Expanding Treatments of The Rotational Spectra of Floppy Molecules

By

J.H. Westerfield

DISSERTATION

Submitted in partial satisfaction of the requirements for the degree of

DOCTOR OF PHILOSOPHY

in

Chemistry

in the

OFFICE OF GRADUATE STUDIES

of the

UNIVERSITY OF CALIFORNIA

DAVIS

Approved:

Kyle N. Crabtree

C. William McCurdy

R. David Britt

Committee in Charge

2023

Contents

Abstract

This dissertation explores the coupling of internal rotation to the overall rotation of molecules and is divided into three distinct sections. The first section is a traditional torsion-rotation problem studying the Ka band spectrum of methyl tert-butyl ether, a gasoline additive. The molecule is extremely prolate ($\kappa = -0.991$) and has three possible large amplitude motions: methoxy methyl torsion, tert-butyl torsion, and geared methyl torsion. These three internal rotations were investigated by MP2/cc-pVDZ calculations, and the methoxy methyl torsion was predicted to be the most influential in the microwave spectrum. Using a recently constructed Ka band chirped-pulsed Fourier Transform Microwave Spectrometer, the torsional-rotational spectrum of this molecule was recorded. Due to the minimal molecular asymmetry, the A state spectrum resembled that of a symmetric top, while the torsion-rotation coupling in the E state spectrum broke the near symmetric pattern and was a more typical asymmetric top spectrum. A total of 405 transitions were recorded and fit using XIAM, and the methyl torsional barrier height was determined to be 495.648(720) cm^{-1}.

The second section describes a new program, westerfit, for C_s molecules with internal rotation and spin angular momentum. The code implements a single diagonalization Rho Axis Method approach for the torsion-rotation alongside a complete treatment of nuclear quardupole interaction and spin-rotation coupling. Unlike other programs designed for internal rotation with spin effects, westerfit includes matrix elements off-diagonal in the rotational angular momentum quantum number, N, rather than the perturbative treatment of the spin-rotation and quadrupole interactions. This full combined approach allows fitting of all symmetrically allowed terms in both the spin-rotation and the quadrupole tensors as well as inclusion of any higher order terms coupling the large amplitude motion to the spin angular momentum. The program was benchmarked against other published programs and found to be capable of reproducing results from three different programs. Particular interest was paid to meta-chlorotoluene as this molecule has a low internal rotation barrier and a spin 3/2 nucleus which make it the exact type of molecule the program was designed to treat. Previous attempts to fit this molecule were complicated in part by XIAM's limitations at very low barrier heights and its perturbative quadrupole treatment. While the new

fit in westerfit does offer reduced RMS error and better precision on the spectroscopic parameters, transitions from excited torsional states will likely be necessary to accurately determine the barrier height.

The final section details the theoretical interactions between the methyl rotation and a single unpaired electron's spin angular momentum. A Hamiltonian for spin-torsion-rotation in the Rho Axis System was determined and the matrix element of the spin-torsion coupling operator was derived as well as possible definitions for calculating the associated parameter. The operator was implemented into the code described in the preceding chapter and was used for the theoretical investigations. The interaction of this operator with other second order operators was explored with the spin-torsion coupling being most sensitive to the torsional barrier height. Coupled cluster parameters for the example molecule, meta-methyl-phenoxyl, were calculated, and spin-torsion-rotation spectra were simulated with the spin-torsion term at zero and at a non-zero value. When the spin-torsion term was changed from zero, most of the simulated transitions underwent a subtle shift that was not uniform in magnitude or direction. The work presented here should provide a foundation for future work on the rotational spectra of radicals with internal rotation.

Acknowledgments

I think it's fairly obvious to anyone who has spoken to me in the last few years that my time in grad school has been an odd and frustrating one. While I don't think UC Davis and I would have ever agreed with each other, there are a handful of people that massively helped make this work possible. First, I'd like to thank my undergrad institution New College of Florida, as it used to be, which was a wonderful place for me. It was where I figured out that I'm Autistic and found my love of torsional-rotational spectroscopy to which this work is entirely focused on. The school was filled with interesting and critical people who had all sort of exciting topics they wanted to study and ways they wished the world would function. It was a place of great growth and comfort for me and I truly doubt I'd have managed a bachelor's from any other school. Despite its many, many flaws, there was a constant level of good faith that I could readily extend to my peers and teachers. Well as readily as a curmudgeonly fellow can manage. I left filled with hope and conviction for what the future could be and I so greatly thank Sean, Victoria, Steve, the Erikas, Han, and the others that helped me develop into who I was by the time I left New College. The problem with leaving a place that one feels so at home in is that the next place won't hold up. I did later jokingly accuse NCF of not adequately preparing me of grad school by setting my expectations for academic environments too high.

Next, I thank the international rotational spectroscopy community. ISMS has been the highlight of my year each year since 2016. I still remember Li Hong Xu's plenary talk from that year and how seeing those dense energy level diagrams and such meticulous detail dedicated to methanol being presented on that giant projector solidified my desire to become a torsional-rotational spectroscopist. The greatest highlight of my time in grad school was November of my first year when Jon Hougen visited UC Davis and we were able to have an extended one-on-one chat about group theory and large amplitude motion wherein he told me he'd do whatever he could to make me a torsional spectroscopist. Unfortunately I was never able to take him up on the offer as he and Xu passed away two months later. I miss them both dearly and hope to one day have a fraction of the impact on the torsion-rotation community has either of them. There are of course those still living such as Isabelle Kleiner, Ha Vinh Lam Nguyen,and Vadim Ilyshun

all of whom have produced such inspiring works. Particular thanks go to Kleiner from whom I've got such strong encouragement during our chats at ISMS. I do so hope to get to work with you more directly in the future. And of course I must thank the dear friends in the community such as Connor, Halley, Blair, Brian, Marie-Aline, and many more for the joy of seeing them both at ISMS and pop up in literature searches. My regrettably named program, westerfit, is a blatant love letter to the rotational spectroscopy community past, present, and future. I again thank Kleiner for thinking the program's name is funny and thus allowing me to permit myself to keep the name.

My greatest thanks must of course go to my union, UAW-2865, which had the greatest hand in maintaining my sanity over the last few years. I had planned to become UAW-2865 member from the moment I learned I'd have a union though I didn't think I'd do much active organizing. I will confess that a solid 30% of why I first went to a UAW-2865 event was to try to meet leftist women. This was of course not how it worked out as I'd become a campus Head Steward, the Guide on the state-wide Executive Board. I loved it and I loved the people I met through it. It was so heart warming to be surrounded by people who would look at the world around us, figure out how to make it better, and push for that. Organizing was exhausting and among the most stressful things I've ever done but to sit by and let the horrible system of the UC continue to harm my peers and my students would have been a morally unforgivable option. I'm sure the six weeks we spent on strike will have lasting physical and mental health costs but the only thing I'd change about it is that I would have gone to a union event sooner and started organizing before the middle of my second year. I have nothing but thanks, fondness, and support for Sophie, Izzy, Deb, Aarthi, Ximena, Marshall, Nathan, Emily, Ellen, Carla, Brennan, Willa, and anyone else who signed their union card & did a walkthrough to help fight for a better UC.

If any future graduate student is reading this, I hope you are having a better time than I did and that you've signed your union card.

CHAPTER 1

Introduction

To provide context for the work contained in this text, a history of the field shall be provided here. While microwave has been shown to have applications in astrochemistry and analytical fields, it remains largely the domain of fundamental molecular interest. Rotational spectroscopy has given deep, accurate insight into molecular structure, and remains one of the most sensitive probes of intra- and inter-molecular interactions. The sensitivity to perturbation and frequency precision associated with rotational spectroscopy make it a powerful tool for confirming ab initio models. However, there remain areas where theory has not been developed to support rotational investigation into all molecules, such as spin-torsion interaction.

1.1. 1920–1939: The Beginning of the Field

The field of molecular rotational spectroscopy began in the 1920s as an expansion of orbital motions of electrons in the hydrogen atom. Dennison determined the energy levels of rigid linear and symmetric molecules as well as determining the separate quantum numbers for overall angular momentum and its projection onto the molecular symmetry axis, which would latter be referred to as J and K respectively [**1**]. This paper also established that the rotational energy levels are heavily dependent on the exact structure of the molecule which makes rotational spectroscopy a very powerful tool for determining the molecular geometry. The exact connection between the moments of inertia and the molecular energy levels is discussed in Chapter 2. Kronig and Rabi restructured Dennison's work into Schrödinger's wave mechanics and determined that the quantum numbers must take on integer values [**2**]. Witmer began the study on rigid asymmetric tops by building on the wave mechanics approach and treating the asymmetry of the molecule as a perturbation on the symmetric top problem [**3**]. Wang expanded Witmer's work in 1929 with matrix mechanics and his namesake unitary transformation for block diagonalizing the asymmetric top Hamiltonian [**4**].

Wang also determined the selection rules of $\Delta J = 0, \pm 1$ and $\Delta K = 0, \pm 1$. While it wouldn't be until after World War II that works of Witmer and Wong would be experimentally tested, the first experimental microwave spectrum was that of ammonia recorded in 1934 [**5**]. This was a single pass direct absorption experiment performed at room temperature and pressure. Due to aggressive pressure broadening and limited resolution, only a single broad feature was recorded, which corresponded to the inversion motion of ammonia.

The theoretical advancements continued in this period, awaiting future experimental technologies. Conveniently for rotational spectroscopy, quantum angular momentum occurs frequently in other aspects of physics and chemistry. Initially, the focus was centered on properties of atoms such as spin-orbit coupling. This topic had been explored thoroughly by the mid 1930s, and Condon and Shortly released their textbook on atomic spectra in 1935 [**6**]. The coupling of vibrations and rotations was also theorized with particular interest to structural distortions emerging from the rotation as well as low energy modes with large nuclear displacements. The structural distortions, referred to as centrifugal distortions, account for how the geometry of the molecule and thus the exact rotational energy levels change with increasing angular momentum within a singular vibrational state. Kivelson and Wilson proposed a Taylor expansion approach of adding fourth order angular momentum operators to account for centrifugal distortion in 1932 [**7**]. By simply adding higher order angular momentum operators, the rotational energy levels are corrected without the need to solve the full vibrational Hamiltonian.

The low frequency vibrational modes with large nuclear displacement are referred to as large amplitude motions. These modes are very anharmonic and complicate rotational spectra by creating additional energy levels thus more transitions so the spectra can no longer be treated by purely rotational models. The classic case of this is methyl rotation. Thermodynamic models to study these torsions were introduced in the 1920s with a particular emphasis on ethane. Quantum mechanical models for infrared and microwave spectra came about in the work of Neilson [**8**] in 1932 and were expanded to include rotational coupling by Dennison and his coworkers [**9**, **10**]. These works introduced a quantum number for torsional angular momentum that takes on integer values

as well as the singly and doubly degenerate symmetries for three-fold internal rotors. The torsion-rotation energy levels were found to be heavily dependent on the potential energy barrier to internal rotation thus expanding the possible information that can be extracted from a molecule's rotational spectrum. While ethane is the prototype for methyl internal rotation, its lack of permanent electric dipole moment greatly inhibits its study via microwave spectroscopy. Thus, methanol became the focus for these models.

1.2. 1940–1962: Expansion of RADAR Technology

World War II led to vast improvement in the generation and detection of microwave radiation due to the growing telecommunications industry. During the testing of radio wave communications, the ammonia inversion band was accidentally remeasured via vapors of a trash boat in the Charles River [**11**]. The postwar period saw a surge of interest in microwave spectroscopy as a result of these advancements. 1947 saw the publication of Hughes and Wilson's description of the Stark-modulated spectrometer [**12**]. This design improved the previously used waveguide instruments by adding a metal septum along the waveguide and applying an oscillating voltage to the septum. The repeated introduction and removal of the electric field removes and restores the degeneracy of the angular momentum projection on the laboratory frame, which in turn alters the transition frequencies. This combined with lock-in amplifiers boosted resolution and sensitivity over previous designs. This Stark-modulated design would be the dominant technique of microwave spectroscopists for nearly 40 years. By 1948, a review article on microwave spectroscopy was written by Gordy [**13**]. This article discussed around 60 molecules that had been measured since 1934 with the bulk occurring after the war. For 17 of these molecules, their structures had been determined by comparing the changes in the moments of inertia across multiple isotopic variations of the molecule. The review also demonstrated the technique's sensitivity to large amplitude inversions and nuclear hyperfine coupling.

One molecule measured in this postwar boom was methanol, which would become the core test case for torsional-rotational spectroscopy. The first reported microwave spectra of methanol was presented in 1947 by Hershberger and Turkevich [**14**]. The paper showed 5 transitions recorded

using a direct absorption cell and was expanded mere months later by Dailey using a stark modulated spectrometer [**15**]. This work reported reported 23 transitions though the spectrum was not analyzed with a torsion-rotation model until 1951 [**10**] wherein multiple moments of inertia for the internal rotor in the analysis which determined corresponding barrier heights ranging from 377–383 cm^{-1}. Over the next decade, internal rotation would remain such a core aspect of rotational spectroscopy that Lin and Swalen released a review article in 1959 [**16**]. It collected and explained both Wilson's Principal Axis Method of torsion-rotation as well as the Internal Axis Method of Neilson and Dennison, which aligns with what modern literature refers to as the Rho Axis Method. It also contains a collection of 35 molecules with their internal rotor barrier heights alongside discussions of the spectral features. The review covered a range of barrier heights from 2–1250 cm^{-1} with the average molecule containing 8 atoms.

In 1951, Wigner introduced the n-j symbols as a means of assessing the matrix elements and wavefunctions of coupled angular momentum problems [**17**]. This, coupled with spherical tensors via the Wigner-Eckart Theorem, provided a clear structure for calculating the energy levels of quantum angular momentum problems [**18**]. These mathematics were developed with the focus on atomic and nuclear problems. However, the attention turned more to molecules by 1951 with Van Vleck's application of angular momentum coupling to polyatomic systems [**19**]. This introduced the idea of time-reversed spin as a means of addressing the "anomalous" commutator relations of the molecular frame angular momentum projections. The anomalous relations emerge from the shift from a laboratory reference frame to a molecular reference frame and are discussed further in the next chapter. Van Vleck's matrix elements established the foundation for more precise studies of molecules with electronic or nuclear spin interacting with the overall rotations. Curl and Kinsey applied Wigner's approach to the problem of asymmetric tops in 1961 and found their results to be consistent with Van Vleck's approach while offering a more algebraic derivation of the matrix elements [**20**].

The first successful report of the rotational spectra of a transient species was the OH radical spectrum on 1955 [**21**]. It used a 300 W discharge oscillating at a frequency of 2 MHz to break down the water vapor as it entered the Zeeman modulated spectrometer. These pre-free jet

spectrometers struggled due to narrow cross-sections leading to the unstable species colliding with the walls more. Additionally, the metal surfaces used for the modulation could help catalyze decay pathways, thus further decreasing the lifetimes of the target molecules [**22**]. The OH measurement used a glass cell inside a waveguide to alleviate this problem and relied on Zeeman modulation instead of Stark modulation. The oscillating magnetic field caused only the radical signal to be detected, preventing spectral congestion from the closed shell species. The transitions were split by Λ doubling from the electronic orbital angular momentum as well as by the magnetic hyperfine interaction of the nuclear spin and the unpaired election. This work provided experimental proof of Van Vleck's matrix elements as well as opened the possibility for future microwave studies on unstable molecules. The first detection of spin-rotation would not come for nearly a decade.

1.3. 1962–1979: Mid-Century Theoretical Advancements

Stark modulated spectrometers would continue to dominate the the world of microwave spectroscopy to such a degree that Hewlett-Packard produced and sold Stark modulated spectrometers from the early 1960's to the early 1970's [**23**]. While it would be a considerable length of time before a new experimental conceit entered the scene, many important theoretical works emerged in this time period. Perhaps the most important of these was Watson's 1967 reduction of the asymmetric top Hamiltonian [**24**]. With the improving resolution and signal to noise since the initial spectrometers, the ability for a simple rigid rotor approximation to model all the details recorded in a spectrum declined. Watson showed that the number of distortion terms at fourth order can be reduced from the previous six down to five. This reduction removes indeterminacies between parameters and simplifies the asymmetric top problem by increasing the independence of the remaining operators. This Hamiltonian has become so ubiquitous in the field that it is colloquially referred to as the "Watsonian" [**25**].

The higher resolution allowed for the first experimental case of spin-rotation coupling in the SO radical [**26**]. This was measured in 1964 with a coating of Corning "K" mixture to reduce the degradation of the radicals. The higher resolution also created a greater need for more precise calculation of rotational energies coupled to spin interactions. Raynes expanded Van Vleck's work on angular momentum coupling for molecules in 1964 to address more of the symmetries and

distortions of asymmetric top molecules [**27**]. Similar to Van Vleck, this work used vector coupling coefficients to determine the matrix elements. Nuclear hyperfine interactions were intially given the spherical tensor treatment in 1966 by Benz [**28**]. This provided an exact treatment as opposed to earlier perturbative approaches [**29**]. Bowater, Brown, and Carrington expanded the spherical tensor approach in rotational spectroscopy for their 1973 study of the HCO radical [**30**]. The radical was produced by reacting F atoms with formaldehyde and the species provides a minimally sized asymmetric top to focus on the internal spin interactions without large amplitude motion or other strong vibrational coupling. The theory given in this work treated all three angular momentum sources (rotation, electron spin, hydrogen spin, all their couplings, and the impacts of the Stark and Zeeman effects. Much was consistent with the prior work aside from some phase factors such as the off-diagonal in N elements in spin-rotation relative to Raynes. A great advantage of this approach is that it can systematically be expanded to include an indefinite number of angular momentum sources [**31**]. In 1979, Brown and Sears would later add a set of fourth order terms for spin-rotation centrifugal distortion as well as a reduction to the second order spin-rotation Hamiltonian [**32**]. These new terms follow the structure established by the Watsonian and allowed for fitting of asymmetric radicals past the rigid rotor approximation.

The torsion-rotation literature would begin to take on its more modern appearance in the 1960s with Woods's 1966 paper [**33**]. The paper by Woods described a general program for abritrary-fold rotors and had a follow-up paper extending it to multiple rotors. The approach Woods laid out involves rotating the molecular coordinates into the Internal Axis System and then solving the torsional energy levels for a given K value via Mathieu equations. Then the coordinates are rotated back to the Principal Axis System to solve the torsion-rotation energy levels. This would go onto form the theoretical basis of the program XIAM. In 1968, Lees and Baker returned attention to methanol with their approach for molecules with a plane of symmetry and a three-fold internal rotor [**34**]. This work features the use of computers to more accurately and easily solve for the non-periodic solutions of the torsion-rotation Hamiltonian that result from higher order distortion terms in the torsional Hamiltonian. Lees and Baker's approach allowed for transitions involving as high as $J = 25$ and $K_a = 10$ to be included in the fit all while simultaneously addressing

v_t = 0, 1, 2, and 3. This would form the theoretical basis for the 1984 work Herbst et al. which introduced the two stage diagonalization approach [**35**]. The two stage approach solves the torsional part of the Hamiltonian and then the torsion-rotation Hamiltonian thus allowing a larger torsional basis to be used in the first stage and a smaller in the second. A balance of performance over a large-basis single stage and accuracy over a small-basis single stage can be achieved.

1.4. 1979–2006: Era of Balle-Flygare Cavity

As radio frequency technologies improved, the Stark-modulated instruments ultimately phased out in phase of Fourier Transform techniques. A particular advantage of these is that they do not require use of a waveguide which allows for use of supersonic jet expansions. These allow the rotational temperature of the gas samples to be heavily reduced thus aggressively simplifying the spectrum by reducing the thermal population of the higher energy rovibrational states. Additionally the increased time before collisions allow for longer coherence times and thus higher resolution measurements. In 1979, to further increase resolution and sensitive, Balle and Flygare placed a resonator cavity inside the vacuum chamber which would be tuned to specific frequency windows [**36**]. The cavity produces standing waves in a 1 MHz window to greatly increase the sensitivity and resolution of the instrument which allows for the study of harder to detect molecules such a species with low dipole moments or transient species.

Jumping to 2000, the McCarthy group introduced a design of discharge nozzles used to produce unstable species [**37**]. The nozzle immediately follows the pulsed valve and contains two copper electrodes spaced by teflon. A high voltage, generally in the range of a few hundred volts, is applied to the electrodes and the molecules are dissociated as they pass between two electrodes. This discharge nozzle was first used for producing long carbon chain molecules such as methylpolyynes. An alternative to the discharge approach, the pyrolysis reactor, as introduced by Chen in 1986 [**38**] and popularized by Ellison in 2014 [**39**]. These reactors work by following the pulsed valve with a silicon carbide rod that a high current is passed through. The electrical current heats the rod to as much as 1600 K which causes the molecules passing through to undergo thermal decomposition.

Perhaps the most important paper in the rotational spectroscopy literature is Herb Pickett's 1994 text on his program program SPFIT/SPCAT [**40**]. The program implemented the spherical tensor approach of Ref. [**30**] alongside a modified Wang transformation to avoid explicit complex algebra in the matrix elements of odd-ordered operators. The code also supports the ability to fit the rotational spectra of multiple vibrational or electronic states at the same time with the option for operators to couple the states. In its current form, SPFIT can support up to 99 vibronic states and 9 spin sources. This, alongside the use of only user-defined operators, makes the program incredibly flexible. This is one of the most cited papers and influential programs in rotational spectroscopy and has had two papers on its usage by other authors: one on more advanced usages [**41**] and a more beginner directed paper [**42**]. In 1998, NASA's Jet Propulsion Laboratory built an online spectral database centered around this program [**43**]. The database contained nearly two million transitions from 331 atomic and molecular species upon release. Each species has the necessary input files for SPFIT/SPCAT including the spectroscopic parameters and a list of observed transitions. In addition, a simulation to higher frequencies and quantum number is provided for each entry so radio astronomers can use the database to identify species in the interstellar medium.

The 1990s saw the release of two key programs for the analysis of large amplitude motion that are still widely used in present day rotational spectroscopy: BELGI-CS [**44**] in 1994 and XIAM [**45**] two years later. The first of these, BELGI-CS, was developed by Hougen, Kleiner, and Godefroid as an implementation of the two stage diagonalization approach given in Ref. [**35**]. This program has been proven to be especially effective at low barrier rotor problems, which feature such large splittings that the rigid rotor model qualitatively fails [**46**]. Many variants, such as ones for C_1 tops, perturbative treatment of hyperfine interactions, and methylamine-like molecules that have a 2 welled oscillator alongside the methyl rotor, have been developed [**47**, **48**, **49**]. XIAM is capable of fitting up to 3 internal rotors along side a perturbative hyperfine treatment. However the smaller torsional basis and more limited number of parameters has given it more trouble in the lower barrier cases. Sven Herbers working alongside Ha Vinh Lam Nguyen updated the code to add in a few more parameters bring closer to BELGI's performance [**50**]. The difference in feature

set and performance as well as quantum number input, have allowed both programs to find and continue serving for different spectroscopic cases around 30 years after their initial release.

There are two other programs available what will be mentioned here for historical completeness: ERHAM [**51**] and IAMCALC [**52**] which were introduced in 1997 and 2001 respectively. While XIAM and BELGI both directly solve the internal rotor Hamiltonian, these two use Fourier series to avoid directly solving the this part of the problem. ERHAM transforms the typical internal rotor parameters into two non-physical fitting parameters. While this method has been effective at fitting complex spectra, it does not provide as much physical insight as BELGI and XIAM. IAMCALC acts as a front-end to SPFIT and uses the Mathieu equations to convert the Hamiltonian into an Internal Axis Method and then generates an input file with the spectroscpic parameters into Fourier series variations. This program does not have accessible documentation aside from the source code and has thus not gained as much popular usage despite the prevalence of SPFIT. The present work takes inspiration from BELGI so the internal mechanisms of that program will be addressed in the next chapter.

1.5. 2006–Present: Modern Microwave Spectroscopy

Brown *et al* introduced the Chirped-Pulse Fourier Transform Microwave Spectrometer design [**53**] in 2006 as an alternative to the cavity design. It used a Gigahertz-spanning, linearly-increasing frequency pulse to cover large frequency bands in a single pulse. The chirped pulse trades the sensitivity of the cavity for greater efficiency at blind searches. Additionally, because it does not require large microwave mirrors, the chirped pulse can be built in a variety of geometries. For example, the room-temperature waveguide returned in designs like the one formerly at New College of Florida [**54**]. This design allows for room temperature rotational spectra to be taken, thus allowing for measurements of higher rotational states and rotational spectra of vibrational states below ~ 200 cm $^{-1}$. In the case of 2-methylfuran, the spectra of first two torsional states were able to be collected simultaneously using the room temperature chirped-pulse. This waveguide setup also does not require as powerful pumps as the traditional jet expansion experiments which can allow for cheaper instruments. Another structure is the cryogenic buffer gas cell designed by Patterson and Daly [**55**]. This design uses cold helium atoms to collisionally cool the molecules of interest

which are then polarized with narrow band chirped pulses that are only $\sim$ 10 MHz wide. The more gentle buffer gas cell over the jet expansions allows for better than room temperature populations of higher energy conformers to be detected such as the gauche conformer of isoprene [**56**]. In addition to offering new instrument geometries, the chirped allowed the average molecule size studied by rotational spectroscopy to increase from $\sim$8.5 atoms to $\sim$13 just in the span if its first decade [**57**]. Thanks to the complementary nature of the chirped pulse and cavity experiments, both have found continued usage in modern day microwave spectroscopy. There now exist instruments that combine both techniques in a single vacuum chamber such as those of the McCarthy and Leopold Groups [**58**, **59**]. These setups use the chirped pulse as an initial cursory survey of the spectrum and then remeasure the transitions at higher resolution with the cavity. The combined setup is able to record transitions at the superior resolution of a cavity without spending time recording regions devoid of transitions.

Discharge and pyrolysis nozzles have also continued to find usage in modern spectroscopy. The discharge nozzles have also been used to produce a variety of radicals from benzene discharge [**60**]. By discharging pure benzene as well as mixtures with O_2 and N_2, over 150 species were assigned alongside 60 isotopic or vibrational variations. One of these pyrolysis reactors has been coupled to a buffer gas cell to study the ozonolysis of isoprene [**61**]. Another was coupled to a jet expansion experiment used to probe phenoxyl [**62**] and 2-furanyloxyl [**63**].

About 15 years after the initial release of BELGI, Vadim Ilyushin released a derivative program called RAM36 [**64**]. This offers both performance and user benefiting features over its predecessor. The key new feature is user-definable operators. BELGI and XIAM both use hard coded Hamiltonians which require the source code to be revised and recompiled to add higher order operators. A quality of life feature included in this program is use of traditional asymmetric top labels for the transitions as opposed to BELGI's variant state labels which makes the program more immediately approachable for rotational spectroscopists who are new to internal rotation. Six years later, a version with perturbative treatment hyperfine interactions was released [**65**].

1.6. Objectives of Present Work

A shortcoming of the previously mentioned programs is their inability to address torsion-rotation and spin-rotation at the same time. This dissertation seeks to combine and expand these approaches to lay the groundwork for a program that can treat C_s molecules with an arbitrary fold internal rotor and a single strong spin source. After covering the background theory, this work will demonstrate a more traditional methyl rotor problem in the case of methyl tert-butyl ether. The new program's development and performance in a variety of test cases is demonstrated in Chapter 4. Lastly, the potential interactions of electron spin and internal rotation will be discussed. An operator and its matrix element will be derived and the impact on the energy levels will be shown.

CHAPTER 2

Theoretical Background

Spectroscopy provides a powerful set of tools for identifying molecules and probing their quantum mechanical properties. Different frequencies of light correspond to different molecular energy levels which can be used to experimentally probe a variety of molecular properties. The Ultraviolet & Visible (UV-Vis) region is dominated by transitions between electronic states and the infrared (IR) region by transitions between vibrational states. Low frequency radio waves can be used to measure transitions between nuclear spins in a magnetic field. While both IR and UV-Vis can achieve rotational resolution, the microwave region allows focus to be more easily placed on molecular rotations within a single vibronic state at a time. Rotational spectroscopy is capable of differentiating between molecules with any amount of structural differences such as conformers, excited vibrational states, and isotopicly substituted species. This is due to full-bodied nature of the end-over-end rotation as opposed to other forms of spectroscopy for which the transitions depend only indirectly on the overall structure. As a result, rotational spectroscopy has been responsible for the majority of molecular identifications in space [**66**]. The naturally narrow linewidths however come with a very high sensitivity to perturbation which leads to more complex spectra and makes the technique a powerful tool for exploring molecular physics. Two common sources of complexity are large amplitude nuclear motion and angular momentum coupling between internal spins and the overall rotation. Since the remaining chapters focus on analysis of such complex rotational spectra, the fundamentals and notation shall be addressed in this chapter.

2.1. An Introduction to Rotational Spectroscopy

To bring the focus to rotational energy, the full molecular Hamiltonian will first be simplified. The Born-Oppenheimer approximation allows the energy to be split into electronic and nuclear parts as the less massive electrons move much faster than the nuclei. This approximation

allows a separate nuclear Hamiltonian to be written for a given electronic state. The kinetic energy of the nuclei is given by [**67**]:

$$\mathcal{T} = \frac{1}{2}\sum_{n} m_n \dot{R}_n^2 \tag{2.1}$$

This expression is summed over each nucleus taking the product of its mass, m_n, and the square of the velocities in the laboratory-fixed axes, $\dot{R}_n$. The nuclear coordinates are chosen to satisfy the Eckart Conditions which allow for the approximate separation of the translational and rotational energies from the vibrational energy. It is more convenient to use the molecule-fixed coordinates so R_n is changed to r_n where r_n satisfy the Eckart Conditions.

$$\sum_{n} m_n \Delta r_n = 0 \tag{2.2}$$

$$\sum_{n} m_n \left(r_n^{(e)} \times \Delta r_n \right) = 0 \tag{2.3}$$

In these equations, Δr_n is the deviation of the nth nucleus from its equilibrium position, $r_n^{(e)}$. The first of these equations defines the coordinate system to be centered at the molecular center of mass. The second expression negates angular momentum from the rotation of the coordinate system. The position vector of a given nucleus can be written as:

$$R_n = R + \Phi^{\dagger}(\phi, \theta, \chi) \left(r_n^{(e)} + \Delta r_n \right) \tag{2.4}$$

Here R is the origin of the molecular-fixed coordinate system in the laboratory frame. The equilibrium coordinates and their displacements are multipled by the transpose of the direction cosine matrix, $\Phi(\phi, \theta, \chi)$. The angles of this rotation are the Euler angles which represent a right-handed rotation $\phi \in [0, 2\pi)$ about the laboratory-fixed Z axis, then a rotation $\theta \in [0, \pi]$about the new molecule-fixed y axis, and finally a rotation $\chi \in [0, 2\pi)$ about the new molecule-fixed z axis [**67**]. Now the velocity of nucleus n can be written as:

$$\dot{R}_n = \dot{R} + \left(\omega \times \left(r_n^{(e)} + \Delta r_n \right) \right) + \dot{\Delta r}_n \tag{2.5}$$

The above expression has introduced the angular velocity, ω, and the time derivative of the displacement, $\dot{\Delta r}_n$. Plugging into Equation 2.1 and simplifying gives an expression for the kinetic

energy separated by the types of motion:

$$2\mathcal{T} = \dot{R}^2 \sum_n m_n + \sum_n m_n \left(\omega \times \left(r_n^{(e)} + \Delta r_n\right)\right)^2 + \sum_n m_n (\Delta\dot{r}_n)^2 + 2\omega \sum_n \left(\Delta r_n \times \Delta\dot{r}_n\right) \quad (2.6)$$

The first term on the right hand side is the translational energy and will be neglected going forward. The second term is the rotational energy with ro-vibrational interaction. The third and fourth terms are the vibrational kinetic energy and the Coriolis coupling of the rotation and vibration, respectively. The rigid rotator approximation forces $\Delta r_n = 0$ which simplifies rotational term and allows for the classical expression to be written with ω as the angular velocity and I as the inertial tensor.

$$2\mathcal{T}_{rot} = \sum_n m_n \left(\omega \times r_n^{(e)}\right)^2 = \omega^\dagger I \omega \quad (2.7)$$

The nuclear energy expression can be completed by adding in the potential energy along each vibrational normal mode, $V(Q_k)$. The vibrational and Coriolis terms can also be rewritten in terms of the normal modes.

$$E_{nuc} = \frac{1}{2}\omega^\dagger I \omega + \frac{1}{2}\sum_k \dot{Q}_k^2 + V(Q_k) + \frac{\omega_\alpha}{2}\sum_{kl} \zeta_{kl}^\alpha Q_k \dot{Q}_l \quad (2.8)$$

The coefficient ζ_{kl}^α is the Coriolis coupling parameter between axis α and modes k and l. The focus will be firmly centered on the rotational component with the occasional look to vibration in the form of centrifugal distortion and large amplitude motion, both of which will be discussed shortly. The Coriolis term will only be included as it appears in the torsional-rotational problem.

The rotational energy levels of a molecule are dependent on the inverse moments of inertia are calculated along the three axes of the molecule which are referred to as rotational constants. They are dubbed A, B, and C as they correspond to the a, b, and c axes of the molecule:

$$A = \frac{\hbar^2}{2I_a}, \qquad B = \frac{\hbar^2}{2I_b}, \qquad C = \frac{\hbar^2}{2I_c} \quad (2.9)$$

The rotational constants are given in energy units here but typically discussed in units of megahertz or wavenumbers for more direct comparison to the units of experimental spectra. As part of the Eckart conditions, the inertial tensor has been diagonalized so there are only 3 terms rather than 9 and this coordinate system is referred to as the Principal Axis System. The Hamiltonian can be

constructed from Equation 2.7 as:

$$\mathscr{H}_{rot}^{(2)} = \frac{1}{2}\omega^{\dagger} I \omega = \frac{1}{2}\sum_{i,j} I_{ij}\omega_i\omega_j \xrightarrow{\text{PAM}} \frac{1}{2}\sum_{i} I_{ii}\omega_i^2 \tag{2.10}$$

The angular velocities are then replaced with the angular momentum operators on the corresponding axes using the following conversion.

$$\mathcal{N}_i = \frac{1}{\hbar} I_i \omega_i \tag{2.11}$$

Compiling all of this gives the rigid rotator Hamiltonian.

$$\mathscr{H}_{rot}^{(2)} = A\mathcal{N}_a^2 + B\mathcal{N}_b^2 + C\mathcal{N}_c^2 \tag{2.12}$$

In the case of the symmetric top, which occurs when two of the rotational constants are identical, the rotational energy levels can be determined from a closed form expression. For a prolate top ($A > B = C$) and the I^r representation ($a, b, c \rightarrow z, x, y$), the Hamiltonian becomes:

$$\mathscr{H}_{rot}^{(2)} = A\mathcal{N}_z^2 + B\left(\mathcal{N}_x^2 + \mathcal{N}_y^2\right) \tag{2.13}$$

Using, the relationship of $\mathcal{N}^2 = \mathcal{N}_z^2 + \mathcal{N}_x^2 + \mathcal{N}_y^2$, the Hamiltonian can be simplified further:

$$\mathscr{H}_{rot}^{(2)} = A\mathcal{N}_z^2 + B\left(\mathcal{N}^2 - \mathcal{N}_z^2\right) = (A-B)\mathcal{N}_z^2 + B\mathcal{N}^2 \tag{2.14}$$

The above operator can be acted on the symmetric top wavefunction to calculate the rotational energy levels. The symmetric top wavefunction has three quantum numbers: the angular momentum, N, its projection on the molecular z-axis, K, and its projection on the laboratory Z-axis, M.

$$|NKM\rangle = (-1)^{M-K}\sqrt{\frac{2N+1}{8\pi^2}}\mathscr{D}^N_{-M-K}(\phi,\theta,\chi) \tag{2.15}$$

In this equation, $\mathscr{D}$ is the Wigner D-matrix and ϕ, θ, χ are the Euler angles. It is important to note that when $K = 0$, $\mathscr{D}^N_{M0} \propto Y^N_M$ where Y^N_M is the spherical harmonic. This work will assume a field-free environment so M will be taken to be zero and will deviate from field convention by using N instead of J to refer to the molecular frame angular momentum in the absence of electron spin. This is done for better conceptual consistencies between chapters. Three mutually commuting

operators may be chosen and by convention these are: the square of the total angular momentum operator, its projection on the molecular z-axis, and its projection on to the laboratory Z axis. These operators have the following matrix elements in the symmetric top basis.

$$\langle NKM|\mathcal{N}^2|NKM\rangle = N(N+1)|NKM\rangle \tag{2.16}$$

$$\langle NKM|\mathcal{N}_z|NKM\rangle = K|NKM\rangle \tag{2.17}$$

$$\langle NKM|\mathcal{N}_Z|NKM\rangle = M|NKM\rangle \tag{2.18}$$

The units of $\hbar$ have been dropped from these matrix elements as they are assumed to be included in the parameter definitions. Using the operators in Equations 2.16 and 2.17, it can be seen that the combination of Equations 2.14 and 2.15 only has on-diagonal elements and thus the energy is calculated as:

$$E_{rot}(N,K) = (A-B)\,K^2 + BN(N+1) \tag{2.19}$$

For an oblate top, when $A = B > C$, in the III^r representation $(a, b, c \rightarrow y, x, z)$, the energy levels are instead:

$$E_{rot}(N,K) = (C-B)\,K^2 + BN(N+1) \tag{2.20}$$

In the case of the prolate top, the energy increases as K increases but for the oblate top, the energy decreses as K increases. When all three moments of inertia are nonequivalent, the molecule is referred to as an asymmetric top and there is no closed form expression for the rotational energy levels. This complication comes from the three molecule-fixed angular momentum projections not commuting and instead obeying the following relation:

$$[\mathcal{N}_i, \mathcal{N}_j] = -\imath e_{ijk}\mathcal{N}_k \tag{2.21}$$

In these relations, f, g, and h are arbitrary projection axes and the Levi-Civita symbol e_{fgh} is equal to 1 if f, g, and h are in a cyclic order of x, y, and z, to -1 if they are in an anticyclic order, and to zero if any axes are repeated [**32**]. The minus sign in the above expression causes these commutation relations to be called "anomalous" and is not present for the space-fixed operators. The angular momentum about the x and y axes can be addressed by constructing raising and

TABLE 2.1. The Four Group, V, with the symmetries of the I^r states based on the even or odd values of K_a and K_c [**31**]

V	E	R_x^π	R_y^π	R_z^π	K_a, K_c	Operator
A	1	1	1	1	ee	$-$
B_x	1	1	-1	-1	oo	$\mathcal{N}_x$
B_y	1	-1	1	-1	oe	$\mathcal{N}_y$
B_z	1	-1	-1	1	eo	$\mathcal{N}_z$

lowering operators:

$$\mathcal{N}_\pm|NK\rangle = (\mathcal{N}_x \pm \imath\mathcal{N}_y)|NK\rangle = \sqrt{N(N+1) - K(K\mp 1)}|NK\mp 1\rangle \tag{2.22}$$

The mismatch of the operator subscript and the direction by which K is changed is a result of the so-called anomalous commutation relations of the molecule-fixed axis system as opposed to the laboratory-fixed axis system. The direction of the molecule's rotation appears to go in opposing directions if viewed from the molecule's perspective or the laboratory's perspective. Using the I^r representation $(a, b, c \to z, x, y)$ and rearranging Equation 2.12 to use the above operators gives the practical form of the rotational Hamiltonian:

$$\mathscr{H}_{rot}^{(2)} = \left(A - \frac{B+C}{2}\right)\mathcal{N}_z^2 + \frac{B+C}{2}\mathcal{N}^2 + \frac{B-C}{4}\left(\mathcal{N}_+^2 + \mathcal{N}_-^2\right) \tag{2.23}$$

The energy levels are obtained by diagonalizing the Hamiltonian in the symmetric top basis. Using the operator definitions in Equations 2.16, 2.17, and 2.22, the matrix can be structured into independent blocks for each N value. By invoking the Wang transformation, the N blocks can be further block-diagonalized by the different irreducible representations of the four group, V, as presented in Table 2.1. After diagonalization, K is not a good quantum number so a different method of labeling the states must be concocted. The states can also be labeled according to symmetry in V. By combining the symmetries with the energetic ordering, the states are instead labeled with "near" quantum numbers K_a and K_c which can be interpreted as K if the molecule were purely prolate or purely oblate respectively. The values of K_a ascend with energy from 0 to N while K_c spans from N down to 0. The sum of K_a and K_c always equals N or $N+1$.

While V is the rotational symmetry group for any asymmetric top rigid rotor no matter its geometry, other interactions break this symmetry. Most of the molecules explored in later chapters

TABLE 2.2. The C_s Group with the symmetries of the I^r states based on the even or odd values of K_a and K_c

C_s	E	σ_{xz}	K_a, K_c	Operators
A_1	1	1	ee, oe	$\mathcal{N}_y$
A_2	1	-1	eo, oo	$\mathcal{N}_x, \mathcal{N}_z$

possess C_s symmetry, with an xz reflection plane in the I^r representation $(x, y, z \rightarrow b, c, a)$. The two group would be most appropriate to describe these states. This is isomorphic to C_s so C_s will be used to more clearly connect to the molecular symmetry group. The C_s group in relation to the state labels K_a and K_c is shown in Table 2.2. Additionally this expands the group theoretically complete Hamiltonian to include an off-diagonal term on the x and z axis. The associated constant, D_{ab}, is calculated from an inverse product of inertia and will be discussed in greater detail in the following section. Below is the adjusted Hamiltonian where $\{,\}$ is an anti-commutator which follows the form of $\{\mathcal{A}, \mathcal{B}\} = \mathcal{AB} + \mathcal{BA}$. This Hamiltonian is not in the rotational Principal Axis System so the rotational constants have been marked with $'$ to prevent confusion with the values in Equation 2.23. The values are still calculated from the moments of inertia along the given axes.

$$\mathscr{H}_{rot}^{(2)} = \left(A' - \frac{B'+C}{2}\right)\mathcal{N}_z^2 + \frac{B'+C}{2}\mathcal{N}^2 + \frac{B'-C}{4}\left(\mathcal{N}_+^2 + \mathcal{N}_-^2\right) + D_{ab}\{\mathcal{N}_z, \mathcal{N}_x\} \tag{2.24}$$

The rigid rotor Hamiltonian has the obvious shortcoming of not accounting for the distortions in molecular geometry that result from increasing kinetic energy. The early methods of accounting for this "centrifugal distortion" used a Taylor expansion of the following form [**31**]:

$$\mathscr{H}_{rot}^{(4)} = \frac{1}{4}\sum_{\alpha,\beta,\gamma,\delta} \tau_{\alpha,\beta,\gamma,\delta}\mathcal{N}_\alpha\mathcal{N}_\beta\mathcal{N}_\gamma\mathcal{N}_\delta \tag{2.25}$$

This summation has an intuitive 81 terms which can be reduced down to 21 by assessing the equivalent terms. A given τ can be calculated from the harmonic force constant matrix, f_{ij}, as well as the derivative of the inertial tensor elements along the normal coordinates, R_i.

$$\tau_{\alpha,\beta,\gamma,\delta} = -\frac{1}{2I^e_{\alpha\alpha}I^e_{\beta\beta}I^e_{\gamma\gamma}I^e_{\delta\delta}}\sum_{i,j}\frac{\partial I_{\alpha\beta}}{\partial R_i}\left(f^{-1}\right)_{ij}\frac{\partial I_{\gamma\delta}}{\partial R_j} \tag{2.26}$$

The centrifugal distortion Hamiltonian can be further reduced to a mere 6 terms by using the symmetries of the Four Group as well as commutator relations which result in this condensed form [**31**].

$$\mathscr{H}_{rot}^{(4)} = \frac{1}{4}\sum_{\alpha,\beta}\tau_{\alpha,\alpha,\beta,\beta}\mathcal{N}_\alpha^2\mathcal{N}_\beta^2 \tag{2.27}$$

Combining with Equation 2.12, the rotational Hamiltonian up to 4th order can be written as:

$$\begin{aligned}\mathscr{H}_{rot} = \mathscr{H}_{rot}^{(2)} + \mathscr{H}_{rot}^{(4)} = (A+6R_6)\mathcal{N}_z^2 + (B-4R_6)\mathcal{N}_x^2 + (C-4R_6)\mathcal{N}_y^2 \\ - D_N\mathcal{N}^4 - D_{NK}\mathcal{N}^2\mathcal{N}_z^2 - D_K\mathcal{N}_z^2 - \frac{\delta_N}{2}\left\{\mathcal{N}^2, \mathcal{N}_+^2 + \mathcal{N}_-^2\right\} \\ + R_5\left\{\mathcal{N}_z^2, \mathcal{N}_+^2 + \mathcal{N}_-^2\right\} + R_6\left\{\mathcal{N}_+^4 + \mathcal{N}_-^4\right\}\end{aligned} \tag{2.28}$$

The relationship between the $\tau_{\alpha,\alpha,\beta,\beta}$ values and the parameters in the above equation are listed in Table 8.7 of [**31**]. Yet another reduction can be applied in the form of a unitary contact transformation designed to remove terms from the Hamiltonian particularly to increase how independent the remaining parameters are when fitting to experimental data [**68**].

$$\widetilde{\mathscr{H}} = \hat{U}\mathscr{H}\hat{U}^{-1} = e^{\imath\hat{G}}\mathscr{H}e^{-\imath\hat{G}} \tag{2.29}$$

The Hamiltonian here is constructed from the group theoretically complete Hamiltonian which in this case contains all the even order operators of the symmetrically invariant irreducible representation, such as N_z^2, N_zN_x, N^4, etc. The reduction operator, $\hat{G}$, is constructed from the odd order operators that are also of the symmetrically invariant irreducible representation such as N_y, $N_zN_xN_y$, N_y^3, etc. This specific case of the transformation is carried out using the second and fourth order operators to construct the Hamiltonian and the third order operators to construct the reduction operator. Among the most common and immediate relevant are those carried out by Watson [**24**] to reduce the centrifugal distortion terms in the asymmetric top Hamiltonian. This brought about two constructions that each lowered the number of fourth order operators down to five. The one implemented in BELGI [**44**] and more common in the torsional literature [**69**, **70**] is the A-reduction:

$$\widetilde{\mathscr{H}_{rot}^{(4)}} = \Delta_N\mathcal{N}^4 + \Delta_{NK}\mathcal{N}^2\mathcal{N}_z^2 + \Delta_K\mathcal{N}_z^4 + \delta_N\left\{\mathcal{N}^2, \mathcal{N}_+^2 + \mathcal{N}_-^2\right\} + \delta_K\left\{\mathcal{N}_z^2, \mathcal{N}_+^2 + \mathcal{N}_-^2\right\} \tag{2.30}$$

TABLE 2.3. Conversion of Parameter Values between Watson A-Reduction and S-Reduction [**31**]

Operator	A-reduction value	S-reduction value
$\mathcal{N}_z^2$	$A + 16R_6$	$A + 6R_6 - \frac{5R_5(B-C)}{2A-B-C}$
$\mathcal{N}_x^2$	$B + \frac{16R_6(A-C)}{B-C}$	$B - 4R_6 + 4R_5 + \frac{2R_5(B-C)}{2A-B-C}$
$\mathcal{N}_y^2$	$C + \frac{16R_6(A-B)}{B-C}$	$C - 4R_6 - 4R_5 + \frac{2R_5(B-C)}{2A-B-C}$
$\mathcal{N}^4$	$D_N - 2R_6$	$D_N + \frac{R_5(B-C)}{2A-B-C}$
$\mathcal{N}^2\mathcal{N}_z^2$	$D_{NK} + 12R_6$	$D_{NK} - \frac{6R_5(B-C)}{2A-B-C}$
$\mathcal{N}_z^4$	$D_K - 10R_6$	$D_K + \frac{5R_5(B-C)}{2A-B-C}$
$\{\mathcal{N}^2, \mathcal{N}_+^2 + \mathcal{N}_-^2\}$	δ_N	δ_N
$\{\mathcal{N}_z^2, \mathcal{N}_+^2 + \mathcal{N}_-^2\}$	$-2R_5 - \frac{4(2A-B-C)R_6}{B-C}$	0
$\mathcal{N}_+^4 + \mathcal{N}_-^4$	0	$R_6 + \frac{R_5(B-C)}{2(2A-B-C)}$

The other construction is the S-reduction and at fourth order, only the last operator is different.

$$\widetilde{\mathscr{H}_{rot}^{(4)}} = D_N\mathcal{N}^4 + D_{NK}\mathcal{N}^2\mathcal{N}_z^2 + D_K\mathcal{N}_z^4 + d_N\left\{\mathcal{N}^2, \mathcal{N}_+^2 + \mathcal{N}_-^2\right\} + d_K\left(\mathcal{N}_+^4 + \mathcal{N}_-^4\right) \tag{2.31}$$

The contact transformation also changes the values of the second order parameters. The conversions for the parameters in Equation 2.28 into the A or S reduced forms are given in Table 2.3. This contact transformation can be extended to indefinitely higher order operators [**31**]. The approach of contact transformations can also be applied to other cases such as torsion-rotation [**70**] and spin-rotation [**32**]. The process of carrying the contact transformation out is described in greater detail in the books [**31**] and [**68**].

2.2. An Introduction to Torsion-Rotation Interaction

Large amplitude motion refers large nuclear displacements such as rotation about a single bond or an amine inversion which converts the structure into an equivalent configuration. The most common of these, and a central focus of this work, is the internal rotation, or torsion, of a methyl group. Remarkably, this means that a very common organic functional group can contribute to higher level of spectral complexity. The torsional energy of a methyl group is dictated largely by two key factors: an internal rotation constant, F, and a potential barrier height based on the torsional angle, $V(\alpha)$. For molecules with C_s symmetry, the torsional angle, α is the dihedral angle between the symmetry plane and a methyl hydrogen. The potential barrier generally follows a three-fold

cosinusoidal structure but can be Fourier expanded to better match the actual potential.

$$V(\alpha) = \frac{V_3}{2}(1 - \cos 3\alpha) + \frac{V_6}{2}(1 - \cos 6\alpha) + \dots \tag{2.32}$$

The function for the potential defined such that the bottom of the well is at zero and V_3 is the full barrier height with minima at $\alpha = 0, \pm 120°$. The internal rotor constant F_0 is calculated from the least inverse moment of inertia of the top, I_α. F_0 is implemented in the Hamiltonian after being scaled by a factor, r, based on the geometry of the molecule with the symbol being changed to F [**46**].

$$F = \frac{\hbar^2}{2rI_\alpha} = \frac{F_0}{r} \tag{2.33}$$

This term r is based on the moments of inertia along each of the molecular axes and the direction cosines between the internal rotor axis and the molecular axes, λ_g.

$$r = 1 - \sum_{g}^{x,y,z} \frac{\lambda_g^2 I_\alpha}{I_g} \tag{2.34}$$

It is also paired with the square of the torsional angular momentum to calculate the kinetic contribution to the torsional energy. Together, the Hamiltonian for the torsion using only the leading term of Equation 2.32 is:

$$\mathscr{H}_{tor} = F\mathcal{P}_\alpha^2 + \frac{V_3}{2}(1 - \cos 3\alpha) \tag{2.35}$$

The eigenfunctions of Equation 2.35 are the free rotor wavefunctions as given by Equation 2.36.

$$|m\rangle = \frac{1}{\sqrt{2\pi}} e^{-\imath m\alpha} \tag{2.36}$$

The quantum number m can take on any integer value and is proportional to the torsional angular momentum. In this basis, the momentum operator has a matrix element of:

$$\langle m|\mathcal{P}_\alpha|m\rangle = m \tag{2.37}$$

The cosine operator creates off-diagonal elements and can be derived as follows:

$$\langle m'|\cos 3\alpha|m\rangle = \int_0^{2\pi} \frac{1}{\sqrt{2\pi}} e^{\imath m'\alpha} \cos 3\alpha \frac{1}{\sqrt{2\pi}} e^{-\imath m\alpha} d\alpha \tag{2.38}$$

TABLE 2.4. Character Table for the $\mathbf{G}_3$ [**47**]

	E	(123)	(132)
$\mathbf{G}_3$	1E	$C_3(z)$	$C_3^2(z)$
A:	1	1	1
E_+:	1	ω	ω^2
E_-:	1	ω^2	ω

$\omega = \exp(2\pi\imath/3)$

Condensing the coefficients and then invoking Euler's formula gives:

$$\frac{1}{2\pi}\int_0^{2\pi} \cos 3\alpha e^{\imath(m'-m)\alpha} d\alpha = \frac{1}{2\pi}\int_0^{2\pi} \cos 3\alpha \left(\cos(m'-m)\alpha + \imath \sin(m'-m)\alpha\right) d\alpha \tag{2.39}$$

Substituting $\Delta m = m' - m$, for convenience and expanding out:

$$\langle m'| \cos 3\alpha |m\rangle = \frac{1}{2\pi}\int_0^{2\pi} \cos 3\alpha \cos(\Delta m\alpha) + \imath \cos 3\alpha \sin(\Delta m\alpha) d\alpha \tag{2.40}$$

The imaginary term goes to zero and the real term is only non-zero when $\Delta m = \pm 3$. This leaves the final result as:

$$\langle m'| \cos 3\alpha |m\rangle = \frac{1}{2}\delta_{m',m\pm 3} \tag{2.41}$$

With these matrix elements, the Hamiltonian can be expressed in the free rotor basis set as Equation 2.42. The energy levels and eigenvectors are obtained by matrix diagonalization.

$$\langle m'|\mathscr{H}_{tor}|m\rangle = (Fm^2 + \frac{V_3}{2})\delta_{m',m} - \frac{V_3}{4}\delta_{m',m\pm 3} \tag{2.42}$$

As can be seen from the matrix elements, the Hamiltonian can be block-diagonalized into three groups of m values: $m \bmod 3 = 0$, $m \bmod 3 = +1$, and $m \bmod 3 = -1$. These three groupings can be mapped onto the irreducible representations of the G_3 permutation-inversion group as shown by Table 2.4 and can be labeled with $\sigma = m \bmod 3$. The E states form pairs of degenerate energy levels with $E_{m,+1} = E_{-m,-1}$. The A states are non-degenerate so long as $V_3 \neq 0$ cm^{-1}. After diagonalization, the energy levels can be labeled with v_t which begins at 0 for the ground state and increases in integer steps. Each v_t value contains a distinct energy level for each symmetry. As $E \to \infty$, the spacing between the $\sigma = 1$ and $\sigma = 0$ states for a given v_t approaches zero and v_t behaves as a vibrational quantum number.

The complications grow and expand as angular momentum from the methyl top couples to the angular momentum of the molecular frame. In the aforementioned case of a molecule with C_s symmetry, the methyl rotor can couple to the a and b axes to give the following torsion-rotation Hamiltonian:

$$\mathscr{H}_{PAM} = A\mathcal{N}_z^2 + B\mathcal{N}_x^2 + C\mathcal{N}_y^2 + F(\mathcal{P}_\alpha - \rho_z\mathcal{N}_z - \rho_x\mathcal{N}_x)^2 + \frac{V_3}{2}(1 - \cos 3\alpha) \tag{2.43}$$

The terms ρ_z and ρ_x are coupling terms between the angular momentum projections on z and x respectively. They are calculated by the following where λ_g is the direction cosine between the internal rotation axis and the g principal axis.

$$\rho_g = \frac{\lambda_g I_\alpha}{I_g} \tag{2.44}$$

The number of operators can be reduced by rotating the molecular coordinate system such that the coupling between methyl rotor and the x axis is removed. This is referred to as the Rho Axis Method (RAM) and is the dominant approach in modern rotational spectroscopy, with adapted forms being used for multi-top problems [**71**]. The Hamiltonian for this method is:

$$\mathscr{H}_{RAM} = A_R\mathcal{N}_z^2 + B_R\mathcal{N}_x^2 + C\mathcal{N}_y^2 + D_{ab}\{\mathcal{N}_z, \mathcal{N}_x\} + F(\mathcal{P}\alpha - \rho_z\mathcal{N}_z)^2 + \frac{V_3}{2}(1 - \cos 3\alpha) \tag{2.45}$$

Here the values of A_R and B_R are not consistent with their principal axis counterparts, thus the need to denote them with this subscript. The cost of this approach is that by leaving the Principal Axis Method, an off-diagonal rotational constant, D_{ab}, is introduced thus complicating the rotational part of this Hamiltonian, especially as $\{\mathcal{N}_z, \mathcal{N}_x\}$ is off-diagonal in K by 1. The value of D_{ab} can be calculated from the angle rotating into the Rho Axis System from the Principal Axis System, $\theta_{RAM} = \arccos\left(\frac{\rho_z}{|\rho|}\right)$ [**46**].

$$D_{ab} = \frac{A_R - B_R}{2}\tan 2\theta_{RAM} \tag{2.46}$$

This process can be viewed as a contact transformation as presented in [**70**]. The RAM approach has proven very effective at low barrier internal rotor problems such as acetic acid [**72**] and 2-butynoic acid [**73**]. This method has been implemented in the programs BELGI [**44**] and its derivative RAM36 [**64**].

TABLE 2.5. Character Table for the $\mathbf{G}_6$ [**68**]

	E	(123)	(23)*	
$\mathbf{G}_6$	1E	$2C_3(z)$	$3\sigma_v$	
A_1:	1	1	1	$\mathcal{N}_y$, $\cos 3\alpha$
A_2:	1	1	-1	$\mathcal{N}_z$, $\mathcal{N}_x$, $\mathcal{P}_\alpha$, $\sin 3\alpha$
E:	2	-1	0	

Large-amplitude motion also causes the standard point group symmetry to be insufficient; instead a group which allows for the feasible permutation of equivalent atoms involved in the LAM is required. By combining the (123) permutation of Table 2.4 and the (23)* permutation-inversion operator which is equivalent to the xz reflection of Table 2.2, the best permutation-inversion group to represent this problem is the $\mathbf{G}_6$ group, as shown in Table 2.5. The symmetry of a given energy level can then be taken as the direct product of the torsional and the rotational symmetries. In the high barrier limit, the (123) permutation is no longer feasible and the Hamiltonian returns to the pure rotational problem.

The main effect of torsional motion on the rotational spectrum is through line splitting. In the ground torsional state, each rotational transition is split into an A and an E component. The separation between the two torsional components is inversely related to the potential barrier height. For the higher barrier cases where the torsional splitting is still resolved, the spectrum follows the asymmetric top selection rules with the additions of $\Delta\sigma = 0$ and $\Delta v_t = 0, 1$. The E states will also show forbidden transitions [**74**] including c-type transitions despite $\mu_c = 0$ for C_s tops. The forbidden transitions emerge from both the reduction in K meaning and $\langle\psi'|\mu_c|\psi\rangle \neq 0$ for E states. As the barrier height decreases, more of these "forbidden" transitions can be observed [**46**]. This labeling ambiguity allows for transitions that would appear forbidden by the standard asymmetric top rules [**75**].

2.3. An Introduction to Angular Momentum Coupling in Rotational Spectra

Internal spin sources like an unpaired electron or a nuclear spin can couple with the molecular angular momentum. Similarly to the large amplitude motion, this lifts the energetic degeneracy of states and creates more transitions. In the case of an unpaired electron, the rotating molecule's moving electric charge creates a magnetic field which couples with the electron's magnetic moment

thus breaking the degeneracy of the electron spin projection states. This "spin-rotation interaction" is calculated from the dot product of the molecular and spin angular momenta. The spin-rotation coupling is generally treated from a Hund's case (b) wavefunction where the total angular momentum, J, is treated as the vector difference of the molecular frame's angular momentum, N, and the electron spin angular momentum, S. The coupled wavefunction is built from a linear combination of the uncoupled states of the spin and the molecular frame angular momentum [**76**]. Regardless of coupling scheme, the resulting energy levels are identical. The weighting factors of the different uncoupled states are defined by the Clebsch-Gordan coefficients. These can be reconstructed into the Wigner 3j symbols which will be the preferred notation of this work. The two symbols are related by the following, with the 3j symbol on the left-hand side and the Clebsch–Gordan coefficient on the right:

$$\begin{pmatrix} j_1 & j_2 & j_3 \\ m_1 & m_2 & m_3 \end{pmatrix} = \frac{(-1)^{j_1-j_2-m_3}}{\sqrt{2j_3+1}} \left(j_1 m_1 j_2 m_2 | j_1 j_2 j_3 - m_3\right) \tag{2.47}$$

Exact calculations and other uses of these terms can be found in [**18**] and [**77**]. Using Wigner 3j symbols, the coupled wavefunction can be written as [**76**]:

$$|JSNK\rangle = \sum_{\Sigma,\Omega} (-1)^{N-S+\Omega} \sqrt{2J+1} \begin{pmatrix} J & S & N \\ \Omega & -\Sigma & -K \end{pmatrix} |S\Sigma\rangle |J\Omega\rangle \tag{2.48}$$

Within the above 3j symbol are the quantum numbers Σ and Ω which are the projections of S and J, respectively, on to the molecular z-axis. The Hamiltonian for the spin-rotation interaction consists of the sum over all the anti-commutators between the spin angular momentum projections and the molecular frame angular momentum projections.

$$\mathscr{H}_{sr} = \frac{1}{2} \sum \epsilon_{gh} \{\mathcal{N}_g, \mathcal{S}_h\} \tag{2.49}$$

The term ϵ_{gh} is the spin-rotation tensor element for the g axis projection of molecular frame angular momentum and the h axis projection of the electron spin angular momentum. The Hamiltonian's anti-commutator structure enforces the Hermitian nature of the Hamiltonian as the projections of N and S do not always commute with each other.

$$[\mathcal{N}_f, \mathcal{N}_g] = -\imath e_{fgh} \mathcal{N}_h \tag{2.50}$$

$$[\mathcal{N}_f, \mathcal{S}_g] = -\imath e_{fgh}\mathcal{S}_h \tag{2.51}$$

$$[\mathcal{S}_f, \mathcal{S}_g] = \imath e_{fgh}\mathcal{S}_h \tag{2.52}$$

Instead of working with these Cartesian operators, this Hamiltonian is often recast as into spherical tensor notation, using the tensor product of the two angular momentum sources and then the scalar product between that and the spin-rotation tensor [**30**]

$$\mathscr{H}_{sr} = \frac{1}{2}\sum_{k=0}^{2} T^k(\epsilon)T^k(\mathcal{N},\mathcal{S}) + T^k(\mathcal{N},\mathcal{S})T^k(\epsilon) \tag{2.53}$$

The spherical tensor form of the spin-rotation tensor relates back to the Cartesian form by the following series of equations [**78**] and the operators are converted to the same structure but replacing ϵ_{gh} with $\mathcal{N}_g\mathcal{S}$.

$$T^0_{\ 0}(\epsilon) = -(\epsilon_{zz} + \epsilon_{xx} + \epsilon_{yy})/\sqrt{3} \tag{2.54}$$

$$T^2_{\ 0}(\epsilon) = (2\epsilon_{zz} - \epsilon_{xx} - \epsilon_{yy})/\sqrt{6} \tag{2.55}$$

$$T^2_{\pm 1}(\epsilon) = \mp((\epsilon_{zx} + \epsilon_{xz}) \pm \imath(\epsilon_{zy} + \epsilon_{yz}))/2 \tag{2.56}$$

$$T^2_{\pm 2}(\epsilon) = ((\epsilon_{xx} - \epsilon_{yy}) \pm \imath(\epsilon_{xy} + \epsilon_{yx}))/2 \tag{2.57}$$

In this form, the spin-rotation tensor does not commute with the operators. The matrix elements can be determined from either the reversed angular momentum method of Van Vleck [**19**] and Raynes [**27**] or the spherical tensor approach of Bowater, Brown, and Carrington [**30**]. Either approach yields identical matrix elements.

$$\langle JSN'K'|\mathscr{H}_{sr}|JSNK\rangle = \sum_{k=0}^{2} \frac{(-1)^{J+S+N'}}{2}\sqrt{2k+1}\sqrt{S(S+1)(2S+1)}\sqrt{(2N+1)(2N'+1)}$$
$$\begin{Bmatrix} N & S & J \\ S & N' & 1 \end{Bmatrix}\left[\sqrt{N(N+1)(2N+1)}\begin{Bmatrix} 1 & 1 & k \\ N' & N & N \end{Bmatrix} + \sqrt{N'(N'+1)(2N'+1)}\begin{Bmatrix} 1 & 1 & k \\ N & N' & N' \end{Bmatrix}\right]$$
$$\sum_q (-1)^{N'-K'}\begin{pmatrix} N' & k & N \\ -K' & q & K \end{pmatrix} T^k_q(\epsilon) \tag{2.58}$$

The terms in {} are Wigner 6j symbols, which are similar to the 3j symbol but used for coupling 3 angular momenta instead of two [**18**]. The exact matrix element presented above does not fully agree with what is printed in [**30**] on two accounts. They introduced an additional phase factor to get the $k = 1$ terms to go to zero while the terms $T^1_q(\epsilon)$ were later shown go to zero by symmetry [**32**]. The other inconsistency is that the stated coupling scheme appears to be in $N = J - S$ despite the paper's claim that it is $J = N + S$.

Another common form of spin interaction in rotational spectroscopy comes from the nuclear spin. Nuclei with spin greater than 1/2 possess a cylindrically symmetric charge distribution, and the interaction between the quadrupole moment of the charge distribution with the electric field gradient of the molecule produces line splitting which is referred to as nuclear hyperfine splitting. In the Hamiltonian, it is parameterized by the nuclear quadrupole tensor, χ, which is a symmetric traceless, rank 2 tensor due to the aforementioned cylindrical symmetry. Each Cartesian element of χ can be calculated by [**31**]:

$$\chi_{gh} = eQ\left(\frac{\partial^2 V}{\partial g \partial h}\right) \tag{2.59}$$

Here e is the elementary charge, Q is the nuclear quadrupole moment, and V is the electrostatic potential of the molecule evaluated at the nucleus. The spherical tensor form can be related back to the Cartesian form by the following equations [**79**].

$$T^2_0(\chi) = \chi_{zz} \tag{2.60}$$

$$T^2_{\pm 1}(\chi) = \mp\sqrt{\frac{2}{3}}\left(\chi_{xz} \pm \imath\chi_{yz}\right) \tag{2.61}$$

$$T^2_{\pm 2}(\chi) = \sqrt{\frac{1}{6}}\left(\chi_{xx} - \chi_{yy} \pm 2\imath\chi_{xy}\right) \tag{2.62}$$

This tensor has 5 independent terms but by including C_s symmetry and keeping the nuclei in the symmetry plane, $\chi_{xy} = \chi_{yz} = 0$. As a result, $T^2_{+1}(\chi) = T^2_{-1}(\chi)$ and $T^2_{-2}(\chi) = T^2_{+2}(\chi)$ which brings the total number of independent terms down to 3. The Hamiltonian for this interaction is constructed from the scalar product of the rank 2 spherical tensor for the quadrupole, $T^2_q(Q)$, and

for the field gradient, $T^2_q(V)$.

$$\mathscr{H}_Q = -\sum_{q=-2}^{2} (T^2_{-q}(Q) \cdot T^2_q(V)) \tag{2.63}$$

Traditionally, the spin of the nucleus is denoted I and it couples to J to give the total angular momentum F. However, for consistency with the implementation used the program described in Chapter 4, it will be written here using S, N, and J respectively. The traditional coupling scheme used for nuclear hyperfine is $J = N + S$ and has been used here for consistency with the literature. This shift in notation is due to the code only supporting one spin source at a time. Evaluating Equation 2.63 from the same wavefunction given in Equation 2.48 yields the following expression for the matrix elements [**28**].

$$\langle JSN'K'|\mathscr{H}_Q|JSNK\rangle =$$

$$\frac{1}{4}(-1)^{N'+N-K'+S+J+1}\sqrt{(2N'+1)(2N+1)} \begin{Bmatrix} J & S & N' \\ 2 & N & S \end{Bmatrix} \frac{\begin{pmatrix} N' & 2 & N \\ -K' & q & K \end{pmatrix}}{\begin{pmatrix} S & 2 & S \\ -S & 0 & S \end{pmatrix}} \chi_q \tag{2.64}$$

The above is only non-zero for $q = K' - K$. This Hamiltonian will go to zero for any spin less than 1 as the triangle conditions [**18**] will not be met in either the leading 6j symbol or in the dividing 3j symbol. The nuclear spin can interact with the overall molecular rotations in the same way as an electronic spin-rotation interaction. Nuclear spin-rotation is mathematically identical to electronic spin-rotation but is generally denoted with C rather than ϵ [**68**] While the difference in coupling scheme may raise concern, removing the additional factors for a second spin source from the nuclear spin rotation expression in [**80**] produces an identical expression to electron spin rotation of both [**80**] and this chapter.

The non-zero spin creates $2S + 1$ different states that share N, K_a, and K_c. In the case of a $S = 1/2$ radical, this doubles the number of distinct states that can undergo transitions. The selection rule of $\Delta J = 0, \pm 1$ creates more transitions than the simple multiplication of $2S+1$ would suggest. The increased basis state mixing from off-diagonal matrix elements and degraded value

of K similar to the torsional problem also allow for transitions that would be forbidden by the standard selection rules. In uncommon cases such as iodine ($S = 5/2$), transitions of $\Delta N = 3$ have been observed.

CHAPTER 3

On Large Amplitude Motion in the Rotational Spectrum of Methyl tert-Butyl Ether

3.1. Introduction

Methyl *tert*-butyl ether (MTBE) is an additive used to raise the octane rating of gasoline and to ease the initial combustion which can be necessary for starting automobiles in colder climates. Due to the imperfections of gasoline storage, MTBE also acts as an environmental pollutant, seepins out of containers and into groundwater leading its detection in public water supplies in 28 states by 2002 [**81**]. MTBE can be tasted at concentrations as low as 7–12 $\mu g L^{-1}$ [**82**]. The unpleasant taste imparted into the water raised public concern about the compound's usage, particularly after incidents in Santa Monica and Maryland. In 1995, high levels of MTBE were found in the water wells of Santa Monica. This lead to thousands more discoveries of MTBE contaminated wells and city officials of Santa Monica suing several major oil companies to carryout a $200 million cleanup. California banned the usage of MTBE as a gasoline additive in 2002. In addition to the unpleasant taste, leeching of MTBE into groundwater is generally accompanied by other more toxic compounds, such as benzene, also entering the wells [**83**]. Various other states have also banned or begun heavily regulating the compound. Outside of the US, Japan and Canada have outright banned use of MTBE as a gasoline additive. MTBE has been shown to be harmful to aquatic life as it is able to break down into formaldehyde or *tert*-butanol [**84**].

Rotational spectroscopy has been used by the Twagirayezu group to detect polar fuel impurities, such as ethanol, toluene, and acetylaldehyde [**85**]. It is capable of differentiating molecules even with similar functional groups, and the signal intensity is proportional to the dipole moment. Because of octane's low dipole moment, it is transparent to rotational spectroscopy. Therefore, rotational spectroscopy is uniquely applicable to spectroscopic studies on gasoline impurities when

compared to THz [**86**] or infrared [**87**] spectroscopy. Ethanol, toluene, and acetylaldehyde have incredibly well-documented spectra as they serve as simple cases of asymmetric tops with internal rotors. In contrast, MTBE has not been previous measured in the millimeter wave region. To date, only 32 lines in the 9 – 18.6 GHz region have been reported [**88**]. While the Twagirayezu group did not search for MTBE, its absence could be from this previously limited number of centimeter wave transitions. Extrapolating up to the 260–290 GHz region investigated by the Twagirayezu group can be particularly difficult with a limited linelist, only a handful of distortion terms, and large frequency uncertainties. This is especially true of torsional problems as the large amplitude motion causes the rigid rotor model to be less applicable to MTBE. All this means that identifying MTBE in a complex mixture using millimeter wave spectroscopy would be challenging.

MTBE also holds its own curiosities from a spectroscopic perspective. The B and C rotational constants differ by only a few percent difference which makes the molecule a very near prolate top thus the impacts of asymmetry on the spectrum are minimal. There are also 3 different potential sources of large amplitude motion in MTBE: methyl group rotation in the methoxy group, tert-butyl group rotation, and methyl rotation within the tert-butyl group. The most visible is the methoxy methyl group which has an internal potential barrier, V_3, of < 500 cm^{-1} thus making MTBE's rotational spectrum a moderate barrier internal rotation problem. The structure is immediately reminiscent of pinacolone [**89**]. This molecule caused great difficulties in resolving a fit due to the coupling of the methyl and the tert-butyl torsions. Pinacolone replaces MTBE's oxygen with a carbonyl group which causes pinacolone to have lower barrier to methyl rotation than MTBE. Much of the following analysis of MTBE is done with inspiration of what was studied on pinacolone due to the structural similarities. Another molecule featuring a tert-butyl group, near symmetry, and large amplitude motion is tert-butyl isocyanate. The microwave spectrum and barrier height of the tert-butyl rotation of this molecule was measured in 1992 [**90**]. The 41 cm^{-1} barrier height is much lower than the analogous barrier in pinacolone and likely MTBE as neither of these two molecules observed splitting associated with this motion. The present work examines the internal motions of MTBE via MP2/cc-pVDZ and the rotational spectrum from 26.5–40 GHz

using a newly completed spectrometer, thus greatly improving the number of observed transitions, improving the fit, and allowing for better prediction of higher frequency spectra.

3.2. Methods

3.2.1. Rotational Spectroscopy. The spectrum of MTBE was recorded using a K_a band (26.5 – 40 GHz) chirped-pulse Fourier transform microwave (CP-FTMW) spectrometer with an instantaneous bandwidth of 13.5 GHz as shown in Figure 3.1. The instrument operates by generating a linear frequency-swept pulse spanning 1.52 – 4.895 GHz over 1 μs using an arbitrary waveform generator (AWG, Tektronix AWG70002A, 16 GSa/s analog bandwith) which is filtered by a 6 GHz low-pass filter (K&L Microwave 6L250-6000/T18000-O/O). This signal is upconverted in a mixer (Marki MWave T3H-18IS) with an 11.52 GHz local oscillator which is generated at 5.76 GHz from a Valon Technology 5009 synthesizer, doubled with a Wright Technologies ASX13-220, and filtered with a 11.52±0.2 GHz bandpass filter (K&L Microwave 6C52-11520/T200-O/O). The resultant 6.625 – 10 GHz chrip is filtered (Mini-Circuits VHF-6010+ 6 GHz high pass filter (HPF), K&L Microwave 8L250-10200/T30000-O/OP 10.2 GHz low pass filter (LPF)), amplified to 13 dBm (Miteq AFSD5-060120-30-26P), and quadrupled (Wright Technologies ASX40-420) to 26.5 – 40 GHz. After a final pair of filters (AMTI H26G40G1 26.5 GHz HPF, Marki MWave FLP-4300 43 GHz LPF) the chrip is sent through a programmable step attenuator (Agilent 84907L) and amplified with a 170W traveling wave tube amplifier (Applied Systems Engineering 187Ka-H). The chirp is broadcast into a stainless steel vacuum chamber via a 24 dBm K_a band horn (Advanced Technical Materials PNR 28-449-6/24) and the molecular free induction decay is collected with a matching horn. To protect the low noise amplifier (Miteq AMF-6F-26004000-25-13P), the signal first goes through a diode limiter (Clear Microwave LT1840H) and a PIN diode switch (Quinstar QSC-ASR000) which is open during the chirped pulse excitation. The amplified FID is down-converted by a mixer (Marki MWave ML1-1644IS) driven with a a 40.96 GHz signal that is generated by a Valon Tech synthesizer (Valon Tech 5009) at a 5.12 GHz and octopuled (Easter Wireless Telecom EWT-31-0351). The lower band from the mixer is selected with a 17.4 GHz LPF (Marki MWave FLP-1740) and amplified (Minicircuits ZVA-183-S+) before being digitized with a 40 GSa/s by a 16 GHz oscilloscope (Tektronix MSO72004C). To ensure phase consistency, the local

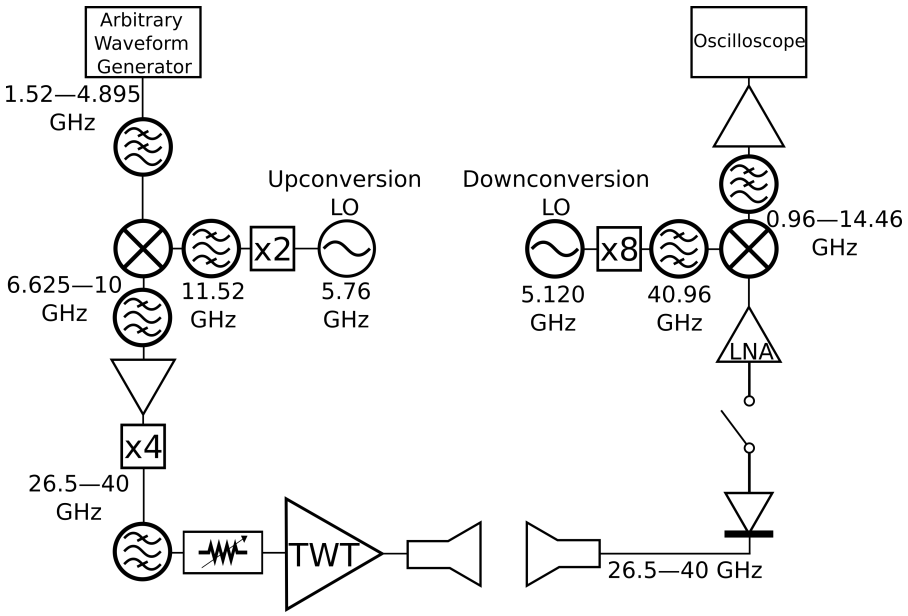

FIGURE 3.1. Block diagram of the K_a band spectrometer

oscillators and timing sources are referenced to the 10 MHz clock of the AWG. The timings of the chirp and gas pulses are controlled by a Quantum Composers 9528 digital pulse generator.

A pulsed super-sonic expansion was generated by a Parker Series 9 solenoid valve with a 500 μm $\varnothing$ apperature driven by an Iota One pulse driver. The sample was introduced by flowing argon through a bubbler of MTBE. The argon pressure was 3.75 bar for one set of averages while only the vapour pressure of the MTBE was used in the second. The valve was actuated at a rate of 5 Hz with pulse width of 650 μs. Each FID was recorded for 15 μs and filtered with a Hanning filter.

3.2.2. Calculations. The structure of MTBE was optimized at the MP2/cc-pVDZ level of theory using CFOUR [**91**] with SCF and geometry convergence criteria of 10^{-8} to acquire the desired spectroscopic parameters. The C_s structure from this calculation is shown in Figure 3.2. Once the geometry was optimized, a finite difference harmonic calculation was carried out. This provided both harmonic vibrational frequencies and approximations of the quartic centrifugal distortion terms. The program Orca was used for a variety of potential energy scans [**92**]. These were done to study the three potential large amplitude motions: the methoxy methyl rotation, the tert-butyl

torsion, and the geared rotation of the methyls inside the tert-butyl group. The first three scans were done as one-dimensional scans where the angle of interest was held fixed and stepped across a 360° range in steps of 1° while the rest of the geometry was reoptimized. This resulted in a set of 361 data points for each motion. This was followed up with two two-dimensional scans wherein the methyl dihedral angle along with another of the two angles were held fixed and stepped across a 240° range in steps of 10° while the rest of the geometry was reoptimized. These pairings were selected to observe how the dominant large amplitude motion will interact with the other two. This produced a 25 by 25 grid for each pair of motions. All of these were done with symmetry turned off to prevent any accidental constraints on the intermediate geometries. Due to the lower likelihood of resolving splitting from either the tert-butyl or the gear motion, a tert-butyl and gear 2D grid was not run at this time.

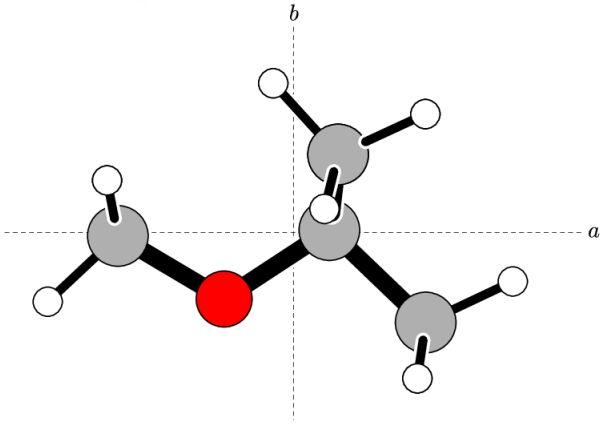

FIGURE 3.2. Methyl tert-butyl ether in the principal axis system

3.2.3. Torsional-Rotational Hamiltonian. This work uses the Rho Axis Method (RAM) as presented XIAM program [**45**], specifically the XIAM_mod [**50**] variant. Unlike other RAM programs, XIAM takes Principal Axis parameters rotates them into the Rho Axis System internally. The RAM has been described Chapter 2 but the expansion to treat two nonequivalent internal rotors will be provided here. The full Hamiltonian is constructed as:

$$\mathscr{H} = \mathscr{H}_{rot} + \mathscr{H}_{tor} + \mathscr{H}_{\alpha\beta} + \Delta_J \mathcal{J}^4 + \Delta_{JK} \mathcal{J}^2 \mathcal{J}_z^2 + \Delta_K \mathcal{J}_z^4 + \frac{\delta_J}{2} \left\{ \mathcal{J}^2, \mathcal{J}_+^2 + \mathcal{J}_-^2 \right\} + \Phi_J \mathcal{J}^6 + \Phi_{JK} \mathcal{J}^4 \mathcal{J}_z^2 \tag{3.1}$$

In addition to introducing torsional operators for the tert-butyl group, a set of top-top coupling terms were also introduced into the fit. This are represented by $\mathscr{H}_{\alpha\beta}$ which is given by:

$$\mathscr{H}_{\alpha\beta} = F_{\alpha\beta}\Big((\mathcal{P}_\alpha - \rho_\alpha \mathcal{J}_z)(\mathcal{P}_\beta - \rho_\beta \mathcal{J}_z) + (\mathcal{P}_\beta - \rho_\beta \mathcal{J}_z)(\mathcal{P}_\alpha - \rho_\alpha \mathcal{J}_z)\Big) + V_{cc}(\cos 3\alpha)(\cos 3\beta) + V_{ss}(\sin 3\alpha)(\sin 3\beta) \quad (3.2)$$

Here α corresponds to the first internal rotor dihedral angle and β corresponds to the second. The term $F_{\alpha\beta}$ couples the kinetic energy of the internal rotors and is derived internally by XIAM from the F_0 values of the methyl and tert-butyl groups. The terms V_{cc} and V_{ss} couple the potential energies and are fit directly. For MTBE, the first internal rotor will refer to the methyl on the methoxy group and the second will refer to the tert-butyl group or the geared methyl group as necessary.

3.3. Results

3.3.1. Calculated Spectroscopic Parameters & Low Frequency Vibrational Modes. The geometry and harmonic frequency calculations provided initial spectroscopic constants including equilibrium rotational constants of $A = 4373.11$ MHz, $B = 2743.30$ MHz, and $C = 2735.80$ MHz as well as dipole projections of $\mu_a = 0.2$ D, $\mu_b = 1.2$ D, and $\mu_c = 0$ D. MTBE is a very prolate asymmetric top with a $\kappa = -0.991$. The Cartesian coordinates of the atoms are given in Table A.1. The 5 lowest frequency normal modes are shown in Table 3.1 in comparison to gas phase measurements [**93**]. The remaining calculated frequencies are listed in Table A.2. Visualizing the normal modes in MOLDEN [**94**] showed the tert-butyl torsion with slight methyl torsion to be the lowest frequency harmonic mode. The frequency discrepancy here likely stems from mode's periodic potential which makes the mode difficult to model in the harmonic oscillator approximation. The harmonic oscillator approximation does not model motions with periodic potentials particularly well. Mode 8 was shown to be the torsion of the methoxy methyl group with slight motion of the geared methyls.

Mode No.	Sym	Exp [**93**]	Calc.	Calc. Int	Type
7	A''	101	17.7966	2.3981	tert-butyl torsion
8	A''	179	178.9342	1.0957	Methoxy methyl torsion
9	A''	219	238.7002	1.3775	Geared methyl torsion
10	A'	262	262.8777	0.3777	COC in plane bend
11	A''	274	293.7098	1.7324	COC out of plane bend

TABLE 3.1. Lowest frequency normal Modes of MTBE calculated at MP2/cc-pVDZ shown against the vapor experimental measurements of [**93**] in cm^{-1}.

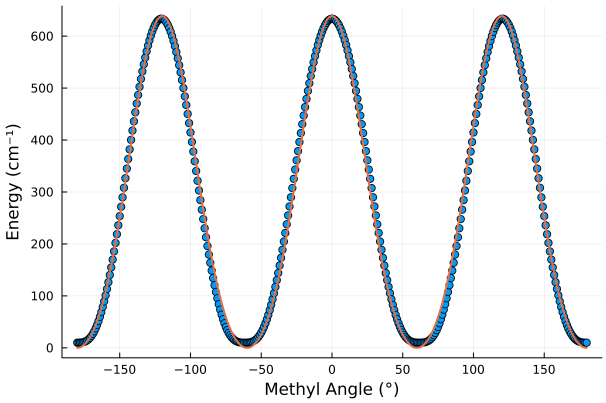

(a) Methoxy methyl dihedral scan

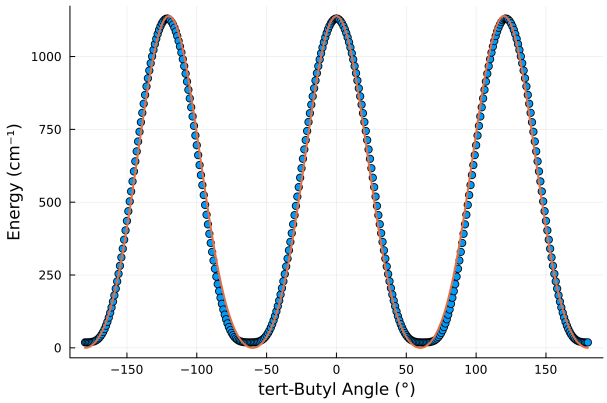

(b) tert-Butyl dihedral scan

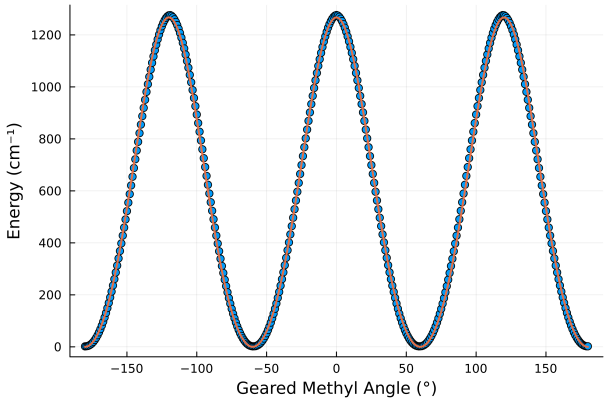

(c) Geared dihedral scan

FIGURE 3.3. MP2/cc-pVDZ potential barriers for the internal rotations of MTBE each fit to the first two expansion terms. Points represent individual ab initio energyies and the curves are the fitted function (3.3)

3.3.2. Internal Barrier Heights. The relaxed 1D potential scans for each of the torsional motions are shown in Figure 3.2. Each potential was fitted to the periodic function:

$$V(\alpha) = \frac{V_3}{2}\left(1 - \cos 3\alpha + \phi\right) + \frac{V_6}{2}\left(1 - \cos 6\alpha + \phi\right) \tag{3.3}$$

Parameter	Methyl	t-Butyl	Geared
V_3	638.68	1139.08	1267.36
V_6	69.19	156.65	100.00

TABLE 3.2. MP2/cc-pVDZ calculated values for the potential terms from the three different internal rotation motions in cm^{-1}

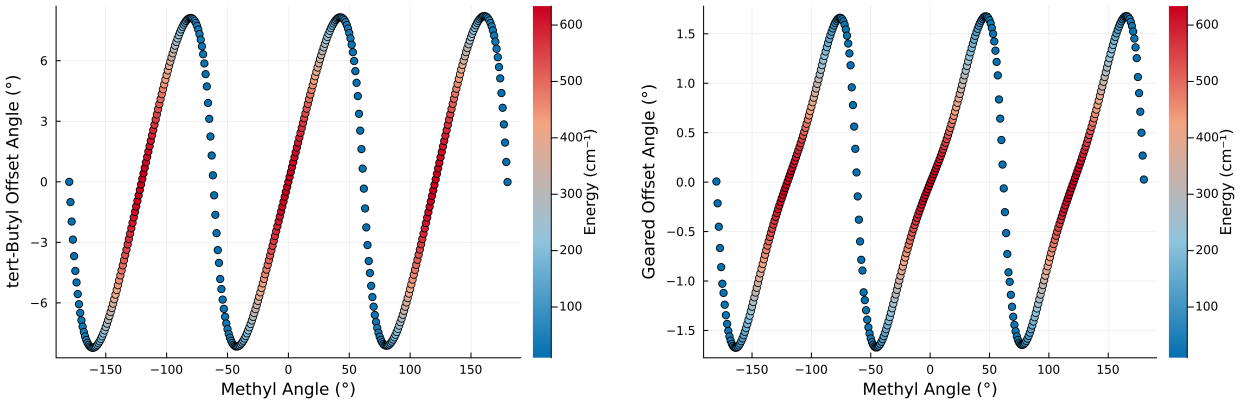

(a) Change in the tert-butyl angle as the methyl angle turns

(b) Change in the geared angle as the methyl angle turns

FIGURE 3.4. MP2/cc-pVDZ potential barrier calculations for the methyl rotation of MTBE. These show how the angles of the other large amplitude motions change with highlighting based on energy. The tert-butyl group shows much more variance as a function of the methyl angle than the geared methyl. In both cases, the step size of the dependent angle along this path is much larger in the well than near the top of the barrier.

ϕ is a phase factor used to match phase of the function to the calculated points. As the phase factor does not alter the torsional energy levels, it is neglected from further discussions. The results of these fits are tabulated in Table 3.2. In the methyl and tert-butyl scans, there is a visible disagreement of the points and fits in the wells and at the $\pm 120°$ peaks which indicates a perturbation, likely from torsional coupling between the modes. MTBE's calculated methoxy methyl barrier (640 cm^{-1}) height is substantially higher than the $C(=O)CH_3$ methyl barrier in pinacolone (156 cm^{-1}). This is consistent with the shift from a methoxy to a methyl ketone group. Using a hybridization interpretation, the electron density at the sp^3 oxygen in the methoxy locks the sp^3 structure of the methyl group into a staggered position thus increasing the the barrier height. The carbonyl oxygen helps pull electron density away from the sp^2 ketone carbon thus lowering the barrier rotation [**95**].

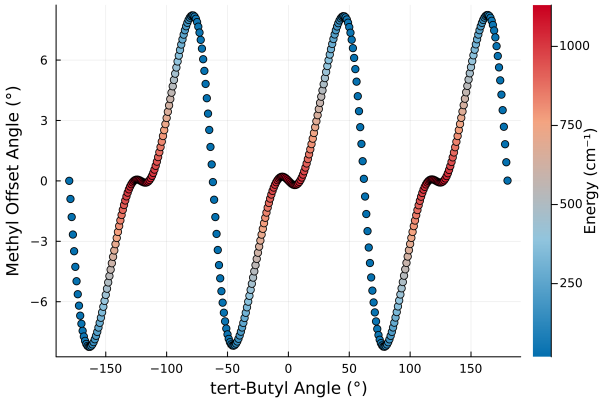

(a) Change in the methyl angle as the tert-butyl angle turns

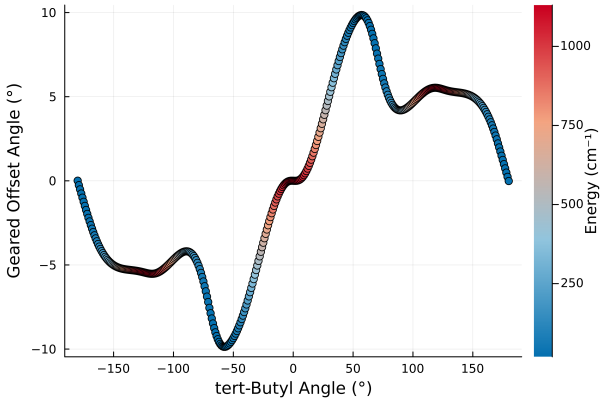

(b) Change in the geared angle as the tert-butyl angle turns

FIGURE 3.5. MP2/cc-pVDZ potential barrier calculations for the tert-Butyl rotation of MTBE. These show how the angles of the other large amplitude motions change with highlighting based on energy. The methyl motion along this path similarly takes larger steps in the well than near the peak. The geared step size is more uniform relative to the energy but spans a larger spatial range

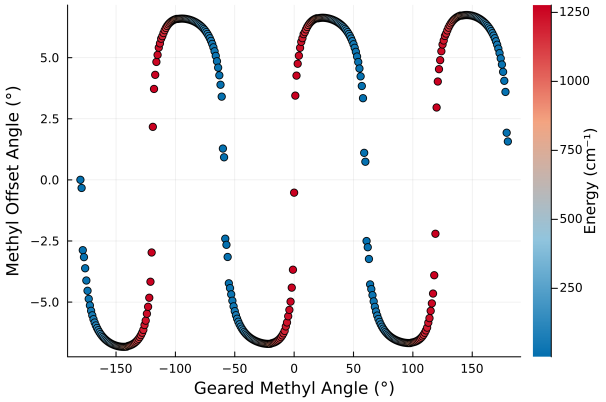

(a) $v_t = 0$

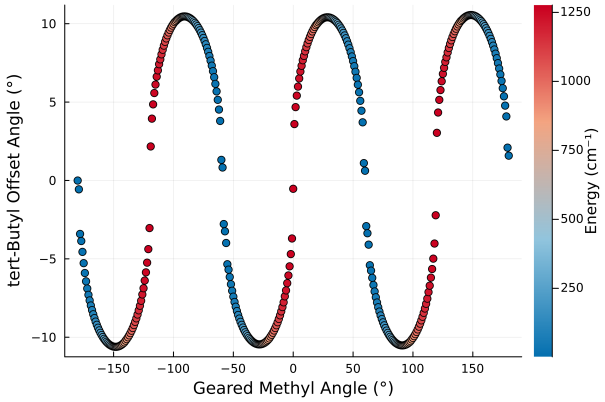

(b) $v_t = 0, 1, 2$

FIGURE 3.6. MP2/cc-pVDZ internal potential barrier for the methyl rotation of MTBE

Figure 3.4 shows how the other torsional angles and the energy change with the methyl angle. Panel a shows the interaction with the tert-butyl angle and displays a roughly 8° swing in either direction within the methyl's V_3 well. This broad spatial distribution shows a probability for torsional coupling between the two internal torsional motions. The curvature of this pathway is similar to the minimum energy pathway of pinacolone [**89**]. A similar interaction was seen in

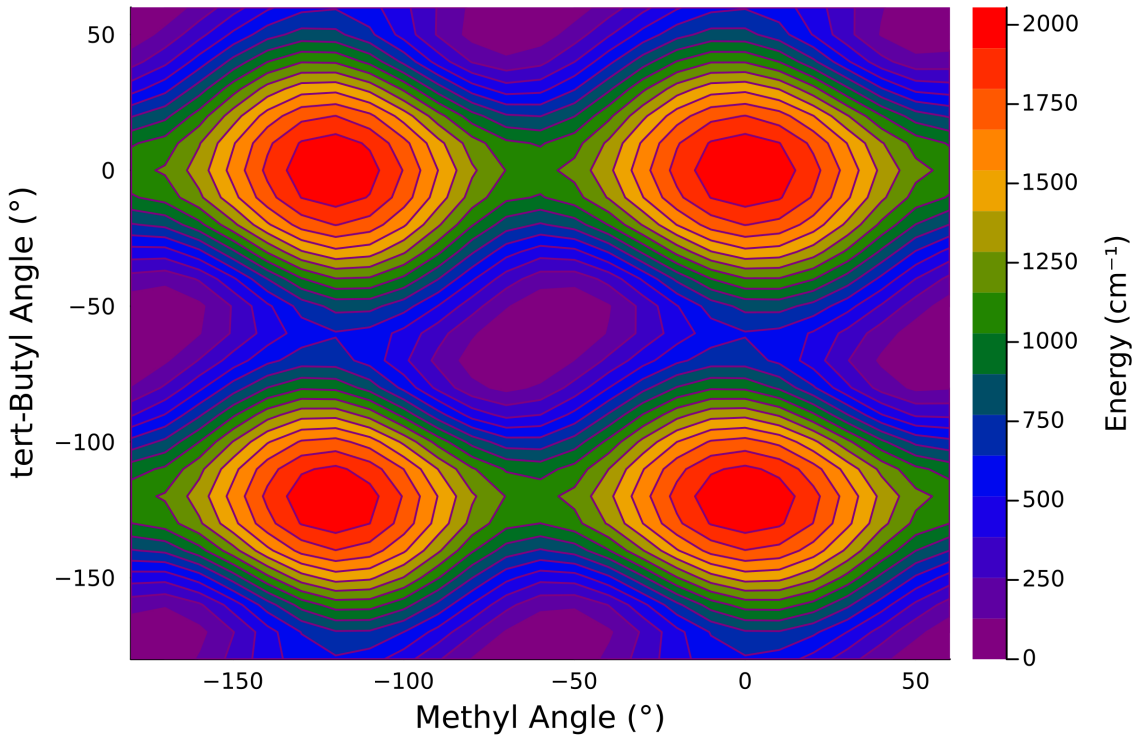

FIGURE 3.7. The 2D MP2/cc-pVDZ PES of MTBE along the tert-butyl and methyl angles. The waving path shown in Figures 3.4a and 3.11a can been seen here as well from the slanted structure of the potential wells

Panel b with the geared methyls but that motion only moved about $\sim 3°$ suggesting less interaction between these motions. Doing a similar calculation about the tert-butyl dihedral angle showed that the methyl undertakes a similar rotation in response. The methyl's rotation is shown in Figure 3.5 which also shows the interaction with the geared motion.

A two dimensional PES was also run along the methyl and tert-butyl angles spanning from $-180°$ to $60°$ in steps of $5°$ and is shown in Figure 3.7. This showed a slanted well structure consistent with the paths shown in Figures 3.4 and 3.5 as well as pinacolone [**89**]. The potential well around $(-60°, -60°)$ is a single well unlike pinacolone for which the analogous well is split in two [**89**]. Compared with pinacolone, MTBE has higher V_3 barriers and lacks the effective V_6 structure which arrives from well splitting. The higher barriers in MTBE make the motions more rigid and reduce the impact of the coupling between the different torsional motions. A similar PES was calculated along the methyl and geared angles, spanning the same range, as shown in Figure

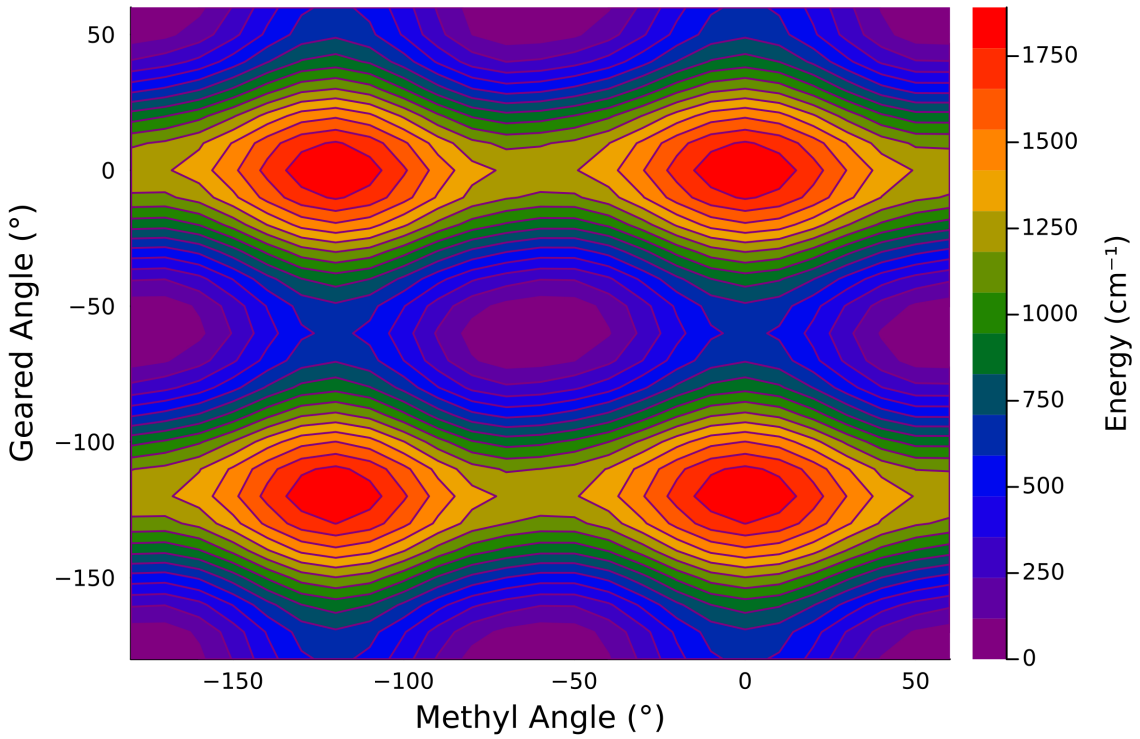

FIGURE 3.8. The 2D MP2/cc-pVDZ PES of MTBE along the geared and methyl angles. The wells are less slanted than in Figure 3.7 indicating that these two modes are less coupled.

Expansion Term	Operator	m-t Fit (cm^{-1})	m-g Fit (cm^{-1})
$V_{3,\alpha}$	$\frac{1}{2}(1-\cos 3\alpha)$	904.1	638.9
$V_{6,\alpha}$	$\frac{1}{2}(1-\cos 6\alpha)$	−1.35	60.9
$V_{3,\beta}$	$\frac{1}{2}(1-\cos 3\beta)$	1282.1	1267.6
$V_{6,\beta}$	$\frac{1}{2}(1-\cos 6\beta)$	0.957	71.4
V_{cc}	$(\cos 3\alpha)(\cos 3\beta)$	156.4	−1.61
V_{ss}	$(\sin 3\alpha)(\sin 3\beta)$	−248.2	−72.04

TABLE 3.3. Potential Terms for MTBE calculated from 1D and 2D Scans at MP2/cc-pVDZ

3.8. The two 2D surfaces were fit to all available potential terms in the XIAM_mod program and are tabulated in Table 3.3. Based on the terms V_{cc} and V_{ss}, the tert-butyl motion is much more heavily coupled to the methyl torsion.

Parameter	Previous [**88**]	This Work	MP2/cc-pVDZ
F_0 (cm^{-1})	5.261(18)	5.23768(704)	5.372
V_3 (cm^{-1})	498.17(173)	495.648(720)	638.68
δ (°)	25.848(196)	26.2998(910)	26.027
A (MHz)	4382.83875(107)	4382.839941(221)	4373.1086
B (MHz)	2732.392089(391)	2732.392478(293)	2743.3015
C (MHz)	2730.755439(380)	2730.755098(280)	2735.8024
Δ_J (kHz)	0.3100(122)	0.31192(281)	0.339727
Δ_{JK} (kHz)	4.274(109)	4.218841(437)	48.0197
Δ_K (kHz)	−3.768(145)	−3.659009(816)	−47.5273
δ_J (kHz)	0.00502(926)	0.01184(200)	0.00791227
Φ_J (Hz)	–	−0.061(11)	–
Φ_{JK} (Hz)	–	0.012(1)	–
RMS (kHz)	17.37	10.79	–
Lines	32	437	–

TABLE 3.4. Fit Results of MTBE

3.3.3. Torsional-Rotational Spectrum. The rotational spectrum of MTBE was measured in the K_a band at roughly 20 K and 40 K thanks to the differing backing pressures. These temperatures were approximated by adjusting the temperature of the simulation to roughly match the intensity distribution in the q-branches. The temperature of the jet does not appear to be uniform and is very likely bimodal so these are only listed as rough approximations. Unlike typical methyl rotor problems which contain doublets with a 1:1 intensity ratio, the spectrum shows a distinctive triplet structure with a 1:2:1 intensity pattern throughout its r branch as highlighted in Figure 3.11. The triplet motif is a result of the very near prolate structure of MTBE. Since $B \approx C$, the asymmetric splitting between the energy levels of A states for $J_{K_a,J-K_a}$ and $J_{K_a,J-K_a+1}$ approaches zero. This degeneracy is broken for the E states by terms such as $\rho F \hat{P}_\alpha \hat{J}_z$ which cause more separation of states sharing J and K_a. There are also 4 distinctive q-branches such as the one shown in Figure 3.10. The q-branches contain the same intensity ratio between the A and the E states though these transitions lack the even structure of the r-branch transitions. The colder spectrum was analysized first and then the higher J transitions of the warmer spectrum were introduced into the fit discussed in the next section.

3.4. Torsional-Rotational Fits

The spectrum was fit using XIAM_mod [**50**] using only a single rotor and the results of this are shown in Table 3.4 with a comparison to the fit from [**88**] and the MP2/cc-pVDZ calculations. This shows generally improved uncertainties on all parameters with a vastly expanded line to parameter ratio. Unlike the structurally similar pinacolone, this fit proved satisfactory and should offer sufficient predictive ability for higher frequency studies. This fit adds 405 lines to the previously reported 32 for a total of 437 transitions with an RMS of 10.79 kHz. The uncertainty of the newly added transitions was set to 10 kHz while the previous work's transitions used an uncertainty of 4 kHz. The highest J value included in the fit is 37 and the highest K_a is 12. The determined V_3 of 5.929 kJ/mol makes this a fairly typical methoxy barrier when compared to Table 3 of [**96**]. The largest point of disagreement between the experimental spectrum and simulations from the fits is in the intensities as can be seen in Figure 3.9. While a large number of transitions appear only in the experimental spectra at these scales, most of these features did have a corresponding feature at the same frequency in the simulation albeit at a much lower intensity.

To provide aid to higher temperature projects such as those similar to [**85**], room temperature simulations shall be provided here. Figure 3.12 shows the spectrum at 298 K up to $J = 70$ in the ground torsional state up to 600 GHz. This J_{max} is the limit of XIAM_mod. The Boltzmann peak can be seen to be around 400 GHz. The intensity in the 260–290 GHz is at roughly half the maximum which should indicate plenty of signal strength from MTBE in a room temperature experiment at this frequency range. The 260–290 GHz band shown in Figure 3.13 is the frequency range of the instrument used in [**85**]. This spectra region is dominated by r branch transitions with the strongest ones having J values in the 30s. The distinctive triplet pattern is still a dominant feature in this region.

3.5. Conclusion

Methyl tert-butyl ether is a floppy near-symmetric prolate top. The only torsional mode observed was the moderate barrier methyl rotor within the methoxy group for which the barrier was measured to be 495.6 cm^{-1}. The secondary motion of the methoxy group rocking relative to

the tert-butyl group was computationally investigated but not directly experimentally observed. The calculated coupling between the motions similar to but less extreme than those of the structurally similar pinacolone. The new Ka band measurements add 405 transitions and reduces the uncertainties on all spectroscopic parameters used in the effective Hamiltonian. The new fit and resulting simulations should be sufficient for higher frequency experiments.

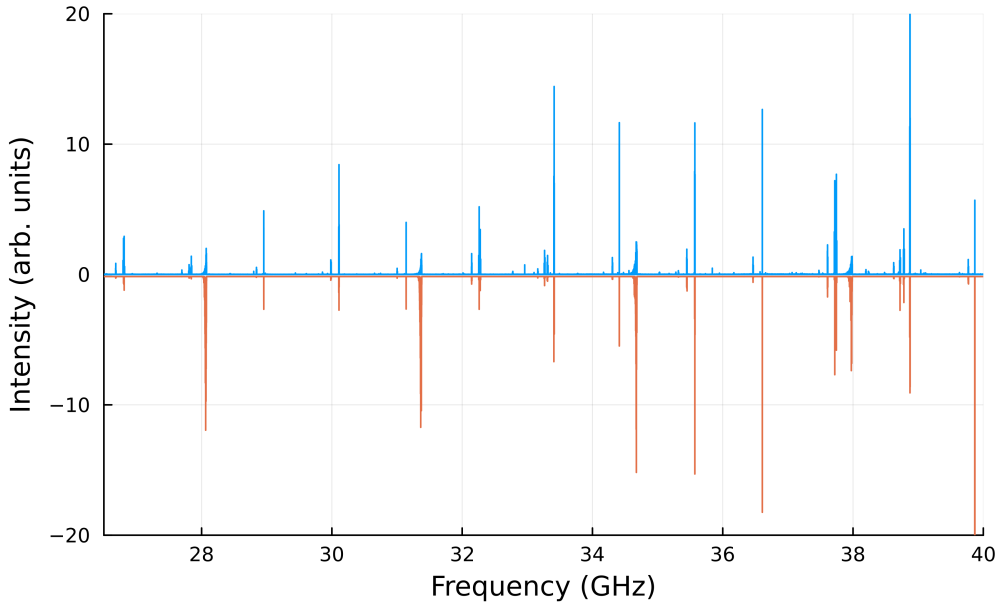

(a) The roughly 20 K Ka band spectrum of MTBE

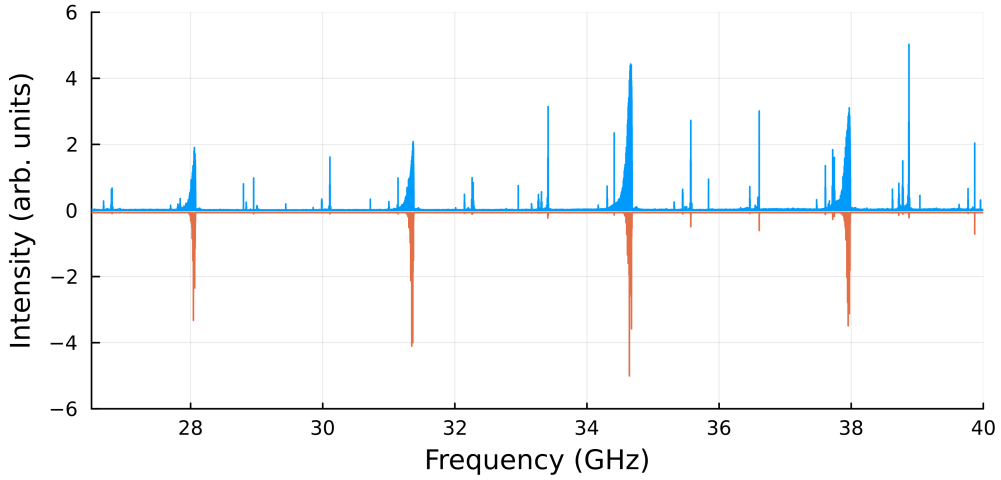

(b) The roughly 40 K Ka band spectrum of MTBE

FIGURE 3.9. Broadband Spectrum of MTBE with the two different temperatures. In both panels, the experimental spectrum is shown on top while the simulated is shown on the bottom.

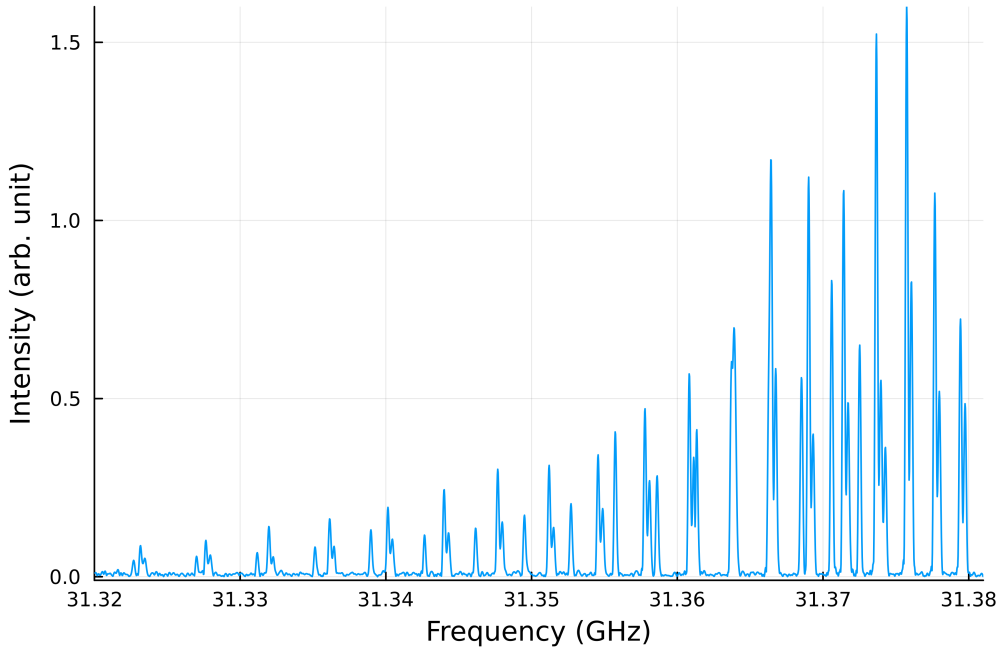

FIGURE 3.10. The $J_{10K_c'} - J_{9K_c''}$ q branch where the A state transitions can be visually distinguished from the E state transitions due to the 2:1 intensity ratio

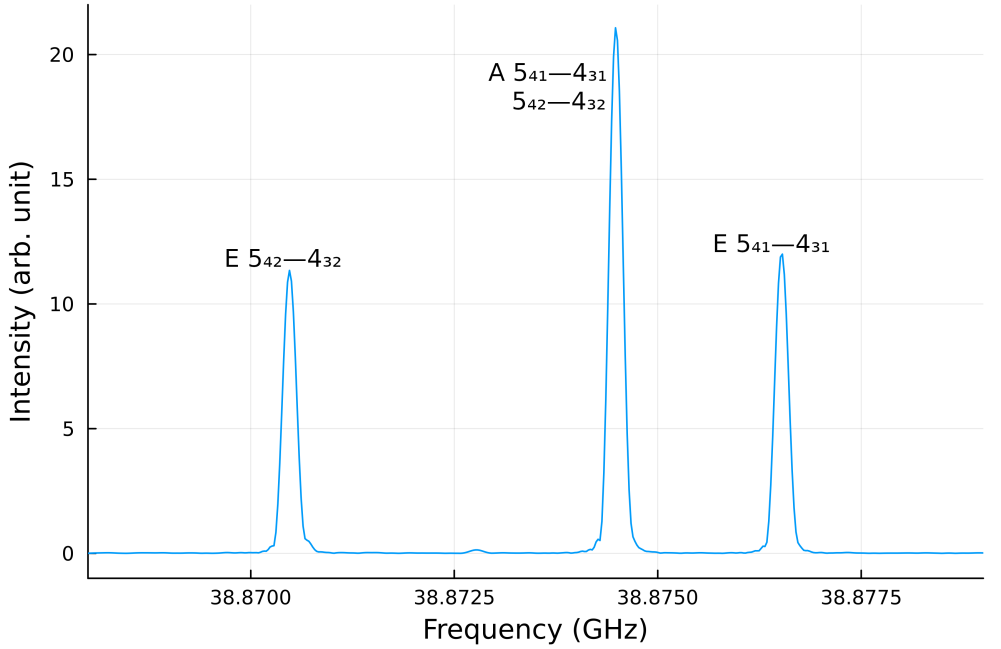

FIGURE 3.11. The $5_{4K_c'} - 4_{3K_c''}$ transitions display the triplet pattern of MTBE where the central A state transition is a blend with around twice the intensity of the the E state transitions which appear on either side

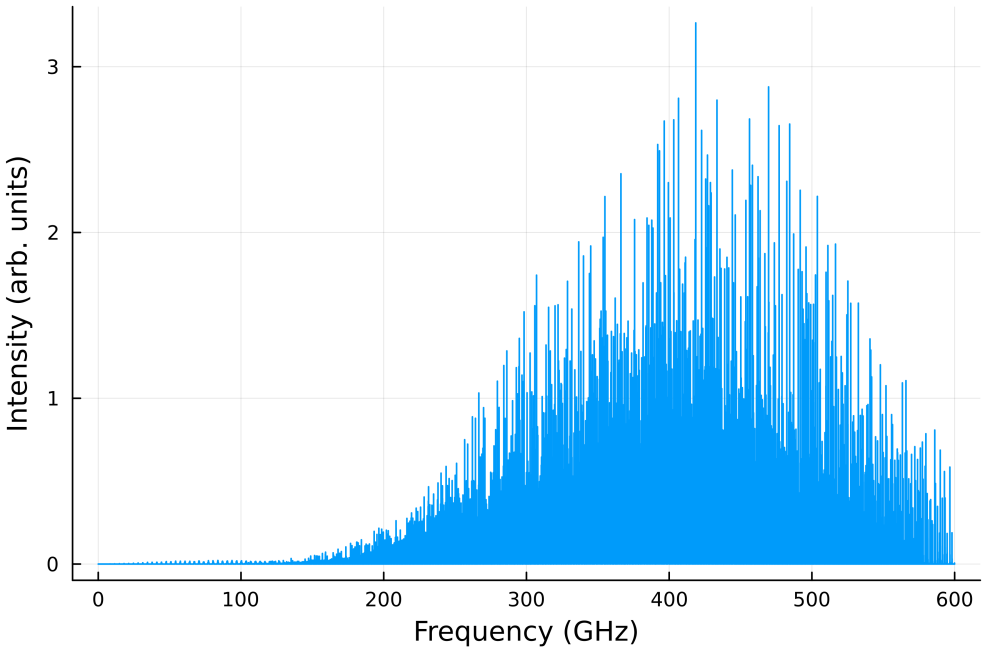

FIGURE 3.12. Simulation of MTBE from 0–600 GHz with up to$J = 70$

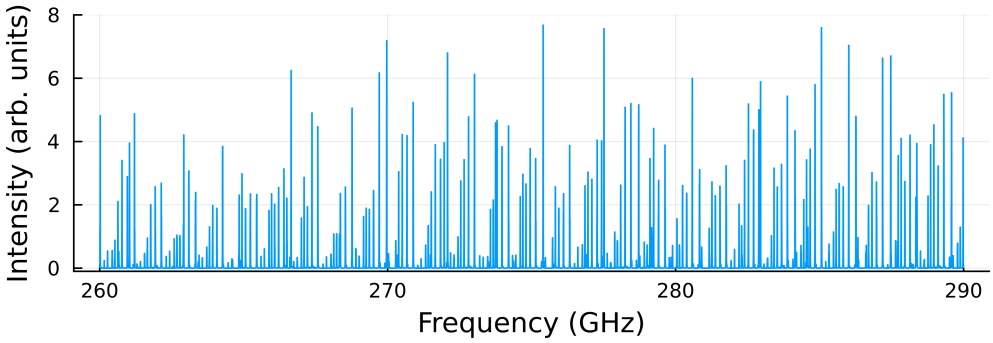

FIGURE 3.13. Simulation of MTBE from 260–290 GHz with up to$J = 70$

CHAPTER 4

On the Developement of a New Program & Application to Meta-Chloro-Toluene

The programs currently available for rotational spectroscopy analysis have proven to be capable of fitting the rotational spectra molecules containing either nuclear quadrupole moments or methyl rotors. Unfortunately, there is not a singular program that can treat both simultaneously. This restriction greatly inhibits the study of molecules containing elements other than hydrogen, carbon, nitrogen, and oxygen as many other elements have nuclear spin greater than 1/2 and larger nuclear quadrupole moments than that of N. Methyl groups are a prevalent structure in organic molecules. The program SPFIT [**40**] uses an efficient spherical tensor method to implement Benz's exact nuclear hyperfine matrix elements [**28**] and is capable of fitting molecules with large nuclear spin values. However it is not capable of treating methyl rotation problems with barrier heights lower than around 500 cm^{-1} [**41**]. Methyl rotors with barriers as low as ~ 1 cm^{-1} have successfully been fit in the Rho Axis Method programs such as BELGI [**44**] and RAM36 [**64**]. The hyperfine variants of these programs [**48**, **65**] and the program XIAM [**45**] are all capable of treating methyl rotors alongside a perturbative hyperfine treatment, limiting their ability treat the nuclear quadrupole interactions of $I > 1/2$ nuclei other than N. This chapter presents a new program, westerfit, designed to combine the quadrupole treatment of SPFIT with the internal rotor treatment of BELGI. In addition to a description of the code, there is a collection of test cases comparing published fits to the same linelists being fit in the new program.

Meta-chlorotoluene (m-Cl-tol), shown in Figure 4.6, was selected as a test case for the new program due to the combination of chlorine's larger spin and electric quadrupole moment relative to nitrogen, a very low methyl internal rotation barrier height, and a preexisting linelist. M-Cl-tol has been previously studied by Nair et al [**97**]. This spectrum was recorded from 5–25 GHz using a

supersonic jet expansion in a Fabry-Pérot cavity. A fit of 336 transitions with a maximum $J = 13$ and maximum $K_a = 5$ was performed in XIAM [**45**] which uses a relatively small torsional basis along with a perturbative treatment of the nuclear hyperfine interactions. This work struggled to fit both the very low V_3 and the larger V_6 simultaneously but did achieve acceptable fits by fixing either of these parameters to an *ab initio* value. It is the goal of the new program to provide a more extensive torsional treatment as well as a complete, non-perturbative hyperfine treatment for more accurate determination of the spectroscopic parameters of m-Cl-tol and other molecules in its class.

4.1. Description of the Program

The program calculates the spin-torsion-rotation energy levels and then transition frequencies and intensities from the parameters input by the user. The program cal also adjust the parameter values to match a list of experimentally measured frequencies in a process referred to as "fitting." The code is written in the Julia [**98**] language and uses the WIGXJPF [**99**] package via Julia's Ccall functionality calculation of Wigner symbols. The input file is divided into three blocks: control settings, second-order terms, and higher order terms. The control settings include all options that are not directly parameters in the Hamiltonian such as the spin value, symmetry fold of the rotor, simulation temperature, and the size of the torsional basis. The second-order block contains the values for all the spectroscopic parameters found in the second order Hamiltonian as well as the scale factors that are used during fitting. The hard-coded part of the Hamiltonian combines Equations 2.45, 2.49, and 5.6. The final block allows for users to define higher order operators along with their parameter values and fitting scale factors. The scale factors in the last two blocks are used in the fitting mode, described in Section 4.1.4, to scale the step size with each fitting iteration or to fix the parameter to its initial value by setting the scale factor to zero.

The code outputs four different files. The energy level calculator writes all of the calculated levels and their labels to a delimited file. The simulator routine produces a file with each line containing the upper and lower quantum numbers of a transition, the frequency, and the intensity. By default this is a delimited file but there is also the option to emulate the SPCAT simulation file structure for interfacing with other programs such as the spectral simulation plotting in AABS.

The fitting routine generates two separate output files. The first one contains the parameters and their adjustments at each iteration of the fitting routine. The last iteration is printed with the uncertainties determined from the fitting process. The other file is a delimited collection of residuals from the fit which contains the inputted line list alongside the calculated frequencies and the observed minus calculated error.

4.1.1. Hamiltonian and Wavefunction. The Hamiltonian is split between a hard-coded second-order Hamiltonian and user-definable terms for the higher order operators. The hard-coded second order Hamiltonian allows for natural input of the terms, which are then transformed into more effective structures. As an example, the user inputs the terms as seen in Equation 2.12 but the code internally treats them as 2.23. The code defaults to an I^r representation ($z, x, y \rightarrow a, b, c$) but the relationship of $A > B > C$ is not enforced by the code which could allow a user to use a different mapping if so needed. All parameters are read in units of MHz with the exception F and V_3 which are input in cm^{-1} for consistency with the convention.

The user-defined operators are defined as the direct product of the anti-commutator of the torsional parts and the anti-commutator of the rotation and spin-rotation operators. This structure allows for the Watson-A reduction of rotation, spin-rotation [**32**], and torsion-rotation [**70**] operators. The pure rotation Watson-S reduction terms can also be used but not the corresponding spin-rotation terms [**32**] due to the lack of $\mathcal{N}_+^n\mathcal{S}_+^m + \mathcal{N}_-^n\mathcal{S}_-^m$. The operators of the Watson-A reduction were selected over the Watson-S as it shows up in more torsional works [**44**, **69**, **70**]. The link between the powers of N_y and $\sin h\alpha$ is to allow for operators found in Xu's global fit of methanol [**69**] while also ensuring use of purely real matrix elements.

$$\hat{O}_{efgh}^{abcd} = \left(P_\alpha^f \cos(g\alpha)\sin(h\alpha) + \sin(h\alpha)(\cos g\alpha)P_\alpha^f\right) \otimes \left(N^a N_z^b (N_+^c + N_-^c)(NS)^d S_z^e N_y^{1-\delta(h,0)} + N_y^{1-\delta(h,0)} S_z^e (NS)^d (N_+^c + N_-^c) N_z^b N^a\right) \quad (4.1)$$

More detailed discussions of these operators can be found in Chapter 2. The input file used for 2-butynoic acid in Section 4.2.1 is shown in Figure 4.1. Additional examples of different Hamiltonians supported by the code, including all those of the fits described in this chapter, can be found on the westerfit github (https://github.com/wes648/westerfit).

```
2ba   @   2023-06-15T13:30:43.433
%CNTRLS
NFOLD = 3
S = 0.0
RUNmode = ESF
TK = 25.0
mcalc = 8
assign = RAM36
LIMIT = 100
INTThresh = 0.0
vtmax = 0
Jmax = 11
turducken = 2
νmax = 20.0

%2NDORDER
A;              11269.90007425439;   1.0
B;             1752.1858813384038;   1.0
C;             1529.5808281741547;   1.0
Dab;           -16.18499786582827;   1.0
ϵzz;                          0.0;   0.0
ϵxx;                          0.0;   0.0
ϵyy;                          0.0;   0.0
ϵxz;                         -0.0;   0.0
χzz;                          0.0;   0.0
χxmy;                         0.0;   0.0
χxz;                          0.0;   0.0
F;                           5.66;   0.0
ρ;            0.07152869750493886;   1.0
Vn;            1.0089940242684279;   1.0
η;                            0.0;   0.0

%PARAMS N^a Nz^b (N₊^c + N₋^c) (NS)^d Sz^e Pₐ^f cos(g*α) sin(h*α) Ny^(1-δ(0,h))
%Op;                          Val;   Scl;   a;   b;   c;   d;   e;   f;   g;   h;  stg
μa;                           2.3;   0.0;   0;   1;   0;   0;   0;   0;   0;   0;   0
μa(3);                      0.008;   0.0;   0;   1;   0;   0;   0;   0;   3;   0;   0
μb;                           1.4;   0.0;   0;   0;   1;   0;   0;   0;   0;   0;   0
μb(3);                      0.008;   0.0;   0;   0;   1;   0;   0;   0;   3;   0;   0
ΔN;         -4.402304488541094e-5;   1.0;   4;   0;   0;   0;   0;   0;   0;   0;   1
ΔNK;          -0.01135174527503434;   1.0;   2;   2;   0;   0;   0;   0;   0;   0;   1
ΔK;         -0.0026470030913908794;   1.0;   0;   4;   0;   0;   0;   0;   0;   0;   1
δN;         -2.4009462733038708e-5;   1.0;   2;   0;   2;   0;   0;   0;   0;   0;   1
δK;          -3.078860557273257e-5;   1.0;   0;   0;   4;   0;   0;   0;   0;   0;   1
FN;           -0.03725315735920008;   1.0;   2;   0;   0;   0;   0;   2;   0;   0;   1
ρN;            0.03520501956210478;   1.0;   2;   1;   0;   0;   0;   1;   0;   0;   1
ρK;           0.015041244206404125;   1.0;   0;   3;   0;   0;   0;   1;   0;   0;   1
ρbc;        -0.0007495062893825343;   1.0;   0;   1;   2;   0;   0;   1;   0;   0;   1
```

FIGURE 4.1. The westerfit input file for 2-butynoic acid as used in Section 4.2.1

The wavefunction used in the code is the product of the free rotor basis and the Hund's case (b) wavefunction. The free rotor basis was selected to properly handle low-barrier torsional cases, and has also been shown to adequately handle high-barrier cases. Hund's case (b) was selected to keep the molecular frame's angular momentum as the rotational pattern-forming quantum number as the spin effects are generally smaller than the indefinitely increasing overall rotation [**100**]. Thus, the program can to handle a wide range of both torsional and spin influences.

4.1.2. Quantum Number Assignment. The state assignments after diagonalization are lacking in true meaning thus making this more a problem of semantics than physics [**40**]. Nevertheless, it is convenient to have the eigenstates labeled in ways reminiscent of the basis states or even just simpler spectroscopic cases. Ideally, when moving from one limiting case to another,

an assignment routine should be able to label states such that a smooth correlation diagram is formed. This consistency can help allow for an intuitive comparison of more complicated energy ladders by building off the more familiar patterns. The K_a, K_c, and v_t labels are standard in the field and desirable for data processing. Additionally, consistency across programs allows for better functionality comparison, and internal consistency can provide a dual energetic and quantum number check. The code contains a handful of approaches to this problem but only the two most functional shall be described here. Both routines performed identically on the test of 2-butynoic acid and m-Cl-tol.

The most difficult struggle in the development of this program has been how to assign the quantum numbers after diagonalization. Fitting routines use these quantum number assignments as the independent values while the Hamiltonian parameters are adjusted to match the simulated frequencies to the observed frequencies. Thus it is necessary to find away to assign labels to the states that do not change as parameters are adjusted and higher order operators are introduced. Further complicating matters, even standard asymmetric rotor energetic trends break down due to the torsion and spin coupling effects. The difficulty of finding meaningful state labels after diagonalization is a documented problem in the torsional literature and various solutions have been proposed for it, though most lack widespread use [**75**, **79**, **101**].

The first method of quantum number assignment is based on that of RAM36 [**65**] but is expanded to account for spin quantum numbers. Since each matrix is built for a specific J and σ pairing, those two are assigned automatically but N, K_a, K_c, and m need to be assigned. This assignment method works by assessing the matrix of eigenvectors outputted by LAPACK's syev routine. First, all the eigenvector elements are squared. Then to assign m, a vector of length $2m+1$ is initialized for each eigenvector. For each m value in the basis set, the $(2S+1)(2J+1)$ elements in the eigenvector that correspond to the target m basis state are added together and placed in the new vector. From here, the routine determines which $(2S+1)(2J+1)$ vectors have the largest value corresponding to $m = 0$. These states are then marked as the ground torsional state. Currently this routine only runs on the ground state but will be adapted to go up to arbitrarily high torsional states. Now that the $m = 0$ states have been determined, N will be assigned. For

the $(2S+1)(2J+1)$ states marked as $m = 0$, a vector of length $2S+1$ is initialized. Then for each N value in the absis set, all the eigenvector elements that correspond the target N value are added together and placed in the vector. Once this is completed, the elements of the vector are analyzed to find the $2N+1$ states corresponding to each N value. Lastly, within each N and m pairing, K_a and K_c are assigned by the simple energetic ordering. This is very consistent with RAM36 in the torsional-rotational case but less so with SPFIT/SPCAT DIAG=3 assignment routine in spin-rotation and hyperfine cases. SPFIT/SPCAT leverage the symmetry of the V group while westerfit is restricted to a subgroup of this. For a pure rotation case, the assignments should be consistent. Some demonstrations of the differences are found and discussed in Section 4.2.

The second and default method uses the expectation values of P_α^2 to group the torsional states, and then the expectation values of N^2 to determine the N states within that torsional state. While the values of $\langle P_\alpha^2 \rangle$ do not tend to map onto obvious values from the basis set, they do tend to form clear clusters. Thus m is assigned by simply sorting the $\langle P_\alpha^2 \rangle$ expectation value and assuming the $(2S+1)(2J+1)$ states with the lowest expectation values are in the ground torsional state. Then, for each N, the $2N+1$ states with expectation values closest to $N(N+1)$ are assigned that N value. Lastly, within each N, K_a and K_c are assigned by energetic sorting.

4.1.3. Calculation of Transition Intensities. The transition intensities are calculated using a combination of the expressions from Gopalakrishnan et al [**102**] and Mekhtiev et al [**103**]. The dipole operator can be expressed as a spherical tensor and Fourier expanded to account for the changes in the dipole moment projections as the methyl group turns. The Fourier expansion of the dipole components can be calculated from a similar potential energy surface calculations as described in Sections 3.2.2 and 4.3.1 except by plotting the dipole projections against the methyl rotor angle rather than the energies. The conversion from Cartesian to spherical tensor form is

structured as:

$$T^1_{-1}(\mu) = T^1_{-1}(\mu^{(0)}) + T^1_{-1}(\mu^{(3)}) = \frac{1}{\sqrt{2}}\left(\mu_x^{(0)} + \mu_x^{(3)}\cos 3\alpha + \imath\mu_y^{(3)}\sin 3\alpha\right) \tag{4.2}$$

$$T^1_{0}(\mu) = T^1_{0}(\mu^{(0)}) + T^1_{0}(\mu^{(3)}) = \mu_z^{(0)} + \mu_z^{(3)}\cos 3\alpha \tag{4.3}$$

$$T^1_{+1}(\mu) = T^1_{+1}(\mu^{(0)}) + T^1_{+1}(\mu^{(3)}) = \frac{-1}{\sqrt{2}}\left((\mu_x^{(0)} + \mu_x^{(3)}\cos 3\alpha - \imath\mu_y^{(3)}\sin 3\alpha\right) \tag{4.4}$$

The superscripts with parenthesis are used to denote Fourier expansion terms while those without mark spherical tensor rank. The dipole moment projection values are based on the Rho Axis coordinates for consistency with the torsional literature [**46**]. Due to the C_s symmetry, $\mu_y^{(0)}$ is rigorously 0 and its Fourier expanded terms are multiplied by $\sin n\alpha$ to ensure the matrix elements are real. The combined matrix element for a given Fourier series dipole component is shown below:

$$\langle J'SN'K'm'|T^1_q(\mu^{(n)})|JSNKm\rangle = (-)^{S+J'-K'+N'+K}\delta_{m',m\pm n}$$
$$\mu^1_q\sqrt{(2J'+1)(2J+1)}\sqrt{(2N'+1)(2N+1)}\begin{pmatrix} N' & 1 & N \\ -K' & q & K\end{pmatrix}\begin{Bmatrix} N & J & S \\ J' & N' & 1\end{Bmatrix} \tag{4.5}$$

The torsion-rotation interactions reduce the symmetry of the rotation group so the selection rules based on values of K_a and K_c are broken. The rigorous remaining selection rules are $|\Delta J| \leq 1$ and $\Delta\sigma = 0$. The intensity for every pair of states with $|\Delta J| \leq 1$ is calculated to determine if a transition is allowed. The program does the calculation by building the dipole matrix for the pair of upper and lower J values and the shared σ value. The dipole matrix is front multiplied by the transpose of the upper J eigenvectors and back multiplied by the lower J eigenvectors. To determine if the transition is included in a simulation, the calculated intensity is compared to a user-defined threshold and if the intensity is above the threshold, the energy difference is calculated. If the frequency is positive and within the bounds provided by the user, the lower energy state is used to determine the thermal factor of the line intensity. Similarly, negative values switch signs and assignment of the upper and lower states, and the thermal factor is determined. Transitions that fall outside of the range are not included. In the future, group theoretical considerations could sort the A states into the A_1 and A_2 irreducible representations of the G_6 group to reduce the number of pairs that must be checked.

4.1.4. Levenberg-Marquardt Implementation. Experimental values for the operators' coefficients, often called the spectroscopic parameters, are determined through comparison with experimentally observed transitions via non-linear least squares fitting. The general process of non-linear least squares fitting is to adjust a set of parameters, x, that are used as variables for a model function, $f(x)$, in order to minimize the norm-2, $||\cdot||$ of the difference between a set of observables, y, and the model function. This norm-2, $||y - f(x)||$, is more commonly referred to as the RMS error in spectroscopic literature. The program performs the least squares fitting through a modified Levenberg-Marquardt routine. The parameters are adjusted by step vector η whose initial value is calculated from the typical weighted Levenberg-Marquardt [**104**, **105**] expression using Fletcher's modification [**106**]. The step direction depends on the Jacobian which is calculated analytically via the Hellmann-Feynman theorem [**107**]. For a given parameter, its derivative at a given state is equal to the expectation value of the parameter's associated operator at said state. Thus the Jacobian element for a specific parameter is calculated from the difference of the expectation values for the parameter's operator for the upper and lower states. Unlike the actual energy levels, this is calculated by matrix multiplication rather than diagonalization allowing for efficient use of analytic derivatives rather than numeric ones. The Hessian is then approximated using the matrix of inverse line uncertainties, or weights W, and the Jacobian of the frequency calculator, J.

$$H = J'WJ \tag{4.6}$$

A defining feature of the LM method is the damping parameters, λ, to control the step size. As the dampening parameter approaches zero, the steps become equivalent to those of the Gauss-Newton method while large dampening parameters restrict the step size and resemble the steepest descent approach. In the traditional LM method, the dampening parameter is simply multiplied by the identity matrix, I. For each iteration, k, the Jacobian, Hessian, dampening term, and model function are all calculated and then the below expression is solved for the step size.

$$(J_k'WJ_k - \lambda_k I)\beta_k = J_k'(y - f_k(x)) \tag{4.7}$$

In the traditional method, the parameters are assumed to be of comparable orders of magnitude and the dampening parameter restricts the step size uniformly. However, given the radically varying orders of magnitude among spectroscopic parameters, it is best to instead use the Fletcher's modification, which uses the diagonals of the approximate Hessian, D, thus tailoring the magnitude of each parameters step to the magnitude of that parameter.

$$(J_k' W J_k - \lambda_k D_k)\beta_k = J_k'(y - f_k(x)) \tag{4.8}$$

The dampening parameter λ_0 is calculated from the product of a scale factor, μ, and a function of the current RMS error. The starting value of the scale factor is arbitrarily defined as 10^{-5} but can be set to a different initial value by the user. This factor increases when the fit steps away from convergence and decreases as the error goes down. [**108**] The full expression for λ on the k-th iteration is:

$$\lambda_k = \frac{\mu_k ||y - f_k(x)|| \big(2 + ||y - f_k(x)||\big)}{2(1 + ||y - f_k(x)||)} \tag{4.9}$$

To accelerate convergence [**108**], the steps can be supplemented by solving the previous expression using the same Jacobian but an updated error yielding a different step vector γ_k.

$$(J_k' W J_k - \lambda_k D_k)\gamma_k = J_k'(y - f_k(x + \beta_k)) \tag{4.10}$$

The final step in a given iteration is determined from:

$$s_k = \beta_k + \left(1 + \frac{\lambda_k \gamma_k' \gamma_k}{\gamma_k' J_k' W J_k \gamma_k}\right) \gamma_k \tag{4.11}$$

The code allows users to define how many nested steps are used and each will be scaled using the same expression [**109**]. The multi-step approach is done to avoid the costs of calculating Jacobian. The speed of the Jacobian calculator generally makes one or two steps using the same Jacobian efficient while more than that loses stability from the Jacobian not be up to date with the parameter values. As the code progresses, the step size and RMS error decrease are compared to convergence criteria. If the change in RMS is less than 10^{-6} MHz or the norm-2 of the step size is less than 10^{-6} times the norm-2 of the parameters, convergence is signaled, and the routine ends. This is is more an assumption that the objective function is close to a minimum and user intuition is needed to

determine if the fit has converged appropriately or not. These conditions generally occur together with one meeting the condition and the other being close. As scale factor μ often becomes much larger than its initial value by the end of a fit, re-initializing μ by staring a new fit with the new parameters can often help escape a false well as the sudden reduction in μ allows for a larger step size.

4.2. Initial Testing

The energy level calculations of westerfit were tested against those published programs by making equivalent input files for each program, calculating the energy levels, and then examining the residuals between the levels calculated by westerfit and the other programs. The energy levels have been directly compared to those of other published programs and found to be consistent with both. These tests were performed by running simulations with identical arbitrary constants for the second order operators in westerfit and either BELGI or SPCAT. The energy levels from each program were then sorted energetically to directly compare the levels while bypassing potential differences in assignment. BELGI was used for the torsional-rotational testing and was examined up to $N = 9$ and $v_t = 2$. This test resulted in an RMS difference of 0.4 Hz over a total of 600 states. The residuals, shown in Figure 4.2a, display very consistent agreement with most states having exact agreement. The handful of outliers deviated by exactly ± 2.998 Hz and resulted from round off error from the last decimal printed by BELGI. The spin-rotation and nuclear quadrupole terms were tested against SPCAT and these tests were run up to $J = 14$ with $S = 1$. First the spin-rotation was tested alongside just the rotational parameters and result in an RMS difference of 0.930 Hz over nearly 700 states. The residuals are plotting in Figure 4.2b with horizontal lines marking the round-off error of SPFIT. This plot shows there is far less agreement that the code had with BELGI. Replacing the spin-rotation terms with the nuclear hyperfine terms produces a nearly identical RMS difference of 0.928 Hz and the residuals are plotted in Figure 4.2c. These differences likely emerge from the Hamiltonian implementations and will be investigated further in future work. Testing both at the same time resulted in an RMS difference of 1.36 MHz, six orders of magnitude higher than the previous tests. The residuals can be seen in Figure 4.2d and display an asymmetry between the positive and negative residuals. The source of this discrepancy has not

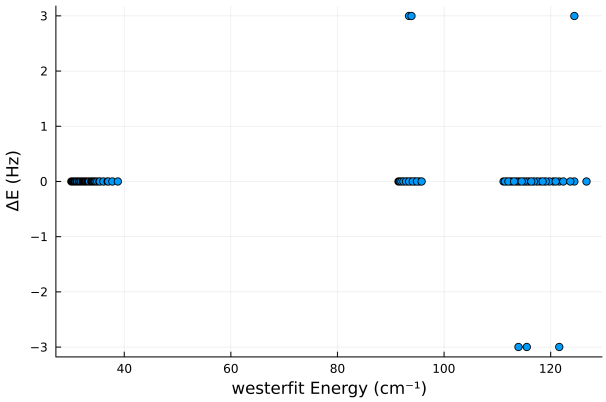

(a) BELGI energy levels minus westerfit energy levels plotted against the westerfit energy of the states for the torsion-rotation test

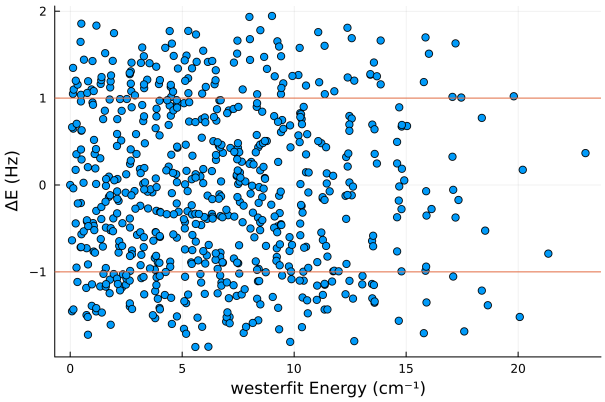

(b) SPCAT energy levels minus westerfit energy levels plotted against the westerfit energy of the states for the spin-rotation test

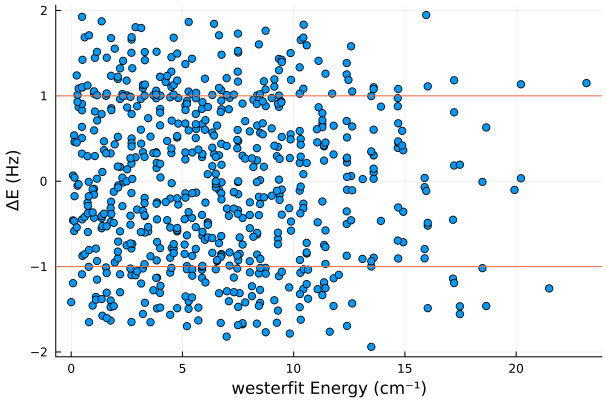

(c) SPCAT energy levels minus westerfit energy levels plotted against the westerfit energy of the states for the nuclear hyperfine test

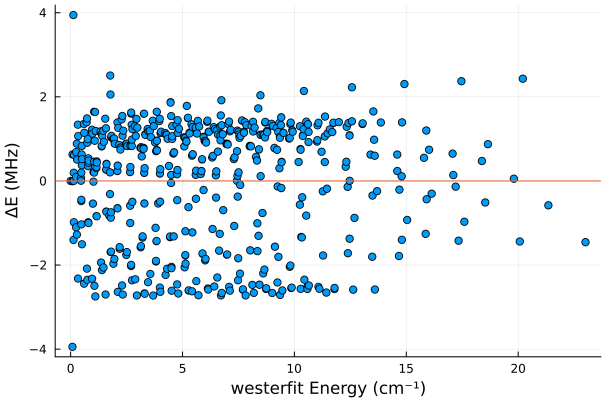

(d) SPCAT energy levels minus westerfit energy levels plotted against the westerfit energy of the states for the combined spin-rotation and nuclear hyperfine test

FIGURE 4.2. Comparison of westerfit energy calculations with those of other published programs. The new program better agrees with BELGI as it is a more exact reproduction of that Hamiltonian than that of SPCAT.

yet been found and did not seem to emerge in the experimental test in Section 4.2.2 which also used both spin-rotation and nuclear hyperfine. These differences are minor, especially given the magnitudes of the energy levels, thus westerfit is generally consistent with the other programs.

After completing this direct comparison of energy levels, performance of the code was tested on specific molecular cases. To test the torsion-rotation treatment, 2-butynoic acid was selected as it is a difficult torsion-rotation problem due to its very low barrier height of 1 cm^{-1}. The spin-rotation and hyperfine implementations were tested against the 1-iodoperfluoropropane

molecule. In building up to the difficult torsional case of m-Cl-tol, 2-fluoro-4-chloro-toluene has been used as a medium-low barrier height case with a strongly coupled quadrupolar nucleus.

4.2.1. Torsion-rotation Test on 2-Butynoic Acid. 2-butynoic acid (2ba) was one of the first 3-fold rotor tests of the RAM36 program and has an almost free internal rotor with a barrier height of 1.0090(4) cm^{-1} [**73**]. A total of 89 transitions were reported from 6–18 GHz, all in the ground torsional state with $N \leq 10$ and $K_a \leq 4$ with experimental uncertainties of 3 kHz. The very low barrier of the rotor makes it an excellent test case of westerfit's ability to treat methyl rotor problems. The experimental frequencies were fit using a Hamiltonian built using the operators shown in Table 4.1. This Hamiltonian is identical to that used in RAM36, and the optimized parameters show quantitative agreement. The residuals are plotted against the observed frequency and the lower N values in Figure 4.3. The strong agreement shows that westerfit performs equally well as RAM36 thus suggesting that the implementation of the torsion-rotation Hamiltonian is correct.

TABLE 4.1. Spectroscopic Parameters of 2-butynoic acid determined by westerift & RAM36. Values in parenthesis are 1σ uncertainties of the last digit

Parameter (units)	Operator	westerfit	RAM36
A (MHz)	$\mathcal{N}_z^2$	11269.9001(11)	11269.90006(66)
B (MHz)	$\mathcal{N}_x^2$	1752.18588(15)	1752.18588(15)
C (MHz)	$\mathcal{N}_y^2$	1529.58083(15)	1529.58083(15)
D_{ab} (MHz)	$\{\mathcal{N}_z, \mathcal{N}_x\}$	−16.185(24)	−16.1845(48)
F (cm^{-1})	$\mathcal{P}_\alpha^2$	5.66(fixed)	5.66(fixed)
ρ	$\mathcal{P}_\alpha \mathcal{N}_z$	0.071528698(37)	0.071528698(37)
V_3 (cm^{-1})	$\frac{1}{2}(1 - \cos 3\alpha)$	1.00899(41)	1.00900(42)
$-D_N$ (kHz)	$\mathcal{N}^4$	−0.0440(17)	−0.0440(17)
$-D_{NK}$ (kHz)	$\mathcal{N}^2\mathcal{N}_z^2$	−11.3517(96)	−11.351(11)
$-D_K$ (kHz)	$\mathcal{N}_z^4$	−2.65(21)	−2.65(21)
d_1 (kHz)	$\{\mathcal{N}^2, \mathcal{N}_+^2 + \mathcal{N}_-^2\}$	−0.0120(7)	−0.01200(65)
d_2 (kHz)	$\mathcal{N}_+^4 + \mathcal{N}_-^4$	−0.0154(19)	−0.0154(19)
F_N (kHz)	$\mathcal{P}_\alpha \mathcal{N}^2$	−37.253(95)	−37.255(96)
ρ_{bc} (kHz)	$\{\mathcal{N}_z, \mathcal{N}_+^2 + \mathcal{N}_-^2\}\mathcal{P}_\alpha$	−0.750(62)	−0.748(63)
ρ_N (kHz)	$\mathcal{P}_\alpha \mathcal{N}_z \mathcal{N}^2$	35.205(35)	35.204(36)
ρ_K (kHz)	$\mathcal{P}_\alpha \mathcal{N}_z^3$	15.04(74)	15.05(74)
Number of lines		89	89
rms (kHz)		2.5	2.6

4.2.2. Hyperfine test on trans-1-iodoperfluoropropane. The lack of an isolated spin-rotation experimental test is due to the limited amount of spectra that did not also show spin-spin

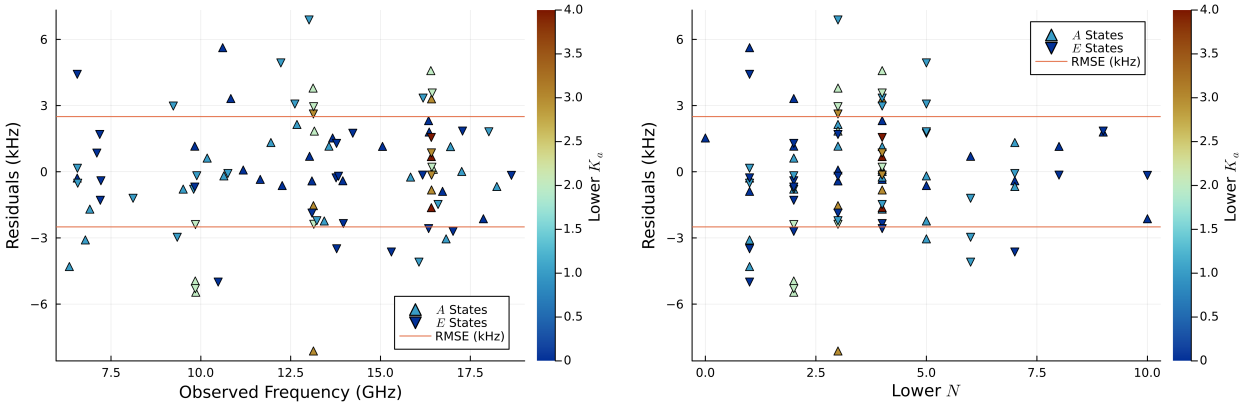

(a) Residuals for 2ba plotted against frequency

(b) Residuals for 2ba plotted against lower N

FIGURE 4.3. Residuals for 2ba plotted against either frequency lower N. Highlighting indicates lower K_a and the horizontal line indicates the fit RMSE

interaction and westerfit's current inability to treat multiple spin sources. To test the combination of both spin-rotation interaction and nuclear quadrupole implementations, the molecule trans-1-iodoperfluoropropane (ipfp) was selected. Its rotational spectrum was previously recorded from 1–4 & 8–18 GHz with experimental uncertainties of 25 kHz and 776 transitions were reported with up to $N = 50$ and $K_a = 15$. The spectrum was fitted using SPFIT, including the full quadrupole tensor and the on-diagonal nuclear spin-rotation tensor terms in the I^r representation [**110**]. Additionally, trans-1-iodoperfluoropropane provides the exotic case of each diagonal element of the quadrupole tensor being larger in magnitude than the corresponding rotational constant. Similarly to the torsional test, there is rather good agreement between the two fits as shown in Table 4.2. There is however slightly more disagreement than the previous test likely largely emerging from differences in quantum number assignments and perhaps with some contribution from westerfit being a less exact reproduction of SPFIT's Hamiltonian than it is of RAM36's. The residuals of the westerfit fit are shown in Figure 4.4 and appear unstructured suggesting there are no systematic issues with the fit. Despite the differences, the parameters, fit RMSE, and magnitudes of uncertainty are all sufficiently comparable between the two fits as to say that westerfit is capable of adaquately treating even strongly coupled nuclear spin cases.

4.2.3. A higher barrier halo-toluene: 2-fluoro-4-chlorotoluene. The molecule 2-fluoro-4-chlorotoluene (2-F-4-Cl-tol) was previously recorded from 4–25 GHz in a Balle-Flygare cavity

TABLE 4.2. Spectroscopic parameters for trans-1-iodoperfluoropropane determined by westerfit & SPFIT. Values in parenthesis are 1σ uncertainties of the last digit

Parameter (units)	westerfit	SPFIT
A (MHz)	1572.12814(11)	1572.127966(99)
B (MHz)	398.458628(35)	398.458568(34)
C (MHz)	382.831179(35)	382.831125(34)
χ_{aa} (MHz)	−1798.4057(57)	−1798.4013(48)
$\chi_{bb} - \chi_{cc}$ (MHz)	−366.213(26)	−366.224(13)
$\lvert\chi_{ab}\rvert$ (MHz)	991.7039(43)	991.7058(35)
C_{aa} (kHz)	1.98(15)	2.19(16)
C_{bb} (kHz)	0.90(15)	0.91(11)
C_{cc} (kHz)	1.36(15)	1.30(10)
$-D_N$ (kHz)	−0.008408(38)	−0.008305(39)
$-D_{NK}$ (kHz)	−0.01023(11)	−0.00986(12)
$-D_K$ (kHz)	−0.0516(12)	−0.05172(94)
d_1 (kHz)	−0.004145(12)	−0.000394(11)
d_2 (kHz)	0.0000444(26)	0.0000377(25)
Number of lines	776	776
rms (kHz)	5.0	5.14

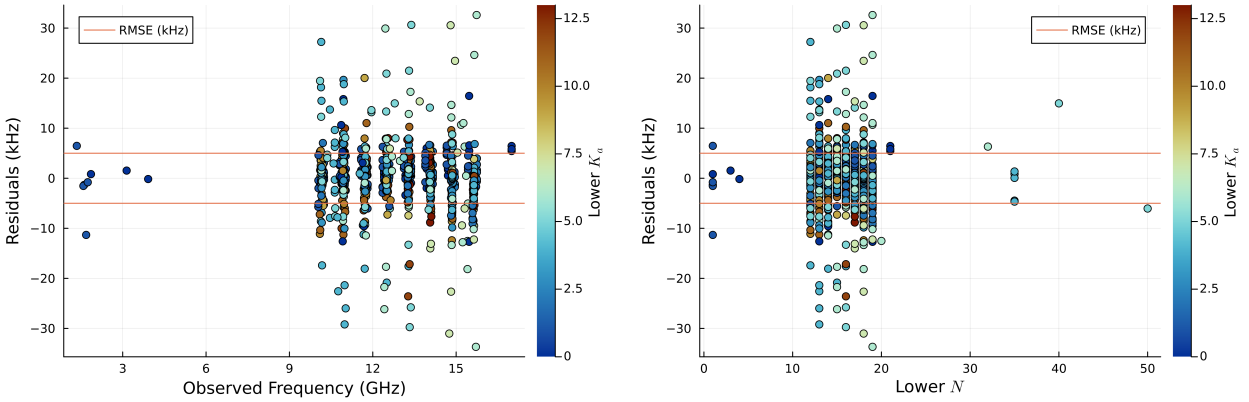

(a) Residuals for ipfp plotted against frequency

(b) Residuals for ipfp plotted against lower N

FIGURE 4.4. Residuals for ipfp plotted against either frequency lower N. Highlighting indicates lower K_a and the horizontal line indicates the fit RMSE

FTMW spectrometer. A total of 312 transitions up to $N = 15$ and $K_a = 2$ all in the ground torsional state with an experimental accuracy of 2 kHz [**111**] were fit in RAM36hf. This molecule provides an interesting interaction of the RAS and the axes of the quadrupole moment as well as a lower barrier test case. In the PAS, both the methyl rotor and the chlorine atom are off-axis and thus require more coupling terms for proper treatment. However, in the RAS, the chlorine is

also moved much closer to the ρ axis. As a result, the value of χ_{xz} is heavily diminished and was excluded from the Hamiltonian in [**111**]. Two experimental transitions at 11985.9111 MHz and 11986.9271 MHz were excluded due to a suspected typographical error in the original work [**111**]. These are the $13/2 \rightarrow 11/2$ and $17/2 \rightarrow 15/2$ hyperfine components of the E state $8_{18} \rightarrow 7_{17}$ in the E states. These transitions are listed as being ∼660 MHz apart from the other two transitions in the set. As a comparison, the $9_{19} \rightarrow 8_{18}$ cluster in the E states is only spread by 0.41 MHz. The complete treatment of the nuclear quadrupole in westerfit did allow for χ_{xz} to be determined alongside a reduction in the RMS error. The parameters for both fits of this data are shown in Table 4.3 with all parameters taking on their RAM values. However, C, χ_{zz}, and ρ all experienced a reduction in precision with ρ being fit to four less digits of precision. The residuals of the new fit are shown in Figure 4.5. These discrepancies may have emerged from differences in the nuclear quadrupole implementations as well as the subtle changes in quantum state labels from impact of the Hamiltonian matrix elements off-diagonal in N on the eigenvectors. This test has shown that westerfit is capable of simultaneously addressing methyl torsions and nuclear quadrupole moments.

TABLE 4.3. Spectroscopic parameters for 2-F-4-Cl-tol determined by westerfit & RAM36hf. Values in parenthesis are 1σ uncertainties of the last digit

Parameter (units)	westerfit	RAM36hf
A (MHz)	3030.11(19)	3036.35(23)
B (MHz)	864.753(83)	859.11(23)
C (MHz)	672.15(83)	672.4555(45)
D_{ab} (MHz)	−113.7(12)	−125.9(14)
χ_{aa} (MHz)	−70.23(26)	−69.443(72)
$\chi_{bb} - \chi_{cc}$ (MHz)	3.63(28)	2.329(51)
χ_{ab} (MHz)	−12.1(26)	–
F (cm^{-1})	5.392521(fixed)	5.392521(fixed)
ρ	0.01831(24)	0.018022728(84)
V_3 (cm^{-1})	223.751(91)	227.22(12)
$-D_N$ (kHz)	−0.00821(17)	−0.00809(22)
V_{3N} (kHz)	0.283(14)	−0.380(19)
Number of lines	310	312
rms (kHz)	5.7	7.5

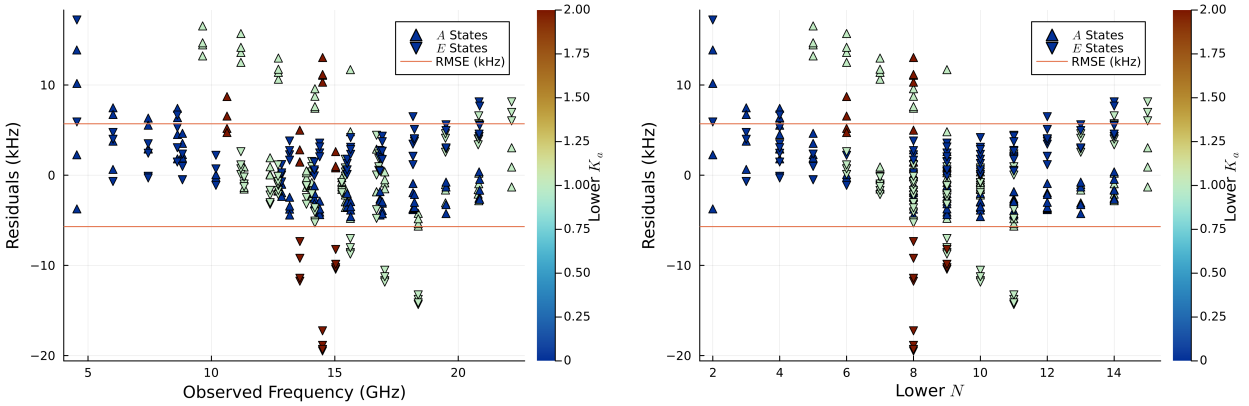

(a) Residuals for 2-F-4-Cl-tol plotted against frequency

(b) Residuals for 2-F-4-Cl-tol plotted against lower N

FIGURE 4.5. Residuals for 2-F-4-Cl-tol plotted against the transition frequency and highlighted by the lower K_a state. The A and E states trend in opposing directions as lower J increases.

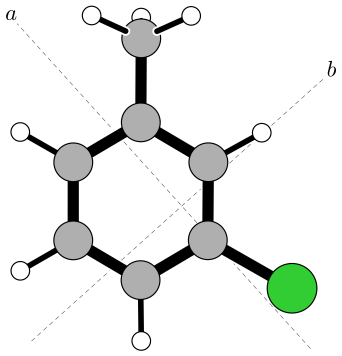

FIGURE 4.6. The MP2/cc-pwCVDZ structure of Cl-tol and its principal axes

4.3. Meta-Chlorotoluene

4.3.1. Improved ab initio Calculations. The geometry results of Ref. [**97**] showed that m-Cl-tol has a C_1 structure at its equilibrium geometry. After confirming this with an MP2/cc-pVDZ calculation in ORCA [**92**] with symmetry disabled, the structure of m-Cl-tol was optimized at MP2/cc-pwCVDZ in CFOUR [**91**] using a fully C_1 Z-matrix. The self-consistent field (SCF) was set to converge when the largest change in the density matrix was 10^{-9} and geometry convergence was set to 10^{-9} Hartree/Bohr. A relaxed potential energy scan was calculated with the same SCF convergence but the geometry convergence relaxed to 10^{-5} Hartree/Bohr. This scan was run by

fixing the methyl rotor dihedral angle and optimizing the rest of the geometry. The angle was incremented with a 1° step-size across a full 360° span. The step energies are plotted against the angle of the methyl group and the phenyl plane in Figure 4.7, showing clear six-fold behavior, and were fit to the following Fourier expansion:

$$V(\alpha) = \frac{V_3}{2}(1 - \cos 3\alpha) + \frac{V_6}{2}(1 - \cos 6\alpha) + \frac{V_9}{2}(1 - \cos 9\alpha) + \frac{V_{12}}{2}(1 - \cos 12\alpha) \tag{4.12}$$

The fit was terminated at the V_{12} term as that was the first term to be less than V_3. The potential terms are tabulated in Table 4.4. The PES makes for a very unusual spectroscopic case as the V_6 term is dominant over a nonzero V_3 term. In general, an expansion led by the V_6 term is indicative of a C_{2v} symmetry in the molecular frame. This makes V_3 zero by symmetry, such as the cases of toluene or para-fluorotoluene. Other meta substituted toluenes such as meta-fluorotoluene [**112**] or 3,4-difluorotoluene [**113**] are led by a V_3 term such as the case of meta-fluorotoluene which has a V_3 of about 17 cm^{-1}. It is more typical for terms in this Fourier expansion to be on the order of 5% of the preceding term, thus making the fit of this molecule of particular interest.

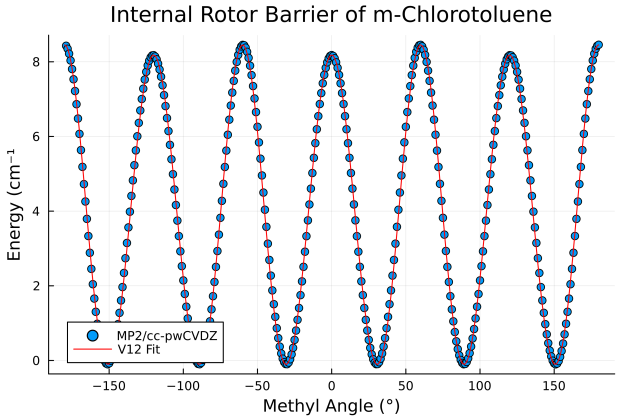

FIGURE 4.7. MP2/cc-pwCVDZ relaxed methyl rotor scan of m-Cl-tol and then fit up to Equation 4.12

4.3.2. Refit of Spectrum. First just the A states were fit to provide the initial estimations of the hyperfine and distortion terms as shown in Table 4.5. Both fits were conducted in the I^r representation. This fit showed reasonable agreement with a comparable analysis with SPFIT though they did not report an exact line count or RMS for this fit [**97**].

Expansion Term	Operator	MP2/cc-pwCVDZ (cm^{-1})
V_3	$\frac{1}{2}(1-\cos 3\alpha)$	0.1207
V_6	$\frac{1}{2}(1-\cos 6\alpha)$	8.4047
V_9	$\frac{1}{2}(1-\cos 9\alpha)$	−0.3921
V_{12}	$\frac{1}{2}(1-\cos 12\alpha)$	0.0465

TABLE 4.4. Fit potential terms for m-Cl-tol

Parameter	westerfit	SPFIT [**97**]
A (MHz)	3373.33218(53)	3373.33216(42)
B (MHz)	1195.33775(37)	1195.337969(43)
C (MHz)	882.501635(37)	882.5014296(262)
χ_{aa} (MHz)	−59.8964(3)	−59.8964(23)
$\chi_{bb}-\chi_{cc}$ (MHz)	−5.9533(39)	−5.9533(31)
χ_{ab} (MHz)	33.036(45)	33.0452(287)
$-D_N$ (kHz)	−0.03381(17)	−0.037381(171)
$-D_{NK}$ (kHz)	0.0081(15)	0.02951(103)
$-D_K$ (kHz)	−0.870(1)	−0.891(83)
d_1 (kHz)	−0.02381(22)	−0.011901(85)
d_2 (kHz)	−0.00357(19)	−0.1066(46)
Number of Lines	240	
RMS (kHz)	12.7	

TABLE 4.5. Fit of the A state transitions of meta-chlorotoluene.

From here, a full fit of all parameters was attempted using the non-perturbative hyperfine treatment and a global torsional basis including 11 torsional states. However, as pointed out by Dr. Kleiner [**97**, **114**], it is not possible to fit both V_3 and V_6 using information from only the ground torsional state. Table 4.6 shows the results from 3 fits: one in which V_3 and V_6 were adjusted, one in which only V_6 was adjusted, and lastly the V_3 fixed fit from [**97**]. In both fits, the RMS is lower than that of Ref. [**97**] while using a smaller total number of parameters. This limitation was done to improve the uncertainties on the potential terms as the inclusion of additional parameters reduced the precision. The attempt to float both V_3 and V_6 resulted in a substantially lower RMS but neither potential term was fit to even a single digit of precision. In the second fit, V_3 was locked to the MP2/cc-pwcVDZ value as this term contributes less to the torsional barrier structure than the V_6 term. This fit yielded greater precision on all the floated torsional terms. Typically an $\sim$8 cm^{-1} difference between the calculated and experimental torsional barrier would be regarded as good agreement though the general uncertainty on these terms is concerning. Many of the

numerical differences between the two programs result from the RAM approach of westerfit and the XIAM's internal conversion from PAM to RAM [**50**]. The PAM values for the rotational constants and nuclear quadrupole terms can be converted to RAM through δ and the RAM values can be restored to PAM through D_{ab}. Due to the lack of confidence in the potential term values, neither of these conversions have been done here. The residuals for the westerfit $V3$ fixed fit are plotted in Figure 4.8; clearly the high RMS transitions belong to the E states which are more sensitive to the torsional operators in the Hamiltonian. Inclusion of transitions from torsional states above $v_t = 0$ will likely be necessary properly determine the torsional parameters.

TABLE 4.6. Spectroscopic parameters for meta-chloro-toluene determined by westerfit and XIAM. Values in parenthesis are 1σ uncertainties of the last digit

Parameter (units)	westerfit Neither fixed	westerfit V_3 Fixed	XIAM V_3 Fixed [**97**]
A (MHz)	3131.34(32)	3131.305(18)	3334.3779(40)
B (MHz)	1393.7592(24)	1393.7598(17)	1191.3563(11)
C (MHz)	882.5027(24)	882.5027(17)	882.50134(58)
D_{ab} (MHz)	−626.7339(48)	−626.7347(31)	–
χ_{aa} (MHz)	−33.2(24)	−33.2(24)	−60.324(97)
χ_{ab} (MHz)	51.68(33)	51.68(33)	32.47(63)
$\chi_{bb} - \chi_{cc}$ (MHz)	−32.69(25)	−32.69(25)	−5.58(12)
F (cm^{-1})	5.26805(fixed)	5.26805(fixed)	5.30448(fixed)
ρ	0.01663(13)	0.0166422(71)	–
δ(deg)	–	–	42.1036(2)
V_3 (cm^{-1})	0.5(28)	0.1207(fixed)	2.452(fixed)
V_6 (cm^{-1})	14(19)	15.88(8)	−17.197(36)
$-D_N$ (kHz)	−0.0209(22)	−0.0208(22)	0.0283(36)
$-D_{NK}$ (kHz)	0.1500(59)	0.1450(59)	0.018005(fixed)
$-D_K$ (kHz)	−0.8000(21)	−0.7900(21)	0.834915(fixed)
d_1 (kHz)	–	–	−0.0085(24)
d_2 (kHz)	–	–	0.00196(fixed)
$D_{\pi 2J}$ (kHz)	–	–	16.17(65)
$D_{\pi 2K}$ (kHz)	–	–	162(13)
$D_{\pi 2-}$ (kHz)	–	–	15.23(19)
Number of lines	336	336	336
RMS (kHz)	17.7	29.6	41.7

4.4. Conclusion

The program, westerfit, has been developed to provide a complete treatment of the rotational spectra of C_s molecules with one internal rotor and one spin source. The code has been shown to give comparable results to the existing programs which are capable of addressing either

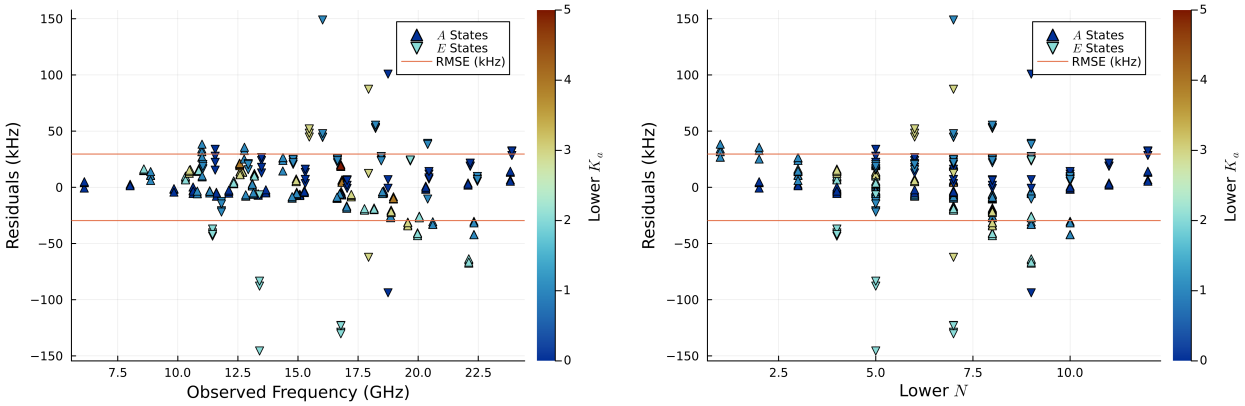

(a) Residuals for m-Cl-tol plotted against frequency (b) Residuals for m-Cl-tol plotted against lower N

FIGURE 4.8. Residuals for m-Cl-tol plotted against the transition frequency and highlighted by the lower K_a state

the torsion or the spin. In the particularly low barrier case of meta-chlorotoluene, westerfit was able to provide a substantial reduction in error as compared to a prior fit attempt using XIAM [**97**]. However, the lack of torsionally excited spectra prevented a complete fit of the unusual potential structure. The code has been publicly released and should serve as a beneficial tool to other spectroscopists attempting to study complicated rotational spectra.

CHAPTER 5

On the Coupling of Electron Spin & Internal Rotation

Radio astronomy has allowed for the astrochemical detection of both radicals and complex organic molecules. However, there have not yet been any detections of methyl containing radical species. This is due to the combined complexity of the unpaired electron's spin-rotation coupling and the methyl rotor's torsion-rotation coupling. The lack of a suitable model and program to study molecules with both complications has prevented study both in the laboratory and in space. The program SPFIT [**40**] has been proven to be an incredibly powerful tool for studying molecules with internal angular momentum coupling such as spin-rotation coupling or nuclear hyperfine coupling. However, it lacks a way to properly treat methyl rotors with barrier heights lower than $\sim$ 500 cm^{-1} [**41**]. The internal rotor problem has been well addressed by Rho Axis Method programs such as BELGI [**44**] and RAM36 [**64**]. These in turn lack the necessary operators and basis set to address the spin-rotation coupling of radical species. The program XIAM [**45**] is able to treat both internal rotation and spin-rotation. Unfortunately, the limited torsional basis in the second diagonalization stage causes it to struggle in low barrier cases and the perturbative spin-rotation treatment prevents its applicability to molecules with large amounts of spin-rotation coupling. In adition, the SR treatment in XIAM is poorly document and does not appear to have been used in any published work.

In order to study this class of molecules, the program in the previous chapter was developed and the specific interactions of the spin and torsion shall be investigated here. A specific molecular example of meta-methyl-phenoxyl (m-MePhO) as shown in Figure 5.1 will be used. The C_s frame allows for many imaginary terms in the Hamiltonian matrix to be ignored and the phenyl ring structure is relatively rigid thus reducing heavy torsion-vibration coupling and allowing the focus to be on the torsional couplings. Additionally the presence of a radical but no other strong spin

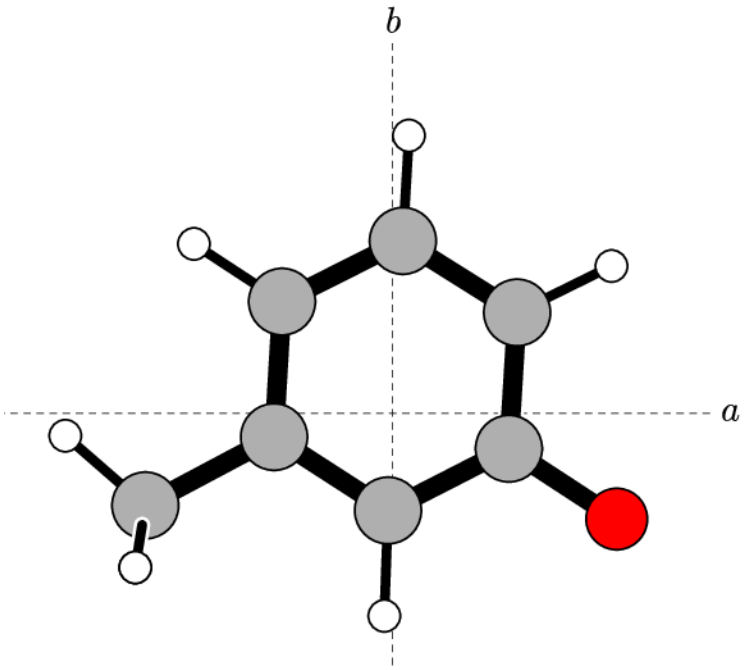

FIGURE 5.1. The structure of meta-methyl-phenoxyl calculated at CCSD(T)/cc-pwCVDZ and shown with its principal axes.

sources limits the amount of spin-spin coupling necessary to make initial explorations into its energetic structure.

This chapter will open with deriving the spin-torsion interaction term and expanding the Rho Axis Method transformation to include spin. Then potential definitions of the spin-torsion interaction parameter will be introduced and discussed. From here the various second order coupling operators will be examined using the *ab initio* parameters for m-MePhO. This will provide context for the relative magnitudes of the spin-torsion coupling for the following section which will examine how the spin-torsion coupling evolves across more general spectroscopic trends. Lastly the simulated spin-torsion-rotation spectrum of m-MePhO will be examined to provide a view as to how the spin-torsion coupling impacts the spectrum.

5.1. Derivation of Spin-Torsion Coupling Interaction

This case is limited to molecules with a C_s frame, a C_{3v} internal rotor, and doublet spin. Per inspection of the $\mathbf{G}_6$ character table, shown in Table 5.1, only two symmetrically allowed

TABLE 5.1. Character Table for the $\mathbf{G}_6$ [**68**]

$\mathbf{G}_6$	E 1E	(123) $2C_3(z)$	(23)* $3\sigma_v$	Operators
A_1:	1	1	1	$\mathcal{J}_y$, $\mathcal{N}_y$, $\mathcal{S}_y$, $\cos 3\alpha$
A_2:	1	1	-1	$\mathcal{J}_z$, $\mathcal{N}_z$, $\mathcal{S}_z$, $\mathcal{J}_x$, $\mathcal{N}_x$, $\mathcal{S}_x$ $\mathcal{P}_\alpha$, $\sin 3\alpha$
E:	2	-1	0	

operators couple the spin and torsion at second order.

$$\mathscr{H}_{st,PAM} = \eta_z \mathcal{P}_\alpha \mathcal{S}_z + \eta_x \mathcal{P}_\alpha \mathcal{S}_x \tag{5.1}$$

By rotating the coordinate system into the Rho Axis System, the methyl top axis is positioned such that the only the z axis coupling remains. Another way to approach this transformation is through application of a contact transformation on the group theoretically complete second order Hamiltonian, $\mathscr{H}_{GC}$. This allows $\mathscr{H}_{RAM}$ to be derived by:

$$\mathscr{H}_{RAM} = e^{-\imath \hat{G}} \mathscr{H}_{GC} e^{\imath \hat{G}} = \mathscr{H}_{GC} + \imath \left[\mathscr{H}_{GC}, \hat{G} \right] + ... \tag{5.2}$$

The expansion is terminated at the first expansion term but could be continued out further by evaluating additional commutators. This Hamiltonian is built from every A_1 operator of second order in Table 5.1. Operators with a power greater than 1 on any projection of $\mathcal{S}$ are neglected as they contribute a constant amount of energy to doublet states. The operators will also be written the "standard form" to ensure Hermiticity and to minimize interdependences between operators [**32**].

$$\begin{aligned}\mathscr{H}_{GC} = a\mathcal{N}_z^2 + b\mathcal{N}_x^2 + c\mathcal{N}_y^2 + d\left(\mathcal{N}_z\mathcal{N}_x + \mathcal{N}_x\mathcal{N}_z\right) + f\mathcal{P}_\alpha^2 + g\mathcal{P}_\alpha\mathcal{N}_z + h\mathcal{P}_\alpha\mathcal{N}_x + j\cos 3\alpha + \\ k\mathcal{N}_z\mathcal{S}_z + l\mathcal{N}_x\mathcal{S}_x + m\mathcal{N}_y\mathcal{S}_y + n\left(\mathcal{N}_z\mathcal{S}_x + \mathcal{S}_x\mathcal{N}_z\right) + p\left(\mathcal{N}_x\mathcal{S}_z + \mathcal{S}_z\mathcal{N}_x\right) + r\mathcal{P}_\alpha\mathcal{S}_z + s\mathcal{P}_\alpha\mathcal{S}_x\end{aligned} \tag{5.3}$$

Similarly, the reduction operator of $\hat{G}$ is constructed through all the A_1 operators of first order in Table 5.1.

$$\hat{G} = \alpha\mathcal{N}_y + \beta\mathcal{S}_y \tag{5.4}$$

Carrying out the algebra, the torsional coupling operators reach this intermediate result:

$$\mathscr{H}_{GC} + \imath[\mathscr{H}_{GC}, \hat{G}] = ... + (g + \alpha h)\mathcal{P}_\alpha \mathcal{N}_z + (h - \alpha g)\mathcal{P}_\alpha \mathcal{N}_y + ... \\ + (r - \alpha s + \beta h - \beta s)\mathcal{P}_\alpha \mathcal{S}_z + (s + \alpha r - \beta g + \beta r)\mathcal{P}_\alpha \mathcal{S}_x \quad (5.5)$$

Setting $\alpha = -\frac{h}{g}$ removes the x-axis torsion-rotation coupling term, thus producing the typical RAM Hamiltonian. All of the terms independent of spin are not modified by the $\beta\mathcal{S}_y$ term so the rotational constants have the same transformation as their spin-free RAM values, thus making this a spin-inclusive extension of the RAM. An additional contact transformation to remove ρ_z and η_z would qualify this as an Internal Axis Method (IAM) [**46**]. Defining $\beta = \frac{sg-hr}{g(g-r)}$ then allows for the removal of the x-axis spin-torsion coupling term. Just one coupling term remains as the y-axis interaction was already removed by symmetry.

$$\mathscr{H}_{st} = \eta \mathcal{P}_\alpha \mathcal{S}_z \quad (5.6)$$

Values of the spectropic parameters are shifted slightly as a result of the contact transformation. However, none are as dramatic as the full removal of an operator. For example, the RAM value of ϵ_{zz} becomes:

$$\epsilon_{zz}^R = \epsilon_{zz} + \frac{\rho_x(\epsilon_{zx} - \epsilon_{xz})}{\rho_z} + \frac{\epsilon_{zx}(\rho_z\eta_x - \rho_x\eta_z)}{\rho_z(2F\rho_z + \eta_z)} \quad (5.7)$$

Equation 5.7 replaces the parameters in Equation 5.3 with their principal axis values, including the removal of d as it equals zero.

The wavefunction for this problem shall be a simple product between the Hund's case (b) function of Equation 2.48 and the free rotor basis of Equation 2.36. The projection onto the laboratory frame will be dropped in this chapter.

$$|\psi\rangle = |m\rangle|JSNK\rangle \quad (5.8)$$

As the torsions are not directly coupled to the other sources of angular momentum, the matrix element calculation can be readily partitioned as:

$$\langle\psi'|\mathcal{P}_\alpha\mathcal{S}_z|\psi\rangle = \langle m'|\mathcal{P}_\alpha|m\rangle\langle J'S'N'K'|\mathcal{S}_z|JSNK\rangle \quad (5.9)$$

The torsional part for this is very simply:

$$\langle m'|\mathcal{P}_\alpha|m\rangle = m\delta_{m',m} \tag{5.10}$$

where δ is the Kronecker delta. The spin contribution to the matrix element can be determined using spherical tensor notation and starting from the Wigner-Eckart Theorem [**18**]:

$$\langle J'S'N'K'|T^1_0(S)|JSNK\rangle = (-)^{N'-K'}\begin{pmatrix} N' & 1 & N \\ -K' & 0 & K \end{pmatrix}\langle J'S'N'||T^1_0(S)||JSN\rangle \tag{5.11}$$

The Wigner 3j symbol requires this term to be on-diagonal in K. The reduced matrix element can be evaluated from Equation 7.1.8 of Edmonds [**18**]:

$$\langle JS'N'||T^1_0(S)||JSN\rangle = (-)^{N+S+J+1}\sqrt{(2N+1)(2N'+1)}\begin{Bmatrix} S' & N' & J \\ N & S & 1 \end{Bmatrix}\langle S'||T^1_0(S)||S\rangle \tag{5.12}$$

The term in $\{\}$ is a Wigner 6j symbol [**18**] and the expression is on-diagonal in J. Because the coupling scheme is $N = J - S$, N in Equation 5.12 corresponds to the J in the expression in Edmonds while J and S correspond to j_1 and j_2. The final reduced matrix element is simply:

$$\langle S'||T^1_0(S)||S\rangle = \delta_{S',S}\sqrt{S(S+1)(2S+1)} \tag{5.13}$$

This term forces the operator to be on-diagonal in S. Reassembling the spherical tensor operator gives the expression:

$$\langle JSN'K|T^1_0(S)|JSNK\rangle = (-)^{N'-K+N+S+J+1}$$
$$\sqrt{(2N+1)(2N'+1)S(S+1)(2S+1)}\begin{pmatrix} N' & 1 & N \\ -K & 0 & K \end{pmatrix}\begin{Bmatrix} S & N' & J \\ N & S & 1 \end{Bmatrix} \tag{5.14}$$

Reintroducing the torsional component, the full matrix element for Equation 5.6 is:

$$\langle JSN'Km|\mathcal{P}_\alpha\mathcal{S}_z|JSNKm\rangle = (-)^{N'-K+N+S+J+1}$$
$$m\sqrt{(2N+1)(2N'+1)S(S+1)(2S+1)}\begin{pmatrix} N' & 1 & N \\ -K & 0 & K\end{pmatrix}\begin{Bmatrix} S & N' & J \\ N & S & 1\end{Bmatrix} \quad (5.15)$$

This operator is on-diagonal in all of the quantum numbers except N which contributes nonzero matrix elements when $\Delta N = 0, \pm 1$ The direct expression for the on-diagonal term is:

$$\langle JSNKm|\mathcal{P}_\alpha\mathcal{S}_z|JSNKm\rangle = 2Km\frac{N(N+1)+S(S+1)-J(J+1)}{N(N+1)} \quad (5.16)$$

and the off-diagonal term is:

$$\langle JSN-1Km|\mathcal{P}_\alpha\mathcal{S}_z|JSNKm\rangle =$$
$$\frac{m\sqrt{(N^2-K^2)}}{2N}\sqrt{\frac{(J+S+N+1)(S+N-J)(J+N-S)(J+S-N+1)}{(2N-1)(2N+1)}} \quad (5.17)$$

The $\mathcal{P}_\alpha\mathcal{S}_z$ operator and matrix element was derived by Hirota for studying the acetyl radical [**22**], and it differs from the one presented here by a factor of two. The spin-torsion parameter was not tested in that paper; as it was left fixed to zero because they onlyonly fit states with K_a equal to zero for which the $\mathcal{P}_\alpha\mathcal{S}_z$ operator has a minimal impact.

5.2. Potential Definitions of Spin-Torsion Interaction Term

Now that the spin-torsion operator and its matrix element have been defined, the question becomes how to define the spin-torsion parameter. The definition for this term would be crucial for predicting the magnitude of the operator's impact on a spectrum and then for extracting physical information from the experimentally determined values. One possible definition for the spin-torsion parameter would be to follow the same logic as the definition of the spin-rotation tensor [**115**].

$$\eta \stackrel{?}{=} \frac{\partial^2 E}{\partial\mathcal{S}_z\partial\mathcal{P}_\alpha} \quad (5.18)$$

Hirota proposed the following as an extension of spin-orbit coupling.

$$\eta \stackrel{?}{=} 2FA_{SO}\sum_{m}\frac{|\langle 0|L_z|m\rangle|^2}{E_0 - E_m} \tag{5.19}$$

As neither of these approaches have been implemented into an ab initio package, an alternative approximation becomes necessary. An exceedingly crude but trivially solvable approach is to assume that the spin-torsion, torsion-rotation, and spin-rotation interaction parameters on the z axis follow a consistent mathematical motif. This approach is inspired by the torsion-rotation coupling at second order, $\rho F\mathcal{P}_\alpha\mathcal{N}_z$. The effective torsion-rotation coupling parameter, ρF, is constructed from the structural parameters.

$$\rho F = \rho\frac{F_0}{1-\rho} = \frac{AF_0}{F_0 - A} \tag{5.20}$$

An effective rotational constant, denoted G, can be created to generate a similar mathematical structure as Equation 5.20 for the spin-rotation interaction and can then be determined as:

$$\epsilon_{zz} = \frac{AG}{G-A} \Rightarrow G = \frac{A\epsilon_{zz}}{A+\epsilon_{zz}} \tag{5.21}$$

Finally, this pattern can be continued using F_0 and G which allows the spin-torsion interaction term to be approximated by:

$$\eta \stackrel{?}{=} \frac{FG}{G-F} = \frac{A\epsilon_{zz}F_0}{A\epsilon_{zz} - F_0A - F_0\epsilon_{zz}} \tag{5.22}$$

Equation 5.22 uses the RAM values of all the listed parameters to determine the RAM value of η. However, since the RAM transformation of ϵ_{zz} depends on the PAM values of η_z and η_x, the PAM value of ϵ_{zz} will be used for now. The validity of this approach remains to be seen but, in the absence of more rigorous approaches, it will be used in this chapter.

5.3. *ab initio* Parameters for Meta-Methyl-Phenoxyl

Most of the parameters used in this work were calculated at the CCSD(T)/cc-pwCVDZ level of theory with a UHF reference using a developmental version of CFOUR [**91**]. The SCF, CC, and linear equation convergences were set to 10^{-9} along side the geometry convergence of 10^{-9} Hartree/Bohr. The structure was optimized at this level to obtain the equilibrium rotational constants and the principal axis coordinates are listed in Table C.1. This geometry was run through

the moments.f script from I. Kleiner to determine F and ρ. A potential energy scan was run by stepping the methyl rotor dihedral angle 5° and reoptimizing the rest of the geometry at CCSD/cc-pwCVDZ. For this surface, a fully C_1 z-matrix was used and the geometry convergence criteria was relaxed to the default 10^{-5} Hartree/Bohr. The energy as a function of dihedral angle was fit to Equation 2.32 to obtain V_3 and V_6. The spin-rotation tensor was calculated at CCSD/cc-pwCVDZ. To complete the second order Hamiltonian, η was calculated using the CCSD(T)/cc-pwCVDZ A and F_0 values and the CCSD/cc-pwCVDZ ϵ_{zz} value using Equation 5.22. As in Section 3.2.2, a harmonic frequency calculation at CCSD/cc-pwCVDZ was carried out using finit differences for the gradients, yielding simulated values for the quartic centrifugal distortion terms. The harmonic frequencies and their intensities are listed in Table C.2.

Parameter	Operator	*ab initio*	Unit
A	$\mathcal{N}_z^2$	3666.961^a	MHz
B	$\mathcal{N}_x^2$	1833.626^a	MHz
C	$\mathcal{N}_y^2$	1231.939^a	MHz
D_{ab}	$\{\mathcal{N}_z, \mathcal{N}_x\}$	-715.182^a	MHz
F	$\mathcal{P}_\alpha^2$	5.268^a	cm^{-1}
ρ	$\mathcal{P}_\alpha \mathcal{N}_z$	0.01179^a	–
V_3	$\frac{1}{2}(1-\cos 3\alpha)$	174.861^b	cm^{-1}
ϵ_{zz}	$\mathcal{N}_z \mathcal{S}_z$	306.516^b	MHz
ϵ_{xx}	$\mathcal{N}_x \mathcal{S}_x$	65.3026^b	MHz
ϵ_{yy}	$\mathcal{N}_y \mathcal{S}_y$	-15.104^b	MHz
ϵ_{xz}	$\{\mathcal{N}_x \mathcal{S}_z\}$	-98.938^b	MHz
ϵ_{zx}	$\{\mathcal{N}_z \mathcal{S}_x\}$	-199.655^b	MHz
η	$\mathcal{P}_\alpha \mathcal{S}_z$	-283.378^c	MHz
Δ_N	$\mathcal{N}^4$	0.0628^d	kHz
Δ_{NK}	$\mathcal{N}^2 \mathcal{N}_z^2$	1.231^d	kHz
Δ_K	$\mathcal{N}_z^4$	-0.687^d	kHz
δ_N	$\frac{1}{2}\{\mathcal{N}^2, \mathcal{N}_+^2 + \mathcal{N}_-^2\}$	0.0220^d	kHz
δ_K	$\frac{1}{2}\{\mathcal{N}_z^2, \mathcal{N}_+^2 + \mathcal{N}_-^2\}$	-0.839^d	kHz
V_6	$\frac{1}{2}(1-\cos 3\alpha)$	-6.093^b	cm^{-1}

TABLE 5.2. Predicted parameters for meta-methyl-phenoxyl. [a] CCSD(T)/cc-pwCVDZ, [b] CCSD/cc-pwCVDZ, [c] A, F, ϵ_{zz} via Eq. 5.22,[d] fc-MP2/cc-pwCVDZ

5.4. Impact of Spin-Torsion on Energy Levels for meta-Methyl-Phenoxyl

Using the program developed in Chapter 4 and a torsional basis of 17 states, the energy levels for m-MePhO were calculated up to $J = 31/2$ and $v_t = 2$. This maximum J value was

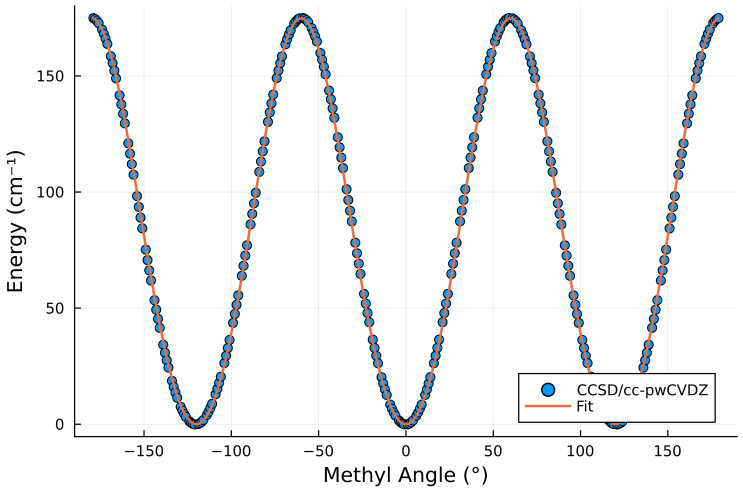

FIGURE 5.2. Potential energy of m-MePhO as a function of the methyl rotor dihedral angle

chosen to give just a few spin-rotational levels of the first torsionally excited states that are above the barrier height for both the A and E torsional symmetries. Looking first at Figure 5.3, clear clusters of energy levels form around six different $\langle \mathcal{P}_\alpha^2 \rangle$ values. The lowest energy cluster is the $v_t = 0$ A state cluster with the $v_t = 0$ E state cluster immediately above it. The next lowest cluster has a parabolic shape and corresponds to the $vt = 1$ states of E symmetry. The parabolic shape emerges from the increased energy difference between states of $\pm K$ [**46**]. The next two clusters are the A states of $v_t = 1$ and $v_t = 2$. In the free rotor limit of the purely torsional case, these states are degenerate so determining the best method of assigning the states after diagonalization in the torsion-rotation case can be difficult. In this specific case, there is a conflict of energy-based assignment versus the expectation value-based assignment. Neither of these A clusters is higher on both expectation value and energy. Because the torsional A state levels alternate between A_1 and A_2, starting with A_1 in the ground state, the higher energy state is assigned to $v_t = 2$ as it has the same symmetry as the ground state. The lower of the two clusters is therefore assigned as $v_t = 1$. This symmetry and energetic assignment are consistent with the correlation diagram given in Figure 2 of [**16**]. The last cluster, isolated from the others, contains the $v_t = 2$ E states.

Before examining the impacts of spin-torsion, a reference point of the other dominant coupling operators will be established. First the various couplings in m-MePhO will be examined.

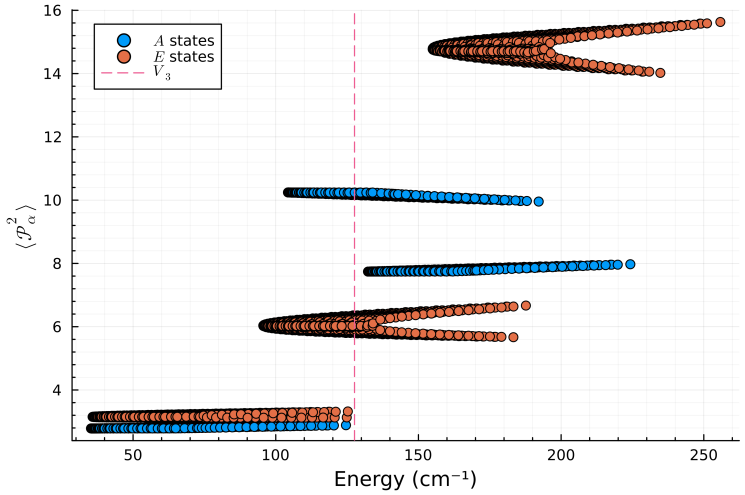

FIGURE 5.3. Expectation values of the torsional angular momentum squared plotted against the energy of each state. The states are highlighted by the torsional symmetry and torsional barrier height is marked for visual reference

Figure 5.4 shows the torsion-rotation coupling expectation values, $\langle \mathcal{P}_\alpha \mathcal{N}_z \rangle$ plotted against the energy. The magnitude of these interactions consistently increase with v_t with the E states having larger expectation values than the A states. The E states generally take on a more parabolic structure of the expectation value while the A states seem to trend in a singular direction within a given v_t. The $v_t = 1$ A states resemble the $v_t = 0$ A states with greater magnitude. In the free rotor and symmetric top limits, the expectation value for this operator would be mK. The highest K value in this simulation is 16. In the ground A states, all mK pairs are zero in this limit and for the ground E, the maximum $|mK| = 16$. However, Figure 5.4a shows that the $v_t = 0$ A states exceed this prediction while the $v_t = 0$ E states undershoot these predictions. On the other end, the highest $|mK|$ would be ≈ 64 for the $m = 4/v_t = 2$ E state of $K = 16$. The spread of $\langle \mathcal{P}_\alpha \mathcal{N}_z \rangle$ values for this torsional state approaches but does not quite reach this value. The energetic contributions from torsion-rotation coupling range from ones to tens of $2\rho F$ which is on the order of ones to tens of GHz.

The next effect of the spin-rotation interaction is shown in Figure 5.5. The $\mathcal{N}_z \mathcal{S}_z$ operator shows a parabolic form within each N grouping. Additionally, as this operator does not act on m, it would be expected that there is no meaningful change in the expectation values from one torsional

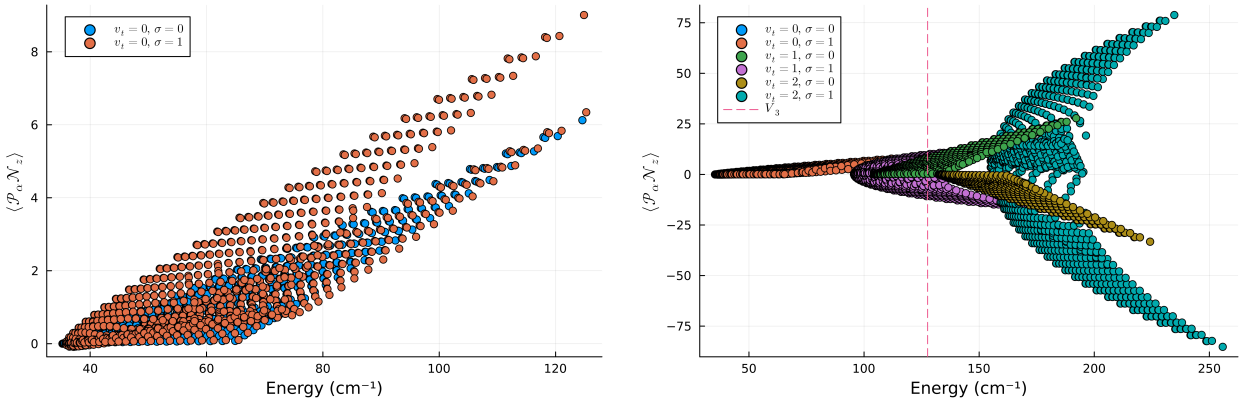

(a) $v_t = 0$ (b) $v_t = 0, 1, 2$

FIGURE 5.4. Expectation values of the torsion-rotation coupling term plotted against the energies of the respective states. This operator contributes more to a given states energy level than the spin-torsion interaction does.

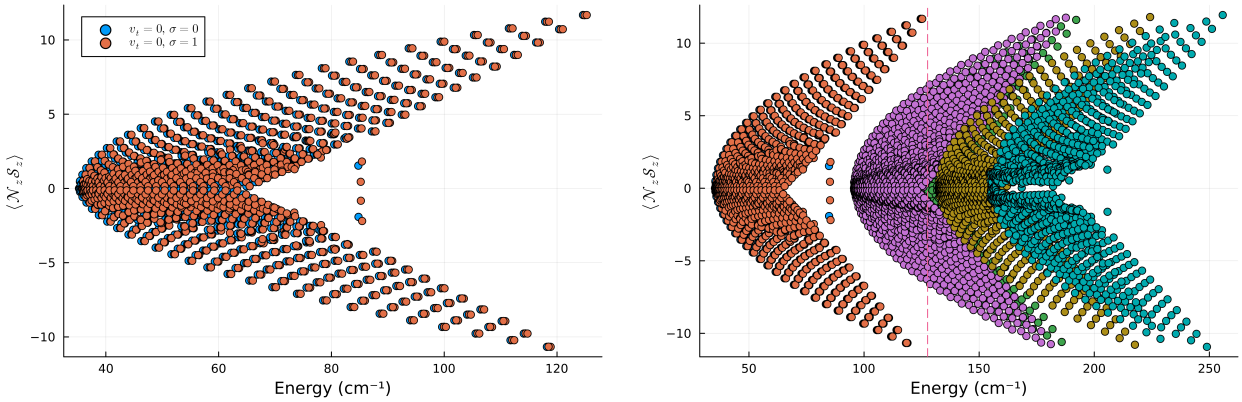

(a) $v_t = 0$ (b) $v_t = 0, 1, 2$

FIGURE 5.5. Expectation values of the z-axis spin-rotation coupling term plotted against the energies of the respective states. This operator also contributes more to a given state's energy level than the spin-torsion interaction does. The coloration in panel b is consistent with Figure 5.4b

state to the next. This prediction is confirmed by Figure 5.5. In an uncoupled representation at the symmetric top limit, $\langle \mathcal{N}_z \mathcal{S}_z \rangle = K\Sigma = \pm K/2$. The maximum value for this would be 8 and this value is very nearly reached thus showing general agreement with the roughly predicted values. The expectation values ranging from ones to almost tens of ϵ_{zz} correspond to energy contributions of hundreds of MHz to ones of GHz.

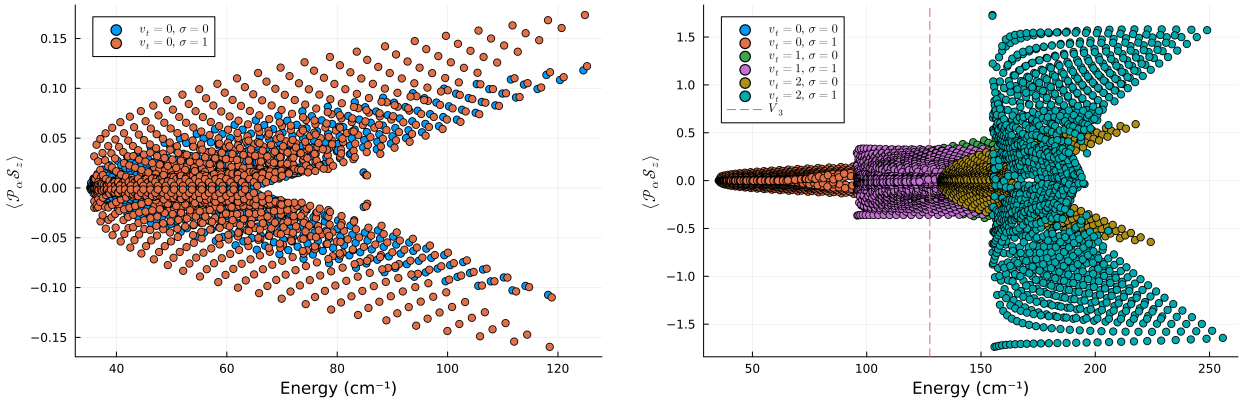

(a) $v_t = 0$ (b) $v_t = 0, 1, 2$

FIGURE 5.6. Expectation values of the spin-torsion coupling term plotted against the energies of the respective states. The magnitudes of the values increase with each v_t and are larger on the E states than the A states.

The spin-torsion interaction is depicted in Figure 5.6. The contribution from the spin-torsion interaction is similar to the spin-rotation interaction at $v_t = 0$, but the magnitude and spread of the values change visibly with increasing in torsional angular momentum like the torsion-rotation interaction. The most critical difference here is the magnitude. In the ground state, this interaction has values almost as much as two orders of magnitude smaller than the spin-rotation coupling. Then in the E states of $v_t = 2$, the maximum contribution is only about a fourth of the spin-rotation interaction. This makes the energetic contribution of this term on the order of tens of megahertz in the ground state and up to hundreds of megahertz in the torsionally excited states.

Digging deeper into the behavior of this operator, Figure 5.7 shows the expectation value plotted against $\langle \mathcal{P}_\alpha \rangle$ with triangle markers to denote if $N - J$ is positive or negative and highlighted by $\sqrt{\langle \mathcal{N}_z^2 \rangle}$ for the $v_t = 0$ and 1 states. This last quantity is used to provide an approximate $|K|$ value as the post-diagonalization quantum number assignment is a complicated procedure, as mentioned in Chapter 4. Panels a and b show the $v_t = 0$ states. For both torsional symmetries, the states with $N = J + 1/2$ tend to have positive contributions while the $N = J - 1/2$ states tend to have negative contributions. The A states tend to have a smoother arc shape while the E show more elaborate shapes stemming from the decreased symmetry with respect to K. Additionally in $v_t = 0$, most of the states with negative contribution have $N < J$ but this becomes more mixed

as v_t increases. There is a clear increase with respect to $|K|$ and in the E states, this relation is roughly parabolic with respect to $\langle \mathcal{P}_\alpha^2 \rangle$. The greatest magnitudes steadily approach $\pm 1/2$ as V_3 decreases, approaching the free rotor limit behavior.

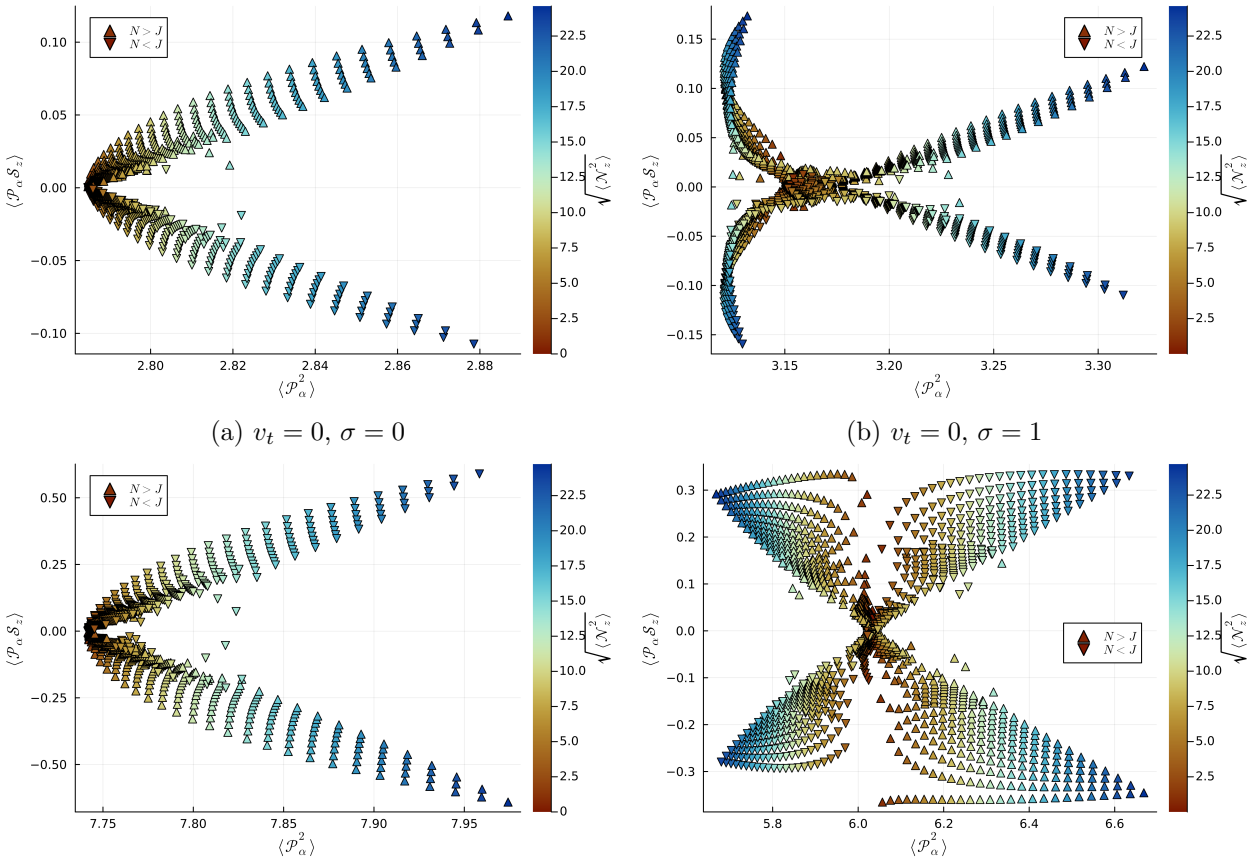

(a) $v_t = 0$, $\sigma = 0$

(b) $v_t = 0$, $\sigma = 1$

(c) $v_t = 1$, $\sigma = 0$

(d) $v_t = 1$, $\sigma = 1$

FIGURE 5.7. Expectation values of the spin-torsion coupling term plotted against the expectation values of the square of the torsional angular momentum operator for the respective states with highlighting based the square root of the z axis projection of the molecular angular momentum.

Stepping to higher torsional levels, Figure 5.7c shows the $v_t = 1$ A states. While this mostly resembles the ground torsional state with just larger values, it can be seen that the relation of $N = J - 1/2$ and $N = J + 1/2$ states has been reversed such that now the states with $N > J$ have the negative contribution, likely as a result of the change from A_1 to A_2 in torsional symmetry. Figure 5.7d shows the $v_t = 1$ E states and the most chaotic spread of values. The $N = J + 1/2$

TABLE 5.3. Reference parameter values used in spin-torsion tests

Parameter	Operator	Value	Unit
A	$\mathcal{N}_z^2$	3000.0	MHz
B	$\mathcal{N}_x^2$	1200.0	MHz
C	$\mathcal{N}_y^2$	1000.0	MHz
F	$\mathcal{P}_\alpha^2$	5.1021	cm^{-1}
ρ	$\mathcal{P}_\alpha \mathcal{N}_z$	0.020014	–
V_3	$\frac{1}{2}(1-\cos 3\alpha)$	100.00	cm^{-1}
ϵ_{zz}	$\mathcal{N}_z \mathcal{S}_z$	300.00	MHz
ϵ_{xx}	$\mathcal{N}_x \mathcal{S}_x$	120.00	MHz
ϵ_{yy}	$\mathcal{N}_y \mathcal{S}_y$	−100.00	MHz
η	$\mathcal{P}_\alpha \mathcal{S}_z$	−273.22	MHz

and $N = J - 1/2$ groups form two clusters with opposing correlations with the $N > J$ trending downward with increasing torsional angular momentum and the $N < J$ trending upwards. Most interestingly is that there are a number of states with low $|K|$ but relatively high spin-torsion interactions which is an occurrence not seen in any other torsional state.

5.5. Interactions of Spin-Torsion With Other Spectroscopic Properties

To provide a more generalized view, a series of simulations were run on a hypothetical molecule with simplified set of parameters. Here we only consider only the on-diagonal terms of the inertial and spin-rotation tensors. Thus the model Hamiltonian appears as:

$$\mathscr{H} = A\mathcal{N}_z^2 + B\mathcal{N}_x^2 + C\mathcal{N}_y^2 + \epsilon_{zz}\mathcal{N}_z\mathcal{S}_z + \epsilon_{xx}\mathcal{N}_x\mathcal{S}_x + \epsilon_{yy}\mathcal{N}_y\mathcal{S}_y + F\left(\mathcal{P}_\alpha - \rho\mathcal{N}_z\right)^2 + \frac{V_3}{2}\left(1-\cos 3\alpha\right) + \eta\mathcal{P}_\alpha\mathcal{S}_z \tag{5.23}$$

The parameters are listed in Table 5.3 and the subfigure using these parameters will be marked with □ for Figures 5.8–5.18 to aid comparison across the sequence of figures. The parameters B, V_3, ρ, ϵ_{zz}, ϵ_{xx}, ϵ_{yy}, and η are adjusted in the different test cases while all others will remain fixed at the listed values. Similarly to Figure 5.7, upward triangle markers will be used to denote states with $N = J + 1/2$ and downward triangle markers will be used for $N = J - 1/2$. Figure 5.8 demonstrates the result of adjusting B from 1100 to 1600 MHz in steps of 100 MHz such that $\kappa = -0.9, -0.8, -0.7, -0.6, -0.5$ and -0.4. The prolate range was selected as the program is currently hard-coded to only support the prolate I^r representation and only couple the torsion-rotation & spin-torsion to the a-axis in this representation. This set of figures shows the difference

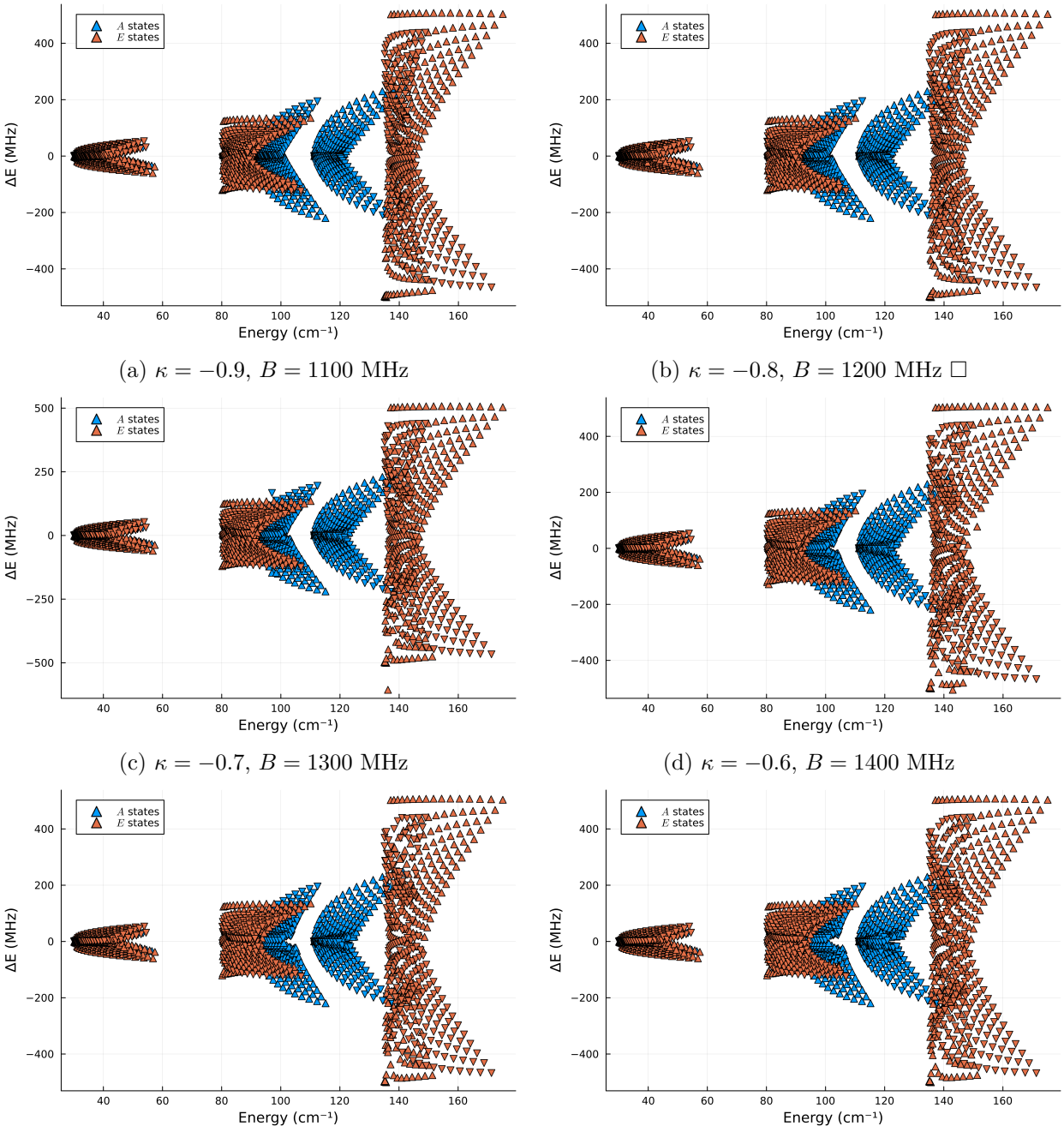

(a) $\kappa = -0.9$, $B = 1100$ MHz

(b) $\kappa = -0.8$, $B = 1200$ MHz □

(c) $\kappa = -0.7$, $B = 1300$ MHz

(d) $\kappa = -0.6$, $B = 1400$ MHz

(e) $\kappa = -0.5$, $B = 1500$ MHz

(f) $\kappa = -0.4$, $B = 1600$ MHz

FIGURE 5.8. The change in energy between including and excluding η in the second order Hamiltonian plotted against the state energies for six different κ values

in energy between including a non-zero η and fixing it zero in the spin-torsion-rotation problem as plotting against the energy of the states for the different κ values. These figures show very little variation with the exception of the $\kappa = -0.7$ plot which seems to experience a slight increase in the energetic shifts. The changes are quite small at only about 0.013% of the total energy. The consistencies here make sense as in an uncoupled basis, the pure rotational Hamiltonian and the spin-torsion coupling operator do not act on the same parts of the wavefunction and would thus be relatively independent.

The spin rotation values were stepped across 1%, 5%, 10%, 20%, 100%, and 1000% of their respective rotational constants with ϵ_{yy} being given a negative value to emulate the structure of m-MePhO's spin-rotation tensor. The spin-torsion coupling parameter, η, was recalculated at each of these by equation 5.22 to account for the change in ϵ_{zz}. Thus the various trials used values of -29.709, -142.99, -273.22, -501.67, -1515.2, and -2777.8 MHz respectively, and these results are shown in Figure 5.9. The energy differences seem to scale rather directly with the parameter increases in subplots a through c. At the larger values, states were less consistently assigned thus creating the large outliers seen in the e and f subfigures. The axes on the last two are restricted to ± 5 GHz and ± 50 GHz respectively in attempt to follow the progression set by a, b, and c. These also seem to show less increase in the energetic change relative to the parameter value starting at subplot d. Due to the amount of outliers in higher torsional states, the results for just the ground A and E states are shown in Figure 5.10. At low ϵ_{gg}/B_{gg} values, the spread of $N = J + 1/2$ and $N = J - 1/2$ states have a generally symmetric arrangement. This symmetry is degraded with larger relative magnitudes of the spin-rotation tensor. While the change in energy remains consistent on both sides, the $N = J + 1/2$ do not extend to as high energy levels and thus have a larger relative impact from the spin-torsion interaction. Figure 5.11 focuses on the ground A states by plotting the change in energy in units of the spin-torsion coupling parameter against the expectation value of $\mathcal{P}_\alpha^2$ with highlighting based on the square root of the expectation value of $\mathcal{N}_z^2$. The first expectation value was chosen to provide a reflection of the amount of torsional angular momentum while the second to provide an approximate $|K|$ value. Each of these cases show the magnitude of the energetic change increase with respect to both torsional angular momentum and

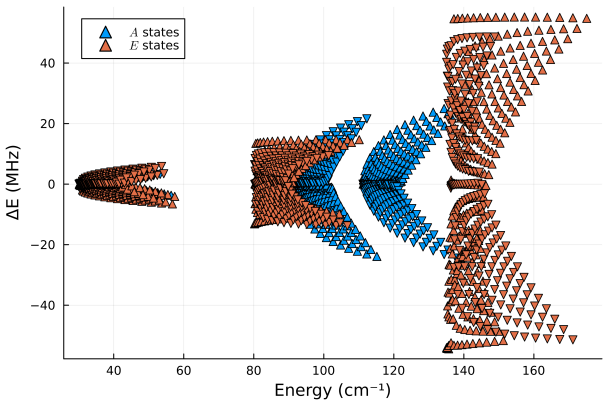

(a) $\epsilon_{gg}/B_{gg} = 1\%$

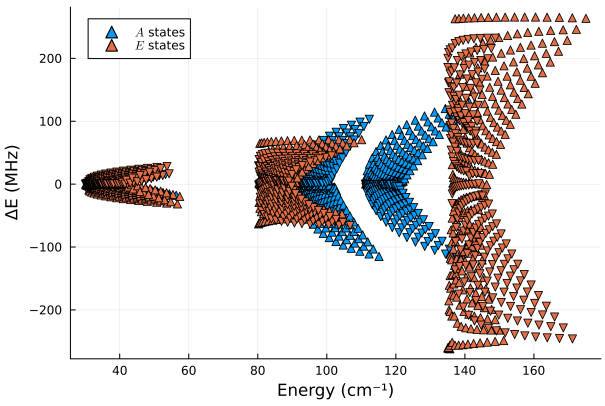

(b) $\epsilon_{gg}/B_{gg} = 5\%$

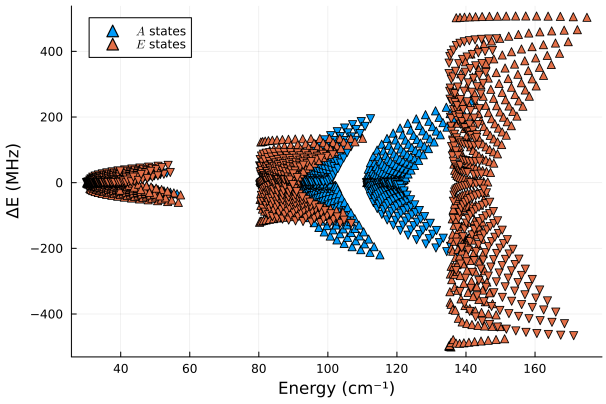

(c) $\epsilon_{gg}/B_{gg} = 10\%$ □

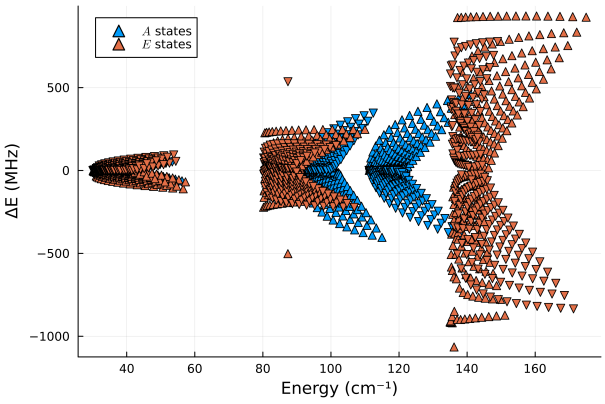

(d) $\epsilon_{gg}/B_{gg} = 20\%$

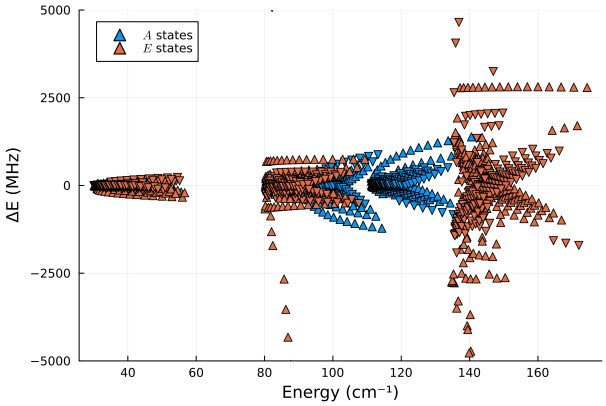

(e) $\epsilon_{gg}/B_{gg} = 100\%$

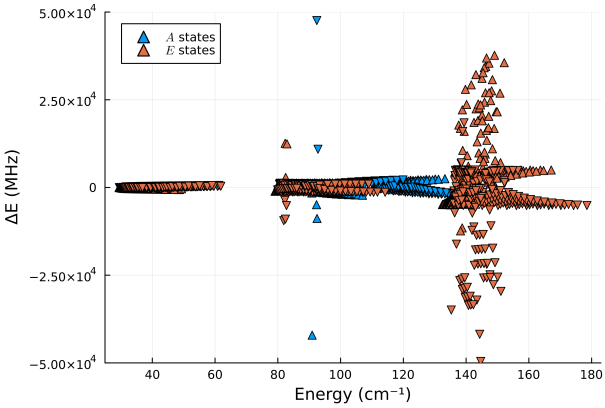

(f) $\epsilon_{gg}/B_{gg} = 1000\%$

FIGURE 5.9. The change in energy between including and excluding η in the second order Hamiltonian plotted against the state energies for six different ϵ_{gg}/B_{gg} values

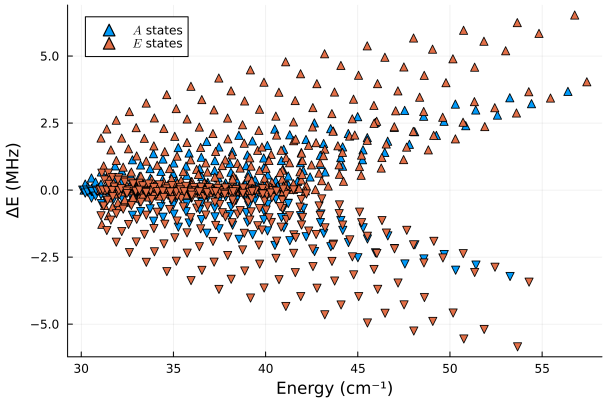

(a) $\epsilon_{gg}/B_{gg} = 1\%$

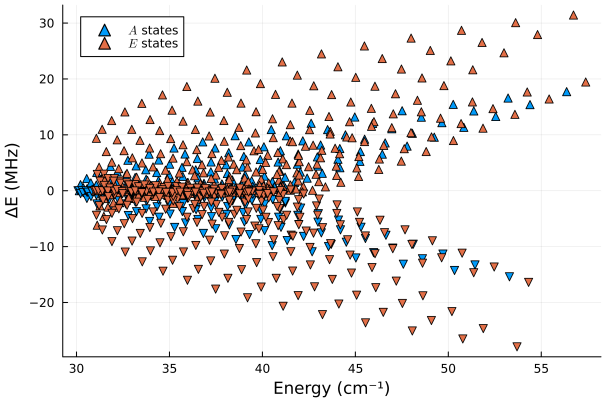

(b) $\epsilon_{gg}/B_{gg} = 5\%$

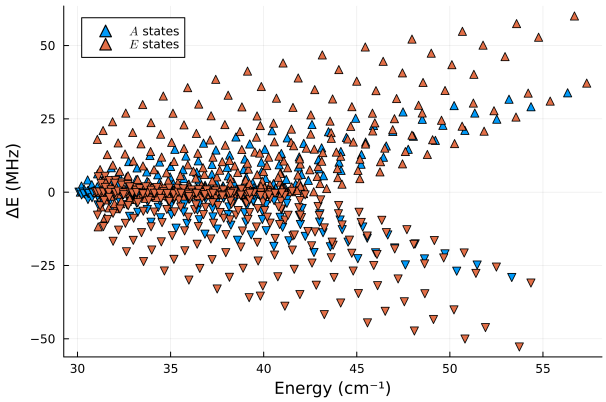

(c) $\epsilon_{gg}/B_{gg} = 10\%$ □

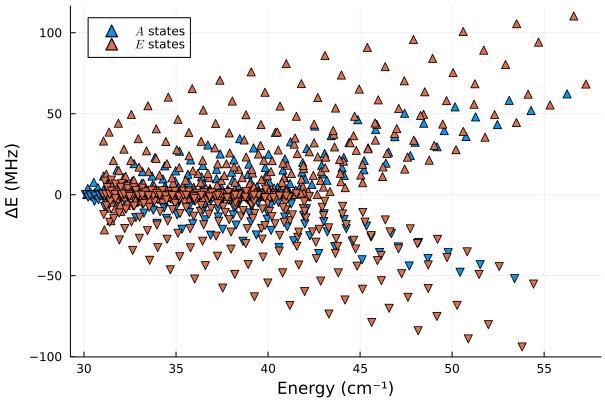

(d) $\epsilon_{gg}/B_{gg} = 20\%$

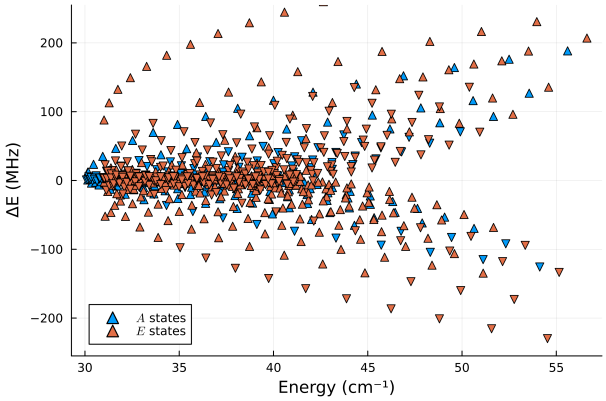

(e) $\epsilon_{gg}/B_{gg} = 100\%$

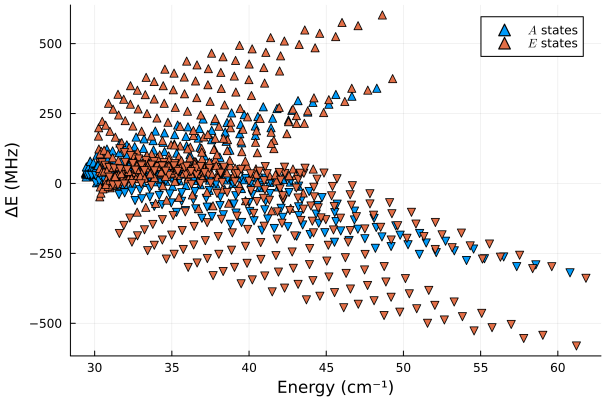

(f) $\epsilon_{gg}/B_{gg} = 1000\%$

FIGURE 5.10. The change in energy between including and excluding η in the second order Hamiltonian plotted against the state energies for six different ϵ_{gg}/B_{gg} values for only the $v_t = 0$ A and E states.

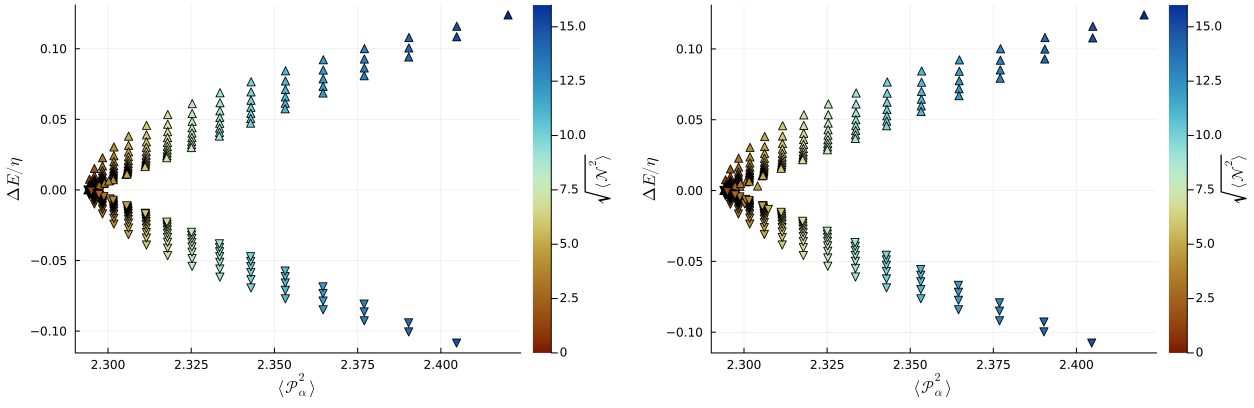

(a) $\epsilon_{gg}/B_{gg} = 1\%$

(b) $\epsilon_{gg}/B_{gg} = 5\%$

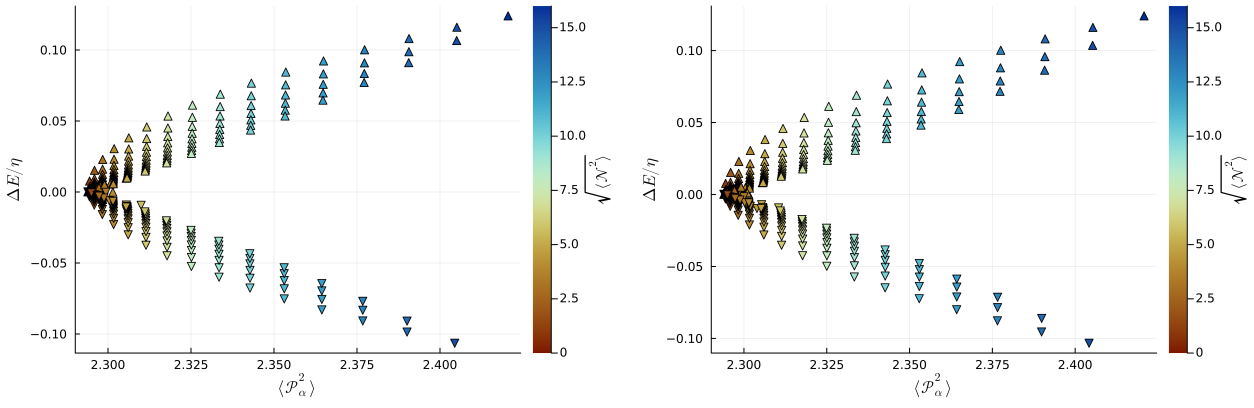

(c) $\epsilon_{gg}/B_{gg} = 10\%$ □

(d) $\epsilon_{gg}/B_{gg} = 20\%$

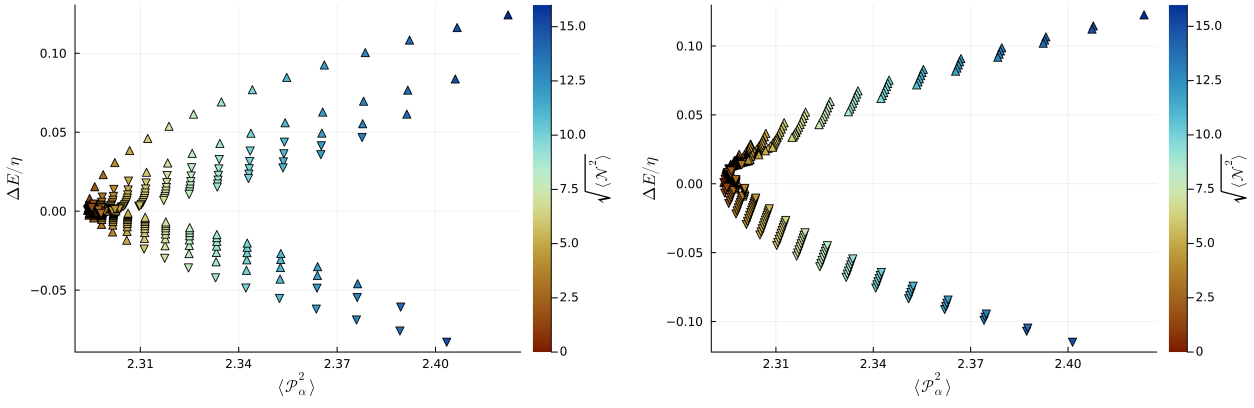

(e) $\epsilon_{gg}/B_{gg} = 100\%$

(f) $\epsilon_{gg}/B_{gg} = 1000\%$

FIGURE 5.11. The change in energy, in units of η, between including and excluding η in the second order Hamiltonian plotted against the $\langle \mathcal{P}_\alpha^2 \rangle$ for the ground A states for six different ϵ_{gg}/B_{gg} values. Subfigure c has 2 outliers cut off at this scale

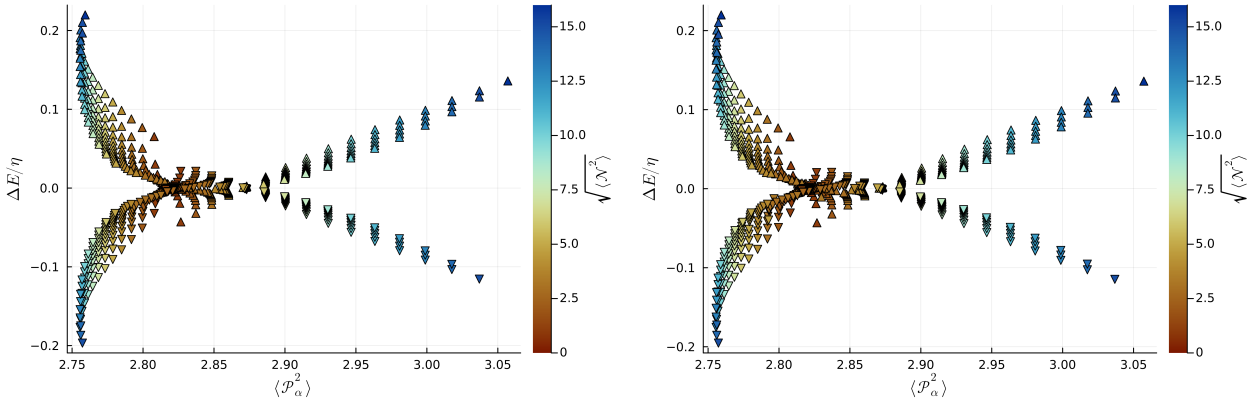

(a) $\epsilon_{gg}/B_{gg} = 1\%$

(b) $\epsilon_{gg}/B_{gg} = 5\%$

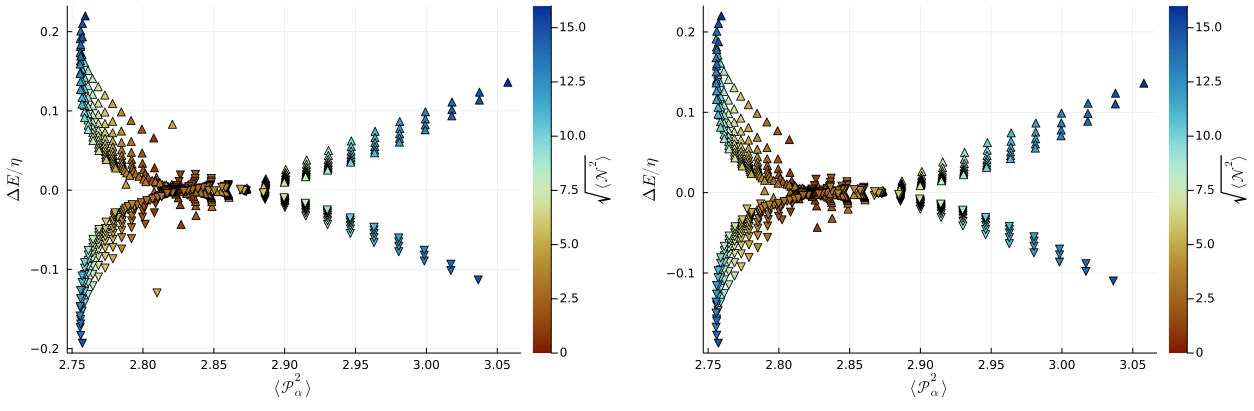

(c) $\epsilon_{gg}/B_{gg} = 10\%$ □

(d) $\epsilon_{gg}/B_{gg} = 20\%$

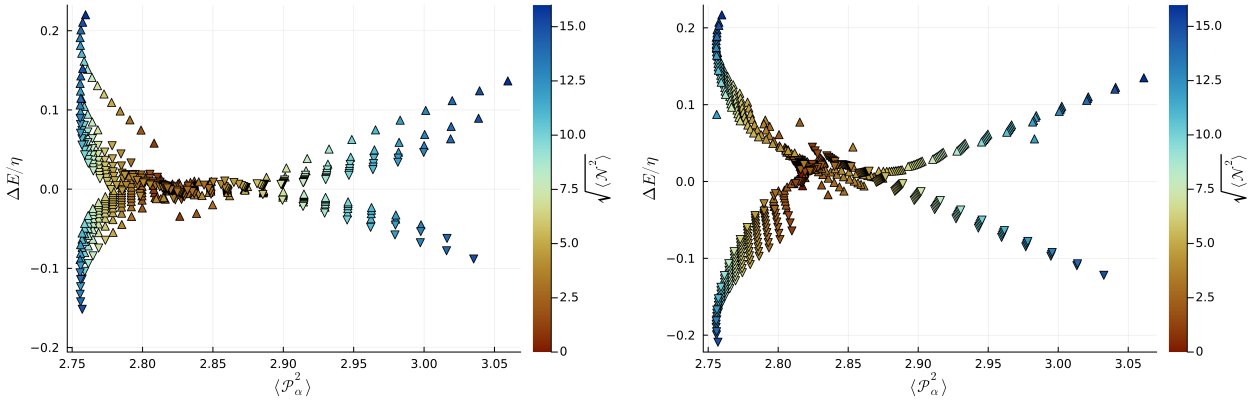

(e) $\epsilon_{gg}/B_{gg} = 100\%$

(f) $\epsilon_{gg}/B_{gg} = 1000\%$

FIGURE 5.12. The change in energy, in units of η, between including and excluding η in the second order Hamiltonian plotted against the $\langle \mathcal{P}_\alpha^2 \rangle$ for the ground E states for six different ϵ_{gg}/B_{gg} values. Panel c has been cropped to hide two outliers

approximate $|K|$ as well as the direction of the change being consistent with the sign of $J - N$. The overall magnitude is consistent across all ϵ_{gg}/B_{gg} values. In the A states, the same overall curvature is observed though there is a reduction in the spread of the energy changes along these curves. Subfigure 5.11e does disagree with trend of direction agreeing with the sign of $J - N$ likely due to the 1:1 ratio between the spin-rotation tensor and the inertial tensor causing a number of states to be assigned differently with and without η. Figure 5.12 focuses on the ground E states. The E states maintain their structure of 2 intersecting curves for $N = J + 1/2$ and $N = J - 1/2$ but with a similar tightening of the vertical spread to the A states, particularly in the $N = J + 1/2$ states. Outliers resulting from state assignment disagreement have been excluded from subfigure e for a clearer view of the trend. This assignment disagreements in subfigure e likely originate from the comparable orders of magnitude in the off-diagonal elements from the pure rotation and the spin-rotation operators. This would result in a more even distribution of basis state contributions thus increasing the difficulty of a confident singular assignment.

Figures 5.13–5.15 examine the interaction of the spin-torsion coupling and the barrier height, using V_3 values of 200, 100, 50, and 25 cm^{-1}. Reducing the barrier height from 200 cm^{-1} to 100 cm^{-1} shows a visible jump in the change in energy particularly in the $v_t > 0$ states. Subfigures d, e, and f unfortunately suffer from heavy state assignment disagreement as both their $v_t = 1$ and $v_t = 2$ A states are above the barrier height thus causing them to be closer to the free rotor basis states of $m = -3$ and $m = +3$ respectively. As they are degenerate in the free rotor limit, meaningfully distinguishing between them becomes increasingly difficult and futile. This leads to differing same quantum number assignment when η is and is not included. Figure 5.14 focuses on the ground A states and uses the same axes and highlighting as Figure 5.11. The change in energy in units of η decreases with the barrier height alongside the $\langle \mathcal{P}_\alpha^2 \rangle$ as V_3 approaches zero, the torsions behave more like free rotor states for which $\langle 0|\mathcal{P}_\alpha|0\rangle = 0$. Additionally since the torsional momentum is decreasing, so does the impact of the spin-torsion interaction. The overall shape of the energy changes is consistent across the different barrier heights. The E states show a more interesting evolution as is visible in Figure 5.15. The $N = J + 1/2$ states and the $N = J - 1/2$ states each form separate curves with an inflection point near $\langle \mathcal{N}_z^2 \rangle = 0$ and opposing sign to one

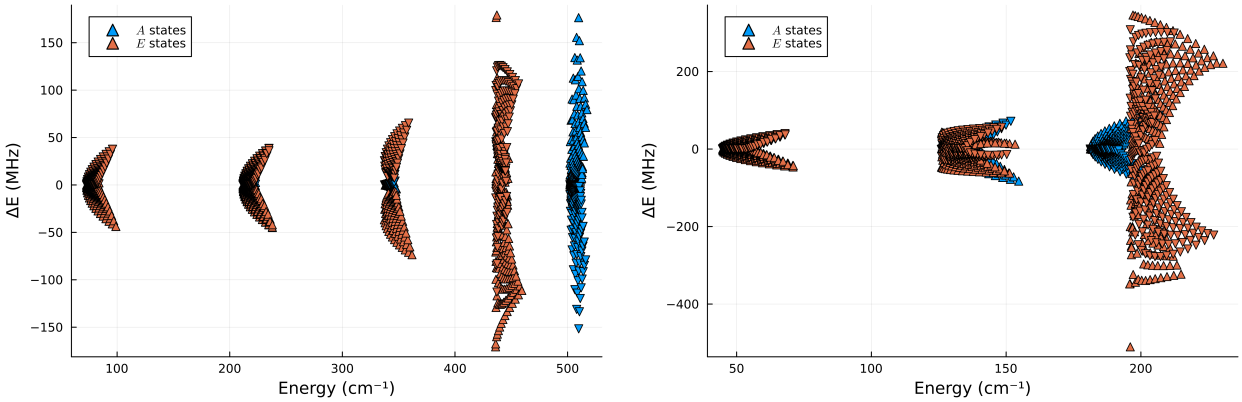

(a) $V_3 = 500$ cm^{-1}

(b) $V_3 = 200$ cm^{-1}

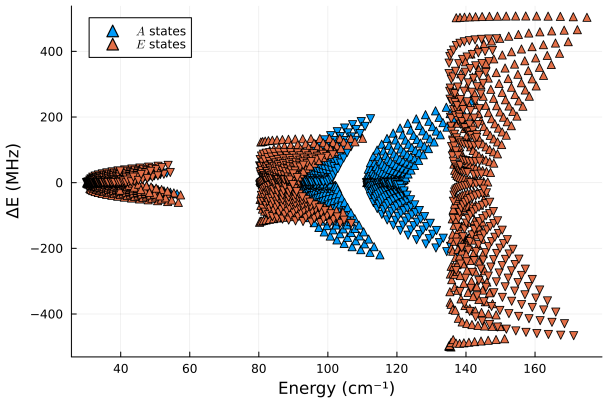

(c) $V_3 = 100$ cm^{-1} □

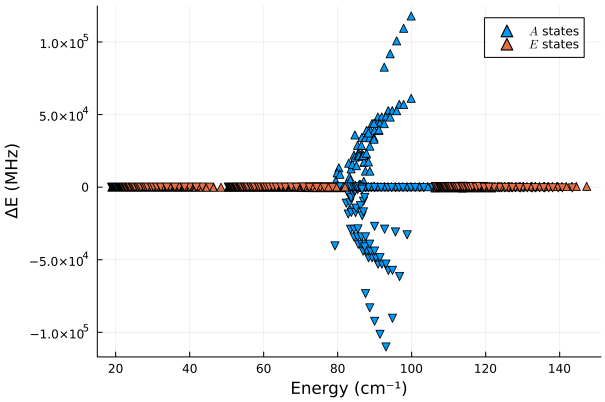

(d) $V_3 = 50$ cm^{-1}

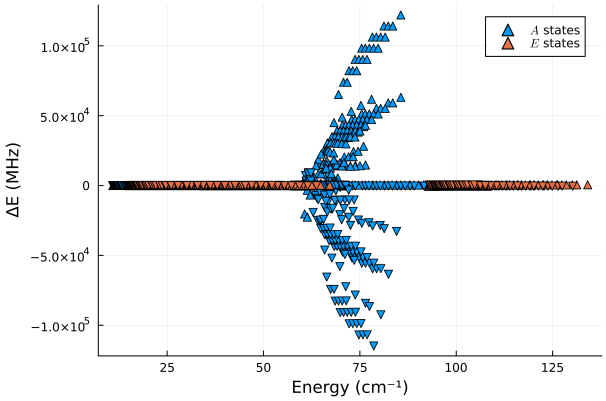

(e) $V_3 = 25$ cm^{-1}

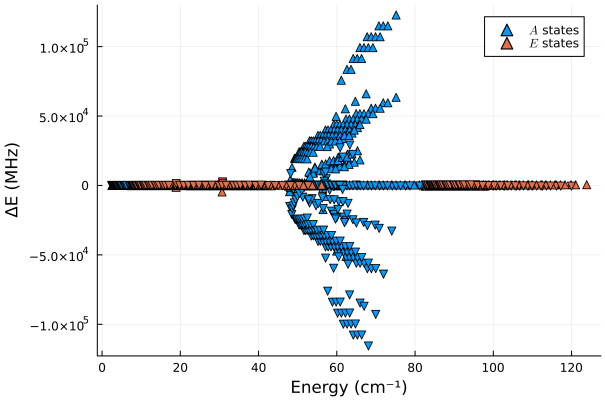

(f) $V_3 = 5$ cm^{-1}

FIGURE 5.13. The change in energy between including and excluding η in the second order Hamiltonian for six different V_3 values plotted against the state energies. The energetic impact increases from a to c but then d, e, and f suffer from too much state mixing of the excited torsional states for obvious visual trends to be concluded

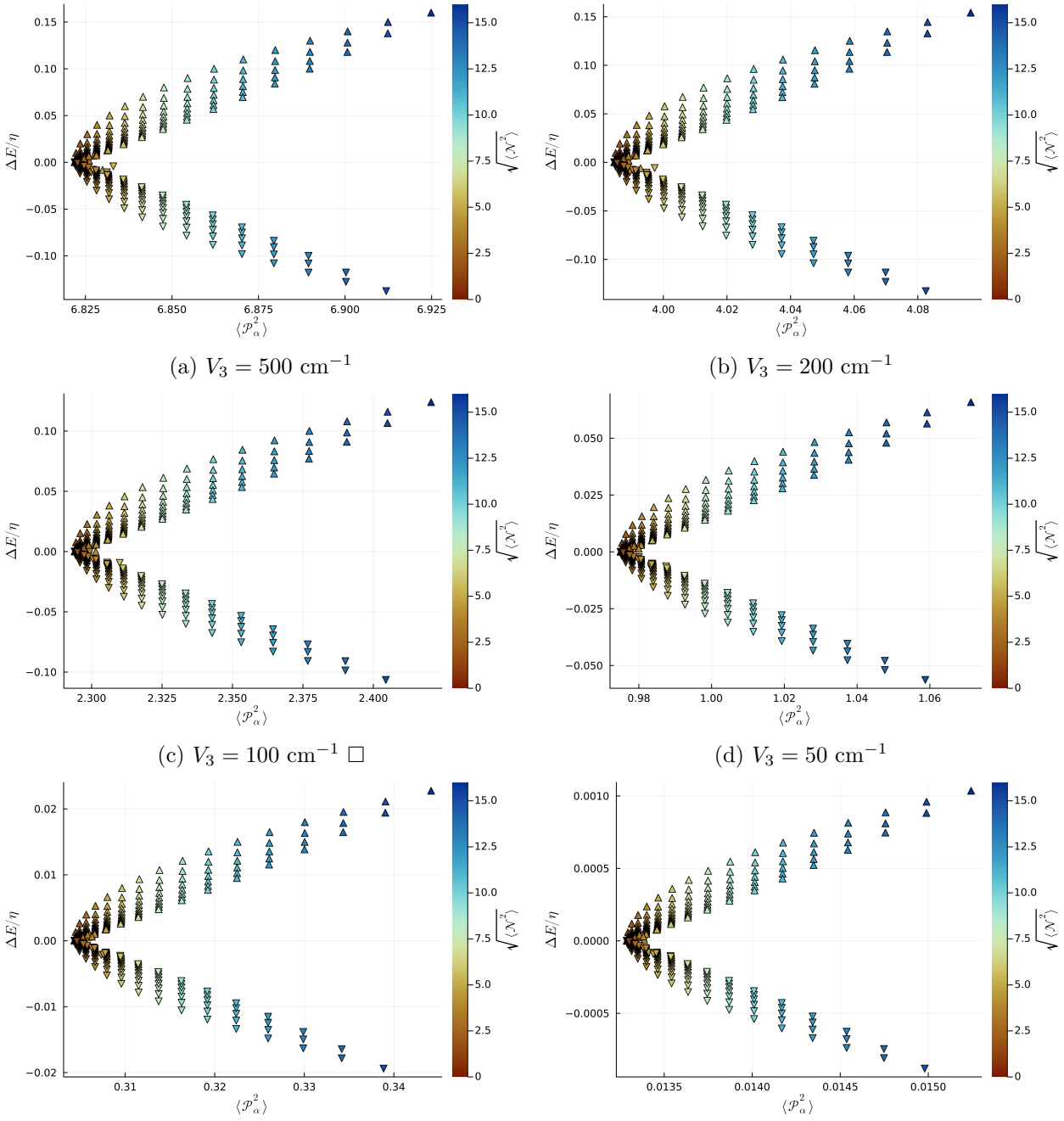

(a) $V_3 = 500$ cm^{-1}

(b) $V_3 = 200$ cm^{-1}

(c) $V_3 = 100$ cm^{-1} □

(d) $V_3 = 50$ cm^{-1}

(e) $V_3 = 25$ cm^{-1}

(f) $V_3 = 5$ cm^{-1}

FIGURE 5.14. The change in energy, in units of η, between including and excluding η in the second order Hamiltonian plotted against the $\langle \mathcal{P}_\alpha^2 \rangle$ for the ground A states for six different V_3 values

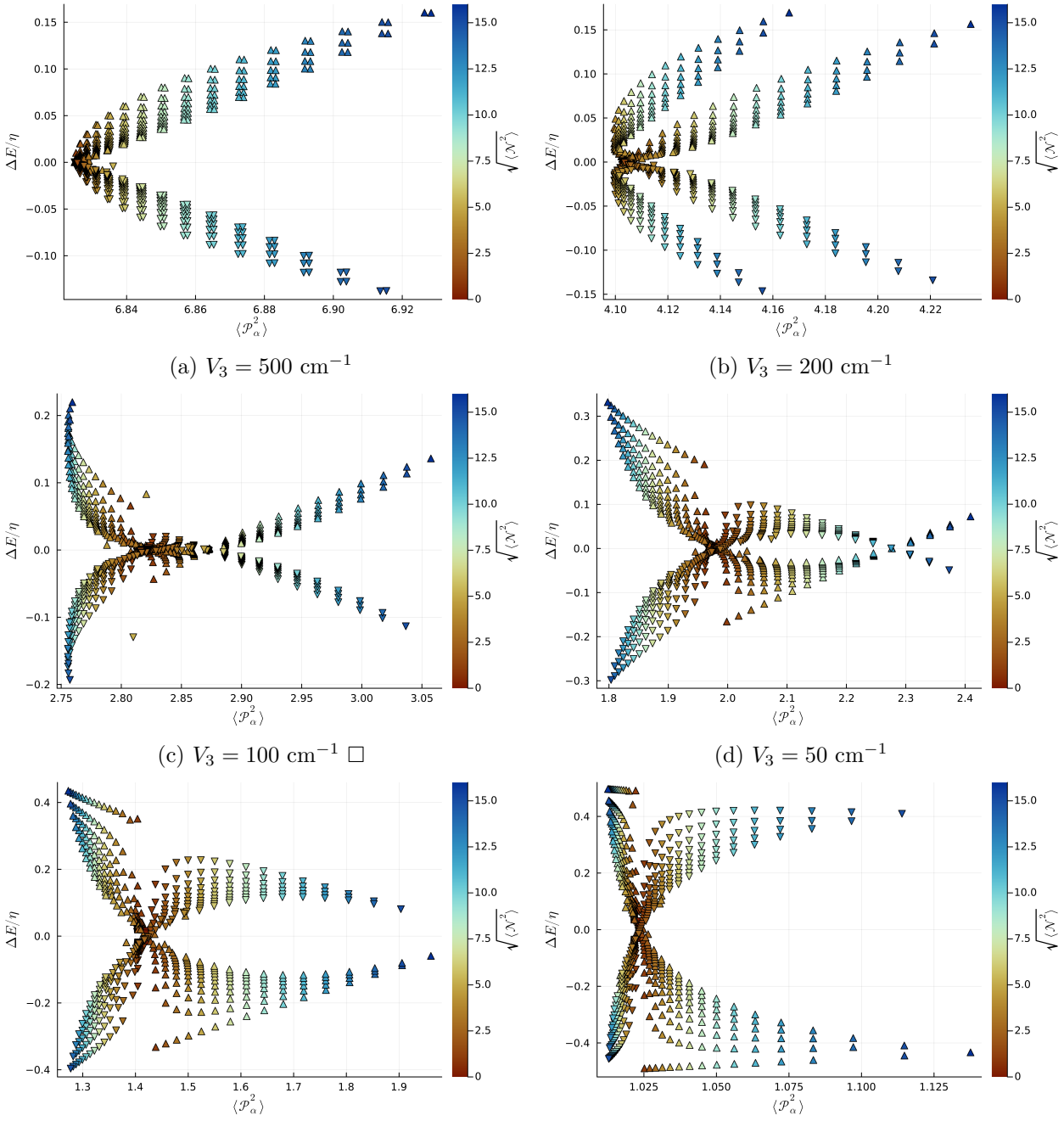

(a) $V_3 = 500$ cm^{-1}

(b) $V_3 = 200$ cm^{-1}

(c) $V_3 = 100$ cm^{-1} □

(d) $V_3 = 50$ cm^{-1}

(e) $V_3 = 25$ cm^{-1}

(f) $V_3 = 5$ cm^{-1}

FIGURE 5.15. The change in energy, in units of η, between including and excluding η in the second order Hamiltonian plotted against the $\langle \mathcal{P}_\alpha^2 \rangle$ for the ground E states for six different V_3 values

another. As V_3 decreases, these curves widen and begin to have a crossing at both low $\langle \mathcal{N}_z^2 \rangle$ and high $\langle \mathcal{N}_z^2 \rangle$ when $\langle \mathcal{P}_\alpha^2 \rangle$ has also increased. Unlike the A states, the magnitude of the energy change increases was V_3 decreases. Figures 5.7a and 5.7b are visually quite consistent with the results of Figures 5.14 and 5.15.

Lastly, the interplay of the torsion-rotation coupling term ρ, and the spin-torsion coupling term η have been inspected. The values of ρ were stepped across 0.01, 0.02, 0.04, 0.06, 0.08, and 0.1 while all other parameters were held fixed. While there have been ρ values as high as 0.7 [**69**] in the case of methanol, the range was capped at 0.1 as $\rho \approx A/F$ and the state assignments using higher ρ values were very inconsistent between the inclusion and exclusion of η. Additionally, only positive values of ρ were used as the term is defined such that $-2F\rho < 0$ [**46**]. The direct comparison of the energy levels is shown in Figure 5.16, revealing much more dramatic changes across the ρ span as the spread of energy levels changes much more than in the rotation and spin-rotation tests. The amount of divergence in all but the $v_t = 2$ E states increases with ρ. The $v_t = 2$ E states remain consistent in the differences across each ρ value. The comparisons of the ground A states are shown in Figure 5.17. These energetic differences show a consistent structure with Figures 5.11 and 5.14. The spread of energy differences in units of η increases as ρ increases. It can also be seen that the $\langle \mathcal{P}_\alpha^2 \rangle$ values also drift upward with ρ. This helps physically justify the the connection between ρ and η as it makes sense that a parameter that can increase the torsional momentum would thus increase the spin-torsion coupling. Continuing the trend, the E states show a much more dynamic sequences of changes in Figure 5.18. The decreased torsional-rotation coupling of subfigure a resembles the lower barrier cases of Figure 5.15. Increasing ρ begins to make E states resemble the curve of the A states.

From this prolonged sequence of figures, it is clear that the impact of the spin-torsion interaction is most sensitive to changes in barrier height and torsion-rotation coupling. While the energy levels did change visibly as the spin-rotation tensor was increased, the proportional impact of the coupling remained generally consistent. The changes in κ did not produce noticeable changes. V_3 typically has the largest off-diagonal elements of the operators in the second order Hamiltonion which causes this parameter to have a large impact on the expectation values of all other operators

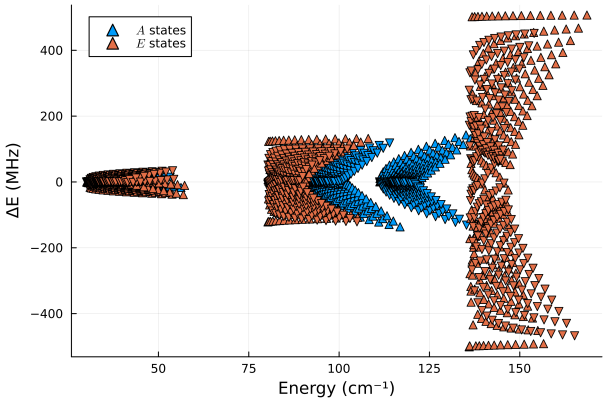

(a) $\rho = 0.01$, $-2F\rho = -3059.1$, MHz

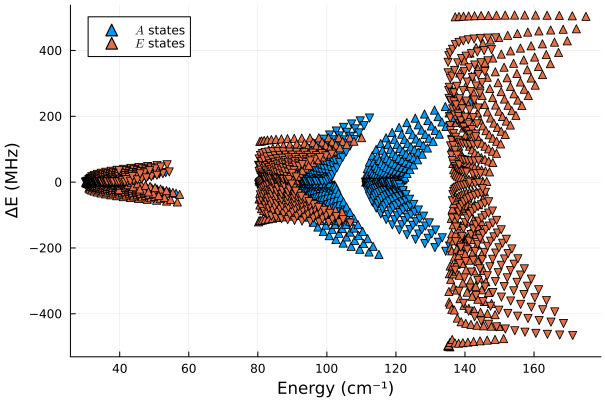

(b) $\rho = 0.02$, $-2F\rho = -6118.2$ MHz □

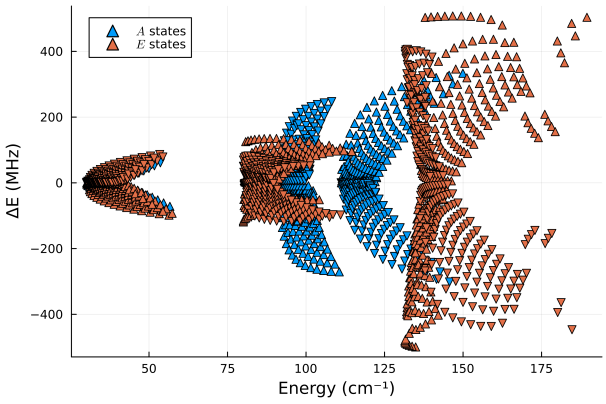

(c) $\rho = 0.04$, $-2F\rho = -12237.$ MHz

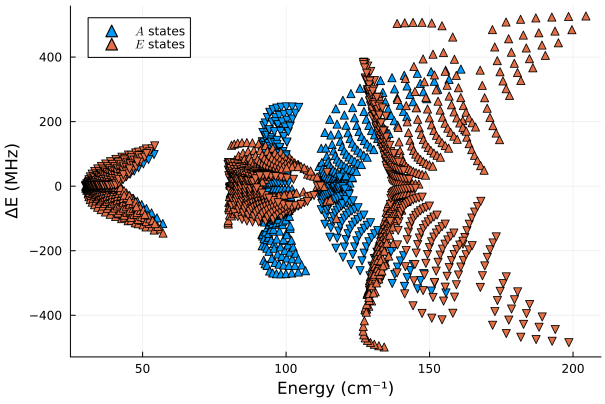

(d) $\rho = 0.06$, $-2F\rho = -18355.$ MHz

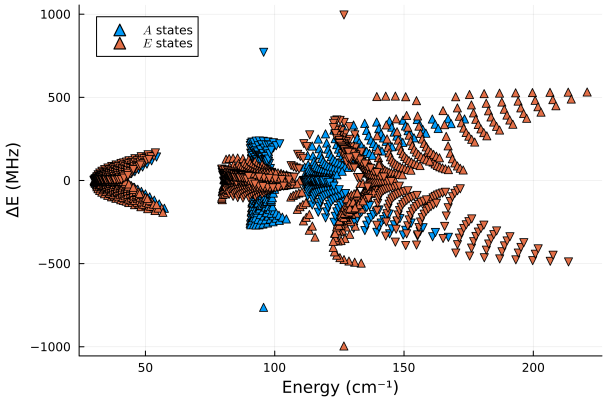

(e) $\rho = 0.08$, $-2F\rho = -24473.$ MHz

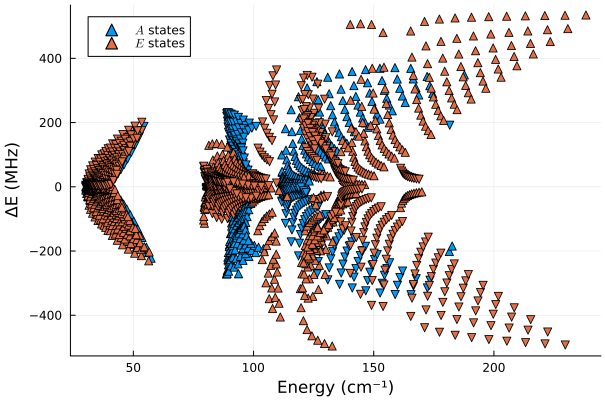

(f) $\rho = 0.1$, $-2F\rho = -30591.$ MHz

FIGURE 5.16. The change in energy between including and excluding η in the second order Hamiltonian for six different ρ values plotted against the state energies

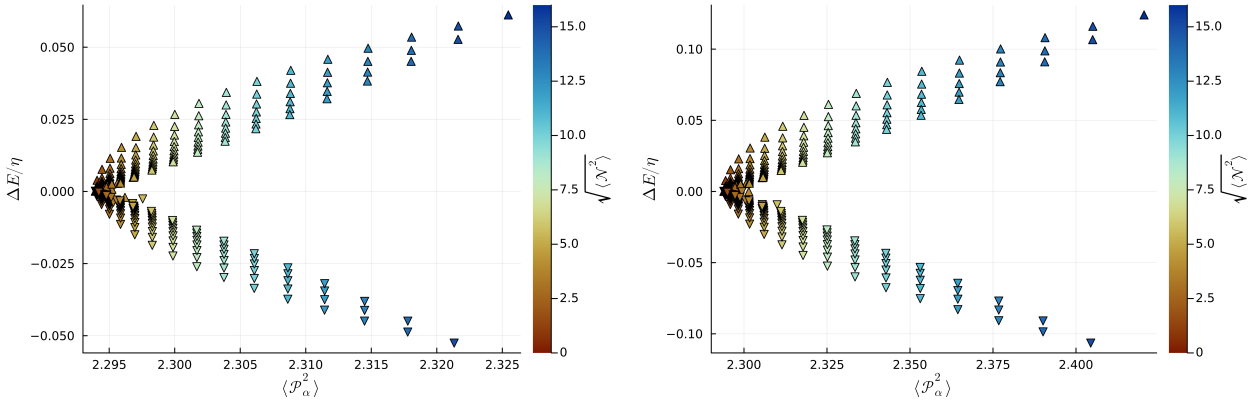

(a) $\rho = 0.01$, $-2F\rho = -3059.1$, MHz

(b) $\rho = 0.02$, $-2F\rho = -6118.2$ MHz □

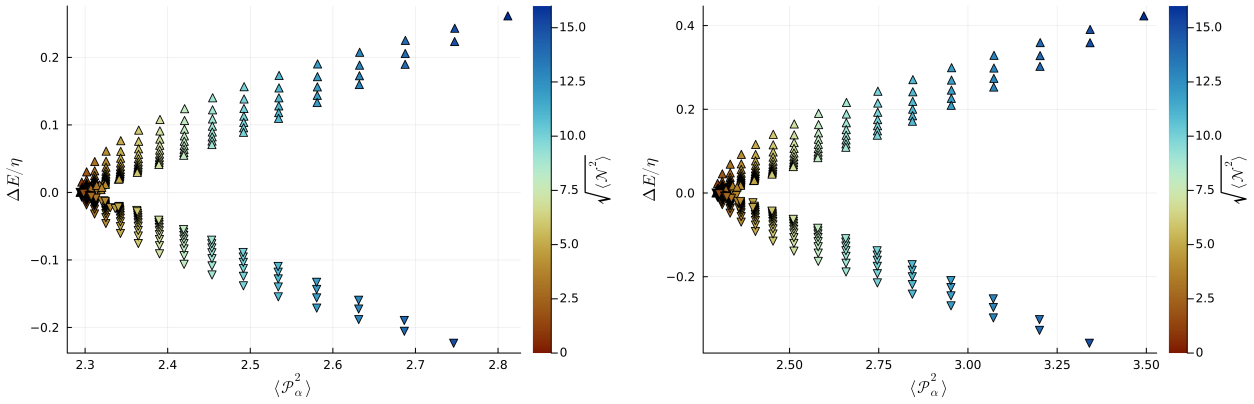

(c) $\rho = 0.04$, $-2F\rho = -12237.$ MHz

(d) $\rho = 0.06$, $-2F\rho = -18355.$ MHz

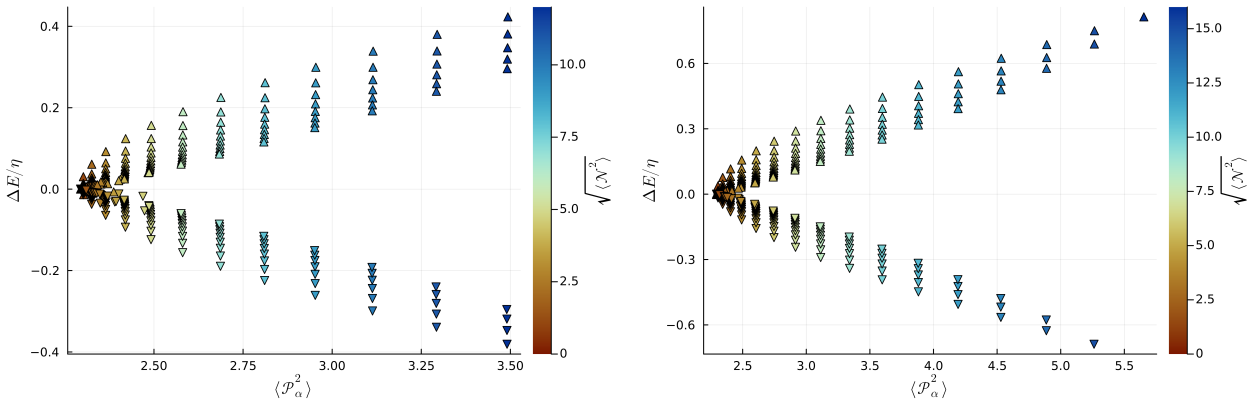

(e) $\rho = 0.08$, $-2F\rho = -24473.$ MHz

(f) $\rho = 0.1$, $-2F\rho = -30591.$ MHz

FIGURE 5.17. The change in energy, in units of η, between including and excluding η in the second order Hamiltonian plotted against the $\langle \mathcal{P}_\alpha^2 \rangle$ for the ground A states for six different ρ values. The magnitude of the interaction increases with ρ

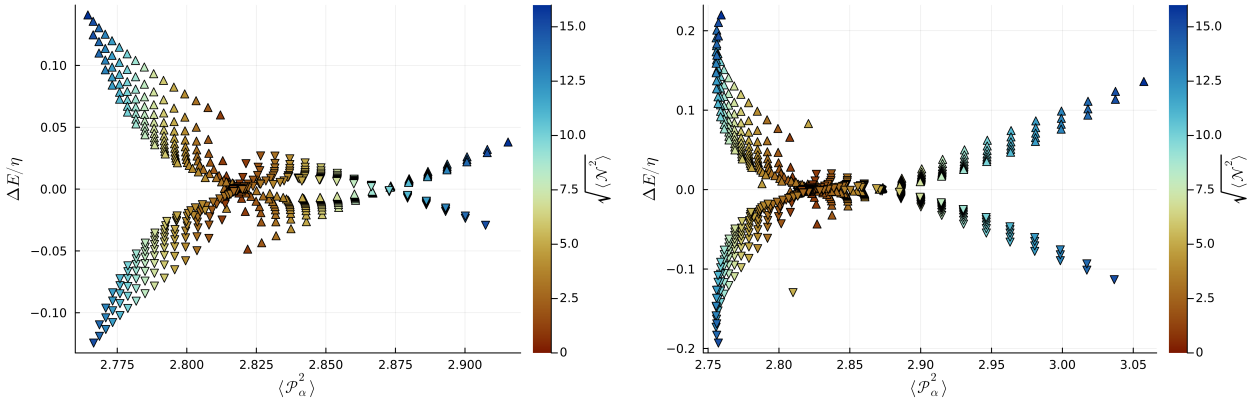

(a) $\rho = 0.01$, $-2F\rho = -3059.1$, MHz

(b) $\rho = 0.02$, $-2F\rho = -6118.2$ MHz □

(c) $\rho = 0.04$, $-2F\rho = -12237.$ MHz

(d) $\rho = 0.06$, $-2F\rho = -18355.$ MHz

(e) $\rho = 0.08$, $-2F\rho = -24473.$ MHz

(f) $\rho = 0.1$, $-2F\rho = -30591.$ MHz

FIGURE 5.18. The change in energy, in units of η, between including and excluding η in the second order Hamiltonian plotted against the $\langle \mathcal{P}_\alpha^2 \rangle$ for the ground E states for six different ρ values

that act on the torsional part of the wavefunction. The parameters ρ and V_3 each pull the $\langle \mathcal{P}_\alpha^2 \rangle$ in opposing directions so the impact of η positively correlated with ρ and negatively correlated with V_3. Because the free rotor basis has large off-diagonal elements compared with the diagonal values at low m, it can make clear state assignment difficult and causes heavy alteration to the expectation values of the on-diagonal operators like $\mathcal{P}_\alpha$. The resulting impact on the expectation values of the torsional angular momentum then heavily shapes how much the spin-torsion interaction alters the spin-torsion-rotation energy levels. As an additional note, the convenience gained from being able to consistently assign states across heavy changes to the second order parameter values has been demonstrated here. A number of the comparisons could have been made far more directly had the assignments been more consistent. Future work will involve efforts to implement more consistent and robust assignment routines.

5.6. Theoretical Spectrum of meta-Methyl-Phenoxyl

Using the parameters listed in Table 5.2, the spin-torsion-rotation spectrum was simulated at 10 K from 0.5–40.0 GHz and the transitions were convolved with a Lorentzian of width 0.4 MHz. This spectrum included up to $J = 51/2$ using only $v_t = 0$ as the ground torsional state is more readily observed in typical microwave experiments. Figure 5.19 shows the broadband simulated spectrum both with and without the spin-torsion coupling parameter. The two spectra look similar with only minor visually distinguishable features at this scale. This agrees with the predictions from the examination of the energy levels that η would generally not have a heavy impact on the spectrum. Figure 5.20 shows a segment of the spectrum from 10.88–11 GHz with separate highlighting for the A and E symmetries as well as a difference of the intensity with and without η at each frequency. Most of the transitions in this region are at least slightly offset as visible by the non-zero differences. Generally these frequency differences are slight resulting in sharp shifts from positive to negative or the reverse. As the transitions do not shift in a uniform direction or amount, it is clear the spin-torsion interaction has a greater impact than simply red or blue shifting the spectrum. The strongest two transitions are the $\frac{8}{2}\,4_{0,4} - \frac{7}{2}\,3_{0,3}$ A-E doublet. This pair is only subtly shifted by inclusion of explicit spin-torsion coupling. The two lowest frequency transitions are the A-E pair of $\frac{19}{2}\,10_{2,8} - \frac{19}{2}\,10_{1,9}$ which are each red-shifted by about half a MHz. The transition that

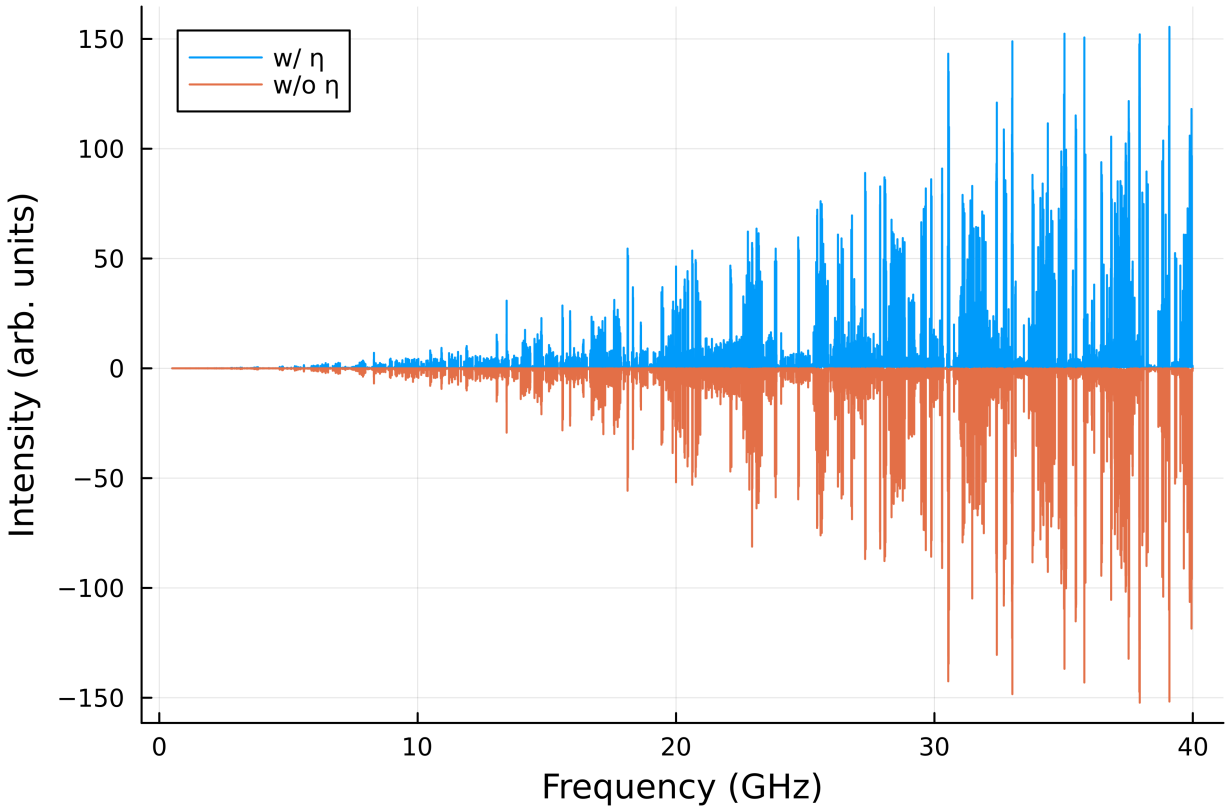

FIGURE 5.19. A broadband plot of the simulated spectrum of m-MePhO at 10 K from 0.5–40.0 GHz. The top spectrum includes the spin-torsion coupling parameter while the bottom one does not. At this view, the impact of the parameter cannot be seen.

is the most displaced is the $E\ \frac{7}{2}\,3_{2,1} - \frac{5}{2}\,3_{0,3}$ which is red-shifted by 1.44 MHz. This transition has the highest K_a relative to N and is consistent with the trend of the spin-torsion coupling being sensitive to $\langle \mathcal{N}_z^2 \rangle$.

Figure 5.21 shows another insert from 25.54–25.74 GHz. In comparison to the previous insert, the transitions here appear to be more impacted by η as seen in the difference spectrum's lineshapes. These difference lines have more tail shape than the lower frequency sample. The four strongest transitions are the A-E doublets of, in order of increasing frequency: $\frac{21}{2}\,10_{1,10} - \frac{19}{2}\,9_{1,9}$, $\frac{19}{2}\,10_{1,10} - \frac{17}{2}\,9_{1,9}$, $\frac{21}{2}\,10_{0,10} - \frac{19}{2}\,9_{0,9}$, and $\frac{19}{2}\,10_{0,10} - \frac{17}{2}\,9_{0,9}$. All of these are shifted minimally by η as evidenced by the very low difference intensities at their frequencies. A more dramatically shifted transition is the $E\ \frac{17}{2}\,9_{46} - \frac{15}{2}\,7_{53}$ which is redshifted by 11.7 MHz.

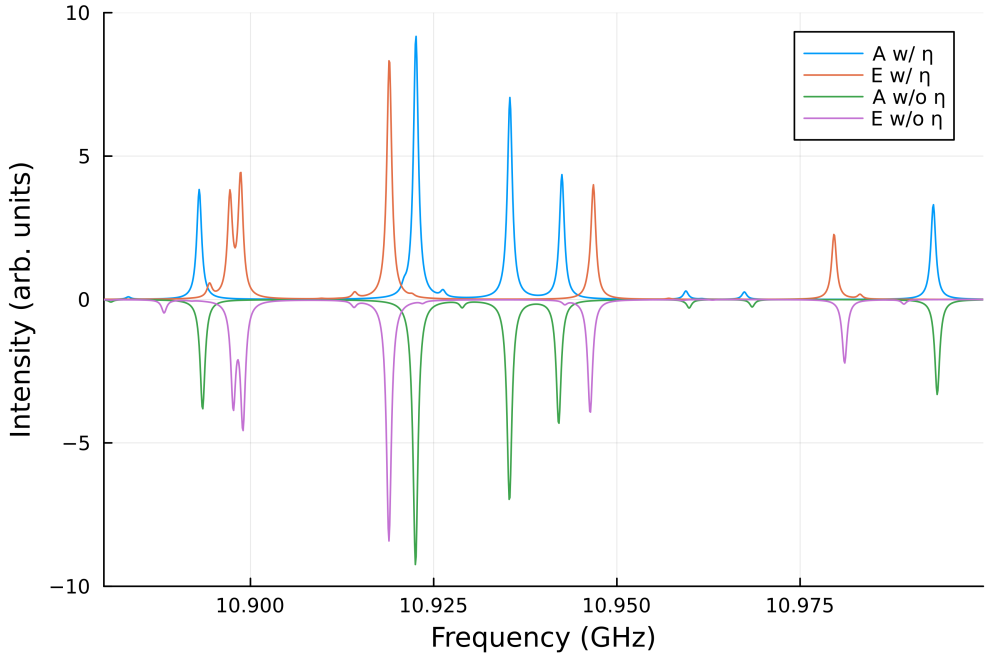

(a) me-MePhO's simulated spectrum from 10.88–11 GHz with separate highlighting for A and E states

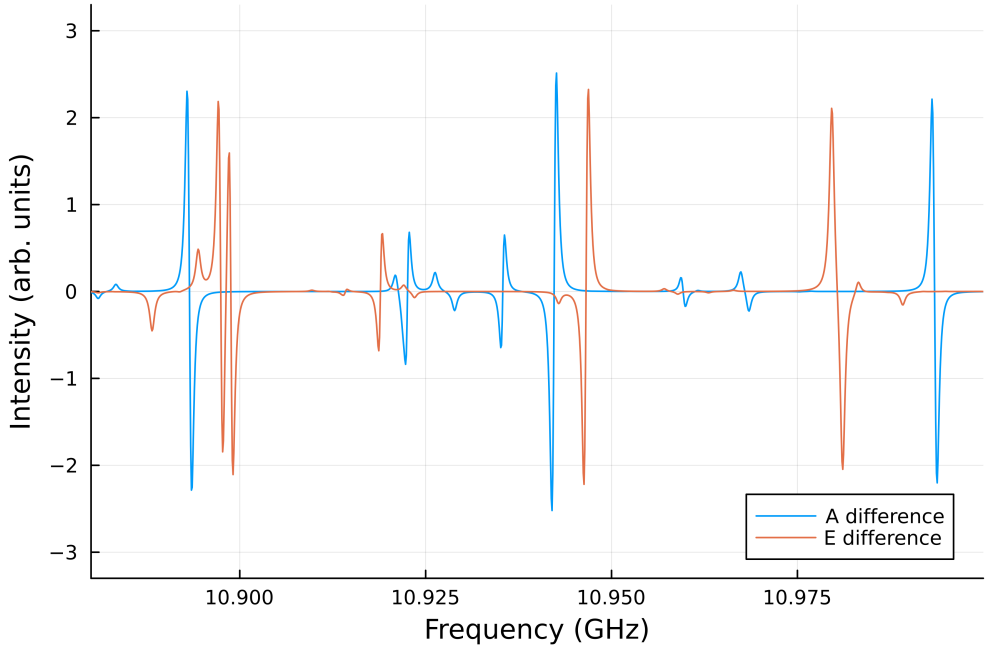

(b) Difference between the $\eta \neq 0$ and $\eta = 0$ spectra from 10.88–11 GHz

FIGURE 5.20. A low frequency segment of the meta-methyl-phenoxyl's simulated spectrum to focus on transitions around $N = 4$

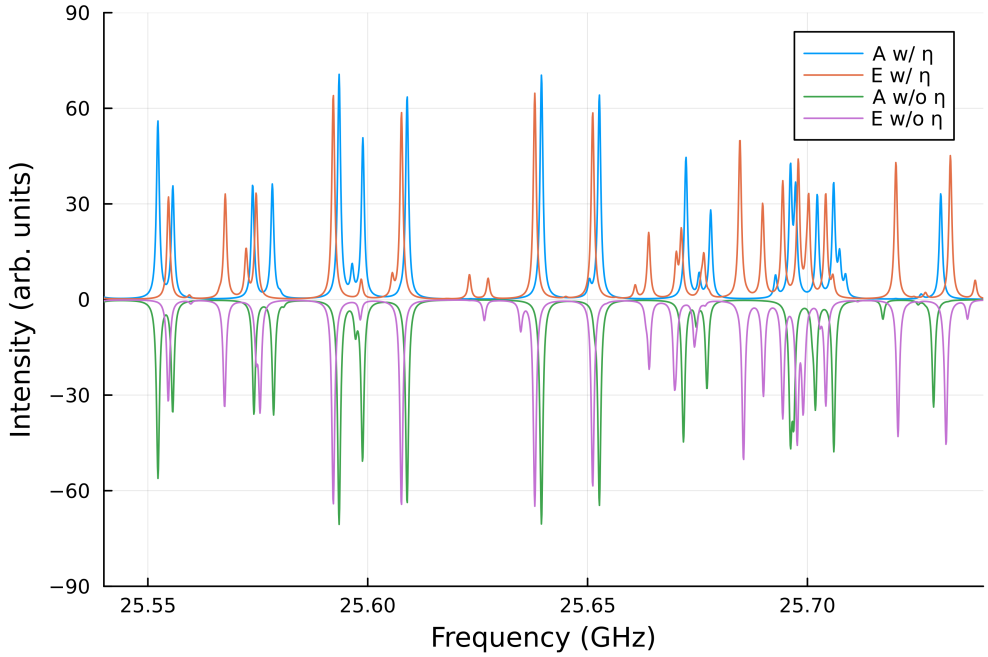

(a) me-MePhO's simulated spectrum from 25.54–25.74 GHz with separate highlighting for A and E states

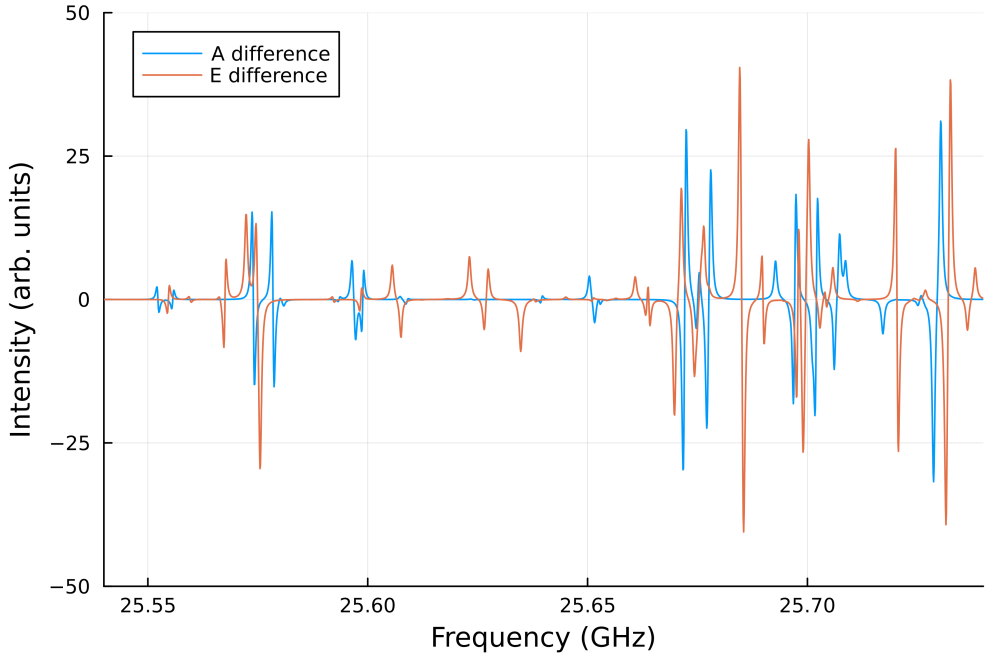

(b) Difference between the $\eta \neq 0$ and $\eta = 0$ spectra from 25.54–25.74 GHz

FIGURE 5.21. A spectral insert showing a 200 MHz window from 25.54–25.74 GHz of me-MePhO's simulated spectrum to focus the view around $N = 10$

Lastly, Figure 5.22 shows the spectrum and difference from 37–37.145 GHz. The impact of the spin-torsion operator is more apparent here as there are more gradual shifts from positive to negative or the reverse in the difference spectrum. The four strongest peaks in the cluster around 37.1 GHz are the A-E pairs of $\frac{27}{2}\,13_{6,7} - \frac{25}{2}\,12_{6,6}$ and $\frac{27}{2}\,13_{6,8} - \frac{25}{2}\,12_{7,6}$. These transitions are shifted by less than half a megahertz. From these inserts, the impact of spin-torsion interaction on the spin-torsion-rotation spectrum is subtle and persistent. Being neither a consistent nor uniform amount of shift, it seems unlikely that fits, particularly those of increasing K_a, without the explicit coupling operator would be able to achieve satisfactory results.

5.7. Conclusion

The spin-torsion operator and its coefficient have been derived in order to expand the Rho Axis Method to include radicals with methyl rotors. The operator's connection to other terms in the second order Hamiltonian was also explored and a particular connection to the potential barrier height was found. The strong linkage between the spin-torsion coupling and potential barrier results from the barrier having a heavy influence on the expectation values of the torsional angular momentum and creating large deviations from the values of the basis states. Additionally, as with many other second order operators, it has a much larger impact on the E states in the ground torsional state. The spectral simulations showed a clear spectral shift as a result of the spin-torsion coupling though future experimental efforts will be necessary to determine the magnitude of this shift. The program and work discussed here should provide a initial basis for the experimental spectroscopists interested in the rotational spectra of complex organic radicals. This work provides a strong motivation for future ab initio calculation of η and exploring its relationship to electronic and molecular structure.

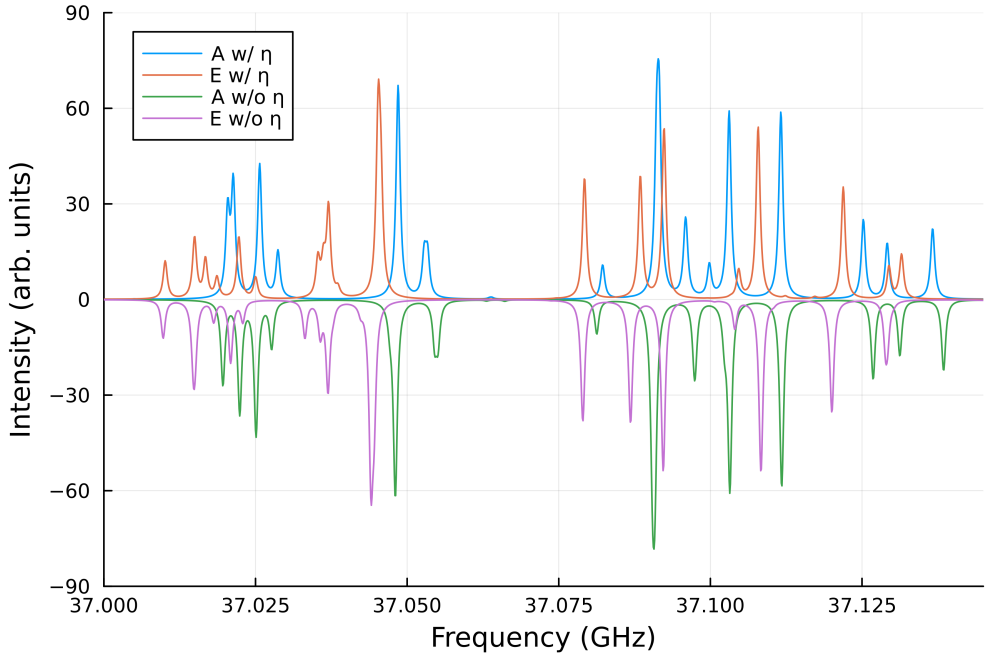

(a) me-MePhO's simulated spectrum from 37–37.145 GHz with separate highlighting for A and E states

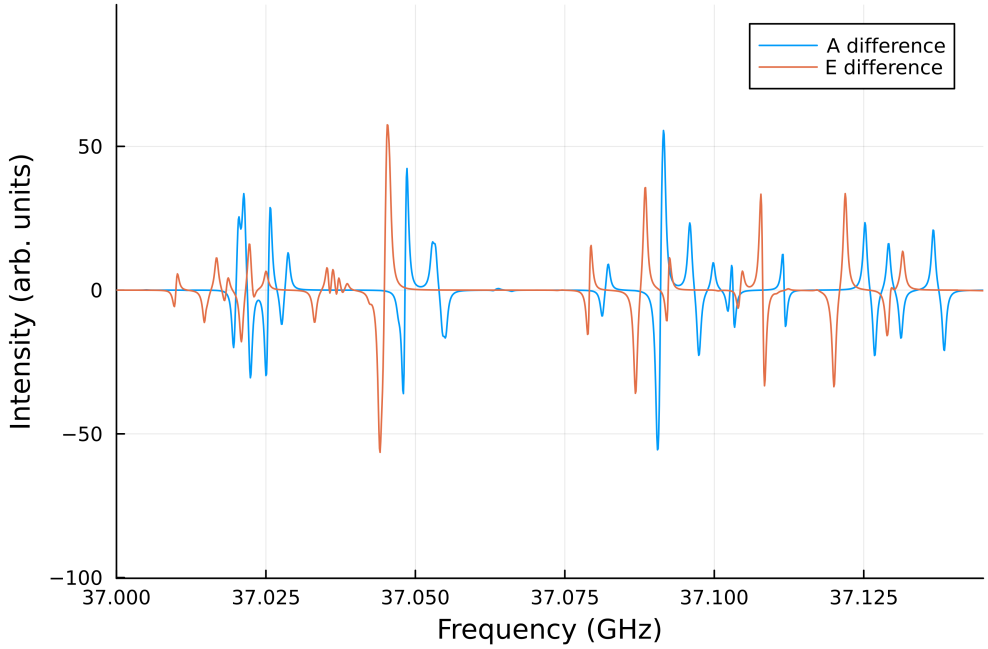

(b) Difference between the $\eta \neq 0$ and $\eta = 0$ spectra from 37–37.145 GHz

FIGURE 5.22. A spectral insert showing a 145 MHz window from 37–37.145 GHz of me-MePhO's simulated spectrum to focus the view around $N = 13$

APPENDIX A

Extended Tables for MTBE

TABLE A.1. MP2/cc-pVDZ Coordinates of Methyl tert-Butyl Ether.

atom	x (Å)	y (Å)	z (Å)
C	−2.57302284	−0.95790007	−0.00000000
C	−1.23333798	−0.24671976	−0.00000000
x	−1.23333798	−0.24671976	1.00000160
H	−3.40508236	−0.23369191	−0.00000000
H	−2.67767003	−1.60213944	−0.89183846
H	−2.67767003	−1.60213944	0.89183846
C	−0.04835568	−1.01059928	−0.00000000
C	−1.15087574	1.15874933	−0.00000000
C	1.29476127	1.04598901	0.00000000
C	1.20894242	−0.36763645	0.00000000
C	0.10635458	1.79046199	0.00000000
H	−0.08652130	−2.10555105	0.00000000
H	−2.06756859	1.75896848	0.00000000
O	2.33084406	−1.09925466	−0.00000000
H	0.16921487	2.88491013	0.00000000
H	2.27632313	1.52906514	0.00000000

TABLE A.2. MP2/cc-pVDZ Harmonic Frequencies of Methyl tert-Butyl Ether

Sym	Freq (cm^{-1})	Intensity (km/mol)	Sym	Freq (cm^{-1})	Intensity (km/mol)
A''	17.7966	2.3981	A''	1389.0635	20.6239
A''	178.9342	1.0957	A'	1395.4595	18.5168
A''	238.7002	1.3775	A'	1412.8939	11.2332
A'	262.8777	0.3777	A''	1465.4034	0.0056
A''	293.7098	1.7324	A'	1471.4836	0.7096
A'	295.9728	0.4568	A''	1479.8989	0.0435
A''	342.6826	0.9321	A'	1484.1250	0.5094
A'	368.8281	0.7681	A''	1490.5040	4.7336
A'	412.9177	0.3557	A'	1497.9752	1.9680
A''	459.8673	6.2739	A''	1505.1709	0.5346
A'	509.0937	1.6176	A'	1514.8823	4.2789
A'	746.6642	5.0142	A'	1522.0329	14.4523
A'	891.1843	14.2625	A'	3054.3266	48.5046
A''	926.7454	0.0106	A''	3084.2111	12.9458
A'	938.1635	0.1046	A'	3086.8468	20.7724
A''	949.3175	0.0580	A'	3091.2850	5.2736
A''	1037.2536	1.8054	A''	3132.0361	58.1400
A'	1040.5070	1.3611	A''	3184.7151	1.3420
A'	1144.7351	80.8842	A'	3187.4378	38.0730
A''	1180.8001	2.0309	A'	3189.8936	4.9988
A'	1207.1908	0.9203	A''	3190.3563	2.8394
A'	1246.5976	107.1851	A'	3193.5805	32.0901
A''	1276.7574	16.2938	A''	3197.5203	22.6845
A'	1304.3221	10.5343	A'	3198.9383	37.3701

TABLE A.3. Fit Results of Methyl tert-Butyl Ether

Transitions used in 3.4																		
N'	K'_a	K'_c	N''	K''_a	K''_c	σ	$Obs(MHz)$	$Calc(MHz)$	N'	K'_a	K'_c	N''	K''_a	K''_c	σ	$Obs(MHz)$	$Calc(MHz)$
2	0	2	1	1	0	1	9271.875	9271.872	7	1	6	6	2	5	1	33317.436	33317.422
2	0	2	1	1	1	0	9275.771	9275.774	4	4	1	3	3	1	1	33407.771	33407.768
2	0	2	1	1	1	1	9278.244	9278.239	4	4	1	3	3	0	0	33411.772	33411.771
2	1	2	1	1	1	0	10924.637	10924.640	12	9	3	11	10	1	0	34169.763	34169.753
2	1	2	1	1	1	1	10925.513	10925.510	12	9	4	11	10	2	1	34174.806	34174.813
2	0	2	1	0	1	1	10926.277	10926.274	9	4	5	8	5	3	1	34303.536	34303.540
2	0	2	1	0	1	0	10926.301	10926.301	9	4	5	8	5	3	0	34305.478	34305.478
2	1	1	1	1	0	1	10927.009	10927.008	9	4	6	8	5	4	1	34309.549	34309.550
2	1	1	1	1	0	0	10927.930	10927.931	6	1	6	5	0	5	0	34412.608	34412.608
2	1	2	1	0	1	1	12573.544	12573.545	6	1	6	5	0	5	1	34412.279	34412.268

Continuation of MTBE Transitions																		
N'	K'_a	K'_c	N''	K''_a	K''_c	σ	$Obs(MHz)$	$Calc(MHz)$	N'	K'_a	K'_c	N''	K''_a	K''_c	σ	$Obs(MHz)$	$Calc(MHz)$
2	1	2	1	0	1	0	12575.166	12575.167	11	11	0	11	10	1	1	34683.653	34683.649
2	1	1	1	0	1	1	12581.408	12581.409	11	11	0	11	10	1	0	34683.653	34683.652
3	0	3	2	1	1	1	14734.253	14734.253	12	11	1	12	10	2	1	34681.521	34681.521
3	0	3	2	1	2	0	14740.564	14740.564	12	11	1	12	10	2	0	34681.521	34681.524
3	0	3	2	1	2	1	14742.120	14742.117	11	11	1	11	10	2	1	34678.317	34678.325
2	2	1	1	1	0	1	15870.569	15870.576	12	11	2	12	10	3	1	34676.209	34676.205
2	2	1	1	1	1	1	15876.941	15876.943	14	11	4	14	10	4	0	34676.737	34676.736
2	2	1	1	1	0	0	15879.502	15879.506	14	11	3	14	10	4	1	34676.737	34676.734
2	2	0	1	1	1	0	15881.150	15881.153	13	11	3	13	10	4	1	34673.873	34673.909
2	2	0	1	1	0	1	15882.864	15882.865	15	11	5	15	10	5	0	34674.075	34674.077
2	2	0	1	1	1	1	15889.233	15889.232	15	11	4	15	10	5	1	34674.075	34674.075
3	1	3	2	1	2	0	16386.942	16386.941	16	11	6	16	10	6	0	34671.243	34671.241
3	1	3	2	1	2	1	16387.520	16387.518	16	11	5	16	10	6	1	34671.243	34671.239
3	0	3	2	0	2	1	16389.390	16389.389	15	11	5	15	10	6	1	34668.794	34668.788
3	0	3	2	0	2	0	16389.431	16389.430	17	11	6	17	10	7	1	34668.227	34668.226
3	1	2	2	1	1	1	16391.221	16391.221	17	11	7	17	10	7	0	34668.227	34668.228
3	1	2	2	1	1	0	16391.876	16391.877	16	11	6	16	10	7	1	34665.960	34665.963
4	1	4	3	2	1	0	16890.314	16890.309	18	11	7	18	10	8	1	34665.039	34665.036
4	1	3	3	2	2	0	16906.767	16906.767	18	11	7	18	10	8	0	34665.039	34665.038
3	1	3	2	0	2	1	18034.789	18034.790	17	11	7	17	10	8	1	34662.960	34662.962
3	1	3	2	0	2	0	18035.807	18035.807	19	11	8	19	10	9	1	34661.666	34661.670
3	1	2	2	0	2	1	18046.355	18046.357	19	11	8	19	10	9	0	34661.666	34661.671
3	1	2	2	0	2	1	18046.355	18046.357	18	11	8	18	10	9	1	34659.779	34659.785
7	3	4	6	4	2	1	26680.064	26680.064	20	11	9	20	10	10	0	34658.131	34658.128
7	3	5	6	4	2	0	26682.263	26682.265	20	11	9	20	10	10	1	34658.131	34658.127
7	3	5	6	4	3	1	26686.130	26686.132	19	11	9	19	10	10	1	34656.436	34656.431
4	2	3	3	1	2	1	26794.007	26794.011	21	11	10	21	10	11	1	34654.404	34654.407
4	2	3	3	1	2	0	26801.440	26801.440	20	11	10	20	10	11	1	34652.909	34652.902
4	2	3	3	1	3	1	26805.574	26805.578	22	11	11	22	10	12	0	34650.510	34650.512
4	2	2	3	1	2	1	26806.287	26806.289	21	11	11	21	10	12	1	34649.197	34649.196
4	2	2	3	1	3	0	26811.324	26811.332	23	11	12	23	10	13	1	34646.441	34646.438
4	2	2	3	1	3	1	26817.854	26817.856	23	11	12	23	10	13	0	34646.441	34646.439

Continuation of MTBE Transitions																		
N'	K'_a	K'_c	N''	K''_a	K''_c	σ	$Obs(MHz)$	$Calc(MHz)$	N'	K'_a	K'_c	N''	K''_a	K''_c	σ	$Obs(MHz)$	$Calc(MHz)$
5	1	5	4	1	4	1	27311.608	27311.614	22	11	12	22	10	13	1	34645.320	34645.315
5	1	5	4	1	4	0	27311.474	27311.467	24	11	13	24	10	14	1	34642.192	34642.189
5	1	4	4	1	3	1	27319.418	27319.409	24	11	13	24	10	14	0	34642.192	34642.190
5	1	4	4	1	3	0	27319.669	27319.686	23	11	13	23	10	14	1	34641.265	34641.258
9	6	3	8	7	1	1	27695.703	27695.713	24	11	14	24	10	15	1	34637.019	34637.026
9	6	4	8	7	1	0	27697.060	27697.064	25	11	14	25	10	15	0	34637.763	34637.764
9	6	4	8	7	2	1	27701.581	27701.580	25	11	14	25	10	15	1	34637.763	34637.764
6	1	6	5	2	3	1	27801.621	27801.624	26	11	15	26	10	16	0	34633.158	34633.163
6	1	6	5	2	3	0	27807.563	27807.555	25	11	15	25	10	16	1	34632.614	34632.618
6	1	6	5	2	4	1	27813.892	27813.895	26	11	16	26	10	17	1	34628.054	34628.034
6	1	5	5	2	3	1	27836.432	27836.430	27	11	16	27	10	17	0	34628.384	34628.385
6	1	5	5	2	4	0	27842.119	27842.125	28	11	17	28	10	18	1	34623.436	34623.433
6	1	5	5	2	4	1	27848.706	27848.700	28	11	18	28	10	18	0	34623.436	34623.432
9	9	0	9	8	1	0	28075.533	28075.548	29	11	18	29	10	19	0	34618.305	34618.302
10	9	1	10	8	2	1	28074.725	28074.721	29	11	18	29	10	19	1	34618.305	34618.304
10	9	1	10	8	2	0	28074.103	28074.112	28	11	18	28	10	19	1	34618.305	34618.341
11	9	2	11	8	3	1	28073.136	28073.140	31	11	20	31	10	21	1	34607.519	34607.520
11	9	3	11	8	3	0	28072.524	28072.532	31	11	21	31	10	21	0	34607.519	34607.517
12	9	3	12	8	4	1	28071.419	28071.416	30	11	20	30	10	21	1	34607.938	34607.948
12	9	3	12	8	4	0	28070.800	28070.809	31	11	21	31	10	22	1	34602.489	34602.489
9	9	1	9	8	2	1	28070.552	28070.553	32	11	21	32	10	22	1	34601.923	34601.865
13	9	4	13	8	5	1	28069.551	28069.548	32	11	22	32	10	22	0	34601.855	34601.862
10	9	2	10	8	3	1	28069.093	28069.124	32	11	22	32	10	23	1	34596.852	34596.855
13	9	4	13	8	5	0	28068.936	28068.942	11	7	5	10	8	3	1	35323.622	35323.624
14	9	5	14	8	6	1	28067.538	28067.537	11	7	5	10	8	2	0	35318.931	35318.932
11	9	3	11	8	4	1	28067.538	28067.551	11	7	4	10	8	2	1	35317.849	35317.853
14	9	5	14	8	6	0	28066.918	28066.931	8	2	6	7	3	4	1	35446.081	35446.078
12	9	4	12	8	5	1	28065.814	28065.835	8	2	7	7	3	4	0	35448.474	35448.443
15	9	6	15	8	7	1	28065.390	28065.382	8	2	6	7	3	5	0	35448.659	35448.701
15	9	6	15	8	7	0	28064.765	28064.777	8	2	7	7	3	5	1	35452.182	35452.177
13	9	5	13	8	6	1	28063.974	28063.977	5	3	3	4	2	3	1	35568.063	35568.058
16	9	7	16	8	8	1	28063.083	28063.083	5	3	2	4	2	2	1	35574.158	35574.149

Continuation of MTBE Transitions																		
N'	K'_a	K'_c	N''	K''_a	K''_c	σ	$Obs(MHz)$	$Calc(MHz)$	N'	K'_a	K'_c	N''	K''_a	K''_c	σ	$Obs(MHz)$	$Calc(MHz)$
16	9	7	16	8	8	0	28062.463	28062.479	5	3	3	4	2	2	0	35571.834	35571.823
14	9	6	14	8	7	1	28061.976	28061.976	5	3	2	4	2	3	0	35571.834	35571.841
17	9	8	17	8	9	1	28060.642	28060.641	10	5	5	9	6	3	1	36463.354	36463.359
17	9	8	17	8	9	0	28060.026	28060.038	10	5	5	9	6	3	0	36465.019	36465.019
15	9	7	15	8	8	1	28059.844	28059.831	10	5	6	9	6	4	1	36469.300	36469.302
18	9	9	18	8	10	0	28057.441	28057.454	7	0	7	6	1	6	0	36607.601	36607.606
16	9	8	16	8	9	1	28057.560	28057.544	7	0	7	6	1	6	1	36607.786	36607.769
18	9	9	18	8	10	1	28058.060	28058.055	12	8	4	11	9	2	1	37475.844	37475.830
19	9	10	19	8	11	1	28055.312	28055.325	12	8	5	11	9	2	0	37476.631	37476.621
17	9	9	17	8	10	1	28055.125	28055.114	12	8	5	11	9	3	1	37481.505	37481.495
19	9	10	19	8	11	0	28054.712	28054.726	9	3	6	8	4	4	1	37606.608	37606.611
20	9	11	20	8	12	0	28051.856	28051.854	9	3	7	8	4	4	0	37608.834	37608.836
18	9	10	18	8	11	1	28052.558	28052.541	9	3	7	8	4	5	1	37612.671	37612.671
20	9	11	20	8	12	1	28052.423	28052.453	6	2	5	5	1	4	1	37713.022	37713.015
21	9	12	21	8	13	0	28048.837	28048.839	6	2	5	5	1	4	0	37719.891	37719.866
21	9	12	21	8	13	1	28049.441	28049.436	6	2	4	5	1	4	1	37725.285	37725.276
19	9	11	19	8	12	1	28049.815	28049.826	6	2	5	5	1	5	1	37738.259	37738.254
20	9	12	20	8	13	1	28046.975	28046.967	6	2	4	5	1	5	0	37744.613	37744.623
22	9	13	22	8	14	1	28046.281	28046.276	6	2	4	5	1	5	1	37750.525	37750.514
22	9	13	22	8	14	0	28045.679	28045.681	12	12	0	12	11	1	0	37988.218	37988.215
23	9	14	23	8	15	0	28042.379	28042.379	12	12	0	12	11	1	1	37987.922	37987.905
23	9	14	23	8	15	1	28042.969	28042.973	13	12	2	13	11	2	0	37985.696	37985.690
21	9	13	21	8	14	1	28043.964	28043.966	13	12	1	13	11	2	1	37985.398	37985.381
22	9	14	22	8	15	1	28040.819	28040.822	14	12	3	14	11	3	0	37982.971	37982.972
24	9	15	24	8	16	1	28039.526	28039.526	12	12	1	12	11	2	1	37982.792	37982.742
24	9	15	24	8	16	0	28038.940	28038.934	14	12	2	14	11	3	1	37982.652	37982.664
23	9	15	23	8	16	1	28037.538	28037.535	15	12	4	15	11	4	0	37980.056	37980.060
25	9	16	25	8	17	1	28035.944	28035.936	13	12	2	13	11	3	1	37980.268	37980.227
25	9	17	25	8	17	0	28035.357	28035.345	15	12	3	15	11	4	1	37979.771	37979.752
24	9	16	24	8	17	1	28034.120	28034.106	16	12	4	16	11	5	0	37976.958	37976.954
26	9	17	26	8	18	1	28032.208	28032.203	14	12	3	14	11	4	1	37977.519	37977.518
26	9	18	26	8	18	0	28031.602	28031.613	15	12	4	15	11	5	1	37974.628	37974.617

Continuation of MTBE Transitions																		
N'	K'_a	K'_c	N''	K''_a	K''_c	σ	$Obs(MHz)$	$Calc(MHz)$	N'	K'_a	K'_c	N''	K''_a	K''_c	σ	$Obs(MHz)$	$Calc(MHz)$
25	9	17	25	8	18	1	28030.549	28030.533	17	12	5	17	11	6	0	37973.658	37973.655
27	9	18	27	8	19	1	28028.331	28028.326	17	12	5	17	11	6	1	37973.353	37973.349
27	9	19	27	8	19	0	28027.757	28027.739	16	12	5	16	11	6	1	37971.537	37971.523
26	9	18	26	8	19	1	28026.827	28026.819	18	12	7	18	11	7	0	37970.161	37970.162
28	9	20	28	8	20	0	28023.720	28023.720	18	12	6	18	11	7	1	37969.858	37969.857
27	9	19	27	8	20	1	28022.951	28022.961	17	12	6	17	11	7	1	37968.248	37968.236
28	9	19	28	8	20	1	28024.301	28024.306	19	12	7	19	11	8	0	37966.478	37966.475
29	9	20	29	8	21	1	28020.167	28020.143	18	12	7	18	11	8	1	37964.760	37964.755
29	9	20	29	8	21	0	28019.562	28019.559	20	12	8	20	11	9	0	37962.596	37962.596
28	9	20	28	8	21	1	28018.957	28018.961	19	12	8	19	11	9	1	37961.091	37961.083
30	9	21	30	8	22	1	28015.865	28015.837	21	12	9	21	11	10	0	37958.523	37958.522
30	9	21	30	8	22	0	28015.253	28015.255	20	12	9	20	11	10	1	37957.229	37957.217
29	9	21	29	8	22	1	28014.837	28014.819	22	12	10	22	11	11	0	37954.257	37954.256
30	9	22	30	8	23	1	28010.564	28010.534	22	12	10	22	11	11	1	37953.950	37953.956
8	4	5	7	5	3	1	28846.210	28846.211	21	12	10	21	11	11	1	37953.165	37953.159
8	4	4	7	5	2	0	28842.122	28842.123	23	12	12	23	11	12	0	37949.796	37949.797
8	4	4	7	5	2	1	28840.192	28840.198	23	12	11	23	11	12	1	37949.485	37949.497
5	1	5	4	0	4	1	28954.060	28954.056	22	12	11	22	11	12	1	37948.922	37948.908
5	1	5	4	0	4	0	28954.528	28954.531	24	12	13	24	11	13	0	37945.139	37945.145
10	7	3	9	8	1	1	29854.281	29854.290	24	12	12	24	11	13	1	37944.817	37944.847
10	7	4	9	8	1	0	29855.351	29855.355	23	12	12	23	11	13	1	37944.488	37944.466
10	7	4	9	8	2	1	29860.063	29860.063	25	12	13	25	11	14	0	37940.286	37940.300
7	2	5	6	3	3	1	29982.861	29982.862	24	12	13	24	11	14	1	37939.834	37939.830
7	2	6	6	3	4	1	29988.971	29988.966	28	12	17	28	11	17	0	37924.581	37924.609
7	2	6	6	3	3	0	29985.289	29985.267	27	12	16	27	11	17	1	37924.797	37924.773
7	2	5	6	3	4	0	29985.390	29985.421	27	12	15	27	11	16	1	37929.727	37929.738
4	3	2	3	2	2	1	30105.235	30105.235	26	12	15	26	11	16	1	37930.026	37929.984
4	3	2	3	2	1	0	30108.996	30108.996	27	12	15	27	11	16	0	37930.026	37930.032
4	3	1	3	2	2	0	30108.996	30109.002	26	12	14	26	11	15	1	37934.975	37934.967
4	3	1	3	2	1	1	30111.334	30111.331	25	12	14	25	11	15	1	37934.975	37935.003
9	5	4	8	6	2	1	30999.930	30999.939	26	12	14	26	11	15	0	37935.254	37935.262
9	5	4	8	6	2	0	31001.582	31001.586	29	12	17	29	11	18	0	37918.992	37918.994

Continuation of MTBE Transitions																		
N'	K'_a	K'_c	N''	K''_a	K''_c	σ	$Obs(MHz)$	$Calc(MHz)$	N'	K'_a	K'_c	N''	K''_a	K''_c	σ	$Obs(MHz)$	$Calc(MHz)$
9	5	5	8	6	3	1	31005.883	31005.885	29	12	18	29	11	19	1	37913.758	37913.776
6	0	6	5	1	5	0	31139.689	31139.692	30	12	18	30	11	19	0	37913.185	37913.187
6	0	6	5	1	5	1	31140.018	31140.016	30	12	18	30	11	19	1	37912.880	37912.898
10	10	0	10	9	1	1	31379.744	31379.746	31	12	19	31	11	20	1	37906.878	37906.901
10	10	1	10	9	1	0	31379.433	31379.442	31	12	20	31	11	20	0	37907.184	37907.189
11	10	2	11	9	2	0	31377.671	31377.677	30	12	19	30	11	20	1	37907.989	37907.990
11	10	1	11	9	2	1	31377.972	31377.980	32	12	21	32	11	21	0	37900.982	37900.998
12	10	2	12	9	3	0	31375.744	31375.751	31	12	20	31	11	21	1	37902.012	37902.013
10	10	1	10	9	2	1	31374.264	31374.275	32	12	21	32	11	22	1	37895.815	37895.845
13	10	3	13	9	4	1	31373.965	31373.968	7	1	7	6	1	6	0	38235.856	38235.840
13	10	3	13	9	5	0	31373.663	31373.665	7	1	7	6	1	6	1	38235.856	38235.861
11	10	2	11	9	3	1	31372.516	31372.517	7	1	6	6	1	5	0	38247.345	38247.330
14	10	4	14	9	5	1	31371.714	31371.721	7	1	6	6	1	5	1	38247.130	38247.127
14	10	4	14	9	5	0	31371.416	31371.419	11	6	5	10	7	3	1	38622.699	38622.696
12	10	3	12	9	4	1	31370.594	31370.599	11	6	5	10	7	3	0	38624.076	38624.073
15	10	5	15	9	6	1	31369.312	31369.314	11	6	6	10	7	4	1	38628.565	38628.558
15	10	5	15	9	6	0	31369.017	31369.012	8	1	8	7	2	5	1	38715.666	38715.680
13	10	4	13	9	5	1	31368.520	31368.522	8	1	8	7	2	5	0	38721.375	38721.359
16	10	6	16	9	7	1	31366.749	31366.747	8	1	8	7	2	6	1	38727.918	38727.930
16	10	6	16	9	7	0	31366.438	31366.445	8	1	7	7	2	5	1	38774.698	38774.678
14	10	5	14	9	6	1	31366.274	31366.285	8	1	7	7	2	6	0	38780.642	38780.651
15	10	6	15	9	7	1	31363.864	31363.889	8	1	7	7	2	6	1	38786.954	38786.928
17	10	7	17	9	8	0	31363.709	31363.718	5	4	2	4	3	2	1	38870.476	38870.466
18	10	8	18	9	9	0	31360.824	31360.831	5	4	2	4	3	1	0	38874.484	38874.479
18	10	8	18	9	9	1	31361.141	31361.132	10	4	6	9	5	4	1	39766.887	39766.888
16	10	7	16	9	8	1	31361.319	31361.333	10	4	6	9	5	4	0	39768.841	39768.838
17	10	8	17	9	9	1	31358.614	31358.618	10	4	7	9	5	5	1	39772.905	39772.894
19	10	9	19	9	10	1	31358.081	31358.084	7	1	7	6	0	6	1	39869.582	39869.588
19	10	9	19	9	10	0	31357.777	31357.784	7	1	7	6	0	6	0	39869.836	39869.825
18	10	9	18	9	10	1	31355.744	31355.743	31	9	23	31	8	23	0	28010.805	28010.807
20	10	10	20	9	11	1	31354.874	31354.876	32	9	23	32	8	24	1	28006.802	28006.795
20	10	10	20	9	11	0	31354.570	31354.577	32	9	24	32	8	24	0	28006.245	28006.217

Continuation of MTBE Transitions																		
N'	K'_a	K'_c	N''	K''_a	K''_c	σ	$Obs(MHz)$	$Calc(MHz)$	N'	K'_a	K'_c	N''	K''_a	K''_c	σ	$Obs(MHz)$	$Calc(MHz)$
19	10	10	19	9	11	1	31352.704	31352.708	11	9	2	10	10	0	1	28705.591	28705.569
21	10	11	21	9	12	1	31351.504	31351.509	11	9	2	10	10	0	0	28706.029	28706.040
21	10	11	21	9	12	0	31351.206	31351.210	5	1	4	4	0	4	1	28979.293	28979.294
20	10	11	20	9	12	1	31349.508	31349.515	12	10	2	11	11	0	0	30861.819	30861.852
22	10	12	22	9	13	1	31347.985	31347.981	6	0	6	5	1	4	1	31114.764	31114.778
22	10	12	22	9	13	0	31347.680	31347.683	30	10	20	30	9	21	1	31314.011	31314.011
21	10	12	21	9	13	1	31346.162	31346.162	30	10	21	30	9	21	0	31313.741	31313.718
23	10	13	23	9	14	1	31344.297	31344.293	29	10	20	29	9	21	1	31313.598	31313.610
23	10	13	23	9	14	0	31343.998	31343.996	31	10	22	31	9	22	0	31308.734	31308.755
22	10	13	22	9	14	1	31342.652	31342.649	30	10	21	30	9	22	1	31308.838	31308.827
24	10	14	24	9	15	1	31340.442	31340.446	31	10	21	31	9	22	1	31309.024	31309.047
24	10	14	24	9	15	0	31340.147	31340.149	32	10	23	32	9	23	0	31303.639	31303.633
23	10	14	23	9	15	1	31338.981	31338.978	31	10	22	31	9	23	1	31303.893	31303.884
25	10	15	25	9	16	1	31336.440	31336.439	32	10	22	32	9	23	1	31303.893	31303.924
25	10	15	25	9	16	0	31336.146	31336.143	33	10	24	33	9	25	1	31293.510	31293.525
24	10	15	24	9	16	1	31335.141	31335.148	34	10	24	34	9	25	0	31292.954	31292.912
25	10	16	25	9	17	1	31331.173	31331.158	35	10	26	35	9	26	0	31287.317	31287.313
26	10	17	26	9	17	0	31331.983	31331.977	35	10	25	35	9	26	1	31287.613	31287.603
26	10	16	26	9	17	1	31332.267	31332.272	34	10	25	34	9	26	1	31288.107	31288.107
27	10	17	27	9	18	1	31327.945	31327.946	35	10	26	35	9	27	1	31282.541	31282.532
27	10	18	27	9	18	0	31327.648	31327.651	36	10	26	36	9	27	1	31281.846	31281.845
26	10	17	26	9	18	1	31327.017	31327.009	36	10	27	36	9	27	0	31281.615	31281.556
28	10	18	28	9	19	1	31323.461	31323.460	37	10	28	37	9	28	0	31275.657	31275.640
28	10	18	28	9	19	0	31323.169	31323.166	37	10	27	37	9	28	1	31275.902	31275.928
27	10	18	27	9	19	1	31322.689	31322.702	36	10	27	36	9	28	1	31276.804	31276.798
29	10	19	29	9	20	1	31318.824	31318.815	6	1	5	5	1	4	1	32783.320	32783.310
29	10	19	29	9	20	0	31318.528	31318.522	6	1	5	5	1	4	0	32783.491	32783.533
28	10	19	28	9	20	1	31318.256	31318.236	4	4	0	3	3	0	1	33413.822	33413.818
11	8	3	10	9	1	1	32012.169	32012.174	12	9	3	11	10	1	1	34169.256	34169.266
11	8	4	10	9	1	0	32012.947	32012.950	30	11	19	30	10	20	0	34612.982	34612.998
11	8	4	10	9	2	1	32017.837	32017.840	30	11	19	30	10	20	1	34612.982	34613.000
8	3	6	7	4	4	1	32149.403	32149.403	33	11	22	33	10	23	0	34596.034	34596.031

Continuation of MTBE Transitions																	
N'	K'_a	K'_c	N''	K''_a	K''_c	σ	$Obs(MHz)$	$Calc(MHz)$	N'	K'_a	K'_c	N''	K''_a	K''_c	σ	$Obs(MHz)$	$Calc(MHz)$
8	3	6	7	4	3	0	32145.548	32145.551	33	11	22	33	10	23	1	34596.034	34596.034
5	2	4	4	1	3	1	32254.023	32254.020	34	11	23	34	10	24	1	34590.026	34590.029
5	2	4	4	1	3	0	32261.107	32261.095	34	11	23	34	10	24	0	34590.026	34590.025
5	2	3	4	1	3	1	32266.296	32266.290	35	11	24	35	10	25	0	34583.817	34583.844
5	2	4	4	1	4	1	32271.463	32271.463	35	11	24	35	10	25	1	34583.817	34583.849
5	2	3	4	1	4	0	32277.581	32277.590	35	11	25	35	10	26	1	34578.945	34578.907
5	2	3	4	1	4	1	32283.739	32283.733	36	11	25	36	10	26	1	34577.486	34577.493
6	1	5	5	1	4	1	32783.320	32783.310	36	11	26	36	10	26	0	34577.486	34577.488
6	1	5	5	1	4	0	32783.491	32783.533	36	11	26	36	10	27	1	34572.585	34572.575
10	6	4	9	7	2	1	33159.189	33159.190	37	11	26	37	10	27	0	34570.951	34570.958
10	6	5	9	7	2	0	33160.551	33160.554	37	11	26	37	10	27	1	34570.951	34570.964
10	6	5	9	7	3	1	33165.051	33165.055	33	12	21	33	11	22	1	37894.315	37894.332
7	1	7	6	2	4	1	33259.083	33259.090	34	12	23	34	11	23	0	37888.016	37888.042
7	1	7	6	2	4	0	33264.910	33264.894	5	4	1	4	3	1	1	38876.521	38876.510
7	1	7	6	2	5	1	33271.348	33271.351	13	9	5	12	10	3	1	39638.577	39638.568
7	1	6	6	2	4	1	33305.170	33305.162	13	9	4	12	10	2	1	39633.020	39633.023
7	1	6	6	2	5	0	33310.986	33310.997									
End of Table																	

APPENDIX B

Observed Transitions Used in Chapter 4 & Calculated Frequencies

TABLE B.1. Fit Results of 2-Butynoic Acid

Transitions used in 4.2.1																		
N'	K'_a	K'_c	m'	N	K_a	K_c	m	Obs (MHz)	Calc (MHz)	N'	K'_a	K'_c	m'	N	K_a	K_c	m	Obs (MHz)	Calc (MHz)
2	1	2	0	1	1	1	0	6340.852	6340.856	4	2	3	1	3	2	2	1	13143.434	13143.436
2	0	2	0	1	0	1	0	6559.941	6559.942	4	2	2	0	3	2	1	0	13159.176	13159.174
2	0	2	1	1	0	1	1	6561.099	6561.095	4	1	3	1	3	1	2	1	13228.712	13228.715
2	2	1	1	1	1	0	1	6565.204	6565.204	4	2	3	0	5	1	4	0	13435.008	13435.010
2	1	1	1	1	1	1	1	6573.932	6573.933	4	1	3	0	3	1	2	0	13564.835	13564.834
2	1	1	0	1	1	0	0	6786.012	6786.015	1	1	1	0	0	0	0	0	13667.467	13667.465
5	0	5	0	4	1	4	0	6910.385	6910.386	1	1	1	1	1	0	1	1	13763.988	13763.989
4	1	4	1	4	0	4	1	7105.787	7105.787	2	1	1	1	2	0	2	1	13776.828	13776.827
3	1	3	1	3	0	3	1	7186.713	7186.711	2	1	2	1	1	0	1	1	13780.175	13780.179
1	1	1	1	2	0	2	1	7202.892	7202.893	3	1	2	1	3	0	3	1	13831.097	13831.097
2	1	2	1	2	0	2	1	7219.083	7219.084	7	1	6	0	7	0	7	0	13950.991	13950.991
7	0	7	1	6	1	5	1	8113.628	8113.629	4	1	3	1	4	0	4	1	13966.498	13966.500
5	0	5	1	4	1	4	1	9233.921	9233.918	5	1	4	1	5	0	5	1	14229.150	14229.148
5	2	4	1	6	1	6	1	9343.330	9343.333	8	1	7	0	8	0	8	0	15055.904	15055.903
3	1	3	0	2	1	2	0	9509.087	9509.088	7	1	6	1	7	0	7	1	15303.212	15303.216
3	1	3	1	2	1	2	1	9800.235	9800.236	5	1	5	0	4	1	4	0	15837.007	15837.008
3	0	3	0	2	0	2	0	9831.069	9831.067	7	0	7	1	6	1	6	1	16070.457	16070.461
3	0	3	1	2	0	2	1	9832.608	9832.609	8	1	7	1	8	0	8	1	16172.040	16172.040
3	2	2	0	2	2	1	0	9844.943	9844.948	5	1	5	1	4	1	4	1	16185.557	16185.553
3	3	1	1	2	2	0	1	9847.591	9847.596	5	0	5	0	4	0	4	0	16338.167	16338.165
3	2	1	1	2	2	1	1	9850.229	9850.232	5	0	5	1	4	0	4	1	16339.702	16339.705
3	2	1	0	2	2	0	0	9859.092	9859.097	9	1	8	0	9	0	9	0	16355.380	16355.378
3	1	2	1	2	1	1	1	9886.879	9886.879	5	2	4	0	4	2	3	0	16400.377	16400.373

Continuation of 2ba Transitions																			
N'	K'_a	K'_c	m'	N	K_a	K_c	m	Obs	Calc	N'	K'_a	K'_c	m'	N	K_a	K_c	m	Obs	Calc
3	1	2	0	2	1	1	0	10176.790	10176.789	5	4	1	1	4	4	1	1	16413.489	16413.487
0	0	0	1	1	0	1	1	10482.286	10482.291	5	4	1	0	4	4	0	0	16414.735	16414.736
1	1	0	0	1	0	1	0	10608.310	10608.304	5	4	2	0	4	4	1	0	16414.735	16414.734
6	0	6	0	5	1	5	0	10640.885	10640.885	5	3	2	1	4	3	1	1	16417.918	16417.917
6	2	4	1	7	1	6	1	10753.105	10753.105	5	3	3	0	4	3	2	0	16419.464	16419.465
2	1	1	0	2	0	2	0	10834.381	10834.377	5	3	2	0	4	3	1	0	16420.206	16420.203
3	1	2	0	3	0	3	0	11180.099	11180.099	5	3	3	1	4	3	2	1	16420.726	16420.726
4	1	3	0	4	0	4	0	11653.320	11653.320	5	2	3	1	4	2	2	1	16430.097	16430.096
6	2	4	0	7	1	7	0	11949.542	11949.540	5	2	4	1	4	2	3	1	16440.064	16440.060
4	2	3	1	5	1	5	1	12226.486	12226.481	5	2	3	0	4	2	2	0	16470.876	16470.876
5	1	4	0	5	0	5	0	12264.311	12264.312	5	1	4	1	4	1	3	1	16602.351	16602.353
6	0	6	1	5	1	5	1	12616.869	12616.866	2	1	2	0	1	0	1	0	16726.580	16726.581
4	1	4	0	3	1	3	0	12674.734	12674.732	4	2	2	0	5	1	5	0	16825.719	16825.722
4	1	4	1	3	1	3	1	13012.394	13012.387	5	1	4	0	4	1	3	0	16949.158	16949.157
6	1	5	0	6	0	6	0	13025.498	13025.498	3	1	3	1	2	0	2	1	17019.318	17019.320
4	0	4	0	3	0	3	0	13091.613	13091.613	3	2	2	0	4	1	3	0	17260.326	17260.326
4	0	4	1	3	0	3	1	13093.309	13093.311	9	1	8	1	9	0	9	1	17283.027	17283.025
4	2	3	0	3	2	2	0	13123.845	13123.841	10	1	9	0	10	0	10	0	17863.403	17863.405
4	3	1	1	3	3	1	1	13131.971	13131.968	4	2	2	1	5	1	4	1	18015.285	18015.283
4	3	2	0	3	3	1	0	13133.110	13133.111	8	0	8	0	7	1	7	0	18237.550	18237.550
4	3	1	0	3	3	0	0	13133.314	13133.322	10	1	9	1	10	0	10	1	18643.783	18643.783
4	2	2	1	3	2	1	1	13138.189	13138.186										
End of Table																			

TABLE B.2. Transitions used in 4.2.2

Iodoperfluoropropane Transitions																			
$2J'$	N'	K'_a	K'_c	$2J$	N	K_a	K_c	Obs (MHz)	Calc (MHz)	$2J'$	N'	K'_a	K'_c	$2J$	N	K_a	K_c	Obs (MHz)	Calc (MHz)
11	13	5	8	10	13	4	9	10457.69	10457.679	15	13	10	3	14	12	10	2	10210.209	10210.207
16	17	5	13	16	17	4	14	10632.40	10632.406	13	13	10	3	12	12	10	2	10095.611	10095.622
18	18	5	14	18	18	4	15	10632.50	10632.507	14	13	10	3	13	12	10	2	10125.722	10125.717

Continuation of I-pF-p transitions																			
$2J'$	N'	K'_a	K'_c	$2J$	N	K_a	K_c	Obs	Calc	$2J'$	N'	K'_a	K'_c	$2J$	N	K_a	K_c	Obs	Calc
10	13	5	8	10	13	4	9	10632.68	10632.682	11	14	10	4	10	13	10	3	10994.603	10994.605
10	13	5	9	10	13	4	10	10632.77	10632.773	14	14	10	4	13	13	10	3	10902.999	10902.994
15	16	5	11	15	16	4	12	10632.92	10632.920	16	14	10	4	15	13	10	3	10984.286	10984.282
19	18	5	14	19	18	4	15	10633.06	10633.059	13	14	10	4	12	13	10	3	10909.446	10909.444
14	16	6	10	13	16	5	11	12818.08	12818.080	13	15	10	5	12	14	10	4	11721.716	11721.724
17	19	7	12	16	19	6	13	15177.99	15177.985	14	15	10	5	13	14	10	4	11693.670	11693.669
18	19	7	12	17	19	6	13	15261.75	15261.753	16	15	10	5	15	14	10	4	11704.346	11704.339
20	19	7	13	19	19	6	14	15423.99	15424.001	17	15	10	5	16	14	10	4	11757.316	11757.316
33	32	7	25	33	32	6	26	15305.30	15305.302	15	15	10	5	14	14	10	4	11685.723	11685.727
21	20	7	13	20	20	6	14	15412.04	15412.045	12	15	10	5	11	14	10	4	11764.611	11764.614
15	13	5	9	14	13	4	10	10755.73	10755.754	15	16	10	6	14	15	10	5	12478.715	12478.718
11	13	5	9	10	13	4	10	10457.74	10457.760	13	16	10	6	12	15	10	5	12537.333	12537.331
33	35	5	30	33	35	4	31	10233.46	10233.462	14	16	10	6	13	15	10	5	12501.627	12501.627
36	35	5	30	36	35	4	31	10233.64	10233.647	16	16	10	6	15	15	10	5	12472.656	12472.654
34	35	5	30	34	35	4	31	10233.72	10233.721	17	16	10	6	16	15	10	5	12489.036	12489.032
32	35	5	30	32	35	4	31	10233.13	10233.130	18	16	10	6	17	15	10	5	12532.766	12532.765
37	35	5	30	37	35	4	31	10233.13	10233.143	16	17	10	7	15	16	10	6	13266.383	13266.384
41	40	6	35	41	40	5	36	12790.06	12790.048	18	17	10	7	17	16	10	6	13273.047	13273.047
47	50	6	45	47	50	5	46	12614.38	12614.391	19	17	10	7	18	16	10	6	13309.505	13309.502
14	14	3	11	13	14	0	14	10940.98	10940.974	15	17	10	7	14	16	10	6	13284.924	13284.928
4	2	0	2	3	1	0	1	1613.61	1613.620	17	17	10	7	16	16	10	6	13261.128	13261.125
2	2	0	2	2	1	0	1	1857.94	1857.938	14	17	10	7	13	16	10	6	13313.676	13313.677
6	4	0	4	5	3	0	3	3141.84	3141.843	19	18	10	8	18	17	10	7	14056.537	14056.534
7	5	0	5	6	4	0	4	3916.16	3916.163	15	18	10	8	14	17	10	7	14089.037	14089.043
14	13	0	13	13	12	0	12	10106.29	10106.295	20	18	10	8	19	17	10	7	14087.215	14087.215
15	13	0	13	14	12	0	12	10107.42	10107.423	18	18	10	8	17	17	10	7	14044.879	14044.875
11	13	0	13	10	12	0	12	10098.78	10098.779	17	18	10	8	16	17	10	7	14048.243	14048.242
12	13	0	13	11	12	0	12	10099.74	10099.746	19	19	10	9	18	18	10	8	14829.646	14829.632
10	13	0	13	9	12	0	12	10102.36	10102.366	20	19	10	9	19	18	10	8	14839.618	14839.616
13	13	0	13	12	12	0	12	10103.05	10103.056	21	19	10	9	20	18	10	8	14865.680	14865.681
12	14	0	14	11	13	0	13	10870.31	10870.312	17	19	10	9	16	18	10	8	14845.527	14845.539
14	14	0	14	13	13	0	13	10871.98	10871.987	21	20	10	10	20	19	10	9	15622.399	15622.402

Continuation of I-pF-p transitions																			
$2J'$	N'	K'_a	K'_c	$2J$	N	K_a	K_c	Obs	Calc	$2J'$	N'	K'_a	K'_c	$2J$	N	K_a	K_c	Obs	Calc
11	14	0	14	10	13	0	13	10873.75	10873.758	22	20	10	10	21	19	10	9	15644.746	15644.748
15	14	0	14	14	13	0	13	10874.48	10874.485	17	20	10	10	16	19	10	9	15645.337	15645.341
16	14	0	14	15	13	0	13	10876.53	10876.530	18	20	10	10	17	19	10	9	15627.087	15627.093
16	15	0	15	15	14	0	14	11645.27	11645.269	20	20	10	10	19	19	10	9	15613.693	15613.697
13	15	0	15	12	14	0	14	11636.76	11636.763	19	20	10	10	18	19	10	9	15615.956	15615.960
12	15	0	15	11	14	0	14	11640.31	11640.309	13	13	11	2	12	12	11	1	10092.253	10092.260
15	15	0	15	14	14	0	14	11641.14	11641.144	12	13	11	2	11	12	11	1	10109.696	10109.706
17	15	0	15	16	14	0	14	11644.48	11644.486	12	14	11	3	11	13	11	2	10943.221	10943.232
18	16	0	16	17	15	0	15	12411.40	12411.409	16	14	11	3	15	13	11	2	10992.314	10992.322
14	16	0	16	13	15	0	15	12405.15	12405.149	14	14	11	3	13	13	11	2	10887.423	10887.419
15	16	0	16	14	15	0	15	12405.48	12405.488	15	14	11	3	14	13	11	2	10914.832	10914.833
16	16	0	16	15	15	0	15	12407.60	12407.607	13	14	11	3	12	13	11	2	10900.195	10900.199
13	16	0	16	12	15	0	15	12408.17	12408.174	11	14	11	3	10	13	11	2	11007.556	11007.562
17	16	0	16	16	15	0	15	12409.72	12409.727	17	15	11	4	16	14	11	3	11762.631	11762.626
18	17	0	17	17	16	0	16	13176.08	13176.086	12	15	11	4	11	14	11	3	11774.801	11774.789
19	17	0	17	18	16	0	16	13177.44	13177.441	14	15	11	4	13	14	11	3	11687.057	11687.061
15	17	0	17	14	16	0	16	13171.78	13171.780	15	15	11	4	14	14	11	3	11676.303	11676.305
16	17	0	17	15	16	0	16	13171.97	13171.975	13	16	11	5	12	15	11	4	12545.725	12545.727
17	17	0	17	16	16	0	16	13173.88	13173.888	16	16	11	5	15	15	11	4	12467.580	12467.572
14	17	0	17	13	16	0	16	13174.61	13174.617	15	16	11	5	14	15	11	4	12474.884	12474.888
19	18	0	18	18	17	0	17	13941.47	13941.473	14	16	11	5	13	15	11	4	12502.579	12502.578
20	18	0	18	19	17	0	17	13942.74	13942.743	17	16	11	5	16	15	11	4	12486.451	12486.446
16	18	0	18	15	17	0	17	13937.58	13937.579	18	16	11	5	17	15	11	4	12538.589	12538.588
17	18	0	18	16	17	0	17	13937.68	13937.692	17	17	11	6	16	16	11	5	13254.367	13254.364
18	18	0	18	17	17	0	17	13939.41	13939.411	16	17	11	6	15	16	11	5	13260.124	13260.124
15	18	0	18	14	17	0	17	13940.23	13940.232	19	17	11	6	18	16	11	5	13314.257	13314.248
19	19	0	19	18	18	0	18	14704.36	14704.368	18	17	11	6	17	16	11	5	13270.552	13270.550
16	19	0	19	15	18	0	18	14705.22	14705.224	14	17	11	6	13	16	11	5	13319.167	13319.170
20	19	0	19	19	18	0	18	14706.28	14706.279	17	18	11	7	16	17	11	6	14050.991	14050.991
21	19	0	19	20	18	0	18	14707.48	14707.480	18	18	11	7	17	17	11	6	14042.254	14042.250
18	20	0	20	17	19	0	19	15467.45	15467.471	20	18	11	7	19	17	11	6	14091.156	14091.155
19	20	0	20	18	19	0	19	15467.51	15467.500	16	18	11	7	15	17	11	6	14074.587	14074.592

Continuation of I-pF-p transitions																		
$2J'$	N'	K'_a	K'_c	$2J$	N	K_a	K_c	Obs	Calc	$2J'$	N'	K'_a	K'_c	$2J$	N	K_a	K_c	Obs	Calc
20	20	0	20	19	19	0	19	15468.91	15468.915	19	18	11	7	18	17	11	6	14054.326	14054.324
17	20	0	20	16	19	0	19	15469.76	15469.764	15	18	11	7	14	17	11	6	14099.552	14099.559
21	20	0	20	20	19	0	19	15470.68	15470.680	18	19	11	8	17	18	11	7	14824.550	14824.541
22	20	0	20	21	19	0	19	15471.81	15471.805	19	19	11	8	18	18	11	7	14824.712	14824.712
20	22	0	22	19	21	0	21	16996.10	16996.095	16	19	11	8	15	18	11	7	14866.871	14866.879
21	22	0	22	20	21	0	21	16996.11	16996.110	21	19	11	8	20	18	11	7	14868.947	14868.948
22	22	0	22	21	21	0	21	16997.30	16997.300	20	20	11	9	19	19	11	8	15610.175	15610.177
1	2	1	1	2	1	1	0	1584.99	1584.996	21	20	11	9	20	19	11	8	15620.624	15620.626
4	2	1	1	3	1	1	0	1742.38	1742.388	19	20	11	9	18	19	11	8	15612.947	15612.955
14	13	1	12	13	12	1	11	10244.83	10244.837	22	20	11	9	21	19	11	8	15647.436	15647.438
15	13	1	12	14	12	1	11	10246.14	10246.143	17	20	11	9	16	19	11	8	15648.901	15648.907
10	13	1	12	9	12	1	11	10241.50	10241.506	18	20	11	9	17	19	11	8	15626.537	15626.543
11	13	1	12	10	12	1	11	10238.68	10238.682	14	14	12	2	13	13	12	1	10876.854	10876.863
13	13	1	12	12	12	1	11	10242.44	10242.447	13	14	12	2	12	13	12	1	10892.207	10892.207
12	14	1	13	11	13	1	12	11024.25	11024.255	15	14	12	2	14	13	12	1	10909.818	10909.812
13	14	1	13	12	13	1	12	11025.03	11025.038	16	14	12	2	15	13	12	1	11000.413	11000.404
11	14	1	13	10	13	1	12	11026.79	11026.801	16	15	12	3	15	14	12	2	11697.217	11697.214
14	14	1	13	13	13	1	12	11027.44	11027.437	12	15	12	3	11	14	12	2	11786.195	11786.190
15	14	1	13	14	13	1	12	11029.69	11029.698	14	15	12	3	13	14	12	2	11681.838	11681.837
16	14	1	13	15	13	1	12	11030.72	11030.722	17	15	12	3	16	14	12	2	11771.543	11771.543
13	15	1	14	12	14	1	13	11808.88	11808.884	15	15	12	3	14	14	12	2	11670.166	11670.172
14	15	1	14	13	14	1	13	11809.49	11809.495	13	15	12	3	12	14	12	2	11723.317	11723.317
12	15	1	14	11	14	1	13	11811.21	11811.222	16	16	12	4	15	15	12	3	12449.976	12449.972
15	15	1	14	14	14	1	13	11811.58	11811.581	15	16	12	4	14	15	12	3	12464.527	12464.525
16	15	1	14	15	14	1	13	11813.63	11813.637	18	16	12	4	17	15	12	3	12542.893	12542.890
17	15	1	14	16	14	1	13	11814.61	11814.617	14	16	12	4	13	15	12	3	12503.076	12503.076
15	16	1	15	14	15	1	14	12593.02	12593.019	13	16	12	4	12	15	12	3	12554.815	12554.816
13	16	1	15	12	15	1	14	12594.74	12594.747	17	16	12	4	16	15	12	3	12477.056	12477.055
17	16	1	15	16	15	1	14	12596.73	12596.733	14	17	12	5	13	16	12	4	13326.578	13326.595
18	16	1	15	17	15	1	14	12597.72	12597.722	17	17	12	5	16	16	12	4	13258.196	13258.202
14	16	1	15	13	15	1	14	12592.55	12592.558	18	17	12	5	17	16	12	4	13272.625	13272.649
19	17	1	16	18	16	1	15	13379.93	13379.932	16	17	12	5	15	16	12	4	13260.283	13260.285

Continuation of I-pF-p transitions																		
$2J'$	N'	K'_a	K'_c	$2J$	N	K_a	K_c	Obs	Calc	$2J'$	N'	K'_a	K'_c	$2J$	N	K_a	K_c	Obs	Calc
15	17	1	16	14	16	1	15	13375.21	13375.214	19	17	12	5	18	16	12	4	13320.451	13320.444
16	17	1	16	15	16	1	15	13375.54	13375.542	15	17	12	5	14	16	12	4	13283.436	13283.435
17	17	1	16	16	16	1	15	13377.15	13377.152	19	18	12	6	18	17	12	5	14052.188	14052.185
14	17	1	16	13	16	1	15	13377.30	13377.301	15	18	12	6	14	17	12	5	14100.576	14100.582
18	17	1	16	17	16	1	15	13378.90	13378.904	20	18	12	6	19	17	12	5	14095.600	14095.605
18	18	1	17	17	17	1	16	14158.40	14158.409	18	18	12	6	17	17	12	5	14035.831	14035.832
15	18	1	17	14	17	1	16	14158.79	14158.798	18	19	12	7	17	18	12	6	14825.294	14825.296
20	18	1	17	19	17	1	16	14161.14	14161.143	21	19	12	7	20	18	12	6	14872.667	14872.667
16	18	1	17	15	17	1	16	14156.77	14156.777	19	19	12	7	18	18	12	6	14820.962	14820.956
17	18	1	17	16	17	1	16	14156.98	14156.986	18	20	12	8	17	19	12	7	15628.296	15628.300
16	19	1	18	15	18	1	17	14939.13	14939.134	22	20	12	8	21	19	12	7	15650.563	15650.564
20	19	1	18	19	18	1	17	14940.08	14940.081	20	20	12	8	19	19	12	7	15607.932	15607.937
21	19	1	18	20	18	1	17	14941.25	14941.255	19	20	12	8	18	19	12	7	15612.117	15612.120
19	19	1	18	18	18	1	17	14938.52	14938.528	16	15	13	2	15	14	13	1	11693.327	11693.322
22	20	1	19	21	19	1	18	15720.17	15720.169	18	16	13	3	17	15	13	2	12551.262	12551.255
20	20	1	19	19	19	1	18	15717.40	15717.409	15	16	13	3	14	15	13	2	12463.768	12463.768
17	20	1	19	16	19	1	18	15718.15	15718.154	13	16	13	3	12	15	13	2	12564.921	12564.915
21	20	1	19	20	19	1	18	15718.86	15718.869	17	16	13	3	16	15	13	2	12479.847	12479.842
15	13	2	11	14	12	2	10	10203.92	10203.914	16	16	13	3	15	15	13	2	12453.193	12453.194
11	13	2	11	10	12	2	10	10196.24	10196.242	14	16	13	3	13	15	13	2	12503.598	12503.592
12	13	2	11	11	12	2	10	10197.39	10197.398	14	17	13	4	13	16	13	3	13334.756	13334.757
10	13	2	11	9	12	2	10	10198.93	10198.929	18	17	13	4	17	16	13	3	13265.853	13265.856
13	13	2	11	12	12	2	10	10200.05	10200.057	16	17	13	4	15	16	13	3	13251.362	13251.361
14	13	2	11	13	12	2	10	10202.16	10202.166	19	17	13	4	18	16	13	3	13325.687	13325.684
13	14	2	12	12	13	2	11	10988.95	10988.950	17	17	13	4	16	16	13	3	13243.295	13243.287
11	14	2	12	10	13	2	11	10989.76	10989.766	18	18	13	5	17	17	13	4	14028.727	14028.725
14	14	2	12	13	13	2	11	10991.33	10991.339	16	18	13	5	15	17	13	4	14064.305	14064.314
15	14	2	12	14	13	2	11	10993.16	10993.163	15	18	13	5	14	17	13	4	14107.288	14107.295
16	14	2	12	15	13	2	11	10994.01	10994.013	19	18	13	5	18	17	13	4	14047.713	14047.709
12	14	2	12	11	13	2	11	10987.77	10987.776	20	18	13	5	19	17	13	4	14098.980	14098.984
13	15	2	13	12	14	2	12	11779.95	11779.952	16	19	13	6	15	18	13	5	14881.767	14881.772
14	15	2	13	13	14	2	12	11781.13	11781.127	21	19	13	6	20	18	13	5	14876.932	14876.926

Continuation of I-pF-p transitions																			
$2J'$	N'	K'_a	K'_c	$2J$	N	K_a	K_c	Obs	Calc	$2J'$	N'	K'_a	K'_c	$2J$	N	K_a	K_c	Obs	Calc
12	15	2	13	11	14	2	12	11781.42	11781.420	18	19	13	6	17	18	13	5	14822.656	14822.652
15	15	2	13	14	14	2	12	11783.27	11783.271	19	20	13	7	18	19	13	6	15606.824	15606.830
16	15	2	13	15	14	2	12	11784.82	11784.821	17	20	13	7	16	19	13	6	15657.624	15657.629
17	15	2	13	16	14	2	12	11785.10	11785.101	21	20	13	7	20	19	13	6	15617.114	15617.116
14	16	2	14	13	15	2	13	12572.63	12572.636	20	20	13	7	19	19	13	6	15602.658	15602.661
16	16	2	14	15	15	2	13	12575.74	12575.736	3	2	1	2	2	1	1	1	1347.783	1347.776
17	17	2	15	16	16	2	14	13368.58	13368.568	4	2	1	2	3	1	1	1	1684.545	1684.557
19	17	2	15	18	16	2	14	13369.41	13369.411	15	13	1	13	14	12	1	12	10045.832	10045.828
18	17	2	15	17	16	2	14	13369.65	13369.658	12	13	1	13	11	12	1	12	10038.812	10038.819
15	17	2	15	14	16	2	14	13365.65	13365.658	10	13	1	13	9	12	1	12	10041.704	10041.704
14	17	2	15	13	16	2	14	13366.22	13366.221	13	13	1	13	12	12	1	12	10042.388	10042.393
16	17	2	15	15	16	2	14	13366.86	13366.866	14	13	1	13	13	12	1	12	10045.503	10045.506
15	18	2	16	14	17	2	15	14160.36	14160.360	13	14	1	14	12	13	1	13	10810.035	10810.033
16	18	2	16	15	17	2	15	14159.34	14159.345	11	14	1	14	10	13	1	13	10811.156	10811.157
18	18	2	16	17	17	2	15	14161.76	14161.767	14	14	1	14	13	13	1	13	10813.235	10813.232
20	18	2	16	19	17	2	15	14162.19	14162.194	16	14	1	14	15	13	1	13	10816.010	10816.008
19	18	2	16	18	17	2	15	14163.22	14163.228	15	14	1	14	14	13	1	13	10816.278	10816.278
16	19	2	17	15	18	2	16	14952.74	14952.745	12	14	1	14	11	13	1	13	10807.763	10807.761
18	19	2	17	17	18	2	16	14953.28	14953.287	12	15	1	15	11	14	1	14	11582.054	11582.053
19	19	2	17	18	18	2	16	14954.62	14954.629	15	15	1	15	14	14	1	14	11583.343	11583.338
17	19	2	17	16	18	2	16	14952.26	14952.268	16	15	1	15	15	14	1	14	11585.665	11585.665
20	20	2	18	19	19	2	17	15747.58	15747.580	17	15	1	15	16	14	1	14	11585.915	11585.916
22	20	2	18	21	19	2	17	15747.92	15747.920	13	15	1	15	12	14	1	14	11579.594	11579.591
21	20	2	18	20	19	2	17	15748.33	15748.332	14	15	1	15	13	14	1	14	11580.634	11580.631
18	20	2	18	17	19	2	17	15745.44	15745.444	18	16	1	16	17	15	1	15	12355.537	12355.532
17	20	2	18	16	19	2	17	15745.88	15745.880	14	16	1	16	13	15	1	15	12349.960	12349.962
19	20	2	18	18	19	2	17	15746.32	15746.321	15	16	1	16	14	15	1	15	12350.852	12350.849
10	13	3	10	9	12	3	9	10164.85	10164.856	13	16	1	16	12	15	1	15	12352.165	12352.168
15	13	3	10	14	12	3	9	10173.39	10173.396	16	16	1	16	15	15	1	15	12353.247	12353.250
11	13	3	10	10	12	3	9	10158.37	10158.373	17	16	1	16	16	15	1	15	12355.396	12355.395
14	13	3	10	13	12	3	9	10159.15	10159.157	15	17	1	17	14	16	1	16	13119.883	13119.881
12	13	3	10	11	12	3	9	10159.54	10159.556	16	17	1	17	15	16	1	16	13120.653	13120.651

Continuation of I-pF-p transitions																		
$2J'$	N'	K'_a	K'_c	$2J$	N	K_a	K_c	Obs	Calc	$2J'$	N'	K'_a	K'_c	$2J$	N	K_a	K_c	Obs	Calc
11	14	3	11	10	13	3	10	10949.80	10949.804	14	17	1	17	13	16	1	16	13121.879	13121.876
16	14	3	11	15	13	3	10	10953.32	10953.327	17	17	1	17	16	16	1	16	13122.790	13122.786
13	14	3	11	12	13	3	10	10945.67	10945.651	18	17	1	17	17	16	1	16	13124.718	13124.717
15	14	3	11	14	13	3	10	10946.74	10946.746	20	18	1	18	19	17	1	17	13893.860	13893.857
14	15	3	12	13	14	3	11	11729.85	11729.858	16	18	1	18	15	17	1	17	13889.394	13889.392
13	15	3	12	12	14	3	11	11730.24	11730.242	17	18	1	18	16	17	1	17	13890.063	13890.065
15	15	3	12	14	14	3	11	11731.05	11731.061	15	18	1	18	14	17	1	17	13891.213	13891.210
16	15	3	12	15	14	3	11	11733.07	11733.072	18	18	1	18	17	17	1	17	13891.978	13891.974
12	15	3	12	11	14	3	11	11734.13	11734.137	19	18	1	18	18	17	1	17	13893.722	13893.719
17	15	3	12	16	14	3	11	11738.76	11738.764	17	19	1	19	16	18	1	18	14658.525	14658.523
13	16	3	13	12	15	3	12	12518.76	12518.759	18	19	1	19	17	18	1	18	14659.117	14659.112
18	16	3	13	17	15	3	12	12522.33	12522.331	16	19	1	19	15	18	1	18	14660.197	14660.193
15	16	3	13	14	15	3	12	12515.22	12515.226	19	19	1	19	18	18	1	18	14660.834	14660.830
14	16	3	13	13	15	3	12	12515.48	12515.481	20	19	1	19	19	18	1	18	14662.421	14662.417
16	16	3	13	15	15	3	12	12516.49	12516.495	21	19	1	19	20	18	1	18	14662.572	14662.566
17	16	3	13	16	15	3	12	12518.44	12518.449	22	20	1	20	21	19	1	19	15430.986	15430.983
15	17	3	14	14	16	3	13	13301.23	13301.240	18	20	1	20	17	19	1	19	15427.299	15427.298
17	17	3	14	16	16	3	13	13302.39	13302.392	19	20	1	20	18	19	1	19	15427.818	15427.817
14	17	3	14	13	16	3	13	13303.95	13303.953	17	20	1	20	16	19	1	19	15428.843	15428.841
18	17	3	14	17	16	3	13	13304.17	13304.175	20	20	1	20	19	19	1	19	15429.370	15429.370
19	17	3	14	18	16	3	13	13306.98	13306.976	21	20	1	20	20	19	1	19	15430.822	15430.821
16	17	3	14	15	16	3	13	13301.14	13301.137	13	13	2	12	12	12	2	11	10145.855	10145.854
18	18	3	15	17	17	3	14	14088.87	14088.878	10	13	2	12	9	12	2	11	10147.637	10147.640
15	18	3	15	14	17	3	14	14089.84	14089.846	14	13	2	12	13	12	2	11	10148.767	10148.768
19	18	3	15	18	17	3	14	14090.45	14090.456	15	13	2	12	14	12	2	11	10152.590	10152.589
20	18	3	15	19	17	3	14	14092.48	14092.483	11	13	2	12	10	12	2	11	10143.237	10143.237
18	19	3	16	17	18	3	15	14874.89	14874.901	12	13	2	12	11	12	2	11	10143.378	10143.379
19	19	3	16	18	18	3	15	14876.05	14876.057	13	14	2	13	12	13	2	12	10923.022	10923.023
16	19	3	16	15	18	3	15	14876.52	14876.526	16	14	2	13	15	13	2	12	10930.828	10930.831
20	19	3	16	19	18	3	15	14877.43	14877.430	11	14	2	13	10	13	2	12	10926.625	10926.626
21	19	3	16	20	18	3	15	14878.87	14878.868	15	14	2	13	14	13	2	12	10927.914	10927.916
17	19	3	16	16	18	3	15	14874.73	14874.732	12	14	2	13	11	13	2	12	10922.869	10922.872

Continuation of I-pF-p transitions																		
$2J'$	N'	K'_a	K'_c	$2J$	N	K_a	K_c	Obs	Calc	$2J'$	N'	K'_a	K'_c	$2J$	N	K_a	K_c	Obs	Calc
19	20	3	17	18	19	3	16	15662.92	15662.923	12	15	2	14	11	14	2	13	11705.246	11705.248
21	20	3	17	20	19	3	16	15665.19	15665.199	13	15	2	14	12	14	2	13	11701.996	11701.998
22	20	3	17	21	19	3	16	15666.17	15666.170	14	15	2	14	13	14	2	13	11702.158	11702.158
18	20	3	17	17	19	3	16	15662.64	15662.643	15	15	2	14	14	14	2	13	11704.161	11704.163
10	13	4	9	9	12	4	8	10136.93	10136.925	16	15	2	14	15	14	2	13	11706.573	11706.572
11	13	4	9	10	12	4	8	10145.08	10145.063	17	15	2	14	16	14	2	13	11708.887	11708.886
12	13	4	9	11	12	4	8	10153.03	10153.034	15	16	2	15	14	15	2	14	12480.799	12480.802
12	14	4	10	11	13	4	9	10986.04	10986.058	18	16	2	15	17	15	2	14	12486.685	12486.685
14	14	4	10	13	13	4	9	10957.27	10957.272	16	16	2	15	15	15	2	14	12482.609	12482.611
11	14	4	10	10	13	4	9	11024.52	11024.531	14	16	2	15	13	15	2	14	12480.636	12480.638
17	15	4	11	16	14	4	10	11733.66	11733.661	17	16	2	15	16	15	2	14	12484.784	12484.784
15	15	4	11	14	14	4	10	11709.54	11709.562	13	16	2	15	12	15	2	14	12483.486	12483.489
12	15	4	11	11	14	4	10	11713.82	11713.825	17	17	2	16	16	16	2	15	13260.602	13260.603
14	15	4	11	13	14	4	10	11718.60	11718.602	15	17	2	16	14	16	2	15	13258.799	13258.801
16	15	4	11	15	14	4	10	11669.15	11669.156	14	17	2	16	13	16	2	15	13261.296	13261.299
13	16	4	12	12	15	4	11	12507.82	12507.821	19	17	2	16	18	16	2	15	13264.176	13264.175
18	16	4	12	17	15	4	11	12514.79	12514.788	16	17	2	16	15	16	2	15	13258.976	13258.978
17	16	4	12	16	15	4	11	12500.52	12500.520	18	17	2	16	17	16	2	15	13262.559	13262.558
16	16	4	12	15	15	4	11	12502.68	12502.709	17	18	2	17	16	17	2	16	14036.639	14036.642
16	17	4	13	15	16	4	12	13287.18	13287.205	18	18	2	17	17	17	2	16	14038.092	14038.093
18	17	4	13	17	16	4	12	13288.17	13288.178	19	18	2	17	18	17	2	16	14039.843	14039.843
14	17	4	13	13	16	4	12	13292.08	13292.080	20	18	2	17	19	17	2	16	14041.311	14041.313
17	17	4	13	16	16	4	12	13287.07	13287.071	15	18	2	17	14	17	2	16	14035.416	14035.411
16	18	4	14	15	17	4	13	14067.68	14067.676	19	19	2	18	18	18	2	17	14815.334	14815.339
18	18	4	14	17	17	4	13	14070.91	14070.917	20	19	2	18	19	18	2	17	14817.371	14817.373
19	18	4	14	18	17	4	13	14072.47	14072.480	21	19	2	18	20	18	2	17	14818.070	14818.067
15	18	4	14	14	17	4	13	14075.28	14075.283	16	19	2	18	15	18	2	17	14819.568	14819.574
20	18	4	14	19	17	4	13	14078.02	14078.022	18	19	2	18	17	18	2	17	14813.858	14813.859
19	19	4	15	18	18	4	14	14854.72	14854.731	17	19	2	18	16	18	2	17	14814.253	14814.256
17	19	4	15	16	18	4	14	14855.18	14855.186	19	20	2	19	18	19	2	18	15590.536	15590.545
16	19	4	15	15	18	4	14	14858.37	14858.386	20	20	2	19	19	19	2	18	15591.720	15591.730
21	19	4	15	20	18	4	14	14861.39	14861.389	17	20	2	19	16	19	2	18	15592.296	15592.305

Continuation of I-pF-p transitions																		
$2J'$	N'	K'_a	K'_c	$2J$	N	K_a	K_c	Obs	Calc	$2J'$	N'	K'_a	K'_c	$2J$	N	K_a	K_c	Obs	Calc
22	20	4	16	21	19	4	15	15644.55	15644.557	21	20	2	19	20	19	2	18	15593.007	15593.013
19	20	4	16	18	19	4	15	15637.20	15637.205	22	20	2	19	21	19	2	18	15594.399	15594.406
18	20	4	16	17	19	4	15	15637.83	15637.838	18	20	2	19	17	19	2	18	15590.396	15590.404
20	20	4	16	19	19	4	15	15638.38	15638.384	15	13	3	11	14	12	3	10	10170.239	10170.238
21	20	4	16	20	19	4	15	15640.72	15640.721	14	13	3	11	13	12	3	10	10155.924	10155.924
17	20	4	16	16	19	4	15	15641.65	15641.656	11	13	3	11	10	12	3	10	10156.391	10156.392
12	13	5	8	11	12	5	7	10103.26	10103.264	12	13	3	11	11	12	3	10	10156.885	10156.887
12	14	5	9	11	13	5	8	10954.69	10954.691	13	13	3	11	12	12	3	10	10157.472	10157.474
14	14	5	9	13	13	5	8	10932.15	10932.150	10	13	3	11	9	12	3	10	10162.180	10162.180
14	15	5	10	13	14	5	9	11718.18	11718.182	16	14	3	12	15	13	3	11	10951.277	10951.274
17	15	5	10	16	14	5	9	11741.20	11741.210	14	14	3	12	13	13	3	11	10941.517	10941.516
15	15	5	10	14	14	5	9	11714.22	11714.225	13	14	3	12	12	13	3	11	10940.408	10940.410
16	16	5	11	15	15	5	10	12494.94	12494.938	12	14	3	12	11	13	3	11	10940.900	10940.893
17	17	5	12	16	16	5	11	13306.02	13306.012	15	14	3	12	14	13	3	11	10943.075	10943.079
16	17	5	12	15	16	5	11	13285.08	13285.094	17	15	3	13	16	14	3	12	11732.743	11732.740
15	17	5	12	14	16	5	11	13328.70	13328.713	15	15	3	13	14	14	3	12	11724.970	11724.969
15	18	5	13	14	17	5	12	14056.96	14056.965	16	15	3	13	15	14	3	12	11727.061	11727.060
13	13	6	7	12	12	6	6	10139.47	10139.475	12	15	3	13	11	14	3	12	11728.587	11728.590
11	13	6	7	10	12	6	6	10159.94	10159.945	14	15	3	13	13	14	3	12	11723.732	11723.732
10	13	6	7	9	12	6	6	10181.04	10181.045	13	15	3	13	12	14	3	12	11724.286	11724.286
15	13	6	7	14	12	6	6	10182.00	10182.004	16	16	3	14	15	15	3	13	12508.164	12508.162
12	13	6	7	11	12	6	6	10144.40	10144.408	17	16	3	14	16	15	3	13	12510.272	12510.270
11	14	6	8	10	13	6	7	10957.62	10957.627	13	16	3	14	12	15	3	13	12511.068	12511.071
16	14	6	8	15	13	6	7	10961.57	10961.572	14	16	3	14	13	15	3	13	12507.382	12507.383
15	14	6	8	14	13	6	7	10934.48	10934.485	15	16	3	14	14	15	3	13	12506.912	12506.912
14	14	6	8	13	13	6	7	10925.19	10925.184	16	17	3	15	15	16	3	14	13289.996	13289.995
13	14	6	8	12	13	6	7	10930.35	10930.360	15	17	3	15	14	16	3	14	13290.358	13290.358
12	15	6	9	11	14	6	8	11735.47	11735.479	18	17	3	15	17	16	3	14	13293.193	13293.192
16	15	6	9	15	14	6	8	11720.51	11720.513	14	17	3	15	13	16	3	14	13293.527	13293.531
13	16	6	10	12	15	6	9	12514.11	12514.113	19	18	3	16	18	17	3	15	14075.963	14075.965
16	17	6	11	15	16	6	10	13292.20	13292.204	18	18	3	16	17	17	3	15	14074.141	14074.147
18	17	6	11	17	16	6	10	13294.82	13294.817	16	18	3	16	15	17	3	15	14073.247	14073.251

Continuation of I-pF-p transitions																		
$2J'$	N'	K'_a	K'_c	$2J$	N	K_a	K_c	Obs	Calc	$2J'$	N'	K'_a	K'_c	$2J$	N	K_a	K_c	Obs	Calc
15	17	6	11	14	16	6	10	13300.59	13300.597	17	18	3	16	16	17	3	15	14072.983	14072.985
17	17	6	11	16	16	6	10	13278.31	13278.312	20	18	3	16	19	17	3	15	14078.573	14078.575
19	18	6	12	18	17	6	11	14063.86	14063.875	19	19	3	17	18	18	3	16	14856.968	14856.974
18	18	6	12	17	17	6	11	14060.04	14060.048	20	19	3	17	19	18	3	16	14858.627	14858.628
20	18	6	12	19	17	6	11	14084.15	14084.159	16	19	3	17	15	18	3	16	14858.451	14858.461
21	19	6	13	20	18	6	12	14860.17	14860.181	21	19	3	17	20	18	3	16	14860.738	14860.745
18	19	6	13	17	18	6	12	14844.94	14844.951	17	19	3	17	16	18	3	16	14856.057	14856.060
19	19	6	13	18	18	6	12	14840.18	14840.195	18	19	3	17	17	18	3	16	14855.871	14855.875
21	20	6	14	20	19	6	13	15736.28	15736.278	19	20	3	18	18	19	3	17	15638.641	15638.646
10	13	7	6	9	12	7	5	10188.53	10188.531	20	20	3	18	19	19	3	17	15639.675	15639.679
12	13	7	6	11	12	7	5	10134.40	10134.404	18	20	3	18	17	19	3	17	15638.765	15638.768
11	13	7	6	10	12	7	5	10153.43	10153.431	17	20	3	18	16	19	3	17	15640.879	15640.882
14	13	7	6	13	12	7	5	10145.45	10145.453	21	20	3	18	20	19	3	17	15641.179	15641.182
13	13	7	6	12	12	7	5	10131.17	10131.174	22	20	3	18	21	19	3	17	15642.929	15642.930
15	13	7	6	14	12	7	5	10187.10	10187.105	15	13	4	10	14	12	4	9	10174.255	10174.274
16	14	7	7	15	13	7	6	10963.64	10963.638	12	13	4	10	11	12	4	9	10152.993	10152.979
14	14	7	7	13	13	7	6	10918.82	10918.825	14	13	4	10	13	12	4	9	10146.726	10146.724
13	14	7	7	12	13	7	6	10923.40	10923.406	12	14	4	11	11	13	4	10	10985.964	10985.971
11	14	7	7	10	13	7	6	10964.78	10964.779	14	14	4	11	13	13	4	10	10957.191	10957.182
15	14	7	7	14	13	7	6	10930.25	10930.245	16	14	4	11	15	13	4	10	10953.234	10953.226
12	14	7	7	11	13	7	6	10939.85	10939.856	17	15	4	12	16	14	4	11	11733.523	11733.519
13	15	7	8	12	14	7	7	11721.49	11721.492	12	15	4	12	11	14	4	11	11713.677	11713.673
17	15	7	8	16	14	7	7	11741.58	11741.585	15	15	4	12	14	14	4	11	11709.382	11709.383
14	15	7	8	13	14	7	7	11708.13	11708.131	17	16	4	13	16	15	4	12	12500.278	12500.278
15	15	7	8	14	14	7	7	11704.52	11704.530	13	16	4	13	12	15	4	12	12507.593	12507.589
16	16	7	9	15	15	7	8	12489.29	12489.291	16	16	4	13	15	15	4	12	12502.451	12502.449
14	16	7	9	13	15	7	8	12503.91	12503.914	18	17	4	14	17	16	4	13	13287.613	13287.612
15	16	7	9	14	15	7	8	12492.53	12492.539	19	17	4	14	18	16	4	13	13295.447	13295.442
18	16	7	9	17	15	7	8	12520.84	12520.837	14	17	4	14	13	16	4	13	13291.723	13291.722
17	16	7	9	16	15	7	8	12497.72	12497.723	16	17	4	14	15	16	4	13	13286.162	13286.161
13	16	7	9	12	15	7	8	12519.01	12519.011	17	17	4	14	16	16	4	13	13286.662	13286.654
18	17	7	10	17	16	7	9	13281.12	13281.126	19	18	4	15	18	17	4	14	14072.099	14072.103

Continuation of I-pF-p transitions																		
$2J'$	N'	K'_a	K'_c	$2J$	N	K_a	K_c	Obs	Calc	$2J'$	N'	K'_a	K'_c	$2J$	N	K_a	K_c	Obs	Calc
19	17	7	10	18	16	7	9	13301.87	13301.877	20	18	4	15	19	17	4	14	14078.407	14078.408
16	17	7	10	15	16	7	9	13277.45	13277.457	15	18	4	15	14	17	4	14	14074.742	14074.745
14	17	7	10	13	16	7	9	13297.65	13297.653	18	18	4	15	17	17	4	14	14070.337	14070.341
15	17	7	10	14	16	7	9	13288.70	13288.709	18	19	4	16	17	18	4	15	14853.261	14853.261
17	17	7	10	16	16	7	9	13273.41	13273.412	19	19	4	16	18	18	4	15	14853.856	14853.863
19	18	7	11	18	17	7	10	14066.56	14066.559	20	19	4	16	19	18	4	15	14855.662	14855.663
18	18	7	11	17	17	7	10	14057.32	14057.328	21	19	4	16	20	18	4	15	14860.275	14860.268
17	18	7	11	16	17	7	10	14070.09	14070.106	16	19	4	16	15	18	4	15	14857.594	14857.594
20	18	7	11	19	17	7	10	14089.63	14089.633	17	20	4	17	16	19	4	16	15640.512	15640.515
16	19	7	12	15	18	7	11	14856.47	14856.471	19	20	4	17	18	19	4	16	15636.724	15636.729
20	20	7	13	19	19	7	12	15623.92	15623.933	21	20	4	17	20	19	4	16	15639.114	15639.116
18	20	7	13	17	19	7	12	15646.35	15646.361	14	13	5	9	13	12	5	8	10132.787	10132.786
17	20	7	13	16	19	7	12	15635.87	15635.877	10	13	5	9	9	12	5	8	10172.993	10172.994
19	20	7	13	18	19	7	12	15638.17	15638.183	13	13	5	9	12	12	5	8	10142.254	10142.246
21	20	7	13	20	19	7	12	15642.22	15642.233	11	14	5	10	10	13	5	9	10950.523	10950.523
12	13	8	5	11	12	8	4	10131.61	10131.608	15	14	5	10	14	13	5	9	10946.913	10946.915
13	13	8	5	12	12	8	4	10122.63	10122.634	14	14	5	10	13	13	5	9	10932.158	10932.164
14	13	8	5	13	12	8	4	10140.82	10140.821	13	14	5	10	12	13	5	9	10945.843	10945.842
15	13	8	5	14	12	8	4	10194.31	10194.309	12	15	5	11	11	14	5	10	11726.678	11726.677
10	13	8	5	9	12	8	4	10200.98	10200.984	13	15	5	11	12	14	5	10	11722.581	11722.587
14	14	8	6	13	13	8	5	10913.52	10913.523	14	16	5	12	13	15	5	11	12491.956	12491.940
12	14	8	6	11	13	8	5	10942.01	10942.019	18	16	5	12	17	15	5	11	12516.942	12516.938
13	14	8	6	12	13	8	5	10920.41	10920.417	13	16	5	12	12	15	5	11	12482.124	12482.118
15	14	8	6	14	13	8	5	10926.40	10926.409	17	16	5	12	16	15	5	11	12492.183	12492.184
16	14	8	6	15	13	8	5	10969.22	10969.218	15	16	5	12	14	15	5	11	12499.292	12499.289
11	14	8	6	10	13	8	5	10974.26	10974.262	14	17	5	13	13	16	5	12	13367.583	13367.591
17	15	8	7	16	14	8	6	11745.71	11745.714	18	18	5	14	17	17	5	13	14051.840	14051.834
12	15	8	7	11	14	8	6	11747.73	11747.738	19	18	5	14	18	17	5	13	14008.404	14008.402
14	15	8	7	13	14	8	6	11703.08	11703.089	16	18	5	14	15	17	5	13	14054.482	14054.473
16	15	8	7	15	14	8	6	11710.93	11710.937	21	19	5	15	20	18	5	14	14858.209	14858.202
15	15	8	7	14	14	8	6	11698.63	11698.628	19	19	5	15	18	18	5	14	14846.723	14846.716
15	16	8	8	14	15	8	7	12487.88	12487.889	16	19	5	15	15	18	5	14	14851.784	14851.782

Continuation of I-pF-p transitions																		
$2J'$	N'	K'_a	K'_c	$2J$	N	K_a	K_c	Obs	Calc	$2J'$	N'	K'_a	K'_c	$2J$	N	K_a	K_c	Obs	Calc
17	16	8	8	16	15	8	7	12494.73	12494.736	14	13	6	8	13	12	6	7	10150.064	10150.063
18	16	8	8	17	15	8	7	12523.40	12523.407	12	14	6	9	11	13	6	8	10944.441	10944.442
13	16	8	8	12	15	8	7	12524.30	12524.308	15	15	6	10	14	14	6	9	11710.313	11710.313
16	16	8	8	15	15	8	7	12484.36	12484.365	14	15	6	10	13	14	6	9	11724.666	11724.670
14	16	8	8	13	15	8	7	12502.08	12502.087	17	15	6	10	16	14	6	9	11748.585	11748.582
17	17	8	9	16	16	8	8	13269.12	13269.119	13	15	6	10	12	14	6	9	11750.618	11750.622
16	17	8	9	15	16	8	8	13271.91	13271.915	18	16	6	11	17	15	6	10	12415.921	12415.927
15	17	8	9	14	16	8	8	13283.68	13283.695	16	16	6	11	15	15	6	10	12491.065	12491.062
18	17	8	9	17	16	8	8	13278.04	13278.037	15	16	6	11	14	15	6	10	12452.798	12452.784
18	18	8	10	17	17	8	9	14053.23	14053.230	17	16	6	11	16	15	6	10	12475.408	12475.414
19	18	8	10	18	17	8	9	14061.01	14061.012	14	17	6	12	13	16	6	11	13292.840	13292.839
17	18	8	10	16	17	8	9	14055.62	14055.622	19	17	6	12	18	16	6	11	13356.777	13356.771
15	18	8	10	14	17	8	9	14080.52	14080.530	16	18	6	13	15	17	6	12	14067.864	14067.867
20	18	8	10	19	17	8	9	14081.50	14081.503	17	19	6	14	16	18	6	13	14838.102	14838.121
16	18	8	10	15	17	8	9	14065.65	14065.653	21	19	6	14	20	18	6	13	14860.101	14860.107
19	19	8	11	18	18	8	10	14836.87	14836.881	16	19	6	14	15	18	6	13	14827.419	14827.415
20	19	8	11	19	18	8	10	14843.83	14843.835	20	20	6	15	19	19	6	14	15654.196	15654.188
21	19	8	11	20	18	8	10	14861.84	14861.848	19	20	6	15	18	19	6	14	15629.592	15629.598
18	19	8	11	17	18	8	10	14839.30	14839.308	21	19	7	13	20	18	7	12	14753.181	14753.193
17	19	8	11	16	18	8	10	14848.28	14848.288	18	19	7	13	17	18	7	12	14800.558	14800.546
16	19	8	11	15	18	8	10	14859.72	14859.729	13	14	0	14	12	12	3	9	10165.284	10165.288
20	20	8	12	19	19	8	11	15620.19	15620.194	15	14	4	11	14	12	5	8	10361.298	10361.295
21	20	8	12	20	19	8	11	15626.78	15626.782	15	14	4	10	14	12	5	7	10361.463	10361.461
18	20	8	12	17	19	8	11	15633.13	15633.144	11	14	4	11	10	12	5	8	10648.526	10648.529
22	20	8	12	21	19	8	11	15643.65	15643.651	11	14	4	10	10	12	5	7	10648.693	10648.698
19	20	8	12	18	19	8	11	15623.62	15623.630	14	15	0	15	13	13	3	10	11642.957	11642.963
17	20	8	12	16	19	8	11	15639.40	15639.410	16	15	4	12	15	13	5	9	11950.642	11950.636
14	13	9	4	13	12	9	3	10136.39	10136.389	16	15	4	11	15	13	5	8	11950.965	11950.958
12	13	9	4	11	12	9	3	10125.88	10125.879	15	16	9	7	14	13	10	4	12641.089	12641.088
15	13	9	4	14	12	9	3	10202.75	10202.762	18	17	5	13	17	15	6	10	12690.081	12690.082
13	13	9	4	12	12	9	3	10114.46	10114.461	18	17	5	12	17	15	6	9	12690.094	12690.093
10	13	9	4	9	12	9	3	10214.14	10214.154	14	17	5	13	13	15	6	10	12976.939	12976.932

Continuation of I-pF-p transitions																			
$2J'$	N'	K'_a	K'_c	$2J$	N	K_a	K_c	Obs	Calc	$2J'$	N'	K'_a	K'_c	$2J$	N	K_a	K_c	Obs	Calc
11	13	9	4	10	12	9	3	10161.59	10161.595	16	19	6	13	15	17	7	10	13688.465	13688.458
14	14	9	5	13	13	9	4	10904.28	10904.282	20	20	6	15	19	18	7	12	15047.918	15047.916
13	14	9	5	12	13	9	4	10912.69	10912.699	18	20	6	15	17	18	7	12	15210.767	15210.771
16	14	9	5	15	13	9	4	10975.93	10975.931	17	20	6	15	16	18	7	12	15305.689	15305.692
15	14	9	5	14	13	9	4	10922.50	10922.500	14	14	10	5	14	13	10	4	10966.037	10966.042
11	14	9	5	10	13	9	4	10983.13	10983.132	13	16	7	9	13	15	7	8	12614.539	12614.534
17	15	9	6	16	14	9	5	11751.10	11751.098	17	20	6	15	16	19	6	14	15710.783	15710.796
14	15	9	6	13	14	9	5	11704.08	11704.067	16	19	7	13	16	18	7	12	14959.397	14959.385
15	15	9	6	14	14	9	5	11694.06	11694.067	16	19	6	13	15	18	6	12	14827.422	14827.415
16	15	9	6	15	14	9	5	11707.63	11707.627	16	18	7	11	15	17	7	10	14093.557	14093.563
13	15	9	6	12	14	9	5	11729.23	11729.234	13	14	0	14	12	13	0	13	10872.272	10872.271
12	15	9	6	11	14	9	5	11758.94	11758.944	13	14	0	14	13	13	0	13	10917.818	10917.828
16	16	9	7	15	15	9	6	12478.22	12478.221	13	13	3	10	12	12	3	9	10157.718	10157.716
18	16	9	7	17	15	9	6	12527.69	12527.693	13	13	3	10	12	13	0	13	10864.705	10864.700
13	16	9	7	12	15	9	6	12527.80	12527.815	13	13	3	10	13	13	0	13	10910.259	10910.256
16	17	9	8	15	16	9	7	13268.04	13268.047	14	15	0	15	13	14	0	14	11635.393	11635.391
14	17	9	8	13	16	9	7	13306.90	13306.901	14	15	0	15	14	14	0	14	11681.224	11681.232
17	17	9	8	16	16	9	7	13264.52	13264.524	13	14	3	11	13	13	3	10	10980.368	10980.374
18	17	9	8	17	16	9	7	13275.54	13275.544	14	14	3	11	13	13	3	10	10948.546	10948.546
19	17	9	8	18	16	9	7	13305.35	13305.356	16	15	4	12	15	14	4	11	11668.941	11668.943
19	18	9	9	18	17	9	8	14058.73	14058.732	16	15	4	12	16	14	4	11	11528.423	11528.422
20	18	9	9	19	17	9	8	14083.85	14083.849	16	14	5	10	15	13	5	9	11009.942	11009.942
15	18	9	9	14	17	9	8	14084.56	14084.573	16	14	5	10	16	14	4	11	10587.729	10587.727
18	18	9	9	17	17	9	8	14049.26	14049.259	16	14	5	10	15	14	4	11	10728.247	10728.249
16	18	9	9	15	17	9	8	14064.52	14064.531	15	16	9	7	14	15	9	6	12479.645	12479.645
17	18	9	9	16	17	9	8	14052.05	14052.049	15	14	10	5	14	13	10	4	10922.503	10922.502
17	19	9	10	16	18	9	9	14846.14	14846.154	18	17	5	12	17	16	5	11	13386.711	13386.698
20	19	9	10	19	18	9	9	14841.59	14841.598	18	16	6	10	17	15	6	9	12415.921	12415.931
21	20	9	11	20	19	9	10	15624.24	15624.242	18	16	6	10	17	16	5	11	13112.541	13112.536
18	20	9	11	17	19	9	10	15627.95	15627.962	16	18	7	11	15	18	6	12	15232.515	15232.520
20	20	9	11	19	19	9	10	15616.99	15616.994	16	18	7	11	16	18	6	12	15408.421	15408.427
11	13	10	3	10	12	10	2	10163.36	10163.366	20	19	7	13	20	19	6	14	15358.430	15358.427

Continuation of I-pF-p transitions																				
$2J'$	N'	K'_a	K'_c	$2J$	N	K_a	K_c	Obs	Calc	$2J'$	N'	K'_a	K'_c	$2J$	N	K_a	K_c	Obs	Calc
12	13	10	3	11	12	10	2	10114.95	10114.957	20	19	7	13	19	18	7	12	14817.722	14817.729
End of Table																				

TABLE B.3. Fit Results of 2-fluoro-4-chlorotoluene

Transitions used in the fit described in 4.2.3																					
$2J'$	N'	K'_a	K'_c	$2J$	N	K_a	K_c	m	Obs (MHz)	Calc (MHz)	$2J'$	N'	K'_a	K'_c	$2J$	N	K_a	K_c	m	Obs (MHz)	Calc (MHz)
3	3	0	3	1	2	0	2	0	4545.035	4545.024	24	10	0	10	22	9	0	9	0	14172.097	14172.101
5	3	0	3	3	2	0	2	0	4545.075	4545.078	22	10	0	10	20	9	0	9	0	14172.124	14172.129
9	3	0	3	7	2	0	2	0	4549.306	4549.304	18	10	0	10	16	9	0	9	1	14171.276	14171.270
7	3	0	3	5	2	0	2	0	4549.402	4549.394	20	10	0	10	18	9	0	9	1	14171.306	14171.301
9	3	0	3	7	2	0	2	1	4549.225	4549.235	24	10	0	10	22	9	0	9	1	14171.538	14171.532
7	3	0	3	5	2	0	2	1	4549.318	4549.324	22	10	0	10	20	9	0	9	1	14171.564	14171.559
5	4	0	4	3	3	0	3	0	6011.701	6011.695	18	10	1	10	16	9	0	9	0	14387.827	14387.838
7	4	0	4	5	3	0	3	0	6011.815	6011.803	20	10	1	10	18	9	0	9	0	14388.022	14388.034
11	4	0	4	9	3	0	3	0	6013.732	6013.718	24	10	1	10	22	9	0	9	0	14388.113	14388.125
9	4	0	4	7	3	0	3	0	6013.846	6013.834	22	10	1	10	20	9	0	9	0	14388.304	14388.316
5	4	0	4	3	3	0	3	1	6011.521	6011.536	18	10	1	10	16	9	0	9	1	14386.173	14386.157
7	4	0	4	5	3	0	3	1	6011.631	6011.644	20	10	1	10	18	9	0	9	1	14386.368	14386.354
11	4	0	4	9	3	0	3	1	6013.550	6013.559	24	10	1	10	22	9	0	9	1	14386.460	14386.445
9	4	0	4	7	3	0	3	1	6013.664	6013.675	22	10	1	10	20	9	0	9	1	14386.649	14386.634
7	5	0	5	5	4	0	4	0	7438.439	7438.430	20	10	2	9	18	9	2	8	0	15032.575	15032.554
9	5	0	5	7	4	0	4	0	7438.569	7438.558	22	10	2	9	20	9	2	8	0	15032.746	15032.728
13	5	0	5	11	4	0	4	0	7439.646	7439.634	18	10	2	9	16	9	2	8	0	15032.939	15032.922
11	5	0	5	9	4	0	4	0	7439.773	7439.762	24	10	2	9	22	9	2	8	0	15033.120	15033.100
7	5	0	5	5	4	0	4	1	7438.138	7438.146	20	10	2	9	18	9	2	8	1	15034.465	15034.485
9	5	0	5	7	4	0	4	1	7438.267	7438.275	22	10	2	9	20	9	2	8	1	15034.636	15034.659
13	5	0	5	11	4	0	4	1	7439.345	7439.350	18	10	2	9	16	9	2	8	1	15034.829	15034.852
11	5	0	5	9	4	0	4	1	7439.471	7439.479	24	10	2	9	22	9	2	8	1	15035.010	15035.029
7	5	1	5	5	4	0	4	0	8622.379	8622.394	22	11	0	11	20	10	1	10	0	15283.919	15283.918
13	5	1	5	11	4	0	4	0	8624.059	8624.050	20	11	0	11	18	10	1	10	0	15284.071	15284.072

Continuation of 2-F-4-Cl-tol Transitions																					
$2J'$	N'	K'_a	K'_c	$2J$	N	K_a	K_c	m	Obs (MHz)	Calc (MHz)	$2J'$	N'	K'_a	K'_c	$2J$	N	K_a	K_c	m	Obs	Calc
9	5	1	5	7	4	0	4	0	8624.162	8624.156	24	11	0	11	22	10	1	10	0	15284.108	15284.107
11	5	1	5	9	4	0	4	0	8625.828	8625.834	26	11	0	11	24	10	1	10	0	15284.260	15284.259
7	5	1	5	5	4	0	4	1	8617.585	8617.594	22	11	0	11	20	10	1	10	1	15284.497	15284.501
13	5	1	5	11	4	0	4	1	8619.265	8619.250	20	11	0	11	18	10	1	10	1	15284.649	15284.654
9	5	1	5	7	4	0	4	1	8619.366	8619.356	24	11	0	11	22	10	1	10	1	15284.686	15284.690
11	5	1	5	9	4	0	4	1	8621.031	8621.034	26	11	0	11	24	10	1	10	1	15284.838	15284.841
9	6	0	6	7	5	0	5	0	8826.308	8826.301	20	11	1	10	18	10	1	9	0	17024.347	17024.327
11	6	0	6	9	5	0	5	0	8826.443	8826.435	22	11	1	10	20	10	1	9	0	17024.430	17024.410
15	6	0	6	13	5	0	5	0	8827.121	8827.111	26	11	1	10	24	10	1	9	0	17024.593	17024.571
13	6	0	6	11	5	0	5	0	8827.238	8827.231	24	11	1	10	22	10	1	9	0	17024.622	17024.602
9	6	0	6	7	5	0	5	1	8825.879	8825.883	20	11	1	10	18	10	1	9	1	17023.056	17023.087
11	6	0	6	9	5	0	5	1	8826.015	8826.018	22	11	1	10	20	10	1	9	1	17023.121	17023.151
15	6	0	6	13	5	0	5	1	8826.693	8826.694	26	11	1	10	24	10	1	9	1	17023.282	17023.311
13	6	0	6	11	5	0	5	1	8826.810	8826.813	24	11	1	10	22	10	1	9	1	17023.331	17023.361
11	6	1	5	9	5	1	4	0	9643.083	9643.044	22	11	1	11	20	10	1	10	0	15425.975	15425.981
9	6	1	5	7	5	1	4	0	9643.508	9643.471	20	11	1	11	18	10	1	10	0	15426.028	15426.034
13	6	1	5	11	5	1	4	0	9643.695	9643.657	24	11	1	11	22	10	1	10	0	15426.177	15426.182
15	6	1	5	13	5	1	4	0	9644.130	9644.089	26	11	1	11	24	10	1	10	0	15426.231	15426.235
13	7	0	7	11	6	0	6	0	10182.771	10182.768	22	11	1	11	20	10	1	10	1	15425.786	15425.783
11	7	0	7	9	6	0	6	0	10182.697	10182.695	20	11	1	11	18	10	1	10	1	15425.839	15425.836
13	7	0	7	11	6	0	6	1	10182.243	10182.243	24	11	1	11	22	10	1	10	1	15425.987	15425.984
17	7	0	7	15	6	0	6	1	10182.706	10182.704	26	11	1	11	24	10	1	10	1	15426.042	15426.037
15	7	0	7	13	6	0	6	1	10182.837	10182.837	20	11	0	11	18	10	0	10	0	15500.063	15500.071
13	7	2	6	11	6	2	5	0	10630.291	10630.265	22	11	0	11	20	10	0	10	0	15500.077	15500.083
15	7	2	6	13	6	2	5	0	10630.424	10630.406	26	11	0	11	24	10	0	10	0	15500.276	15500.283
11	7	2	6	9	6	2	5	0	10631.455	10631.439	24	11	0	11	22	10	0	10	0	15500.289	15500.294
17	7	2	6	15	6	2	5	0	10631.641	10631.614	20	11	0	11	18	10	0	10	1	15499.546	15499.541
13	7	1	6	11	6	1	5	0	11193.528	11193.487	22	11	0	11	20	10	0	10	1	15499.559	15499.553
11	7	1	6	9	6	1	5	0	11193.754	11193.714	26	11	0	11	24	10	0	10	1	15499.759	15499.753
15	7	1	6	13	6	1	5	0	11194.009	11193.969	24	11	0	11	22	10	0	10	1	15499.771	15499.765
17	7	1	6	15	6	1	5	0	11194.240	11194.198	20	11	1	11	18	10	0	10	0	15642.021	15642.032

Continuation of 2-F-4-Cl-tol Transitions																					
$2J'$	N'	K'_a	K'_c	$2J$	N	K_a	K_c	m	Obs (MHz)	Calc (MHz)	$2J'$	N'	K'_a	K'_c	$2J$	N	K_a	K_c	m	Obs	Calc
13	7	1	6	11	6	1	5	1	11192.799	11192.834	22	11	1	11	20	10	0	10	0	15642.133	15642.146
11	7	1	6	9	6	1	5	1	11193.025	11193.061	26	11	1	11	24	10	0	10	0	15642.247	15642.259
15	7	1	6	13	6	1	5	1	11193.280	11193.316	24	11	1	11	22	10	0	10	0	15642.358	15642.369
17	7	1	6	15	6	1	5	1	11193.511	11193.545	20	11	1	11	18	10	0	10	1	15640.737	15640.723
15	8	1	7	13	7	1	6	0	12712.246	12712.207	22	11	1	11	20	10	0	10	1	15640.848	15640.836
13	8	1	7	11	7	1	6	0	12712.351	12712.313	26	11	1	11	24	10	0	10	1	15640.963	15640.949
17	8	1	7	15	7	1	6	0	12712.630	12712.591	24	11	1	11	22	10	0	10	1	15641.072	15641.059
19	8	1	7	17	7	1	6	0	12712.739	12712.699	24	12	0	12	22	11	1	11	0	16689.881	16689.883
15	8	1	7	13	7	1	6	1	12711.492	12711.531	22	12	0	12	20	11	1	11	0	16689.979	16689.982
13	8	1	7	11	7	1	6	1	12711.597	12711.636	26	12	0	12	24	11	1	11	0	16690.048	16690.046
17	8	1	7	15	7	1	6	1	12711.875	12711.914	24	12	0	12	22	11	1	11	1	16690.178	16690.173
19	8	1	7	17	7	1	6	1	12711.984	12712.022	22	12	0	12	20	11	1	11	1	16690.267	16690.272
15	8	1	8	13	7	1	7	0	11324.260	11324.260	26	12	0	12	24	11	1	11	1	16690.336	16690.336
13	8	1	8	11	7	1	7	0	11324.427	11324.430	28	12	0	12	26	11	1	11	1	16690.430	16690.433
17	8	1	8	15	7	1	7	0	11324.620	11324.622	22	12	1	11	20	11	1	10	0	18380.095	18380.084
19	8	1	8	17	7	1	7	0	11324.795	11324.794	24	12	1	11	22	11	1	10	0	18380.167	18380.155
15	8	1	8	13	7	1	7	1	11324.340	11324.341	28	12	1	11	26	11	1	10	0	18380.281	18380.269
13	8	1	8	11	7	1	7	1	11324.506	11324.511	26	12	1	11	24	11	1	10	0	18380.349	18380.337
17	8	1	8	15	7	1	7	1	11324.700	11324.703	22	12	1	11	20	11	1	10	1	18378.580	18378.606
17	9	0	9	15	8	1	8	0	12375.993	12375.985	24	12	1	11	22	11	1	10	1	18378.653	18378.678
19	9	0	9	17	8	1	8	0	12376.243	12376.238	28	12	1	11	26	11	1	10	1	18378.766	18378.791
15	9	0	9	13	8	1	8	0	12376.372	12376.368	26	12	1	11	24	11	1	10	1	18378.834	18378.860
21	9	0	9	19	8	1	8	0	12376.625	12376.616	24	12	1	12	22	11	1	11	1	16781.566	16781.560
17	9	0	9	15	8	1	8	1	12377.479	12377.491	22	12	1	12	20	11	1	11	1	16781.604	16781.599
19	9	0	9	17	8	1	8	1	12377.731	12377.745	26	12	1	12	24	11	1	11	1	16781.736	16781.730
15	9	0	9	13	8	1	8	1	12377.858	12377.874	28	12	1	12	26	11	1	11	1	16781.775	16781.769
21	9	0	9	19	8	1	8	1	12378.110	12378.122	22	12	0	12	20	11	0	11	0	16831.936	16831.943
15	9	0	9	13	8	0	8	0	12846.057	12846.061	24	12	0	12	22	11	0	11	0	16831.936	16831.945
17	9	0	9	15	8	0	8	0	12846.112	12846.115	28	12	0	12	26	11	0	11	0	16832.113	16832.119
21	9	0	9	19	8	0	8	0	12846.389	12846.391	26	12	0	12	24	11	0	11	0	16832.113	16832.120
19	9	0	9	17	8	0	8	0	12846.439	12846.441	22	12	0	12	20	11	0	11	1	16831.461	16831.453

Continuation of 2-F-4-Cl-tol Transitions																						
$2J'$	N'	K'_a	K'_c	$2J$	N	K_a	K_c	m	Obs (MHz)	Calc (MHz)	$2J'$	N'	K'_a	K'_c	$2J$	N	K_a	K_c	m	Obs	Calc
15	9	0	9	13	8	0	8	1	12845.470	12845.466	24	12	0	12	22	11	0	11	1	16831.461	16831.455
17	9	0	9	15	8	0	8	1	12845.525	12845.522	28	12	0	12	26	11	0	11	1	16831.638	16831.630
21	9	0	9	19	8	0	8	1	12845.803	12845.798	26	12	0	12	24	11	0	11	1	16831.638	16831.630
19	9	0	9	17	8	0	8	1	12845.846	12845.842	22	12	1	12	20	11	0	11	0	16923.795	16923.807
17	9	1	8	15	8	1	7	0	14192.724	14192.690	24	12	1	12	22	11	0	11	0	16923.857	16923.869
15	9	1	8	13	8	1	7	0	14192.749	14192.715	28	12	1	12	26	11	0	11	0	16923.980	16923.991
19	9	1	8	17	8	1	7	0	14193.036	14193.001	26	12	1	12	24	11	0	11	0	16924.040	16924.051
21	9	1	8	19	8	1	7	0	14193.067	14193.031	22	12	1	12	20	11	0	11	1	16922.792	16922.781
17	9	1	8	15	8	1	7	1	14191.841	14191.879	24	12	1	12	22	11	0	11	1	16922.855	16922.843
15	9	1	8	13	8	1	7	1	14191.865	14191.904	28	12	1	12	26	11	0	11	1	16922.978	16922.965
19	9	1	8	17	8	1	7	1	14192.152	14192.190	26	12	1	12	24	11	0	11	1	16923.038	16923.024
21	9	1	8	19	8	1	7	1	14192.182	14192.220	26	13	0	13	24	12	0	12	0	18167.270	18167.279
17	9	1	9	15	8	1	8	0	12698.631	12698.632	24	13	0	13	22	12	0	12	0	18167.276	18167.284
15	9	1	9	13	8	1	8	0	12698.741	12698.743	28	13	0	13	26	12	0	12	0	18167.418	18167.427
19	9	1	9	17	8	1	8	0	12698.923	12698.925	30	13	0	13	28	12	0	12	0	18167.426	18167.433
21	9	1	9	19	8	1	8	0	12699.037	12699.037	26	13	0	13	24	12	0	12	1	18166.832	18166.824
17	9	1	9	15	8	1	8	1	12698.590	12698.590	24	13	0	13	22	12	0	12	1	18166.839	18166.829
15	9	1	9	13	8	1	8	1	12698.700	12698.701	28	13	0	13	26	12	0	12	1	18166.981	18166.972
19	9	1	9	17	8	1	8	1	12698.882	12698.883	30	13	0	13	28	12	0	12	1	18166.990	18166.978
21	9	1	9	19	8	1	8	1	12698.996	12698.995	24	13	1	13	22	12	0	12	0	18225.967	18225.979
15	9	1	9	13	8	0	8	0	13168.426	13168.436	26	13	1	13	24	12	0	12	0	18225.998	18226.010
17	9	1	9	15	8	0	8	0	13168.750	13168.762	30	13	1	13	28	12	0	12	0	18226.122	18226.132
21	9	1	9	19	8	0	8	0	13168.801	13168.812	28	13	1	13	26	12	0	12	0	18226.150	18226.161
19	9	1	9	17	8	0	8	0	13169.118	13169.129	24	13	1	13	22	12	0	12	1	18225.174	18225.161
15	9	1	9	13	8	0	8	1	13166.311	13166.293	26	13	1	13	24	12	0	12	1	18225.204	18225.192
17	9	1	9	15	8	0	8	1	13166.636	13166.621	30	13	1	13	28	12	0	12	1	18225.328	18225.314
21	9	1	9	19	8	0	8	1	13166.689	13166.672	28	13	1	13	26	12	0	12	1	18225.356	18225.343
19	9	1	9	17	8	0	8	1	13166.998	13166.980	28	14	1	14	26	13	1	13	0	19483.808	19483.816
17	9	2	7	15	8	2	6	0	14504.952	14504.897	26	14	1	14	24	13	1	13	0	19483.830	19483.839
19	9	2	7	17	8	2	6	0	14505.146	14505.092	30	14	1	14	28	13	1	13	0	19483.934	19483.942
15	9	2	7	13	8	2	6	0	14505.520	14505.467	28	14	1	14	26	13	1	13	1	19483.519	19483.509

Continuation of 2-F-4-Cl-tol Transitions																					
$2J'$	N'	K'_a	K'_c	$2J$	N	K_a	K_c	m	Obs (MHz)	Calc (MHz)	$2J'$	N'	K'_a	K'_c	$2J$	N	K_a	K_c	m	Obs	Calc
21	9	2	7	19	8	2	6	0	14505.723	14505.666	26	14	1	14	24	13	1	13	1	19483.541	19483.532
17	9	2	7	15	8	2	6	1	14501.326	14501.371	30	14	1	14	28	13	1	13	1	19483.645	19483.635
19	9	2	7	17	8	2	6	1	14501.519	14501.565	28	14	0	14	26	13	0	13	0	19505.406	19505.418
15	9	2	7	13	8	2	6	1	14501.895	14501.943	26	14	0	14	24	13	0	13	0	19505.418	19505.426
21	9	2	7	19	8	2	6	1	14502.099	14502.143	30	14	0	14	28	13	0	13	0	19505.534	19505.545
17	9	2	8	15	8	2	7	0	13579.675	13579.653	32	14	0	14	30	13	0	13	0	19505.546	19505.554
19	9	2	8	17	8	2	7	0	13579.846	13579.841	28	14	0	14	26	13	0	13	1	19505.000	19504.990
15	9	2	8	13	8	2	7	0	13580.180	13580.179	26	14	0	14	24	13	0	13	1	19505.011	19504.999
21	9	2	8	19	8	2	7	0	13580.396	13580.373	30	14	0	14	28	13	0	13	1	19505.127	19505.117
17	9	2	8	15	8	2	7	1	13583.241	13583.259	32	14	0	14	30	13	0	13	1	19505.138	19505.126
19	9	2	8	17	8	2	7	1	13583.396	13583.446	30	15	0	15	28	14	1	14	0	20808.498	20808.506
15	9	2	8	13	8	2	7	1	13583.729	13583.782	28	15	0	15	26	14	1	14	0	20808.529	20808.538
21	9	2	8	19	8	2	7	1	13583.961	13583.976	30	15	0	15	28	14	1	14	1	20808.352	20808.341
19	10	0	10	17	9	1	9	0	13849.227	13849.222	28	15	0	15	26	14	1	14	1	20808.382	20808.373
21	10	0	10	19	9	1	9	0	13849.444	13849.441	30	15	1	15	28	14	1	14	0	20831.762	20831.771
17	10	0	10	15	9	1	9	0	13849.465	13849.464	32	15	1	15	30	14	1	14	0	20831.872	20831.880
23	10	0	10	21	9	1	9	0	13849.684	13849.680	28	15	1	15	26	14	1	14	0	20831.779	20831.790
19	10	0	10	17	9	1	9	1	13850.195	13850.202	30	15	1	15	28	14	1	14	1	20831.459	20831.446
21	10	0	10	19	9	1	9	1	13850.413	13850.421	32	15	1	15	30	14	1	14	1	20831.569	20831.556
17	10	0	10	15	9	1	9	1	13850.433	13850.443	28	15	1	15	26	14	1	14	1	20831.476	20831.465
23	10	0	10	21	9	1	9	1	13850.653	13850.659	30	15	0	15	28	14	0	14	0	20845.625	20845.635
17	10	1	9	15	9	1	8	0	15630.311	15630.292	28	15	0	15	26	14	0	14	0	20845.638	20845.646
19	10	1	9	17	9	1	8	0	15630.321	15630.284	32	15	0	15	30	14	0	14	0	20845.735	20845.746
23	10	1	9	21	9	1	8	0	15630.546	15630.517	30	15	0	15	28	14	0	14	1	20845.240	20845.228
17	10	1	9	15	9	1	8	1	15629.217	15629.253	28	15	0	15	26	14	0	14	1	20845.254	20845.239
19	10	1	9	17	9	1	8	1	15629.229	15629.264	32	15	0	15	30	14	0	14	1	20845.351	20845.339
23	10	1	9	21	9	1	8	1	15629.464	15629.498	30	15	1	15	28	14	0	14	0	20868.888	20868.900
21	10	1	9	19	9	1	8	1	15629.501	15629.536	28	15	1	15	26	14	0	14	0	20868.888	20868.897
19	10	1	10	17	9	1	9	0	14065.384	14065.387	32	15	1	15	30	14	0	14	0	20869.000	20869.011
17	10	1	10	15	9	1	9	0	14065.459	14065.462	30	15	1	15	28	14	0	14	1	20868.347	20868.333
21	10	1	10	19	9	1	9	0	14065.625	14065.628	28	15	1	15	26	14	0	14	1	20868.347	20868.331

Continuation of 2-F-4-Cl-tol Transitions																					
$2J'$	N'	K'_a	K'_c	$2J$	N	K_a	K_c	m	Obs (MHz)	Calc (MHz)	$2J'$	N'	K'_a	K'_c	$2J$	N	K_a	K_c	m	Obs	Calc
23	10	1	10	21	9	1	9	0	14065.701	14065.704	32	15	1	15	30	14	0	14	1	20868.458	20868.444
19	10	1	10	17	9	1	9	1	14065.255	14065.255	32	16	0	16	30	15	1	15	0	22164.050	22164.055
17	10	1	10	15	9	1	9	1	14065.333	14065.330	30	16	0	16	28	15	1	15	0	22164.069	22164.079
21	10	1	10	19	9	1	9	1	14065.497	14065.496	34	16	0	16	32	15	1	15	0	22164.143	22164.151
23	10	1	10	21	9	1	9	1	14065.574	14065.572	32	16	0	16	30	15	1	15	1	22163.837	22163.823
17	10	0	10	15	9	0	9	0	14171.834	14171.839	30	16	0	16	28	15	1	15	1	22163.859	22163.846
19	10	0	10	17	9	0	9	0	14171.864	14171.869	34	16	0	16	32	15	1	15	1	22163.934	22163.919
End of Table																					

TABLE B.4. Fit Results of m-Chlorotoluene

Transitions used in 4.3.2																					
$2J'$	N'	K'_a	K'_c	$2J$	N	K_a	K_c	m	Obs (MHz)	Calc (MHz)	$2J'$	N'	K'_a	K'_c	$2J$	N	K_a	K_c	m	Obs (MHz)	Calc (MHz)
5	3	0	3	3	2	0	2	0	6107.166	6107.162	19	8	5	3	17	7	5	2	0	16779.249	16779.228
3	3	0	3	1	2	0	2	0	6107.197	6107.198	13	8	5	3	11	7	5	2	0	16780.155	16780.136
7	3	0	3	5	2	0	2	0	6110.907	6110.903	17	8	5	4	15	7	5	3	0	16773.726	16773.706
9	3	0	3	7	2	0	2	0	6110.920	6110.915	15	8	5	4	13	7	5	3	0	16774.663	16774.643
9	4	0	4	7	3	0	3	0	8015.691	8015.688	19	8	5	4	17	7	5	3	0	16778.194	16778.173
11	4	0	4	9	3	0	3	0	8015.710	8015.708	13	8	5	4	11	7	5	3	0	16779.104	16779.084
9	4	2	2	7	3	2	1	0	8579.101	8579.086	17	9	0	9	15	8	0	8	0	16815.440	16815.446
7	4	2	2	5	3	2	1	0	8581.217	8581.202	15	9	0	9	13	8	0	8	0	16815.527	16815.534
11	4	2	2	9	3	2	1	0	8585.095	8585.078	19	9	0	9	17	8	0	8	0	16815.722	16815.727
5	4	2	2	3	3	2	1	0	8587.161	8587.144	21	9	0	9	19	8	0	8	0	16815.809	16815.816
7	4	1	3	5	3	1	2	0	8866.661	8866.649	15	9	0	9	13	8	0	8	1	17043.367	17043.368
9	4	1	3	7	3	1	2	0	8867.294	8867.283	17	9	0	9	15	8	0	8	1	17043.537	17043.530
5	4	1	3	3	3	1	2	0	8867.984	8867.978	21	9	0	9	19	8	0	8	1	17043.711	17043.709
11	4	1	3	9	3	1	2	0	8868.940	8868.926	19	9	0	9	17	8	0	8	1	17043.872	17043.865
9	5	0	5	7	4	0	4	0	9838.578	9838.580	17	9	1	8	15	8	1	7	0	18853.806	18853.833
13	5	0	5	11	4	0	4	0	9839.627	9839.629	15	9	1	8	13	8	1	7	0	18853.927	18853.954
11	5	0	5	9	4	0	4	0	9839.667	9839.668	19	9	1	8	17	8	1	7	0	18854.046	18854.072

Continuation of m-Cl-Tol Transitions																					
$2J'$	N'	K'_a	K'_c	$2J$	N	K_a	K_c	m	Obs	Calc	$2J'$	N'	K'_a	K'_c	$2J$	N	K_a	K_c	m	Obs	Calc
7	5	0	5	5	4	0	4	0	9838.682	9838.687	21	9	1	8	19	8	1	7	0	18854.174	18854.200
11	5	2	3	9	4	2	2	0	10866.925	10866.911	17	9	1	8	15	8	1	7	1	18226.504	18226.451
9	5	2	3	7	4	2	2	0	10867.391	10867.376	19	9	1	8	17	8	1	7	1	18226.702	18226.649
13	5	2	3	11	4	2	2	0	10869.933	10869.916	15	9	1	8	13	8	1	7	1	18226.955	18226.902
7	5	2	3	5	4	2	2	0	10870.288	10870.273	21	9	1	8	19	8	1	7	1	18227.161	18227.105
9	5	2	3	7	4	2	2	1	11444.579	11444.620	17	9	1	9	15	8	1	8	0	16735.035	16735.040
11	5	2	3	9	4	2	2	1	11444.808	11444.851	15	9	1	9	13	8	1	8	0	16735.174	16735.181
7	5	2	3	5	4	2	2	1	11445.522	11445.559	19	9	1	9	17	8	1	8	0	16735.304	16735.310
13	5	2	3	11	4	2	2	1	11445.574	11445.616	21	9	1	9	19	8	1	8	0	16735.447	16735.453
9	5	1	4	7	4	1	3	0	11011.800	11011.790	17	9	1	9	15	8	1	8	1	16642.457	16642.433
11	5	1	4	9	4	1	3	0	11012.409	11012.399	15	9	1	9	13	8	1	8	1	16642.623	16642.602
7	5	1	4	5	4	1	3	0	11012.534	11012.524	19	9	1	9	17	8	1	8	1	16642.724	16642.699
13	5	1	4	11	4	1	3	0	11013.159	11013.149	21	9	1	9	19	8	1	8	1	16642.898	16642.875
11	5	2	4	9	4	2	3	0	10317.884	10317.876	17	9	2	7	15	8	2	6	0	19974.370	19974.411
9	5	2	4	7	4	2	3	0	10318.417	10318.408	19	9	2	7	17	8	2	6	0	19974.539	19974.580
13	5	2	4	11	4	2	3	0	10320.969	10320.959	15	9	2	7	13	8	2	6	0	19974.769	19974.812
7	5	2	4	5	4	2	3	0	10321.291	10321.285	21	9	2	7	19	8	2	6	0	19974.945	19974.986
11	5	3	2	9	4	3	1	0	10514.038	10514.022	17	9	2	8	15	8	2	7	0	18165.305	18165.324
9	5	3	2	7	4	3	1	0	10516.239	10516.225	19	9	2	8	17	8	2	7	0	18165.463	18165.481
13	5	3	2	11	4	3	1	0	10520.745	10520.730	15	9	2	8	13	8	2	7	0	18165.803	18165.823
7	5	3	2	5	4	3	1	0	10523.047	10523.031	21	9	2	8	19	8	2	7	0	18165.969	18165.989
11	5	3	3	9	4	3	2	0	10473.444	10473.429	19	9	3	6	17	8	3	5	0	19567.729	19567.762
9	5	3	3	7	4	3	2	0	10475.619	10475.607	17	9	3	6	15	8	3	5	0	19567.742	19567.776
13	5	3	3	11	4	3	2	0	10480.117	10480.103	15	9	3	6	13	8	3	5	0	19568.849	19568.880
7	5	3	3	5	4	3	2	0	10482.443	10482.428	21	9	3	6	19	8	3	5	0	19568.867	19568.898
9	6	0	6	7	5	0	5	0	11604.226	11604.234	19	9	3	7	17	8	3	6	0	18874.382	18874.402
11	6	0	6	9	5	0	5	0	11604.235	11604.239	17	9	3	7	15	8	3	6	0	18874.416	18874.436
13	6	0	6	11	5	0	5	0	11604.852	11604.857	15	9	3	7	13	8	3	6	0	18875.472	18875.495
15	6	0	6	13	5	0	5	0	11604.982	11604.987	21	9	3	7	19	8	3	6	0	18875.525	18875.547
9	6	0	6	7	5	0	5	1	11554.666	11554.651	19	9	4	6	17	8	4	5	0	18969.579	18969.589
11	6	0	6	9	5	0	5	1	11554.788	11554.760	17	9	4	6	15	8	4	5	0	18969.817	18969.828
15	6	0	6	13	5	0	5	1	11555.465	11555.443	21	9	4	6	19	8	4	5	0	18971.588	18971.596

Continuation of m-Cl-Tol Transitions																					
$2J'$	N'	K'_a	K'_c	$2J$	N	K_a	K_c	m	Obs	Calc	$2J'$	N'	K'_a	K'_c	$2J$	N	K_a	K_c	m	Obs	Calc
13	6	0	6	11	5	0	5	1	11555.578	11555.544	15	9	4	6	13	8	4	5	0	18971.790	18971.800
11	6	1	6	9	5	1	5	0	11326.638	11326.641	19	10	0	10	17	9	0	9	0	18562.663	18562.668
9	6	1	6	7	5	1	5	0	11327.053	11327.058	17	10	0	10	15	9	0	9	0	18562.747	18562.751
13	6	1	6	11	5	1	5	0	11327.175	11327.179	21	10	0	10	19	9	0	9	0	18562.892	18562.895
15	6	1	6	13	5	1	5	0	11327.627	11327.630	23	10	0	10	21	9	0	9	0	18562.975	18562.979
11	6	1	6	9	5	1	5	1	11040.223	11040.206	17	10	0	10	15	9	0	9	1	18746.623	18746.624
13	6	1	6	11	5	1	5	1	11040.734	11040.714	19	10	0	10	17	9	0	9	1	18746.729	18746.722
9	6	1	6	7	5	1	5	1	11041.200	11041.183	23	10	0	10	21	9	0	9	1	18746.988	18746.887
15	6	1	6	13	5	1	5	1	11041.500	11041.482	21	10	0	10	19	9	0	9	1	18746.890	18746.984
15	6	2	4	13	5	2	3	0	13186.393	13186.382	19	10	1	9	17	9	1	8	0	20608.181	20608.214
9	6	2	4	7	5	2	3	0	13186.448	13186.435	17	10	1	9	15	9	1	8	0	20608.290	20608.323
11	6	2	4	9	5	2	3	0	13184.730	13184.719	21	10	1	9	19	9	1	8	0	20608.380	20608.410
13	6	2	4	11	5	2	3	0	13184.789	13184.778	23	10	1	9	21	9	1	8	0	20608.488	20608.521
13	6	2	4	11	5	2	3	1	13399.700	13399.788	19	10	1	9	17	9	1	8	1	20395.689	20395.651
11	6	2	4	9	5	2	3	1	13399.789	13399.872	21	10	1	9	19	9	1	8	1	20395.873	20395.834
15	6	2	4	13	5	2	3	1	13401.128	13401.273	17	10	1	9	15	9	1	8	1	20395.873	20395.883
9	6	2	4	7	5	2	3	1	13401.196	13401.203	23	10	1	9	21	9	1	8	1	20396.123	20396.085
11	6	1	5	9	5	1	4	0	13098.214	13098.212	19	10	1	10	17	9	1	9	0	18514.821	18514.825
9	6	1	5	7	5	1	4	0	13098.627	13098.626	17	10	1	10	15	9	1	9	0	18514.929	18514.935
13	6	1	5	11	5	1	4	0	13098.696	13098.693	21	10	1	10	19	9	1	9	0	18515.042	18515.046
15	6	1	5	13	5	1	4	0	13099.118	13099.115	23	10	1	10	21	9	1	9	0	18515.154	18515.158
11	6	1	5	9	5	1	4	1	11815.732	11815.752	19	10	1	10	17	9	1	9	1	18464.197	18464.171
13	6	1	5	11	5	1	4	1	11815.832	11815.854	17	10	1	10	15	9	1	9	1	18464.304	18464.280
9	6	1	5	7	5	1	4	1	11817.354	11817.367	21	10	1	10	19	9	1	9	1	18464.422	18464.394
15	6	1	5	13	5	1	4	1	11817.470	11817.485	23	10	1	10	21	9	1	9	1	18464.530	18464.507
13	6	3	3	11	5	3	2	0	12692.723	12692.709	19	10	2	8	17	9	2	7	0	22105.840	22105.908
11	6	3	3	9	5	3	2	0	12693.584	12693.570	21	10	2	8	19	9	2	7	0	22105.998	22106.063
15	6	3	3	13	5	3	2	0	12696.597	12696.583	17	10	2	8	15	9	2	7	0	22106.110	22106.173
9	6	3	3	7	5	3	2	0	12697.422	12697.409	23	10	2	8	21	9	2	7	0	22106.267	22106.333
13	6	3	4	11	5	3	3	0	12587.311	12587.300	19	10	2	9	17	9	2	8	0	20047.569	20047.596
11	6	3	4	9	5	3	3	0	12588.228	12588.214	21	10	2	9	19	9	2	8	0	20047.717	20047.742
15	6	3	4	13	5	3	3	0	12591.211	12591.197	17	10	2	9	15	9	2	8	0	20047.937	20047.964

Continuation of m-Cl-Tol Transitions																					
$2J'$	N'	K'_a	K'_c	$2J$	N	K_a	K_c	m	Obs	Calc	$2J'$	N'	K'_a	K'_c	$2J$	N	K_a	K_c	m	Obs	Calc
9	6	3	4	7	5	3	3	0	12591.985	12591.974	23	10	2	9	21	9	2	8	0	20048.089	20048.115
13	6	4	3	11	5	4	2	0	12568.167	12568.145	19	10	2	9	17	9	2	8	1	19673.669	19673.645
11	6	4	3	9	5	4	2	0	12570.213	12570.192	21	10	2	9	19	9	2	8	1	19673.782	19673.758
15	6	4	3	13	5	4	2	0	12575.024	12575.003	17	10	2	9	15	9	2	8	1	19674.233	19674.209
9	6	4	3	7	5	4	2	0	12577.035	12577.016	23	10	2	9	21	9	2	8	1	19674.351	19674.327
13	6	4	2	11	5	4	1	0	12571.830	12571.809	21	11	0	11	19	10	0	10	0	20316.250	20316.252
11	6	4	2	9	5	4	1	0	12573.882	12573.862	19	11	0	11	17	10	0	10	0	20316.325	20316.327
15	6	4	2	13	5	4	1	0	12578.693	12578.672	23	11	0	11	21	10	0	10	0	20316.440	20316.439
9	6	4	2	7	5	4	1	0	12580.703	12580.682	25	11	0	11	23	10	0	10	0	20316.515	20316.514
13	7	0	7	11	6	0	6	0	13342.333	13342.340	19	11	0	11	17	10	0	10	1	20449.326	20449.319
11	7	0	7	9	6	0	6	0	13342.409	13342.415	21	11	0	11	19	10	0	10	1	20449.376	20449.364
15	7	0	7	13	6	0	6	0	13342.809	13342.815	25	11	0	11	23	10	0	10	1	20449.536	20449.528
17	7	0	7	15	6	0	6	0	13342.889	13342.896	23	11	0	11	21	10	0	10	1	20449.586	20449.572
11	7	0	7	9	6	0	6	1	13482.944	13482.931	21	11	1	10	19	10	1	9	0	22321.292	22321.334
13	7	0	7	11	6	0	6	1	13483.157	13483.133	19	11	1	10	17	10	1	9	0	22321.413	22321.443
17	7	0	7	15	6	0	6	1	13483.539	13483.521	23	11	1	10	21	10	1	9	0	22321.453	22321.495
15	7	0	7	13	6	0	6	1	13483.738	13483.711	25	11	1	10	23	10	1	9	0	22321.574	22321.606
13	7	1	7	11	6	1	6	0	13144.805	13144.810	21	11	1	10	19	10	1	9	1	22464.423	22464.416
11	7	1	7	9	6	1	6	0	13145.077	13145.083	19	11	1	10	17	10	1	9	1	22464.521	22464.516
15	7	1	7	13	6	1	6	0	13145.227	13145.232	23	11	1	10	21	10	1	9	1	22464.611	22464.602
17	7	1	7	15	6	1	6	0	13145.511	13145.516	25	11	1	10	23	10	1	9	1	22464.689	22464.683
13	7	1	7	11	6	1	6	1	12929.945	12929.924	23	12	0	12	21	11	0	11	0	22074.237	22074.233
15	7	1	7	13	6	1	6	1	12930.274	12930.253	21	12	0	12	19	11	0	11	0	22074.303	22074.301
11	7	1	7	9	6	1	6	1	12930.353	12930.338	25	12	0	12	23	11	0	11	0	22074.395	22074.391
17	7	1	7	15	6	1	6	1	12930.812	12930.792	26	12	0	12	25	11	0	11	0	22074.462	22074.459
15	7	3	4	13	6	3	3	0	14923.332	14923.326	21	12	0	12	19	11	0	11	1	22166.216	22166.197
13	7	3	4	11	6	3	3	0	14923.667	14923.662	23	12	0	12	21	11	0	11	1	22166.229	22166.208
17	7	3	4	15	6	3	3	0	14925.771	14925.764	26	12	0	12	25	11	0	11	1	22166.387	22166.368
11	7	3	4	9	6	3	3	0	14926.061	14926.055	25	12	0	12	23	11	0	11	1	22166.399	22166.378
11	7	3	4	9	6	3	3	1	15469.538	15469.493	23	13	0	13	21	12	0	12	0	23835.082	23835.069
13	7	3	4	11	6	3	3	1	15469.821	15469.769	25	13	0	13	23	12	0	12	0	23835.024	23835.009
17	7	3	4	15	6	3	3	1	15469.963	15469.915	28	13	0	13	26	12	0	12	0	23835.211	23835.204

Continuation of m-Cl-Tol Transitions																					
$2J'$	N'	K'_a	K'_c	$2J$	N	K_a	K_c	m	Obs	Calc	$2J'$	N'	K'_a	K'_c	$2J$	N	K_a	K_c	m	Obs	Calc
15	7	3	4	13	6	3	3	1	15470.123	15470.071	26	13	0	13	25	12	0	12	0	23835.150	23835.144
15	8	0	8	13	7	0	7	0	15075.963	15075.971	25	13	0	13	23	12	0	12	1	23898.307	23898.275
13	8	0	8	11	7	0	7	0	15076.051	15076.057	23	13	0	13	21	12	0	12	1	23898.317	23898.285
17	8	0	8	15	7	0	7	0	15076.324	15076.330	26	13	0	13	25	12	0	12	1	23898.446	23898.418
19	8	0	8	17	7	0	7	0	15076.412	15076.419	28	13	0	13	26	12	0	12	1	23898.459	23898.427
13	8	0	8	11	7	0	7	1	15303.883	15303.880	13	7	0	7	11	6	1	6	0	12824.803	12824.810
15	8	0	8	13	7	0	7	1	15304.086	15304.073	11	7	0	7	9	6	1	6	0	12825.287	12825.294
19	8	0	8	17	7	0	7	1	15304.316	15304.309	15	7	0	7	13	6	1	6	0	12825.178	12825.186
17	8	0	8	15	7	0	7	1	15304.536	15304.520	17	7	0	7	15	6	1	6	0	12825.681	12825.687
15	8	1	8	13	7	1	7	0	14946.266	14946.270	15	8	0	8	13	7	1	7	0	14755.962	14755.971
13	8	1	8	11	7	1	7	0	14946.454	14946.461	13	8	0	8	11	7	1	7	0	14756.259	14756.269
17	8	1	8	15	7	1	7	0	14946.598	14946.604	17	8	0	8	15	7	1	7	0	14756.274	14756.284
19	8	1	8	17	7	1	7	0	14946.794	14946.800	19	8	0	8	17	7	1	7	0	14756.582	14756.591
15	8	1	8	13	7	1	7	1	14798.144	14798.120	13	8	1	8	11	7	0	7	0	15266.245	15266.250
13	8	1	8	11	7	1	7	1	14798.413	14798.393	15	8	1	8	13	7	0	7	0	15266.267	15266.270
17	8	1	8	15	7	1	7	1	14798.460	14798.435	19	8	1	8	17	7	0	7	0	15266.625	15266.628
19	8	1	8	17	7	1	7	1	14798.746	14798.724	17	8	1	8	15	7	0	7	0	15266.646	15266.650
15	8	1	7	13	7	1	6	0	17026.506	17026.523	11	7	1	7	9	6	0	6	0	13662.199	13662.204
13	8	1	7	11	7	1	6	0	17026.678	17026.697	13	7	1	7	11	6	0	6	0	13662.336	13662.340
17	8	1	7	15	7	1	6	0	17026.812	17026.829	17	7	1	7	15	6	0	6	0	13662.720	13662.725
19	8	1	7	17	7	1	6	0	17026.975	17026.993	15	7	1	7	13	6	0	6	0	13662.859	13662.861
15	8	1	7	13	7	1	6	1	16023.944	16023.900	17	9	0	9	15	8	1	8	0	16625.138	16625.147
17	8	1	7	15	7	1	6	1	16024.143	16024.099	15	9	0	9	13	8	1	8	0	16625.332	16625.342
13	8	1	7	11	7	1	6	1	16024.669	16024.621	19	9	0	9	17	8	1	8	0	16625.397	16625.406
19	8	1	7	17	7	1	6	1	16024.975	16024.826	21	9	0	9	19	8	1	8	0	16625.598	16625.607
15	8	2	6	13	7	2	5	0	17765.222	17765.242	1	2	2	1	1	1	1	0	0	10995.843	10995.816
17	8	2	6	15	7	2	5	0	17765.395	17765.414	3	2	2	1	3	1	1	0	0	10995.957	10995.923
13	8	2	6	11	7	2	5	0	17765.839	17765.859	7	2	2	1	5	1	1	0	0	10999.893	10999.861
19	8	2	6	17	7	2	5	0	17766.020	17766.039	5	2	2	1	3	1	1	0	0	11006.671	11006.632
15	8	2	6	13	7	2	5	1	16782.871	16783.000	3	2	2	1	1	1	1	0	0	11010.786	11010.759
17	8	2	6	15	7	2	5	1	16782.908	16783.038	3	3	2	2	1	2	1	1	0	12760.749	12760.724
13	8	2	6	11	7	2	5	1	16783.927	16784.050	9	3	2	2	7	2	1	1	0	12765.640	12765.607

Continuation of m-Cl-Tol Transitions																					
$2J'$	N'	K'_a	K'_c	$2J$	N	K_a	K_c	m	Obs	Calc	$2J'$	N'	K'_a	K'_c	$2J$	N	K_a	K_c	m	Obs	Calc
19	8	2	6	17	7	2	5	1	16783.977	16784.101	5	3	2	2	3	2	1	1	0	12767.596	12767.564
17	8	3	5	15	7	3	4	0	17216.308	17216.316	7	3	2	2	5	2	1	1	0	12772.335	12772.299
15	8	3	5	13	7	3	4	0	17216.373	17216.381	7	5	1	5	5	4	0	4	0	10632.978	10632.983
19	8	3	5	17	7	3	4	0	17217.889	17217.897	9	5	1	5	7	4	0	4	0	10633.708	10633.707
13	8	3	5	11	7	3	4	0	17218.030	17218.036	13	5	1	5	11	4	0	4	0	10634.192	10634.194
15	8	3	5	13	7	3	4	1	17935.429	17935.416	11	5	1	5	9	4	0	4	0	10634.975	10634.974
13	8	3	5	11	7	3	4	1	17935.558	17935.546	9	5	1	5	9	4	0	4	0	10638.981	10638.985
17	8	3	5	15	7	3	4	1	17935.665	17935.727	9	6	1	6	7	5	0	5	0	12121.350	12121.355
19	8	3	5	17	7	3	4	1	17935.742	17935.654	11	6	1	6	9	5	0	5	0	12121.766	12121.769
17	8	3	6	15	7	3	5	0	16794.965	16794.968	15	6	1	6	13	5	0	5	0	12122.193	12122.196
15	8	3	6	13	7	3	5	0	16795.007	16795.013	13	6	1	6	11	5	0	5	0	12122.483	12122.486
19	8	3	6	17	7	3	5	0	16796.498	16796.504	11	6	2	5	9	5	2	4	0	12326.100	12326.097
13	8	3	6	11	7	3	5	0	16796.662	16796.667	9	6	2	5	7	5	2	4	0	12327.896	12327.891
17	8	4	4	15	7	4	3	0	16860.662	16860.657	13	6	2	5	11	5	2	4	0	12326.166	12326.160
15	8	4	4	13	7	4	3	0	16861.142	16861.136	15	6	2	5	13	5	2	4	0	12327.809	12327.805
19	8	4	4	17	7	4	3	0	16863.537	16863.531	11	6	0	6	9	5	1	5	0	10809.107	10809.112
13	8	4	4	11	7	4	3	0	16863.975	16863.970	13	6	0	6	11	5	1	5	0	10809.545	10809.550
17	8	4	5	15	7	4	4	0	16828.161	16828.157	9	6	0	6	7	5	1	5	0	10809.932	10809.937
15	8	4	5	13	7	4	4	0	16828.670	16828.663	15	6	0	6	13	5	1	5	0	10810.418	10810.421
19	8	4	5	17	7	4	4	0	16831.052	16831.046	5	4	2	3	3	3	1	2	0	14367.921	14367.907
13	8	4	5	11	7	4	4	0	16831.464	16831.460	11	4	2	3	9	3	1	2	0	14370.895	14370.869
17	8	5	3	15	7	5	2	0	16774.779	16774.759	7	4	2	3	5	3	1	2	0	14372.480	14372.456
15	8	5	3	13	7	5	2	0	16775.715	16775.695	9	4	2	3	7	3	1	2	0	14375.315	14375.288
End of Table																					

APPENDIX C

Additional Computational Results of meta-Methyl-Phenoxyl

TABLE C.1. CCSD(T)/cc-pwCVDZ Coordinates of Meta-Methyl-Phenoxyl. A dummy atom was required to build the C_s structure in the z-matrix and has been included here as reference for ease of future use.

atom	x (Å)	y (Å)	z (Å)
C	−2.57302284	−0.95790007	−0.00000000
C	−1.23333798	−0.24671976	−0.00000000
x	−1.23333798	−0.24671976	1.00000160
H	−3.40508236	−0.23369191	−0.00000000
H	−2.67767003	−1.60213944	−0.89183846
H	−2.67767003	−1.60213944	0.89183846
C	−0.04835568	−1.01059928	−0.00000000
C	−1.15087574	1.15874933	−0.00000000
C	1.29476127	1.04598901	0.00000000
C	1.20894242	−0.36763645	0.00000000
C	0.10635458	1.79046199	0.00000000
H	−0.08652130	−2.10555105	0.00000000
H	−2.06756859	1.75896848	0.00000000
O	2.33084406	−1.09925466	−0.00000000
H	0.16921487	2.88491013	0.00000000
H	2.27632313	1.52906514	0.00000000

TABLE C.2. MP2/cc-pwCVDZ Harmonic vibrational frequencies for meta-methylphenoxyl

Symmetry	Frequency (cm^{-1})	Intensity (km/mol)
A''	99.4803	1.5868
A''	236.0530	0.7689
A''	291.9830	1.8687
A'	314.7844	2.1174
A''	494.0467	1.8517
A'	497.0857	4.3366
A'	501.7042	13.2967
A'	538.8682	2.1285
A''	616.3099	4.8040
A''	744.0449	13.7159
A'	753.7599	193.4353
A'	759.3548	4.7190
A''	871.2238	42.7564
A''	956.5066	1.0248
A'	986.8986	5.1974
A'	998.9436	12.2234
A''	1015.3064	6.7574
A'	1021.5093	21.5011
A''	1070.9072	0.1305
A''	1091.7648	4.0707
A'	1112.8956	1.4148
A'	1143.4727	23.2879
A'	1213.8641	8.6282
A'	1234.8884	15.2288
A'	1305.5971	0.5103
A'	1412.2509	0.1136
A'	1457.5953	0.6880
A''	1484.3475	7.1463
A'	1492.6408	3.9034
A'	1528.3330	8.4789
A'	1589.8029	54.6212
A'	1701.5994	21.1775
A'	3077.1651	20.6908
A''	3167.0691	8.4087
A'	3185.4240	5.8080
A'	3226.1893	4.0263
A'	3242.6665	8.0591
A'	3247.5689	0.7004
A'	3266.2473	1.2587

Bibliography

[1] David M. Dennison. The rotation of molecules. *Phys. Rev.*, 28:318–333, Aug 1926.

[2] R. de L. Kronig and I. I. Rabi. The symmetrical top in the undulatory mechanics. *Phys. Rev.*, 29:262–269, Feb 1927.

[3] Enos E. Witmer. The quantization of the rotational motion of the polyatomic molecule by the new wave mechanics. *Proceedings of the National Academy of Sciences of the United States of America*, 13(2):60–65, 1927.

[4] S. C. Wang. On the asymmetrical top in quantum mechanics. *Phys. Rev.*, 34:243–252, Jul 1929.

[5] C. E. Cleeton and N. H. Williams. Electromagnetic waves of 1.1 cm wave-length and the absorption spectrum of ammonia. *Phys. Rev.*, 45:234–237, Feb 1934.

[6] E. U. Condon and G. H. Shortley. *Theory of Atomic Spectra*. Cambridge University Press, 1935.

[7] Daniel Kivelson and Jr. Wilson, E. Bright. Approximate Treatment of the Effect of Centrifugal Distortion on the Rotational Energy Levels of Asymmetric-Rotor Molecules. *The Journal of Chemical Physics*, 20(10):1575–1579, 12 2004.

[8] Harald H. Nielsen. The torsion oscillator-rotator in the quantum mechanics. *Phys. Rev.*, 40:445–456, May 1932.

[9] James S. Koehler and David M. Dennison. Hindered rotation in methyl alcohol. *Phys. Rev.*, 57:1006–1021, Jun 1940.

[10] Donald G. Burkhard and David M. Dennison. The molecular structure of methyl alcohol. *Phys. Rev.*, 84:408–417, Nov 1951.

[11] Walter Gordy. Early events and some later developments in microwave spectroscopy. *Journal of Molecular Structure*, 97:17–32, 1983. Determination of Molecular Structure by Microwave Spectroscopy and Electron Diffraction.

[12] Richard H. Hughes and E. Bright Wilson. A microwave spectrograph. *Phys. Rev.*, 71:562–563, Apr 1947.

[13] Walter Gordy. Microwave spectroscopy. *Rev. Mod. Phys.*, 20:668–717, Oct 1948.

[14] W. D. Hershberger and John Turkevich. Absorption of methyl alcohol and methylamine for 1.25-cm waves. *Phys. Rev.*, 71:554–554, Apr 1947.

[15] B. P. Dailey. First-order Stark effect in the microwave spectrum of methyl alcohol. *Phys. Rev.*, 72:84–85, Jul 1947.

[16] Chun C. Lin and Jerome D. Swalen. Internal rotation and microwave spectroscopy. *Rev. Mod. Phys.*, 31:841–892, Oct 1959.

[17] E. P. Wigner. On matrices which reduce kronecker products of representations of s.r. groups. (unpublished), 1951.

[18] A. R. Edmonds. *Angular Momentum in Quantum Mechanics*. Princeton University Press, 1957.

[19] J. H. Van Vleck. The coupling of angular momentum vectors in molecules. *Rev. Mod. Phys.*, 23:213–227, Jul 1951.

[20] Jr. Curl, R. F. and James L. Kinsey. Calculation of Interaction Matrix Elements for Asymmetric Rotors with Resultant Electronic Spin and Nuclear Spin. *The Journal of Chemical Physics*, 35(5):1758–1765, 08 2004.

[21] G. C. Dousmanis, T. M. Sanders, and C. H. Townes. Microwave spectra of the free radicals OH and OD. *Phys. Rev.*, 100:1735–1754, Dec 1955.

[22] E. Hirota, A. Mizoguchi, Y. Ohshima, K. Katoh, Y. Sumiyoshi, and Y. Endo. Interplay of methyl-group internal rotation and fine and hyperfine interaction in a free radical: Fourier transform microwave spectroscopy of the acetyl radical. *Molecular Physics*, 105(5-7):455–466, 2007.

[23] Howard W. Harrington, John Robert Hearn, and Roger F. Rauskolb. The routine rotational microwave spectrometer. 1971.

[24] James K.G. Watson. Simplification of the molecular vibration-rotation Hamiltonian. *Molecular Physics*, 15(5):479–490, 1968.

[25] Takeshi Oka. Watson's papers on the vibration-rotation interaction. *Journal of Molecular Spectroscopy*, 384:111588, 2022.

[26] F. X. Powell and Jr. Lide, David R. Microwave Spectrum of the SO Radical. *The Journal of Chemical Physics*, 41(5):1413–1419, 07 2004.

[27] W. T. Raynes. Spin splittings and rotational structure of nonlinear molecules in doublet and triplet electronic states. *The Journal of Chemical Physics*, 41(10):3020–3032, 07 2004.

[28] H.P. Benz, A. Bauder, and Hs.H. Günthard. Exact quadrupole interaction energies in rotational spectra. *Journal of Molecular Spectroscopy*, 21(1):156–164, 1966.

[29] C.H. Townes and A.L. Schawlow. *Microwave Spectroscopy*. Dover, 1955.

[30] I. C. Bowater, J. M. Brown, and Alan Carrington. Microwave spectroscopy of nonlinear free radicals - i. general theory and application to the Zeeman effect in HCO. *Proceedings of the Royal Society of London. A. Mathematical and Physical Sciences*, 333(1594):265–288, 1973.

[31] Walter Gordy and Robert L. Cook. *Microwave Molecular Spectra*. Wiley, 1984.

[32] J.M. Brown and T.J. Sears. A reduced form of the spin-rotation Hamiltonian for asymmetric-top molecules, with applications to HO_2 and NH_2. *Journal of Molecular Spectroscopy*, 75(1):111–133, 1979.

[33] R.C. Woods. A general program for the calculation of internal rotation splittings in microwave spectroscopy. *Journal of Molecular Spectroscopy*, 21(1):4–24, 1966.

[34] R. M. Lees and J. G. Baker. Torsion–Vibration–Rotation Interactions in Methanol. I. Millimeter Wave Spectrum. *The Journal of Chemical Physics*, 48(12):5299–5318, 09 2003.

[35] Eric Herbst, J.K. Messer, Frank C. De Lucia, and Paul Helminger. A new analysis and additional measurements of the millimeter and submillimeter spectrum of methanol. *Journal of Molecular Spectroscopy*, 108(1):42–57, 1984.

[36] T. J. Balle, E. J. Campbell, M. R. Keenan, and W. H. Flygare. A new method for observing the rotational spectra of weak molecular complexes: KrHCl. *The Journal of Chemical Physics*, 71(6):2723–2724, 07 2008.

[37] M. C. McCarthy, W. Chen, M. J. Travers, and P. Thaddeus. Microwave spectra of 11 polyyne carbon chains. *The Astrophysical Journal Supplement Series*, 129(2):611, aug 2000.

[38] Peter Chen, Steven D. Colson, William A. Chupka, and Jerome A. Berson. Flash pyrolytic production of rotationally cold free radicals in a supersonic jet. resonant multiphoton spectrum of the $3p^2a_2$" $leftarrow$ x^2a_2" origin band of methyl. *The Journal of Physical Chemistry*, 90(11):2319–2321, 1986.

[39] Qi Guan, Kimberly N. Urness, Thomas K. Ormond, Donald E. David, G. Barney Ellison, and John W. Daily. The properties of a micro-reactor for the study of the unimolecular decomposition of large molecules. *International Reviews in Physical Chemistry*, 33(4):447–487, 2014.

[40] Herbert M. Pickett. The fitting and prediction of vibration-rotation spectra with spin interactions. *Journal of Molecular Spectroscopy*, 148(2):371–377, 1991.

[41] Brian J. Drouin. Practical uses of SPFIT. *Journal of Molecular Spectroscopy*, 340:1–15, 2017.

[42] Stewart E. Novick. A beginner's guide to Pickett's SPCAT/SPFIT. *Journal of Molecular Spectroscopy*, 329:1–7, 2016.

[43] H.M. Pickett, R.L. Poynter, E.A. Cohen, M.L. Delitsky, J.C. Pearson, and H.S.P. Müller. Submillimeter, millimeter, and microwave spectral line catalog. *Journal of Quantitative Spectroscopy and Radiative Transfer*, 60(5):883–890, 1998.

[44] J.T. Hougen, I. Kleiner, and M. Godefroid. Selection rules and intensity calculations for a C_s asymmetric top molecule containing a methyl group internal rotor. *Journal of Molecular Spectroscopy*, 163(2):559–586, 1994.

[45] H. Hartwig and H. Dreizler. The microwave spectrum of trans-2,3-dimethyloxirane in torsional excited states. *Zeitschrift für Naturforschung A*, 51(8):923–932, 1996.

[46] I. Kleiner. Asymmetric-top molecules containing one methyl-like internal rotor: Methods and codes for fitting and predicting spectra. *Journal of Molecular Spectroscopy*, 260(1):1–18, 2010.

[47] Isabelle Kleiner and Jon T. Hougen. Rho-axis-method Hamiltonian for molecules having one methyl rotor and C_1 point-group symmetry at equilibrium. *The Journal of Chemical Physics*, 119(11):5505–5509, 08 2003.

[48] Raphaela Kannengießer, Wolfgang Stahl, Ha Vinh Lam Nguyen, and Isabelle Kleiner. ^{14}N nuclear quadrupole coupling and methyl internal rotation in n-tert-butylacetamide as observed by microwave spectroscopy. *The Journal of Physical Chemistry A*, 120(23):3992–3997, 2016.

[49] Isabelle Kleiner and Jon T. Hougen. A hybrid program for fitting rotationally resolved spectra of floppy molecules with one large-amplitude rotatory motion and one large-amplitude oscillatory motion. *The Journal of Physical Chemistry A*, 119(43):10664–10676, 2015. PMID: 26439709.

[50] Sven Herbers and Ha Vinh Lam Nguyen. Next level achievement of the XIAM code in modeling the microwave spectrum of m-methylanisole. *Journal of Molecular Spectroscopy*, 370:111289, 2020.

[51] Peter Groner. Effective rotational Hamiltonian for molecules with two periodic large-amplitude motions. *The Journal of Chemical Physics*, 107(12):4483–4498, 09 1997.

[52] Douglas T. Petkie, Thomas M. Goyette, Paul Helminger, Herb M. Pickett, and Frank C. De Lucia. The energy levels of the v5/2v9 dyad of hno3 from millimeter and submillimeter rotational spectroscopy. *Journal of Molecular Spectroscopy*, 208(1):121–135, 2001.

[53] Gordon G. Brown, Brian C. Dian, Kevin O. Douglass, Scott M. Geyer, and Brooks H. Pate. The rotational spectrum of epifluorohydrin measured by chirped-pulse Fourier transform microwave spectroscopy. *Journal of Molecular Spectroscopy*, 238(2):200–212, 2006.

[54] Ian A. Finneran, Steven T. Shipman, and Susanna L. Widicus Weaver. Rotational spectroscopy of 2-methylfuran from 8.7 to 960GHz. *Journal of Molecular Spectroscopy*, 280:27–33, 2012. Broadband Rotational Spectroscopy.

[55] David Patterson and John M. Doyle. Cooling molecules in a cell for FTMW spectroscopy. *Molecular Physics*, 110(15-16):1757–1766, 2012.

[56] Jessica P. Porterfield, J. H. Westerfield, Lincoln Satterthwaite, David Patterson, P. Bryan Changala, Joshua H. Baraban, and Michael C. McCarthy. Rotational characterization of the elusive gauche-isoprene. *The Journal of Physical Chemistry Letters*, 10(8):1981–1985, 2019.

[57] G. Barratt Park and Robert W. Field. Perspective: The first ten years of broadband chirped pulse Fourier transform microwave spectroscopy. *The Journal of Chemical Physics*, 144(20):200901, 05 2016.

[58] Kyle N. Crabtree, Marie-Aline Martin-Drumel, Gordon G. Brown, Sydney A. Gaster, Taylor M. Hall, and Michael C. McCarthy. Microwave spectral taxonomy: A semi-automated combination of chirped-pulse and cavity Fourier-transform microwave spectroscopy. *The Journal of Chemical Physics*, 144(12):124201, 03 2016.

[59] Christopher T. Dewberry, Rebecca B. Mackenzie, Susan Green, and Kenneth R. Leopold. 3D-printed slit nozzles for Fourier transform microwave spectroscopy. *Review of Scientific Instruments*, 86(6):065107, 06 2015.

[60] Michael C. McCarthy, Kin Long Kelvin Lee, P. Brandon Carroll, Jessica P. Porterfield, P. Bryan Changala, James H. Thorpe, and John F. Stanton. Exhaustive product analysis of three benzene discharges by microwave spectroscopy. *The Journal of Physical Chemistry A*, 124(25):5170–5181, 2020. PMID: 32437151.

[61] Jessica P. Porterfield, Sandra Eibenberger, David Patterson, and Michael C. McCarthy. The ozonolysis of isoprene in a cryogenic buffer gas cell by high resolution microwave spectroscopy. *Phys. Chem. Chem. Phys.*, 20:16828–16834, 2018.

[62] A. O. Hernandez-Castillo, Chamara Abeysekera, John F. Stanton, and Timothy S. Zwier. Structural characterization of phenoxy radical with mass-correlated broadband microwave spectroscopy. *The Journal of Physical Chemistry Letters*, 10(11):2919–2923, 2019.

[63] Chamara Abeysekera, A.O. Hernandez-Castillo, John F. Stanton, and Timothy S. Zwier. Broadband microwave spectroscopy of 2-furanyloxy radical: Primary pyrolysis product of the second-generation biofuel 2-methoxyfuran. *The Journal of Physical Chemistry A*, 122(34):6879–6885, 2018. PMID: 30063137.

[64] Vadim V. Ilyushin, Zbigniew Kisiel, Lech Pszczókowski, Heinrich Mäder, and Jon T. Hougen. A new torsion–rotation fitting program for molecules with a sixfold barrier: Application to the microwave spectrum of toluene. *Journal of Molecular Spectroscopy*, 259(1):26–38, 2010.

[65] Vadim Ilyushin. Millimeter wave spectrum of nitromethane. *Journal of Molecular Spectroscopy*, 345:64–69, 2018.

[66] Michael C. McCarthy and Brett A. McGuire. Aromatics and cyclic molecules in molecular clouds: A new dimension of interstellar organic chemistry. *The Journal of Physical Chemistry A*, 125(16):3231–3243, 2021. PMID: 33749264.

[67] Alfred Bauder. *Fundamentals of Rotational Spectroscopy*. John Wiley & Sons, Ltd, 2011.

[68] P.R. Bunker and P. Jensen. *Molecular Symmetry and Spectroscopy*. NRC Press, second edition, 1999.

[69] Li-Hong Xu, J. Fisher, R.M. Lees, H.Y. Shi, J.T. Hougen, J.C. Pearson, B.J. Drouin, G.A. Blake, and R. Braakman. Torsion–rotation global analysis of the first three torsional states (v_t=0, 1, 2) and terahertz database for methanol. *Journal of Molecular Spectroscopy*, 251(1):305–313, 2008. Special issue dedicated to the pioneering work of Drs. Edward A. Cohen and Herbert M. Pickett on spectroscopy relevant to the Earth's atmosphere and astrophysics.

[70] Kuniaki Nakagawa, Shozo Tsunekawa, and Takeshi Kojima. Effective torsion-rotation Hamiltonian for methanol-type molecules. *Journal of Molecular Spectroscopy*, 126(2):329–340, 1987.

[71] Ha Vinh Lam Nguyen, Isabelle Kleiner, Steven T. Shipman, Yoshiaki Mae, Kazue Hirose, Shota Hatanaka, and Kaori Kobayashi. Extension of the measurement, assignment, and fit of the rotational spectrum of the two-top molecule methyl acetate. *Journal of Molecular Spectroscopy*, 299:17–21, 2014.

[72] Vadim V. Ilyushin, Christian P. Endres, Frank Lewen, Stephan Schlemmer, and Brian J. Drouin. Submillimeter wave spectrum of acetic acid. *Journal of Molecular Spectroscopy*, 290:31–41, 2013.

[73] Vadim Ilyushin, Roberto Rizzato, Luca Evangelisti, Gang Feng, Assimo Maris, Sonia Melandri, and Walther Caminati. Almost free methyl top internal rotation: Rotational spectrum of 2-butynoic acid. *Journal of Molecular Spectroscopy*, 267(1):186–190, 2011.

[74] Dudley R. Herschbach and Jerome D. Swalen. Internal Barrier of Propylene Oxide from the Microwave Spectrum. II. *The Journal of Chemical Physics*, 29(4):761–776, 08 2004.

[75] V. Ilyushin. A new scheme of K-labeling for torsion–rotation energy levels in low-barrier molecules. *Journal of Molecular Spectroscopy*, 227(2):140–150, 2004.

[76] J.M. Brown and B.J. Howard. An approach to the anomalous commutation relations of rotational angular momenta in molecules. *Molecular Physics*, 31(5):1517–1525, 1976.

[77] Richard N. Zare and William G. Harter. *Angular Momentum: Understanding Spatial Aspects in Chemistry and Physics*. Wiley, second edition, 1988.

[78] Jinjun Liu. Rotational and fine structure of open-shell molecules in nearly degenerate electronic states. *The Journal of Chemical Physics*, 148(12):124112, 03 2018.

[79] Juan Ortigoso and Jon T. Hougen. Rotational energy surfaces of molecules exhibiting internal rotation. *The Journal of Chemical Physics*, 101(4):2710–2719, 08 1994.

[80] Eizi Hirota. *High-Resolution Spectroscopy of Transient Molecules*. Springer, 1985.

[81] Michael J. Moran, John S. Zogorski, and Paul J. Squillace. MTBE and gasoline hydrocarbons in ground water of the United States. *Groundwater*, 43(4):615–627, 2005.

[82] Annemarie van Wezel, Leo Puijker, Cees Vink, Ans Versteegh, and Pim de Voogt. Odour and flavour thresholds of gasoline additives (MTBE, ETBE and TAME) and their occurrence in dutch drinking water collection areas. *Chemosphere*, 76(5):672–676, 2009.

[83] Paul J. Squillace, James F. Pankow, Nic E. Korte, and John S. Zogorski. Review of the environmental behavior and fate of methyl tert-butyl ether. *Environmental Toxicology and Chemistry*, 16(9):1836–1844, 1997.

[84] I Werner, C.S Koger, L.A Deanovic, and D.E Hinton. Toxicity of methyl-tert-butyl ether to freshwater organisms. *Environmental Pollution*, 111(1):83–88, 2001.

[85] Artressa L. Christophe, Jalon T. Barnes, Sylvestre Twagirayezu, Aleksandr Mikhonin, Matthew T. Muckle, and Justin L. Neill. Direct measurements of small polar impurities in gasoline mixtures using molecular rotational resonance spectroscopy. *Applied Spectroscopy*, 73(11):1334–1339, 2019. PMID: 31219324.

[86] Enis Arik, Hakan Altan, and Okan Esenturk. Dielectric properties of ethanol and gasoline mixtures by terahertz spectroscopy and an effective method for determination of ethanol content of gasoline. *The Journal of Physical Chemistry A*, 118(17):3081–3089, 2014. PMID: 24701997.

[87] Xiong Li, YanDe Liu, Xiaogang Jiang, Aiguo Ouyang, Xudong Sun, and Guantian Wang. Determination and quantification of kerosene in gasoline by mid-infrared and raman spectroscopy. *Journal of Molecular Structure*, 1210:127760, 2020.

[88] R.D. Suenram, F.J. Lovas, W. Pereyra, G.T. Fraser, and A.R.Hight Walker. Rotational spectra, structure, and electric dipole moments of methyl and ethyltert-butyl ether (MTBE and ETBE). *Journal of Molecular Spectroscopy*, 181(1):67–77, 1997.

[89] Yueyue Zhao, Ha Vinh Lam Nguyen, Wolfgang Stahl, and Jon T. Hougen. Unusual internal rotation coupling in the microwave spectrum of pinacolone. *Journal of Molecular Spectroscopy*, 318:91–100, 2015.

[90] J.-U Grabow, N Heineking, and W Stahl. The microwave spectrum of tert-butyl isocyanate. *Journal of Molecular Spectroscopy*, 154(1):129–136, 1992.

[91] Devin A. Matthews, Lan Cheng, Michael E. Harding, Filippo Lipparini, Stella Stopkowicz, Thomas-C. Jagau, Péter G. Szalay, Jürgen Gauss, and John F. Stanton. Coupled-cluster techniques for computational chemistry: The CFOUR program package. *The Journal of Chemical Physics*, 152(21):214108, 2020.

[92] Frank Neese. The ORCA program system. *WIREs Computational Molecular Science*, 2(1):73–78, 2012.

[93] Atsuhiko Suwa, Hiroshi Ohta, and Shigehiro Konaka. Molecular structures of tert-butyl alcohol and tert-butyl methyl ether as studied by gas electron diffraction combined with vibrational spectroscopy. *Journal of Molecular Structure*, 172:275–290, 1988.

[94] G. Schaftenaar and J.H. Noordik. Molden: a pre- and post-processing program for molecular and electronic structures. *Journal of Computer-Aided Molecular Design*, 14:123–134, 2000.

[95] Noel L. Owen David G. Lister, John N. MacDonald. *Internal Rotation and Inversion: An Introduction to Large Amplitude Motion in Molecules*. Academic Press, 1978.

[96] Weixing Li, Annalisa Vigorito, Camilla Calabrese, Luca Evangelisti, Laura B. Favero, Assimo Maris, and Sonia Melandri. The microwave spectroscopy study of 1,2-dimethoxyethane. *Journal of Molecular Spectroscopy*, 337:3–8, 2017. Spectroscopy and Inter/Intramolecular Dynamics in Honor of Walther Caminati - Part 2.

[97] K.P. Rajappan Nair, Sven Herbers, Alberto Lesarri, and Jens-Uwe Grabow. Molecular systems with nearly-free internal rotation and nuclear quadrupole coupling: Meta-chlorotoluene. *Journal of Molecular Spectroscopy*, 361:1–7, 2019.

[98] Jeff Bezanson, Alan Edelman, Stefan Karpinski, and Viral B Shah. Julia: A fresh approach to numerical computing. *SIAM review*, 59(1):65–98, 2017.

[99] H. T. Johansson and C. Forssén. Fast and accurate evaluation of Wigner $3j$, $6j$, and $9j$ symbols using prime factorization and multiword integer arithmetic. *SIAM Journal on Scientific Computing*, 38(1):A376–A384, 2016.

[100] Robert W. Field. *Spectra and Dynamics of Small Molecules*. Springer Cham, 2015.

[101] Juan Ortigoso, Isabelle Kleiner, and Jon T. Hougen. The K-rotational labeling problem for eigenvectors from internal rotor calculations: Application to energy levels of acetaldehyde below the barrier. *The Journal of Chemical Physics*, 110(24):11688–11699, 06 1999.

[102] Sandhya Gopalakrishnan, Christopher C. Carter, Lily Zu, Vadim Stakhursky, György Tarczay, and Terry A. Miller. Rotationally resolved b–x electronic spectra of both conformers of the 1-propoxy radical. *The Journal of Chemical Physics*, 118(11):4954–4969, 2003.

[103] Mirza A. Mekhtiev, Peter D. Godfrey, and Jon T. Hougen. Linestrengths of torsion–rotation transitions of methanol for j$\leq$ 22,k$\leq$ 14, and vt$\leq$ 2 from Hamiltonian-based calculations. *Journal of Molecular Spectroscopy*, 194(2):171–178, 1999.

[104] Kenneth Levenberg. A method for the solution of certain non-linear problems in least squares. *Quarterly Applied Mathematrics*, 2:164–168, 1944.

[105] Donald W. Marquardt. An algorithm for least-squares estimation of nonlinear parameters. *Journal of the Society for Industrial and Applied Mathematics*, 11(2):431–441, 1963.

[106] R. Fletcher. Modified marquardt subroutine for non-linear least squares. Technical report, Atomic Energy Research Establishment, 1971.

[107] R. P. Feynman. Forces in molecules. *Phys. Rev.*, 56:340–343, Aug 1939.

[108] Zahra Rezaeiparsa and Ali Ashrafi. A new adaptive levenberg–marquardt parameter with a nonmonotone and trust region strategies for the system of nonlinear equations. *Mathematical Sciences*, 2023.

[109] Xiao Yang. A higher-order Levenberg–Marquardt method for nonlinear equations. *Applied Mathematics and Computation*, 219(22):10682–10694, 2013.

[110] C.T. Dewberry, G.S. Grubbs, and S.A. Cooke. A molecule with small rotational constants containing an atom with a large nuclear quadrupole moment: The microwave spectrum of trans-1-iodoperfluoropropane. *Journal of Molecular Spectroscopy*, 257(1):66–73, 2009.

[111] K. P. Rajappan Nair, Sven Herbers, Jens-Uwe Grabow, and Ha Vinh Lam Nguyen. Neighborhood matters: Steric effects on methyl internal rotation and chlorine nuclear quadrupole coupling in 2-fluoro-4-chlorotoluene. *Journal of Molecular Structure*, 1246:131096, 2021.

[112] K.P. Rajappan Nair, Sven Herbers, Ha Vinh Lam Nguyen, and Jens-Uwe Grabow. The structure and low-barrier methyl torsion of 3-fluorotoluene. *Spectrochimica Acta Part A: Molecular and Biomolecular Spectroscopy*, 242:118709, 2020.

[113] K.P. Rajappan Nair, Sven Herbers, and Jens-Uwe Grabow. Structure and methyl torsion of halogenated toluenes: Rotational spectrum of 3,4-difluorotoluene. *Journal of Molecular Spectroscopy*, 355:19–25, 2019.

[114] Safa Khemissi, Martin Schwell, Isabelle Kleiner, and Ha Vinh Lam Nguyen. Approaching the free rotor limit: Extremely low methyl torsional barrier observed in the microwave spectrum of 2,4-dimethylfluorobenzene. International Symposium on Molecular Spectroscopy, 2023.

[115] György Tarczay, Péter G. Szalay, and Jürgen Gauss. First-principles calculation of electron spin-rotation tensors. *The Journal of Physical Chemistry A*, 114(34):9246–9252, 2010. PMID: 20684654.